UNIVERSITY OF OKLAHOMA

GRADUATE COLLEGE

INTEGRATED DIAGENETIC, STRUCTURAL AND PALEOMAGNETIC STUDY OF REMAGNETIZED FOLDED MISSISSIPPIAN-TRIASSIC UNITS FROM THE SOUTHERN CANADIAN CORDILLERA, ALBERTA & BRITISH COLUMBIA

A DISSERTATION

SUBMITTED TO THE GRADUATE FACULTY

in partial fulfillment of the requirements for the

Degree of

DOCTOR OF PHILOSOPHY

By

MATTHEW S. ZECHMEISTER
Norman, Oklahoma
2010

INTEGRATED DIAGENETIC, STRUCTURAL AND PALEOMAGNETIC STUDY OF REMAGNETIZED FOLDED MISSISSIPPIAN-TRIASSIC UNITS FROM THE SOUTHERN CANADIAN CORDILLERA, ALBERTA & BRITISH COLUMBIA

A DISSERTATION APPROVED FOR THE
THE CONOCOPHILLIPS SCHOOL OF GEOLOGY AND GEOPHYSICS

BY

Dr. R. Douglas Elmore, Chair

Dr. Eric Ferré

Dr. Ze'ev Reches

Dr. Randy Keller

Dr. Shankar Mitra

Dr. Richard Henry

© Copyright by MATTHEW S. ZECHMEISTER, 2010
All Rights Reserved.

ACKNOWLEDGMENTS

This research was supported in part by an ExxonMobil Student Research Grant, an American Association of Petroleum Geologists R.E. McClelland Memorial Research Grant, a Geological Society of America Graduate Student Research Grant (Allan V. Cox Student Research Award) and an Institute for Rock Magnetism (IRM) Visiting Research Fellowship. Special thanks to Josh Feinberg and Mike Jackson for help with acquisition and processing data as well as with providing stimulating discussions during my visit to the IRM. Thanks also to Vanessa O'Brien, Johari Pannalal, Andrew Theil, and Beth Helmke for assistance during field sampling over four seasons as well as my family for their never ending support during my 12 year collegiate journey. Also I would like to thank all of my committee members, whose comments and suggestions greatly improved this dissertation. Finally I would like to thank my advisor, Doug Elmore for taking in a stray dog and giving me the opportunity and support necessary to complete my dissertation.

TABLE OF CONTENTS

LIST OF TABLES

CHAPTER 1:

CHAPTER 2:

CHAPTER 3:

LIST OF FIGURES

Chapter 1:

Chapter 2:

Chapter 3:

ABSTRACT

Determining the timing and origin of fluid-related diagenetic events relative to orogenesis is crucial for understanding the interaction between orogenesis and diagenesis. Two folds in Mississippian carbonates (Line Creek anticline and Mt. Kidd anticline/syncline) and one fold in Pennsylvanian-Triassic units (Kent anticline) was investigated in the Southern Canadian Cordillera to test for a link between fluid flow, hydrocarbon migration/alteration and the formation of a multi-component remagnetization. This issue was investigated using an integrated diagenetic, structural and paleomagnetic approach. Geochemical, petrographic and fluid inclusion analysis was used to determine the nature of the diagenetic events while combined rock magnetic and paleomagnetic analysis was used to determine the magnetic carriers and age of both a high temperature and intermediate temperature chemical remanent magnetization (HTCRM and ITCRM, respectively). The timing of the HTCRM, contained in magnetite, is Early Cretaceous (~Aptian) and pre-tilting at Line Creek, although is inconclusive at Mt. Kidd due to its syn-tilting nature. The ITCRM is post tilting and Late Tertiary at Mt. Kidd, although is inconclusive at Line Creek due to its syn-tilting result A bedding parallel vein contact test shows direct correlation to the total component magnetic intensity of the HTCRM while a tectonic vein contact test shows a correlation to the total component intensity of the ITCRM. Elevated $^{87}Sr/^{86}Sr$ data indicates that the rocks have been altered by radiogenic fluids. C/O isotopes show evidence for a wide range warm fluids which is confirmed by fluid inclusion homogenization temperatures (149-212°C). The geochemical and petrographic results are consistent with the interpretation that the HTCRM formed as a result of a regional

migration of hydrocarbons and/or evolved basinal fluids. The ITCRM is interpreted to be the result of thermal sulfate reduction (TSR), caused by alteration of hydrocarbons, based on the observation of multiple by-products of TSR.

Because of the possibility of structural complications the conventional tilt test results where integrated with small circle intersection analysis (SCI) and calcite twin strain analysis. The Line Creek anticline formed during low to moderate burial, low deviatoric strain, kink folding, brittle deformation and contained no structural complications leading to a reliable age determination. On the other hand the Mt. Kidd anticline-syncline pair formed under higher burial temperatures, higher deviatoric strain and ductile deformation leading to structural complications affecting the HTCRM. These structural complications led to erroneous age determinations and required a modification of the HTCRM data set, based on the SCI results. This modification cleared up some deformation related discrepancies allowing for the determination that the early syn-tilting remagnetization at Mt. Kidd can be attributed to either strain modification or spurious rotations of a pre-tilting HTCRM. The ITCRM is a late syn-tilting to post tilting Tertiary remagnetization contained in pyrrhotite and has been determined to not have been affected by any structural complications.

Chapter 1: Preface

Integrated diagenetic, structural and paleomagnetic studies of remagnetized carbonates in fold and thrust belts can provide useful information on the timing of diagenetic events relative to orogenesis [e.g., McCabe and Elmore, 1989; Stamatakos et. al., 1996; Enkin et al., 2000; Katz et. al., 2000; Elmore et al., 2001; O'Brien et. al., 2007]. Multiple diagenetic processes have been shown to produce remagnetizations in fold and thrust belts [Elmore, 2001]. These processes may result in the formation of chemical remanent magnetizations (CRMs) via clay diagenesis [e.g., Katz et al., 2000], maturation/alteration of organic matter [e.g., Banerjee, et al., 1997; Blumstein et al,, 2004], and/or alteration caused by fluid migration of evolved basinal fluids and/or hydrocarbons [e.g., McCabe and Elmore, 1989; Enkin et al., 2000; O'Brien et al., 2007]. Moderate to high burial temperatures can also lead to the thermal resetting of a particular population of magnetic grains resulting in the formation of thermoviscous remanent magnetizations (TVRMs) [e.g., Kent, 1985]. Stress reorganization of domain walls [e.g., Hudson et al., 1989; Borradaile, 1997] or strain alterations of preexisting magnetizations during deformation [e.g., Kodama, 1988; Elmore et al., 2006] have also been proposed as remagnetization mechanisms. The objective of this study is to combine the results of rock magnetic, paleomagnetic, geochemical, petrographic, and strain studies in order to determine the origin and timing of CRMs in folded rocks in the Southern Canadian Cordillera.

Chapter 2 of this study focuses on the detailed rock magnetic characterization of a multi-component remagnetization in Mississippian carbonates from the Canadian Cordillera. The purpose of this study is to determine if the intermediate temperature

component resides in pyrrhotite. Previous studies in the Canadian Cordillera suggested that this intermediate temperature component is a TVRM in multi-domain magnetite (e.g., Enkin et al., 2000; Robion et al., 2004). Based on unblocking temperatures it appears that the high temperature component is contained in magnetite and the intermediate component is contained in pyrrhotite. This study utilized a variety of room temperature as well as low temperature rock magnetic experiments in order to gain a clear picture of the magnetic minerals responsible for each CRM. It is crucial to understand which magnetic minerals, as well as their granularity, carry each CRM since specific magnetic minerals relate to specific diagenetic events and particular grain sizes are susceptible to thermoviscous as well as strain/stress remagnetization.

Chapter 3 focused on an integrated diagenetic and paleomagnetic analysis in order to determine the diagenetic origin and timing of each component observed in the Canadian Cordillera. This study utilized standard tilt tests conducted on individual folds as well as vein conduit tests to investigate the relationship between folding, fluid migration, and the different CRMs. Geochemical analysis (stable carbon and oxygen isotopes and $^{86}Sr/^{87}Sr$ isotopes), and a variety of petrographic techniques where used to investigate the diagenetic features. Transmitted light and electron microprobe microscopy were used to determine lithology, identify diagenetic features and investigate the origin of magnetic minerals. Cathodoluminescence (CL) and fluid inclusion microscopy were used to investigate the nature of the vein forming fluids.

Chapter 4 focused on the origin of multiple syn-tilting remagnetizations found in the Canadian Cordillera. Syn-tilting magnetizations are a class of remagnetizations that are apparently acquired during folding but whose origin is still highly debated (e.g.,

Hudson et al., 1989; Elmore et al., 2006). This study investigated syn-tilting remagnetizations within asymmetrical folds comprised of Mississippian carbonates outlined in the previous chapters. The influence of fold and ramp geometry as well as deformation mechanisms on tilt test results were considered. This study integrated fold kinematic analysis and calcite strain analysis with small circle intersection (SCI) analysis [Shipunov, 1997; Waldhöer and Appel, 2006] in order to gain a clearer picture regarding the origin of syn-tilting remagnetizations.

Chapter 2: Rock magnetic characterization of a multi-component remagnetization in Mississippian Carbonates from the Canadian Cordillera, SW Alberta and SE British Columbia

M.S. Zechmeister[a*], E.C. Ferré[b], R. D. Elmore[a]

[a]*The ConocoPhillips School of Geology and Geophysics, the University of Oklahoma, Norman, OK 73019, USA (zechmeim@ou.edu; delmore@ou.edu*

[b]*Department of Geology, Southern Illinois University, Carbondale, IL 62901, USA (eferre@geo.siu.edu)*

Abstract:

Detailed paleomagnetic and rock magnetic analysis was conducted on Mississippian carbonates from the Canadian Cordillera (SE British Columbia and SW Alberta) to determine the dominant remanence carriers of a pervasive multi-component natural remanent magnetization, as well as evaluate the accuracy of rock magnetic techniques commonly employed to determine magnetic mineralogy. Paleomagnetic analysis of the carbonates reveals that two stable components are present after removal of the modern viscous remanent magnetization (VRM; <200°C). The next component is an intermediate temperature component that is removed between 200 and 340°C and is interpreted as a chemical remanent magnetization (CRM) carried by pyrrhotite. The characteristic remanent magnetization has a maximum unblocking temperature of 540°C and is interpreted to be a CRM carried by magnetite. Initial attempts to characterize the magnetic carriers using standard isothermal remanent magnetization (IRM) acquisition curves revealed that the samples are dominated by low coercivity components, but this approach failed to distinguish between pyrrhotite and magnetite. Hysteresis loops are wasp-waisted and the ratios of hysteresis parameters are consistent with published trendlines for remagnetized samples. First order reversal curve analysis reveals a spread of coercivities up to ~70 mT. Low-temperature (LT) experiments

indicate a large concentration of super paramagnetic grains, a suppressed Verwey transition, which could be attributed to the unblocking of a range of magnetite grain sizes. In addition these experiments indicate a maximum magnetization between 200-250 K and a LT magnetic transition at 34 K, both of which are indicative of pyrrhotite. Cumulative log Gaussian analysis of IRM data combined with LT data allowed characterization of three separate components. The first component has low coercivity and is attributed to multi-domain magnetite that is interpreted to carry the VRM. The second component has moderate coercivities and is attributed to pseudo-single domain to single domain magnetite that forms a CRM. The third component is a moderate to high coercivity component attributed to the CRM in single domain pyrrhotite.

1. Introduction

Paleomagnetic and rock magnetic studies of remagnetized carbonates in fold and thrust belts have provided important insight into diagenetic and tectonic events associated with orogenesis [e.g., Kent, 1985; McCabe and Elmore, 1989; Stamatakos et. al., 1995; Enkin et al., 2000; Katz et. al., 2000; Elmore et al., 2001; O'Brien et. al., 2007]. Secondary magnetizations have generally been attributed to multiple processes including burial diagenesis [Katz et al., 2000], fluid flow [Enkin et al., 2000], maturation of organic matter [Banerjee and Elmore, 1997], high burial temperatures [Kent, 1985] and strain/stress [e.g., Hudson et al., 1989; Borradaile, 1997; Elmore et al., 2006]. One of the central issues regarding secondary magnetizations is proper characterization of the magnetic carriers. Commonly remagnetizations associated with fold and thrust belts contain complex multi-component natural remanent magnetizations (NRMs). Accurate characterization of magnetic carriers and magnetic granulometry

distributions is crucial when attempting to relate magnetizations to depositional or diagenetic/tectonic processes, since certain magnetic minerals relate to specific diagenetic events. In most studies characterization is achieved, using a variety of paleomagnetic and room temperature rock magnetic experiments.

Paleomagnetic results obtained from three folds in Mississippian carbonates from the Front Range and Foothills of the Canadian Cordillera suggests that a multi-component NRM is carried by magnetite and pyrrhotite. The purpose of this study is to characterize rock magnetically, this multi-component remagnetization in order to determine if pyrrhotite is indeed an important remanence carrier. In recent years pyrrhotite has been increasingly recognized as an important carrier of a paleomagnetic signal [e.g., Dekkers et al., 1989; Rochette et al., 1990; Jackson et al., 1993; Xu et al., 1998; Horng et al., 1998; Crouzet et al., 2002; Weaver et al., 2002; Gillet and Karlin, 2004; Font et al., 2006; Preeden et al., 2008]. Pyrrhotite is considered an important redox and temperature indicator that can form during diagenesis [Hall, 1986]. Even small amounts of pyrrhotite with magnetizations on the order of 10^{-4} Am^2/kg or less may contribute to the NRM [Rochette et al., 1990]. One reason that pyrrhotite may have been discounted as a dominant remanence carrier in the past is due to the fact pyrrhotite and magnetite have overlapping room temperature coercivities. Another possible reason is because pyrrhotite may be interpreted as thermally remagnetized magnetite. Pyrrhotite is generally considered to have a maximum unblocking temperature of 325°C although temperatures as high as 350°C have been reported [Rochette et al., 1990], which may contribute to this misinterpretation. In order to properly characterize the magnetic mineralogy this study has utilized multiple room

temperature and low temperature (LT) experiments in conjunction with detailed paleomagnetic analysis to characterize this multi-component NRM.

2. Previous Rock Magnetic Studies in Fold and Thrust Belts

The majority of detailed rock magnetic studies of remagnetized Paleozoic carbonates have been conducted in the Appalachians [e.g., Kent 1985; Jackson, 1990; Saffer and McCabe, 1992; Jackson et al., 1993; McCabe and Channell, 1994; Stamatakos et al., 1995; Evans et al., 2000; Elmore et al., 2001; Lewchuk et al., 2002]. These studies found a pervasive Pennsylvanian-Permian (Kiaman) chemical remanent magnetization (CRM) contained in magnetite and/or hematite. A few of these studies also observed a Cenozoic thermoviscous remanent magnetization (TVRM) that was determined to reside in multi-domain (MD) magnetite.

These studies concluded that "wasp-waisted" hysteresis loops are a common feature of remagnetized carbonates and are the result of a bimodal distribution of coercivities [e.g., Jackson et al., 1990; Channell and McCabe, 1994; Suk and Halgedhl, 1996]. This distribution may be explained by a mixture of super paramagnetic (SP), single domain (SD), pseudo-single domain (PSD) and/or MD grains of one or more magnetic minerals [e.g. Jackson et al., 1993; Roberts et al., 1995; Tauxe et al., 1996]. Jackson et al. [1990] determined that the less stable coarse-grained PSD/MD grains did not contribute significantly to the Kiaman CRM, yet that they did contribute to the Cenozoic TVRM, although Jackson et al., [1993] then suggested, based on unblocking temperatures, that the Cenozoic TVRM may be carried by pyrrhotite. Jackson et al. [1993] also observed, which has subsequently been observed in other studies from different fold belts on other continents [e.g., McCabe and Channell, 1994; Weil and

Van der Voo, 2002] that M_{rs}/M_s vs. H_{cr}/H_c data, follow a power-law distribution when plotted on a logarithmic scale. These ratios have higher average M_{rs}/M_s values compared to curves generated experimentally for various magnetite grain size mixtures [Parry, 1982]. This trend from remagnetized carbonates has been considered to be a possible "fingerprint" of remagnetized carbonates [Jackson et al., 1992] representing the complex variations associated with remagnetized carbonates.

Several paleomagnetic studies of remagnetized Paleozoic carbonates within the Canadian Cordillera have isolated a multi-component NRM [e.g. Lewchuk et al., 1998; Enkin et al., 2000; Robion et al., 2004]. Enkin et al. [2000] determined the regional extent of remagnetizations throughout the Canadian Rockies and did not focus on individual structures, while most other studies focused on drill cores obtained from Paleozoic hydrocarbon reservoirs on the western edge of the Western Canada Sedimentary Basin (WCSB [e.g., Lewchuk et al., 1998; Symons et al., 1999; Cioppa et al., 2000; 2001; 2003]. These studies investigated the timing of remagnetizations in relation to: (1) dolomitization [Lewchuk et al., 1998], (2) fluid flow [Enkin et al., 2000; Lewchuk et al., 2000; Cioppa et al., 2000], and (3) hydrocarbon generation [Cioppa and Symons, 2000], using room temperature isothermal remanent magnetization (IRM) acquisition data in a variety of forms (i.e., IRM acquisition curves, saturation IRM crossover plots, tri-axial thermal decay of IRM) [Lowrie, 1990]. In one study, LT saturation IRM (LT-SIRM) experiments were used to identify the Verwey transition [Cioppa and Symons, 2000]. A widespread dual polarity NRM residing in magnetite was interpreted to be present throughout the Canadian Rockies. The characteristic remanent magnetization (ChRM) was determined to be a CRM carried by magnetite

with an intermediate temperature component that was interpreted to be a TVRM that also resides in magnetite [e.g., Lewchuk et al., 1998; Enkin et al., 2000; Robion et al., 2004]. Possible early diagenetic magnetizations were observed only in micritic limestones [Cioppa et al., 2001] or anhydrite nodules [Lewchuk et al., 1998]. In most of these aforementioned studies, magnetite was considered the dominant carrier of the remagnetizations with pyrrhotite being considered a non remanence carrying phase [i.e., Lewchuk et al., 1998; Cioppa et al., 2001]. In a study of the Debolt Formation an intermediate temperature component, similar within the temperature range of the TVRM was observed and appeared to be carried by pyrrhotite or a pyrrhotite/magnetite mixture, however, the magnetic carrier was not conclusively identified [Cioppa et al., 2003].

3. Geological/Tectonic Setting

The foreland fold and thrust belt in the Canadian Cordillera is divided into three sub units from west to east: the Main Ranges, the Front Ranges, and the Foothills (Figure 1) and is the result of west to east directed horizontal compression due to terrane accretion which accommodated up 200 km of horizontal shortening [e.g., Price and Mountjoy, 1970; Price, 1981; Fermor and Moffat, 1992]. Contraction in the foreland fold and thrust belt was expressed as thin-skinned detachment thrusting and folding of Mesoproterozoic to Cretaceous strata over Cretaceous and older strata [e.g., Monger and Price, 1979; McMechan and Thompson, 1989; Price, 1994]. Deformation was active from the late Jurassic to the Eocene and spanned both the Columbian (Mid Jurassic–Late Cretaceous) and Laramide orogenies (Late Cretaceous to Paleocene) with most of the shortening occurring in the Late Cretaceous (~89 Ma)[Price, 1994].

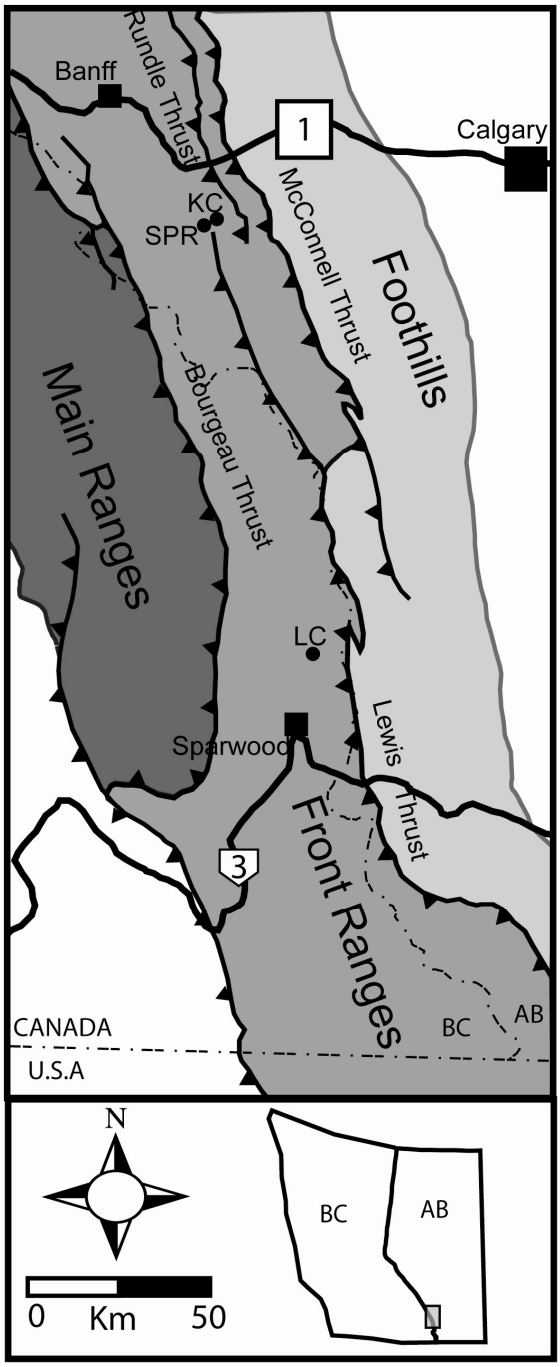

Figure 1: Generalized tectonic map of the Canadian Fold and Thrust belt highlighting major tectonic units (Main Ranges, Front Range, and Foothills; Modified from Enkin et al., 2000). Sampling locations, Kananaskis Country (KC), Line Creek (LC) and Oldman River (OR) are indicated by the black dots.

Obduction of terranes onto the North American peri-cratonic terranes began in the Late Triassic and continued into the Eocene. This obduction initiated shortening and thickening in the Omencia Belt west of the foreland belt along both east and west directed faults resulting in north south oriented folds [Evenchick et al., 2007 and references there in]. This led to significant uplift in the Omencia Belt by the Late to Middle Jurassic followed by the first appearance of western derived sediments and increased subsidence in the foreland belt due to tectonic loading [Poulton et al., 1993]. Initiation of thrusting in the westernmost portion of the foreland belt began in the Early Cretaceous and progressed eastward [Carr and Simony, 2006]. The majority of shortening occurred during the Late Cretaceous-to Eocene, during which the major thrust motions along the Lewis and McConnell thrust sheets occurred [Price, 1981]. This effectively doubled the width of the foreland belt, which was followed by cessation of contractional deformation which led to exhumation and erosion [Price and Mountjoy, 1970].

The folds of interest for this study are in the Front Ranges along Line Creek (LC), British Columbia and Kananaskis Country (KC), Alberta (Mt. Kidd) and in the western edge of the Foothills along Oldman River (OR), Alberta (Figure 1). All of the folds are asymmetrical with steep (KC and LC) to overturned (OR) front limbs and shallow back limbs. These folds comprise various facies of the Mississippian Rundle Group, specifically the Etherington, Mount Head, and Livingstone formations. These units are predominantly platform to basin carbonates deposited within a passive margin setting [e.g., Hardebol et al., 2006], have undergone varying degrees of dolomitization, hydrothermal alteration [e.g., Al-Asam, 2000], and contain degraded hydrocarbons.

At Oldman River the Mount Head and Etherington formations were sampled. The Etherington formation is the only non carbonate unit examined, it is grey and black, banded quartz sandstone. The sandstone was cemented with calcite with the dark bands containing degraded hydrocarbons. The Mount Head formation is a series of dark grey carbonates comprising two lithologies: crystalline dolomite and dolomicrites. At Kananaskis Country, the undivided Mount Head/Livingstone unit was sampled and is comprised of grey to black carbonates made up of a variety of lithologies: pelloidal, oolitic and crinodal grainstones, fossiliferous packstones with minor dolomitization, dolomitized coarse crystalline limestone, fine to coarse crystalline dolomite, and dolomicrites. At Line Creek the Mount Head was sampled along with a few sites in the Etherington Formation. The Etherington samples were light to dark grey limestones and dolomites with minor amounts of chert. The Mount Head formation comprises fossiliferous wackstones, oolitic and pelloidal grainstones, dolomicrites, fine crystalline dolomite, and dolomitized wackstones.

4. Methods

Samples for paleomagnetic and rock magnetic analysis were collected with a portable gasoline drill and oriented with an inclinometer and Brunton compass. The majority of the sampling was confined to road cuts that provided freshly exposed material. Fifty four sites (~ 8 samples/site) were collected from both limbs at the LC anticline (Figure 1) on the property of the Elk Valley Coal Company. Forty three sites were collected from a both limbs of a syncline at KC (Figure 1).Thirteen sites were collected from the front limb and back limb of an anticline/syncline pair at OR (Figure 1).

Paleomagnetic samples were marked and cut to standardized lengths (~2.2 cm) with an ASC Scientific dual blade saw. The NRM was measured using a 2G Enterprises cryogenic magnetometer with DC SQUIDS in a magnetically shielded laboratory. Most samples collected at OR during the first sampling season were subjected to a 17 step thermal demagnetization from 100 to 580°C with coarse steps at low to intermediate temperatures. Specimens collected from LC and KC during the second and third sampling seasons were subjected to stepwise thermal demagnetization using 25 steps with closely spaced steps at intermediate temperatures. Prior to thermal demagnetization, the LC and KC samples and some OR samples were subjected to two liquid nitrogen treatments for two hours to remove the unstable remanence in the low coercivity MD grains [e.g., Dunlop et al., 1997; Borradaile et al., 2004]. The NRM was measured after each liquid nitrogen treatment. Thermal demagnetization was accomplished with an ASC Scientific Thermal Specimen Demagnetizer. Demagnetization data was plotted on Zijderveld [1967] diagrams using the Super IAPD program, which were also used for principal component analysis (PCA) [Kirschvink, 1980] were used to determine the magnetic components.

IRM acquisition/decay experiments were after the NRM had been subjected to alternating field (AF) demagnetization from 0 to 100 mT using a 2G Enterprises automated degaussing system. Acquisition of the SIRM was conducted in 25 steps from 10 to 2500 mT using an ASC Scientific Impulse Magnetizer. Finally, the samples were subjected to AF demagnetization again and had an IRM imparted along three perpendicular directions, 120, 500, and 2500 mT, and were thermally demagnetized for 25 steps from 0 to 680°C to produce tri-axial thermal decay curves [Lowrie, 1990]. Log

Gaussian analysis was performed on an IRM imparted using 25 steps using the IRM-CLG 1.0 software of Kruiver et al [2001] to investigate the coercivity spectrum within individual samples.

Hysteresis loops were generated using ≤ 2 g samples on a Princeton Scientific vibrating sample magnetometer (VSM) model 3900-04 at both the Institute for Rock Magnetism at the University of Minnesota as well as at Southern Illinois University, Carbondale. Measurements were performed using a vibration amplitude of 1, a 3-5 sec averaging time and 1 mT steps up to 500 mT. Hysteresis loops were corrected for either paramagnetic or diamagnetic slopes and were then used to determine the coercive force (H_c), saturation magnetization (M_s), and saturation remanent magnetization (M_{rs}), while the coercivity of remanence (H_{cr}) was determined from backfield demagnetization experiments. Due to the weak magnetizations of remagnetized carbonates, Fast Fourier Transform analysis was used to smooth noisy hysteresis loops [Jackson et al., 1990].

First order reversal curves (FORC) were generated to examine variations in the coercivity spectrum [Pike et al., 1999; Roberts et al., 2000]. A Princeton Scientific VSM at the Institute for Rock Magnetism was used to measure ~ 68 FORCs using an averaging time of 1 sec and 5 mT field increments. A saturation field of 500 mT was used along with a Hb range from (-60 to 60 mT) and a Hc range of (0.6 to 150 mT). FORC diagrams were produced using the FORCinel program [Harrison and Feinberg, 2008].

Multiple samples underwent a series of low temperature experiments using a Quantum Design Magnetic Property Measurement System (MPMS) at the Institute for Rock Magnetism. The first experiments involved a room-temperature SIRM which was

then subjected to progressive cooling to 10 K followed by warming to room temperature, all in a zero field. This experiment is useful to determine LT magnetic transitions (i.e., Verwey and 34 K transitions) which are indicative of particular magnetic phases. Recovery of the magnetization during rewarming through a magnetic transition provides important grain size information [Dekkers et al., 1989]. The second set of experiments involved thermal demagnetization of an IRM imparted at 10 K and during warming back to room temperature to examine the contribution of SP grains to the bulk rock magnetic properties.

5. Results

5.1 Paleomagnetic data

LT treatment prior to thermal demagnetization indicates an overall decrease in the NRM intensity for all localities and varies from site to site (5-41% for KC; 10-30% for LC; 5-25% for OR), which suggests a variable concentration of MD grains. Stepwise thermal demagnetization reveals a multi-component NRM at temperatures above those that define the modern VRM (NRM-200°C) in samples from the Front Ranges (KC and LC) and a single component NRM at after removal of the modern VRM in specimens from the Foothills (OR; Figure 2). Orthogonal projections constructed from the thermal demagnetization data show that each locality has a ChRM with a maximum unblocking temperatures between 480-540°C (Figure 2) suggesting magnetite. The ChRM has a northerly declination and steep down inclination in the Front Ranges (KC and LC, Figure 2A, B) and a southerly declination and steep up inclination in the Foothills (OR, Figure 2C), similar to what has been reported by others in the Canadian Rockies [e.g. Enkin et al, 2000]. In the Front Ranges, an intermediate

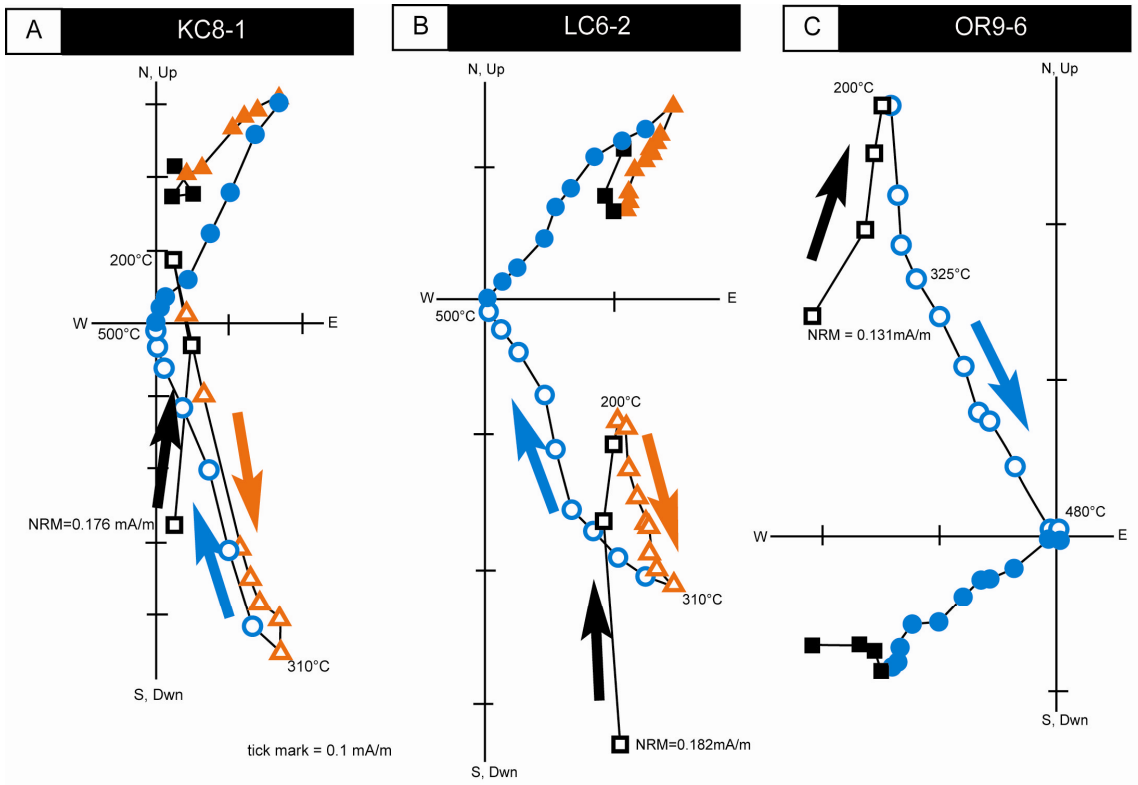

Figure 2: Representative orthogonal projections (Zijderveld diagrams) in geographic coordinates for stepwise thermal demagnetization of KC, LC, and OR localities. Open circles represent the vertical component (inclination) and the closed circles indicate the horizontal component (declination). The normal polarity ChRM is indicated by circles, the reversed polarity intermediate component is indicated by triangles and the modern VRM is indicated by squares. Arrows indicate the direction of thermal decay.

temperature component that has a southerly declination and steep up inclination was observed with a maximum unblocking temperature of ~325-340°C (Figure 2A, B) which suggests pyrrhotite. The intermediate temperature component was not observed in the foothills (OR).

5.2 Isothermal Remanent Magnetization (IRM) Experiments

The majority of curves generated from the 25-step IRM acquisition experiments reached saturation below 500 mT (Figure 3), which suggests that the NRM is controlled by a low to intermediate coercivity phase such as magnetite or pyrrhotite. Many samples have a relatively sharp transition to saturation (Figure 3B & C), however, a few have a more gradual transition (Figure 3A). Some specimens were not fully saturated at 2.5 T, which suggests the presence of a high coercivity phase such as hematite or goethite. Thermal decay of a tri-axial IRM is dominated by the low coercivity component in the majority of the samples with all the curves completely decayed by 580°C suggesting the presence of magnetite (Figure 3). In all two of the three locations, a minor inflection in the tri-axial decay curves is observed around 320°C, which is consistent with the presence of pyrrhotite (Figure 3). In some sites demagnetization was not completed until 680°C, suggesting the presence of hematite.

Cumulative log Gaussian analysis [Kruiver et al., 2000] was performed on the IRM acquisition data to quantitatively examine the coercivity spectrum. The LC and KC samples are similar and require 3 components to fit the raw data (Figure 4A-B; Table 1). The first component is a very low coercivity component which contributed less than 10% of the total IRM and had a coercivity of ~17 mT which is in the range of MD magnetite. The second component is low coercivity component which contributed

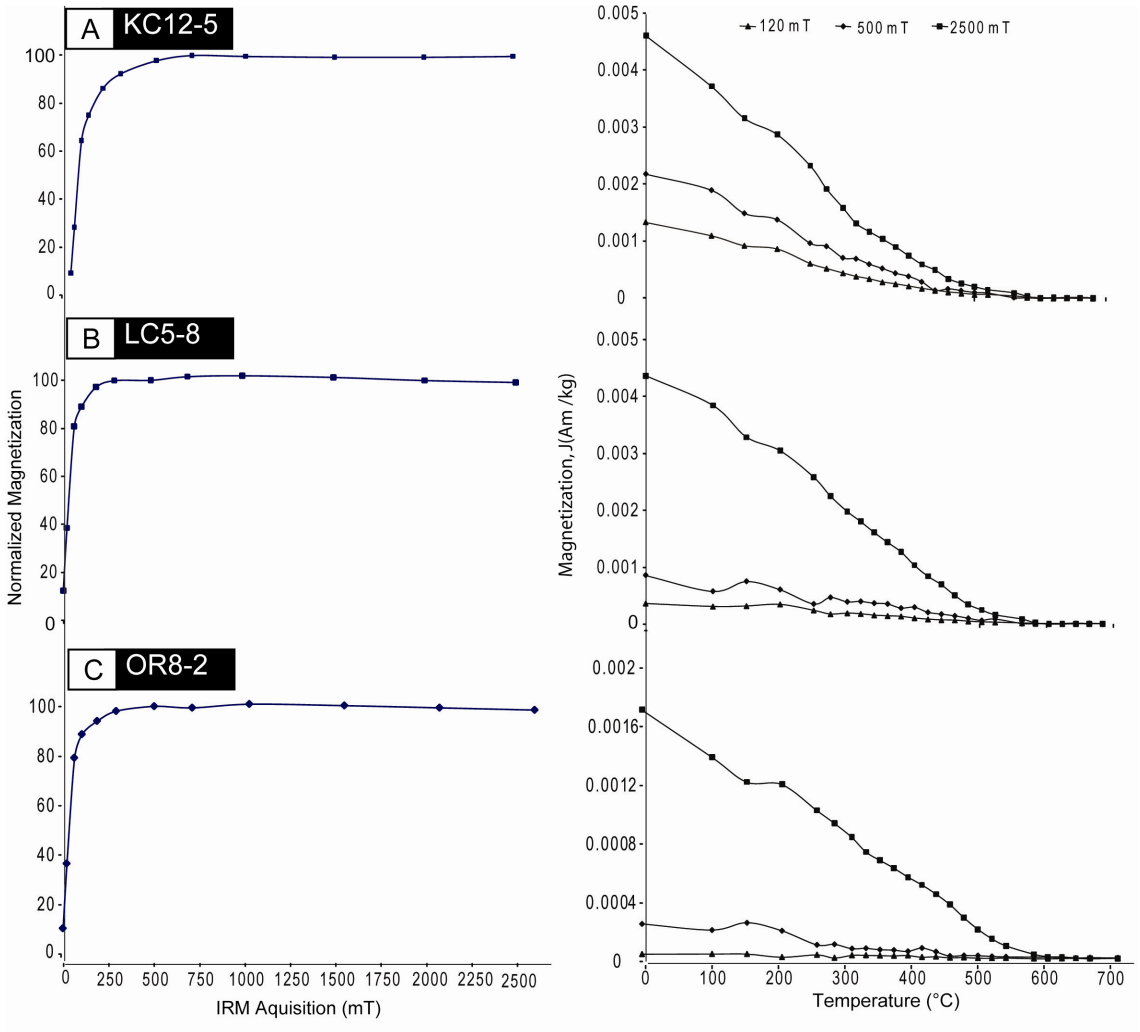

Figure 3: Representative Isothermal Remanent Magnetization (IRM) Acquisition and tri-axial thermal decay curves for KC, LC and OR localities. A) Shallow limb from Mt. Kidd syncline. B) Shallow back limb of Line Creek anticline. C) Back limb of western anticline at Oldman River.

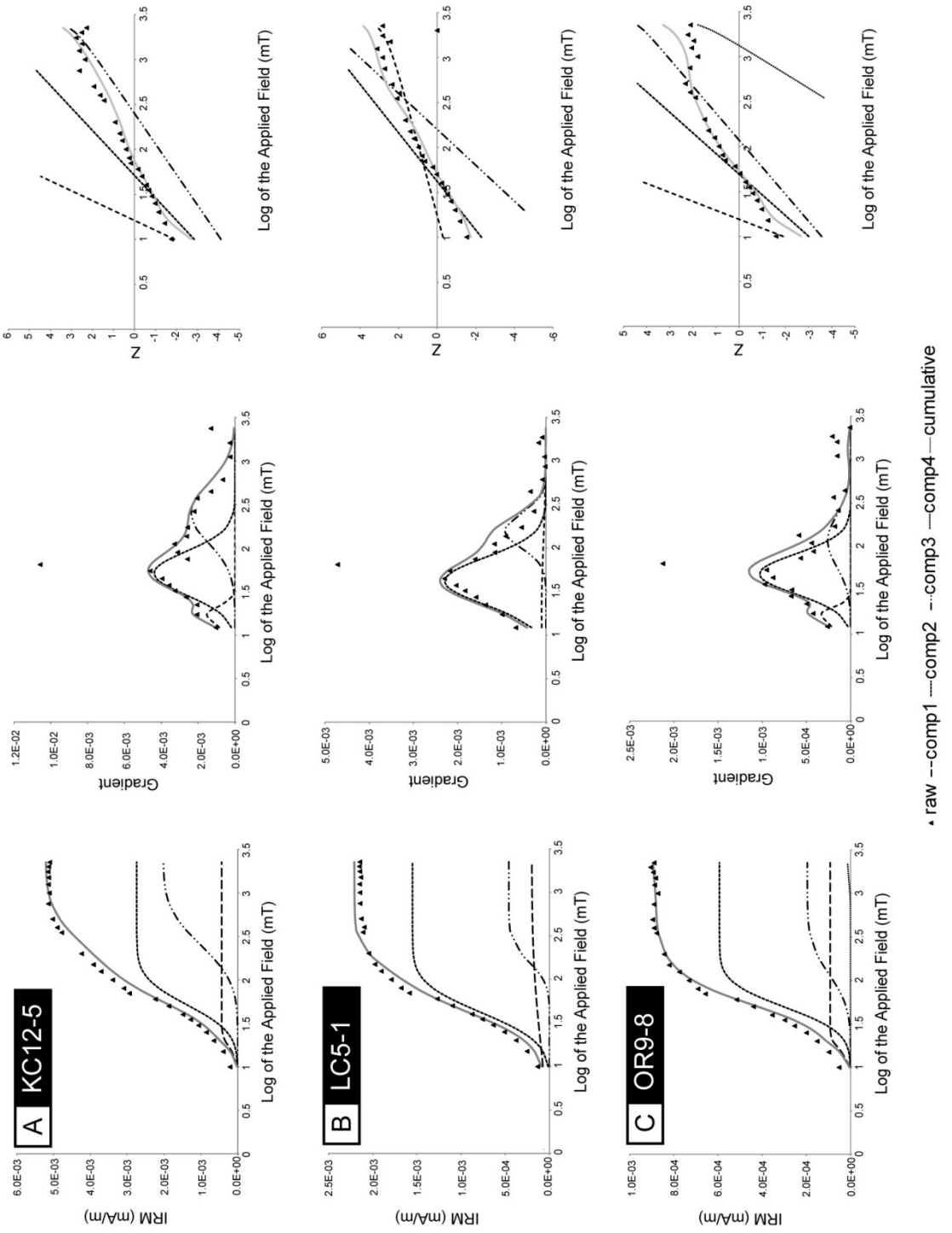

Figure 4: Representative results from cumulative log Gaussian analysis of a 25 step IRM acquisition (Kruiver et al., 2000) for KC, LC and OR. A) Shallow limb from Mt. Kidd syncline with 3 components. B) Shallow back limb of Line Creek anticline with three components. C) Back limb of western anticline at Oldman River with four components

Table 1: component results from LAP-GAP-SAP modeling

Sample	Contribution	SIRM	Log($B_{1/2}$)	$B_{1/2}$	DP	Mineralogy
	%	mA/m	mT	mT	mT	
KC12-5						
1	8.3	4.33 E-4	1.21	16.2	0.11	MD Magnetite
2	52.8	2.75E-03	1.71	51.3	0.25	PSD-SD Magnetite
3	38.9	2.03E-03	2.40	251.2	0.34	Pyrrhotite
LC5-1						
1	9.0	2.00E-04	1.25	17.8	0.80	MD Magnetite
2	70.1	1.55E-03	1.62	41.7	0.27	PSD-SD Magnetite
3	20.9	4.61E-04	2.20	158.5	0.20	Pyrrhotite
OR9-8						
1	10.3	9.25E-05	1.19	15.5	0.10	MD Magnetite
2	66.4	5.94E-04	1.69	49.0	0.23	PSD-SD Magnetite
3	21.8	1.95E-04	2.07	117.5	0.30	Pyrrhotite
4	1.5	1.34E-05	3.13	1349.0	0.16	Hematite

between 50-70% of the IRM and had a coercivity range between 40-52 mT which is in the range for magnetite. The third component is a moderate coercivity component which contributed between 20-40% of the total IRM and had a coercivity between 158-251 mT which overlaps the range for pyrrhotite (Hunt et al., 1995). Samples from Oldman River contained each of the three previous mentioned components, as well as a high coercivity component that only contributed ~1.5% to the IRM and has a coercivity of ~1.3T which is in the range of either goethite or hematite (Figure 4C; Table 1) [Peters and Dekkers, 2003]. The cumulative log Gaussian analysis suggests the presence of pyrrhotite even though no definite intermediate component data was observed in the thermal demagnetization data at Oldman River. This type of modeling gives a more accurate look into how the coercivities are distributed throughout the sample than standard IRM acquisition curves, however, due to the overlap in the coercivity data at room temperature [Peters and Dekkers, 2003], the results obtained are not conclusive for any one particular magnetic mineral.

5.3 Hysteresis and FORC Experiments

In general, all of the hysteresis loops generated were from weak samples, which produced moderately noisy loops, requiring smoothing by fast Fourier transform [Jackson et al., 1990]. Figure 5 shows representative examples of the raw and filtered loops and illustrates the range of loop shapes observed at each locality. The majority of hysteresis loops (50 total) reached saturation below 500 mT (Figure 5) suggesting a dominant low to moderate component such as magnetite or pyrrhotite. These loops also have a wasp-waisted appearance (Figure 5) which is common in remagnetized carbonates and represents a mixture of coercivities [Jackson, 1990; McCabe and

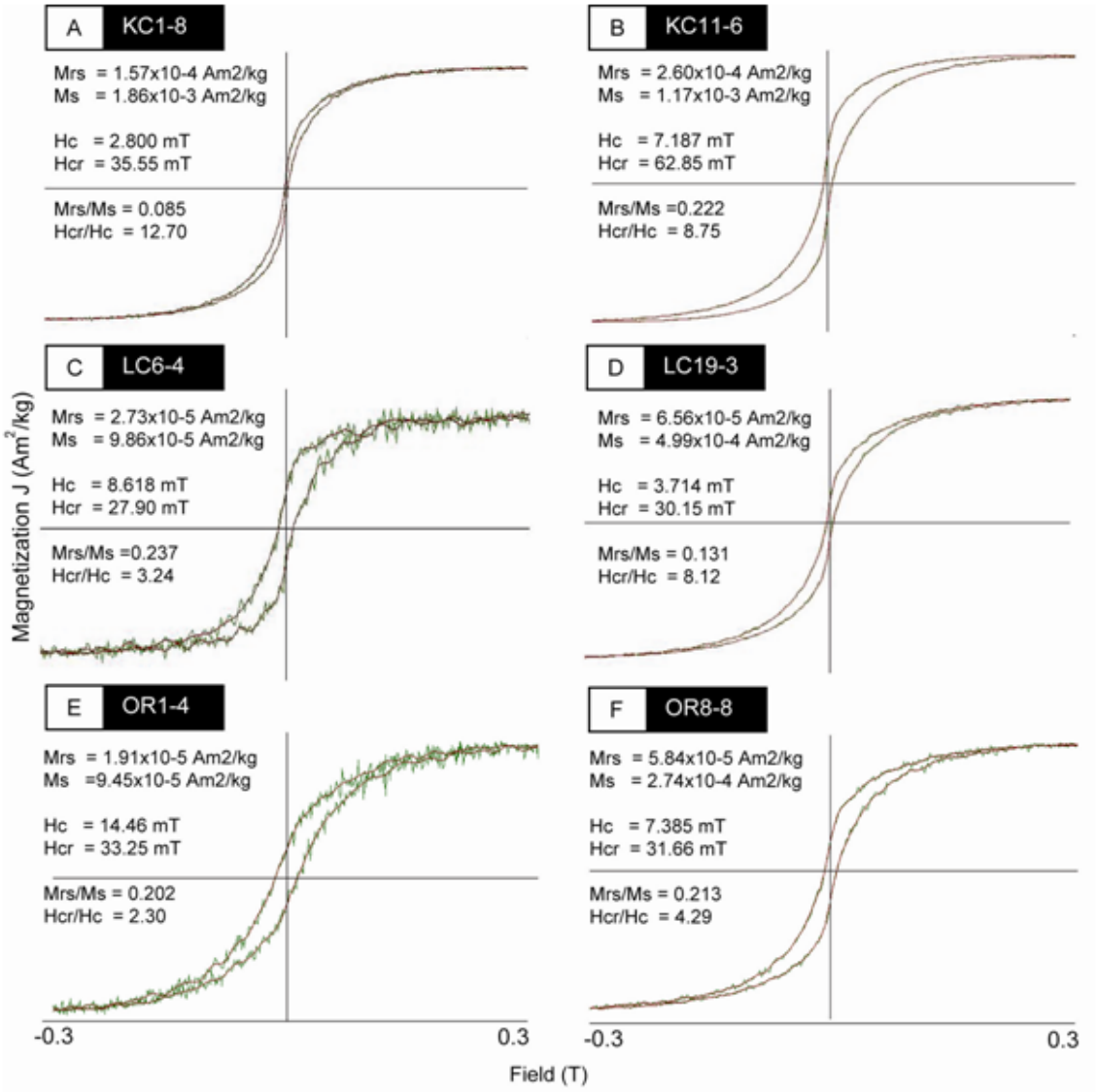

Figure 5: Representative hysteresis loops from all three localities. Light line is the raw data and the dark line is the filtered data. A) KC1-8: Skinny wasp-waisted loop with a large Hcr/Hc ratio indicating a large SP fraction. B) KC11-6 : Wasp-waisted loop with a high Hcr, possibly an indicator of high concentrations of pyrrhotite. C) LC6-4: Goose-necked loop indicating the presence of an oxidized phase most likely hematite. D) LC19-3; Wasp-Waisted loop. E) OR1-4: Non wasp-waisted loop indicating a predominance of SD grains. F) OR8-8: Wasp-waisted loop.

Channell, 1994; Roberts et al., 1995; Tauxe et al., 1996; Weil and Van der Voo, 2002]. Some of the loops are narrow and have very high H_{cr}/H_c ratios (>10) suggesting an overwhelming SP content (e.g. Figure 5A) [i.e., Jackson, 1990; Roberts et al., 1995]. Other samples have H_{cr} values above 50 mT (Figure 5B) suggesting a large amount of a moderate coercivity phase such as pyrrhotite [Dekkers, 1998]. Pyrrhotite is magnetically "harder" than magnetite and pure samples as well as samples containing large concentrations of SD pyrrhotite commonly have H_{cr} values higher than 50 mT [Dekkers, 1988], although none of the samples displayed squared loops which is has been reported for natural pyrrhotite [e.g., Dekkers, 1988]. A few of the loops have a more goose neck appearance (Figure 5C), which suggests that they also contain a small portion of higher coercivity material such as hematite or goethite [e.g., Tauxe et al., 1996].

Plots of M_{rs}/M_s verses H_c/H_{cr} on a log-log plot follow the remagnetization trendlines proposed by Jackson [1990] for cratonic carbonates and McCabe and Channell [1994] for folded limestones from the Craven Basin, Great Britain (Figure 6A). A log-log plot of H_c versus M_{rs}/M_s shows distinct groupings between the front limb and the back limb of the folds at KC and LC with a spread of values observed for OR (Figure 6B). These results suggest a finer grain size in the back limb than in the front limb at KC and LC since H_c and M_{rs}/M_s tend to increase with decreasing grain size for both magnetite and pyrrhotite [e.g., Dunlop, 1986; Dekkers, 1988; Suk and Halgedahl, 1996]. Another possible reason for this grouping may be related to strain enhanced magnetic hardening [e.g., Borradaile, 1991; Jackson et al., 1993; Elmore et al., 2006], yet the steep front limbs, which have higher levels of deformation through

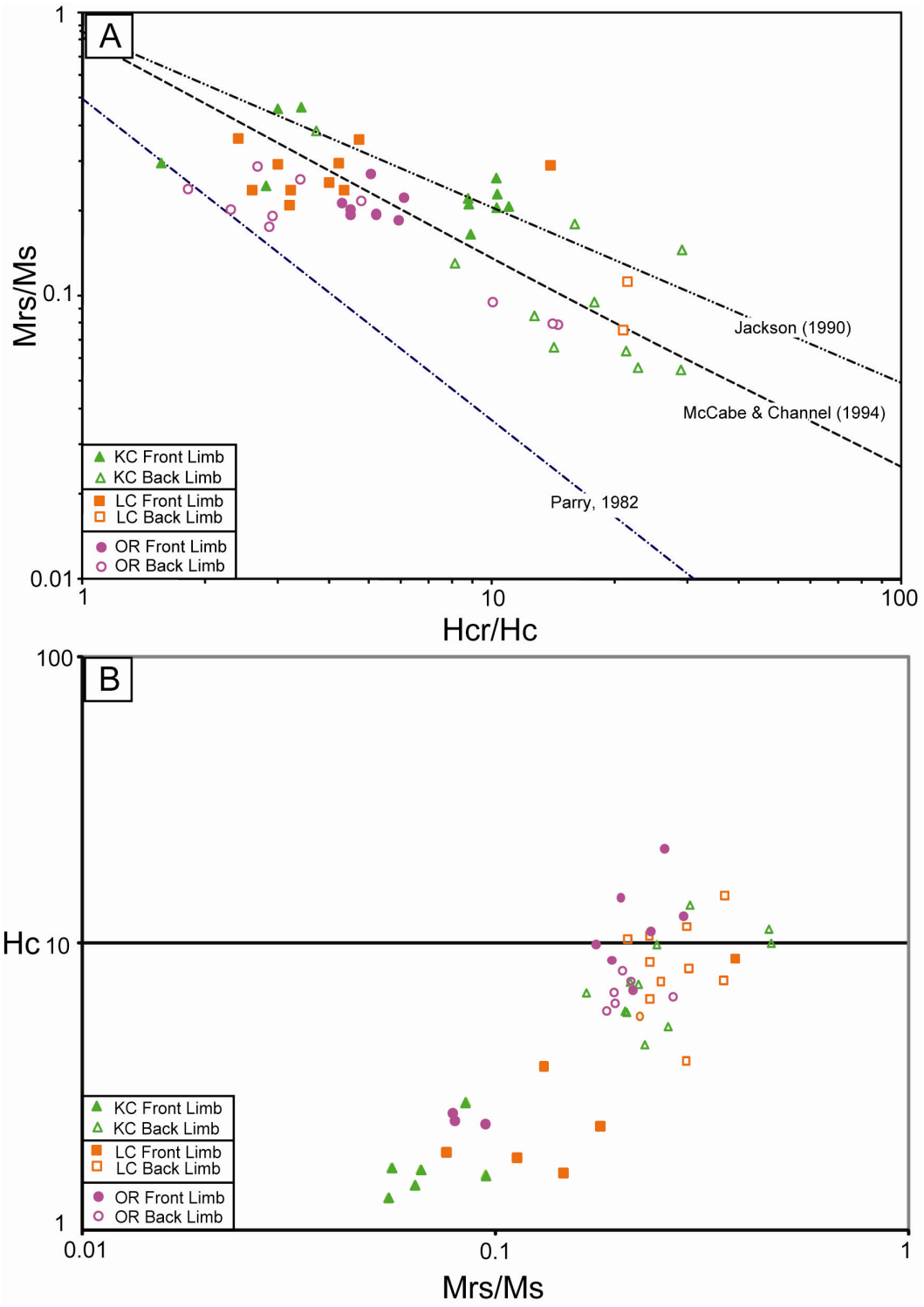

Figure 6: Log-log plots of Hysteresis properties. A) Log-Log plot of the M_{rs}/M_s ratio vs. the H_{cr}/H_c ratio from all field areas. The three lines plotted on the graphs represent the accepted trendlines for samples containing a mixture of grain sizes [Parry, 1982; Jackson, 1990; McCabe and Channell, 1994]. B) Log-Log plot of H_c vs. M_{rs}/M_s ratio from all field areas

thinning either by brittle (LC) or ductile (KC) processes have lower M_{rs}/M_s and H_c values than the shallow back limbs. The results are in direct contrast to what would be expected with strain enhanced magnetic hardening.

FORC experiments were also conducted on selected samples from each fold to examine grain size distributions. Both the KC and LC samples are similar, with a smoothing factor of 2.8 and the majority of the magnetic grain population falling near the low coercivity peak at around 2 m. This suggests a dominance MD magnetite grains, however, there is tail of increasing coercivity observed out to around 70 mT (Figure 7A, B). This observed coercivity range coincides with a mixture of soft components, such as a range of magnetite grain sizes or a possible combination of magnetite and pyrrhotite. The Oldman River sample (Figure 7C) shows a similar large population around H_c = 2 mT and a tail out to ~70 mT. Broad contours which parallel the H_c = 0 axis also exist, suggesting MD grains, however, the large smoothing factor (SF = 11) required makes any conclusive interpretation of these contours suspect.

5.4 Low-temperature experiments

SIRMs imparted at low temperature (~10 K) and warmed to room temperature in a zero field as well as in an applied field show a significant drop in intensity between 10 and 50 K (Figure 8). This feature is indicative of SP grains [Xu et al., 1998; Katz et al., 1998] and the estimation of the SP factor [Hunt et al., 1995] shows a range from 0.4-0.9 indicating variable SP concentrations. Interestingly though, there is no linear correlation between Large H_{cr}/H_c ratios and the SP factor. The majority of the applied field curves and zero field curves did not show the characteristic Verwey transition common for magnetite upon rewarming. This may be due to oxidation of magnetite

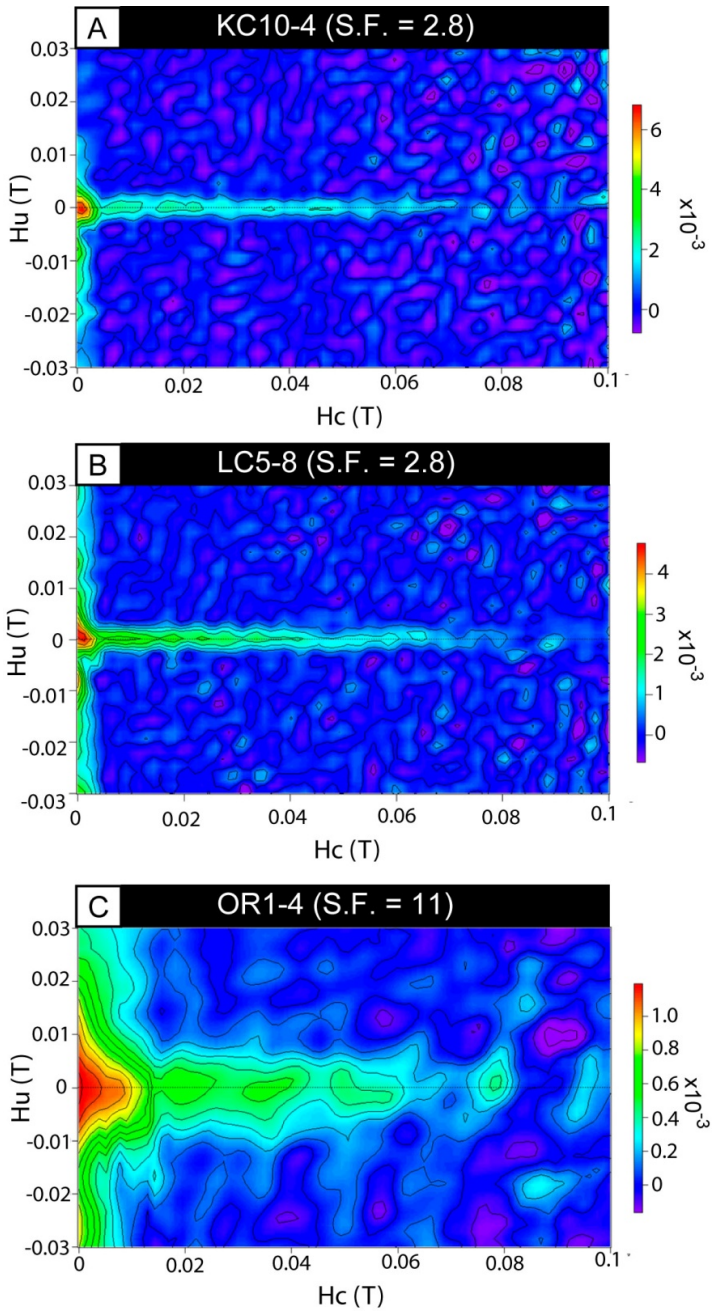

Figure 7: First order reversal curves (FORC) diagrams from each of the three localities with the smoothing factor (SF) shown on each diagram. A) KC10-4: Large concentration of low coercivity designated by the low coercivity peak with a spread out to ~70 mT. B) LC5-8 Similar to KC10-4. C) OR1-4: Weak noise sample with a high smoothing factor, shows similar low coercivity peak but contours only spread out to ~60 mT

[Özdemir et al., 1993]. The majority of the samples showed similar applied field curves and zero field curves (Figure 8B, D), however, a few samples had a applied field curve which did not match up with the zero field curves until they were near room temperature. This suggests the presence of an oxidized phases such as hematite [Özdemir and Dunlop, 2000].

The majority of samples cooled to 10 K after they were imparted with a room temperature (RT) SIRM, displayed a gradually increasing magnetic intensity until it reaches a maximum (M_{max}) between 200-250 K which is diagnostic of pyrrhotite [i.e., Dekkers et al., 1989; Rochette et al., 1990]. Interestingly though only a few of the sites examined showed the 34 K magnetic transition for pyrrhotite (Figure 8B) [Dekkers et al, 1989]. For KC11-8 the cycling of cooling and warming allow for estimation of the pyrrhotite grain size [Rochette et al., 1990]. The ratio of heating over cooling at the 34 K magnetic transition (h/c ratio) (Figure 8B) was 0.98 and the ratio of IRM after and before cycling (R) was 0.95. This suggests that this sample is dominated by ~2 μm pyrrhotite grains which are in the SD range. The only sample to not show the M_{max} between 200 and 250 K was OR1-4 which has an sharp Verwey transition indicating magnetite (Figure 8E). The other RTSIRM samples examined showed a more gradual or suppressed Verwey transition (Figure 8) suggesting the unblocking of a range of magnetite grain sizes with variable coercivities [pers. com. Mike Jackson] or possibly oxidation of magnetite [Özdemir et al., 1993].

6. Discussion

Based on the aforementioned, results the remagnetized carbonates from the studied localities contain complex and highly variable magnetic mineralogy and

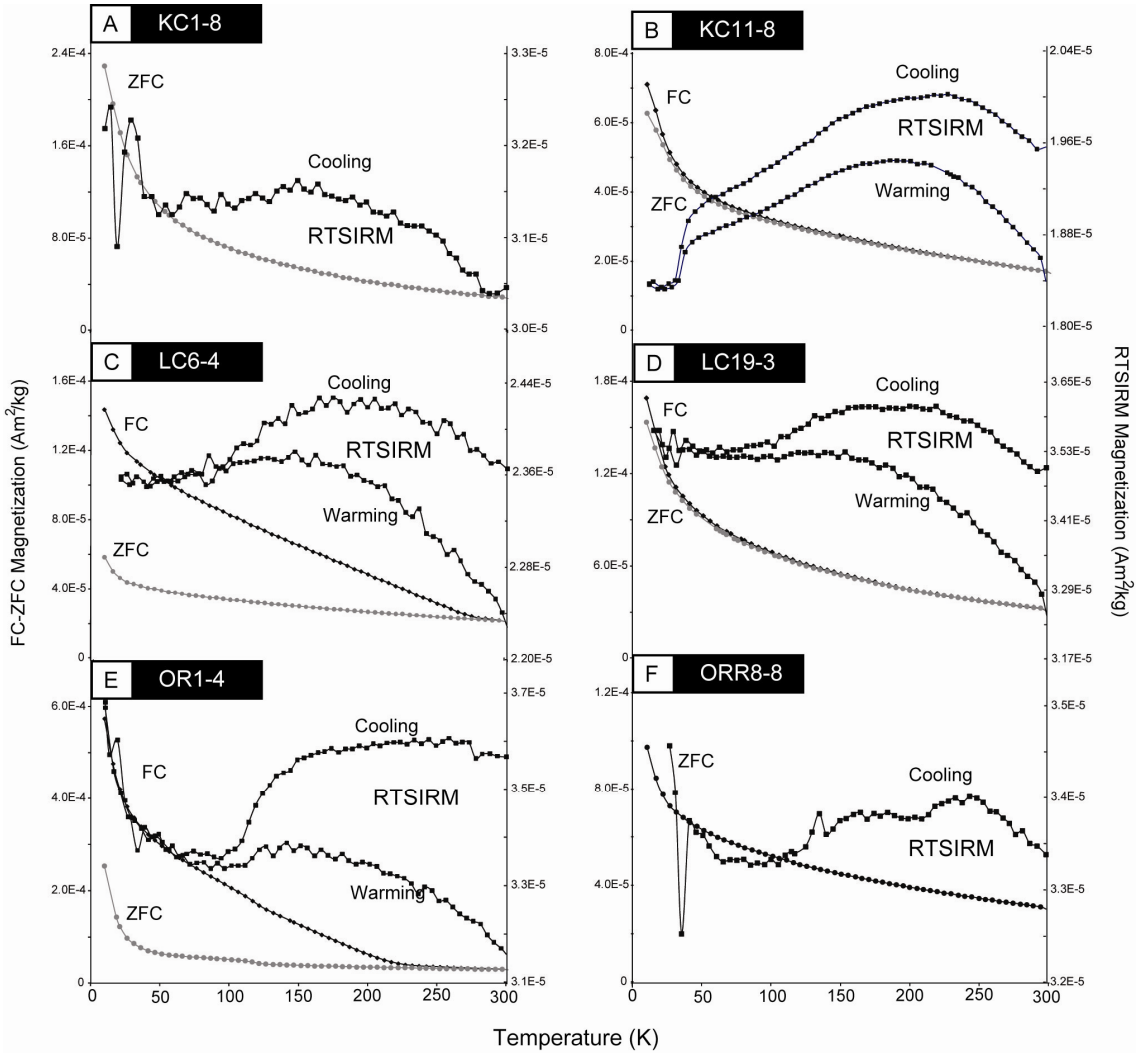

Figure 8: Representative curves generated during low-temperature SIRM experiments. A) Room temperature saturation isothermal remanent magnetization (RTSIRM) cooling curve showing suppressed Verwey transition and a large drop in the zero field curves (ZFC) due to a large SP concentration. B) RTSIRM cooling and warming curves showing a suppressed Verwey transition, a Ms peak between 200-250 K and the 34 K magnetic transition. Applied field curves (FC) and ZFC curves similar and show large SP concentration. C) RTSIRM cooling and warming curves showing a suppressed Verwey transition and a Ms peak between 200-250 K, FC and ZFC do not converge until room temperature suggesting the presence of an oxidized phase. D) Similar to LC6-4 except the FC and ZFC curves similar suggesting a large SP content but no oxidized phase. E) Sharp Verwey transition and no Ms beak between 200-250 K, FC/ZFC curves indicate the presence of an oxidized phase as well as a Verwey transition. F) Suppressed Verwey transition and Ms max between 200-250 K with a ZFC curve indicating a large concentration of SP grains.

variable grain size distributions, even within a single locality. It is therefore necessary to perform a wide range of paleomagnetic and rock magnetic experiments in order to properly characterize the magnetic mineralogy.

6.1 Paleomagnetic/rock magnetic characterization of remanence carriers

By examining the orthogonal projections from stepwise thermal demagnetization, the KC and LC samples contain two components after removal of the modern VRM (Figure 2A, B). The ChRM is steep and of normal polarity with a maximum unblocking temperature between 500-540°C. This range suggests magnetite. The NRM drop due to liquid nitrogen removal of MD magnetite remanence does not significantly alter the ChRM directions. This suggests that the MD grains contribute to the modern VRM whereas PSD-SD magnetite controls the ChRM. The fact that the ChRM is steep even after structural correction indicates that this magnetization is secondary, since these carbonates formed near the equator a primary Mississippian magnetization should have a shallow inclination. This ChRM in magnetite has been observed in other studies throughout the Canadian Rockies and is considered to be the result of diagenetic processes associated with an eastward migrating diagenetic front ahead of Late Cretaceous thrusting [Lewchuk et al., 1998; Symons et al., 1999; Enkin et al., 2000; Cioppa et al., 2003; Robion et al., 2004]. The second, reversed intermediate temperature component has a maximum unblocking temperature of 310-340 °C. The remanence carrier for this component is not as clear as for the ChRM and may be interpreted in one of two ways: (1) It could be a TVRM contained in magnetite as has been proposed in previous studies (e.g., Enkin et al., 2000; Robion et al., 2004). (2) Or it could be a CRM carried by pyrrhotite. At Oldman River the ChRM is reversed, and

resides in magnetite. No definite intermediate temperature component is observed, although a small bend in the data suggest that the intermediate temperature component may be present. This is supported by the fact that Log Gaussian analysis shows that the moderate coercivity component, which is interpreted to be pyrrhotite is present along with the M_{max} between 200 and 250 K. When a magnetite and a pyrrhotite component are of the same polarity it may be difficult to separate the components. This may be why this intermediate temperature component is not observed throughout the Canadian Rockies. No evidence for a high coercivity phase such as hematite or goethite is observed in the thermal demagnetization data. Based on unblocking temperatures alone it is not possible to conclusively determine the carrier of the intermediate temperature component and in order to address this issue it is important to combine the results of multiple rock magnetic experiments with the unblocking temperature spectrum.

Log Gaussian analysis of the IRM acquisition data shows that the IRM is controlled by a mixture of primarily three components. The majority of the IRM is contained in the low coercivity component in the range of PSD-SD magnetite where as the remaining two components fall in the range of pyrrhotite and MD magnetite. FORC analysis also shows that the samples contain a wide distribution of coercivities from 2-70 mT. Both of these methods are useful to quantitatively show how the various coercivities contribute to lab induced magnetizations, but due to the range of coercivities for a particular mineral at room temperature [Peters and Dekkers, 2003], it makes it difficult to say for certain that the range of coercivities observed are due to one specific mineralogy or grain size and require other rock magnetic experiments to supplement these results. Tri-axial IRM decay curves show that the dominant magnetic

mineralogy is magnetite, however, there are small inflections near 325 °C, which coincides with the unblocking temperature of the intermediate temperature component suggesting pyrrhotite.

Room temperature SIRM cooling experiments show M_{max} between 200 and 250 K in the majority of samples investigated, a feature indicative of pyrrhotite. Only a few sites showed the 34 K magnetic transition for pyrrhotite. The amount of recovery was 95% during the complete cooling and warming cycles indicating ~2 μm SD pyrrhotite grains which would have a coercivity range which corresponds to the moderate coercivity component. The lack of a 34 K magnetic transition is not uncommon and may suggest that in these samples the amount of pyrrhotite is negligible when compared to magnetite [Rochette et al., 1990; Jackson et al., 1993]. Discrimination between hexagonal and monoclinic pyrrhotite can be detected by the γ-transition (T_γ = 200-220°C) in hexagonal pyrrhotite as it converts from antiferromagnetic to ferrimagnetic [Rochette et al., 1990] or by a susceptibility increase after quenching from a temperature above the T_γ [Rochette, 1987a], however, this is not possible in these weakly remagnetized rocks because paramagnetic, diamagnetic and ferrimagnetic (i.e., magnetite) contributions strongly influence susceptibility and induced magnetization [Rochette, 1987b] and the only pertinent measurable magnetization is the remanence. Because of this and the range of unblocking temperatures observed (310-350°C) it is probable that both forms exist in variable amounts within these samples.

Other minerals beside pyrrhotite, which can unblock below 350°C, such as some titanomagnetites, maghemite [Lowrie, 1990] or greigite [Roberts, 1995] can be eliminated since these minerals will not possess the M_{max} between 200-250 K and/or the

34 K magnetic transition. Siderite which is antiferromagnetic at low temperatures and shows a large Ms drop between 20 and 40 K [Housen et al., 1996], can lead to misidentification of pyrrhotite [e.g., Horng and Roberts, 2006]. Since the majority of samples examined displayed the M_{max} between 200-250K and siderite has not been observed in any thin sections examined, it can be discounted. Also observed during these experiments were suppressed Verwey transitions suggesting the unblocking of a wide range of magnetite grain sizes (MD-SD) which is supported by the cumulative log Gaussian analysis and FORC results. The oxidation of magnetite, however, cannot be completely disregarded as an explanation for the suppressed Verwey transition [Özdemir et al., 1993].

Based on unblocking temperatures and various rock magnetic experiments the primary remanence carrying components can be summarized as follows: (1) the modern VRM is controlled by very low coercivity MD magnetite (2) The intermediate temperature component is controlled by moderate coercivity SD pyrrhotite which is in contrast to previous work and (3) The high temperature ChRM is controlled by low coercivity PSD-SD magnetite.

6.2 Hysteresis data as a remagnetization "Fingerprint"

Based on the previously described rock magnetic experiments these remagnetized carbonates are dominated by a mixture of SD pyrrhotite as well as SP-MD magnetite, which greatly affect the hysteresis properties. Squared hysteresis loops generally indicate SD pyrrhotite [e.g., Dekkers, 1988], yet this feature is not observed in any of the loops generated and most likely relates to this complex mixture of magnetic minerals. An interesting feature of this data set is that the H_{cr} values for samples that

show the 34 K magnetic transition are greater than 50 mT. Such high coercivities in remagnetized carbonates with complex mixtures of magnetic minerals may be indicative of high concentrations of pyrrhotite, since samples which contain pyrrhotite but no 34 K magnetic transition, tend to have H_{cr} values below 35 mT. This feature may provide a useful way of determining high concentrations of pyrrhotite in remagnetized carbonates using basic room temperature hysteresis loops, since it is often difficult to separate pyrrhotite from magnetite due to overlapping room temperature coercivities. Experiments run on a variety of natural pyrrhotite have shown that H_c values tend to be close to H_{cr} values, unless magnetite is also present in the sample which will reduce H_c [Dekkers, 1988]. This is the case with our samples suggesting a pyrrhotite-magnetite mixture, although H_c is considerably lower (2.8 to 7.187 mT) which is most likely due to large concentrations of SP grains.

Another feature of these remagnetized Paleozoic carbonates is that the ratio of high field properties follows the remagnetization trendline proposed by previous workers [e.g., Jackson 1990]. This data supports the assertion that this trendline is indeed a "fingerprint" for remagnetized Paleozoic carbonates. This trend appears to be independent of location since it has been observed in multiple thrust belts and continents [e.g. Jackson, 1990; McCabe and Channell, 1994; Weil and Van der Voo, 2002; Zegers et al., 2003; Elmore et al., 2006]. Weil and Van der Voo [2002] found that whole rock hysteresis data from Paleozoic carbonates from Spain plotted along the trendline whereas extracts from the same samples did not. They attributed this to the loss of SP grains during the decanting process. Since all of the samples examined in this study had moderate to large SP concentrations the "fingerprint" of remagnetized

carbonates seems to represent the mixture of SP grains with various magnetic mineralogies and grain sizes, which are common in remagnetized carbonates. Unfortunately even though this "fingerprint" may indicate remagnetization due to diagenesis it does not allow for complete separation of mineralogical variations in complex multi-component remagnetizations.

A graph of M_{rs}/M_s versus H_{cr}, which is commonly used to show grain size variations [e.g., Dunlop, 1986; Dekkers, 1988; Suk and Halgedahl, 1996] and to infer strain enhanced magnetic hardening [e.g., Borradaile, 1991; Jackson et al., 1993; Elmore et al., 2006] suggests three possibilities. The first possibility is that the back limbs have finer magnetic grain sizes than the front limbs, however, a pervasive remagnetization event would not be expected to affect limbs differently and would be expected to follow a more spread out trend as is observed in the OR data. The second possibility is that the back limbs have been subject to greater strain enhance magnetic hardening than the front limbs which is in contrast to the observed amounts of macroscopic deformation observed in the field. A third possibility, which is more probable, is that the presence of large variations of pyrrhotite and magnetite in these samples leads to distortion of the hysteresis data making this test unusable. This observation again highlights the need for proper characterization of magnetic mineralogy in remagnetized carbonates.

6.3 Significance of non remanence carrying components

The variety of rock magnetic experiments conducted show that non remanence carrying magnetic grains may also contribute to the bulk rock magnetic properties of remagnetized carbonates. Multiple samples have relatively low M_{rs}/M_s and high (<10)

H_{cr}/H_c ratios. This suggests that SP grains constitute more than half of the total amount of magnetite in a particular sample [e.g., Jackson et al., 1993]. The presence of a variable concentration of SP grains (SP factor 0.3-0.75) is observed applied field curves and zero field curves experiments by a large drop in intensity below 50 K [Hunt et al., 1995]. The presence of a variable concentration of SP grains appears to be a hallmark of the chemical processes which produce remagnetization regardless of geographic location as suggested by other authors [e.g., Jackson, 1990; Suk and Halgedahl, 1996; Weil and Van der Voo, 2002]. No linear trend is observed between the H_{cr}/H_c ratios and the SP factor for a given sample. This indicates that even though all the samples have high concentrations of SP grains the complex mixing of magnetic minerals and grain sizes may overshadow this concentration during room temperature experiments. SP grains add to the complexity of characterizing remagnetized carbonates, however, are not important for characterizing the NRM.

The presence of high coercivity oxidized phases is also observed in multiple rock magnetic experiments. Their presence is shown by goose necked hysteresis loops, and divergence of the applied field and zero field curves which do not merge until near room temperature, tri-axial decay curves that do not fully demagnetize until 680°C and cumulative log Gaussian analysis which display a high coercivity component (~1.3T), that only contributes <10% of the total IRM. Thermal demagnetization of the NRM, however, shows no indications of a high coercivity phase such as hematite or goethite so these oxidized phases are considered to be late stage non-remanence carrying weathering products as observed in other studies [e.g., Blumstein et al., 2004; O'Brien et al., 2007]. As with the SP grains, such oxidized phases contribute to the complexity

of the bulk rock magnetic properties of a given sample but are of little importance to the paleomagnetic component analysis.

6.4 Evaluation of IRM Acquisition data

The use of IRM acquisition curves have been routinely used to determine magnetic mineralogy in rock magnetic and paleomagnetic studies. However, due to the complex grain size and mineralogical variations common to remagnetized carbonates, these curves do not accurately display these variations. The IRM acquisition curves show that saturation is achieved below 500 mT (Figure 3). This allows one to conclude that saturation is controlled by a low coercivity phase such as magnetite or pyrrhotite. The LC and OR samples have relatively sharp transitions to saturation, and their curves are similar to theoretical curves generated for MD magnetite (Figure 3B). The KC sample on the other hand shows a much more subdued transition suggesting a gradual saturation. The curve shape is similar to PSD-SD magnetite, however, it may also be due to pyrrhotite [Lewchuk et al., 1998; Figure 3A]. Because of this apparent complexity in the mixture of coercivities, standard IRM acquisition curves do not allow separation of coercivities with similar and overlapping coercivity spectrums. This experiment tends to be more qualitative than quantitative and is not sufficient to fully characterize remagnetized carbonates.

7. Conclusions

Based on a combination of paleomagnetic and rock magnetic experiments it is clear that the remagnetized Mississippian Carbonates from the Canadian Rockies contain a complex and at times highly variable mixture of magnetic mineralogies and grain sizes. The complex variations in these remagnetized carbonates make a straight-

forward characterization difficult and at times inconclusive. The results of this study suggest that determination of the remanence carriers in multi-component NRMs requires low temperature experiments combined with thermal demagnetization and advanced rock magnetic techniques such as FORC analysis and cumulative log Gaussian analysis.

The specific conclusions are:

1) Based on a combination of thermal demagnetization, Log Gaussian analysis and low temperature experiments these samples contain up to three distinct components: 1) a modern VRM unblocks below 200°C and resides in MD magnetite 2) an intermediate temperature component unblocks between 310 and 325°C and is carried by SD pyrrhotite 3) a high temperature component with a maximum unblocking temperature of 540°C is carried by PSD-SD magnetite. The reversed polarity pyrrhotite component is only observed in rock magnetic experiments at Oldman River, possibly because the high temperature component is also reversed in the Foothills making separation of the two components difficult.
2) Due to the variable of grain size and mineralogies, IRM acquisition curves do not sufficiently separate coercivity variations in remagnetized carbonates. Log Gaussian analysis and FORC analysis offers the most quantitative look at the coercivity distribution in a particular sample, however, due to the wide range of coercivities for a given magnetic mineral at room temperature low temperature experiments are still needed to supplement these experiments

3) A large portion of SP magnetite as well as high coercivity oxidized phases (hematite or goethite) are found in various amounts in these samples. These grains can have a strong influence on the bulk rock magnetic properties but do not affect the NRM of these remagnetized carbonates.

4) The coercivity (H_{cr}) obtained from high field experiments most likely represents an average of the various grain sizes and mineralogies present in a sample. A large concentration of pyrrhotite appears to increase H_{cr} above 50 mT. This may represent a diagnostic feature of large concentrations of pyrrhotite in a sample the same way that high H_{cr}/H_c ratios represent large concentrations of SP grains.

5) The ratio of M_{rs}/M_s plotted against H_c/H_{cr} on a log-log plot show that the data from Paleozoic carbonates in the Canadian Rockies follows the established trend of remagnetized carbonates. The presence of large quantities of SP grains seems to be the main cause of the data following this particular trend. Also having variable concentrations of pyrrhotite does have an effect on hysteresis properties and may cause inaccurate determination of features such as grain size determination and/or strain enhanced magnetic hardening.

References Cited

Al-Aasm, I. S. (2000), Chemical and isotopic constraints for recrystallization of sedimentary dolomites from the Western Canada Sedimentary Basin, Aquatic Geochemistry, 6(2), 227-248.

Banerjee, S., R. D. Elmore, and M. H. Engel (1997), Chemical remagnetization and burial diagenesis; testing the hypothesis in the Pennsylvanian Belden Formation, Colorado, Journal of Geophysical Research, 102(B11), 24,825-824,842.

Blumstein, A. M., R. D. Elmore, M. H. Engel, C. Elliot, and A. Basu (2004), Paleomagnetic dating of burial diagenesis in Mississippian carbonates, Utah, Journal of Geophysical Research, B, Solid Earth and Planets, 109, no.4, 16.

Borradaile, G. J. (1997), Deformation and paleomagnetism, Surveys in Geophysics, 18(4), 405-435.

Borradaile, G. J., K. Lucas, and R. S. Middleton (2004), Low-temperature demagnetization isolates stable magnetic vector components in magnetite-bearing diabase, Geophysical Journal International [Geophys. J. Int.]. 157(2), 526-536.

Channell, J. E. T., and C. McCabe (1994), Comparison of magnetic hysteresis parameters of unremagnetized and remagnetized limestones, Journal of Geophysical Research, 99(B3), 4613-4623.

Cioppa, M. T., and D. T. A. Symons (2000), Timing of hydrocarbon generation and migration; paleomagnetic and rock magnetic analysis of the Devonian Duvernay Formation, Alberta, Canada, in Journal of Geochemical Exploration, vol.69-70, edited by J. J. Pueyo, E. Cardellach, K. Bitzer and C. Taberner, pp. 387-390, Elsevier, Amsterdam-New York.

Cioppa, M. T., I. S. Al-Aasm, D. T. A. Symons, and K. P. Gillen (2003), Dating penecontemporaneous dolomitization in carbonate reservoirs; paleomagnetic, petrographic, and geochemical constraints, AAPG Bulletin, 87(1), 71-88.

Cioppa, M. T., I. S. Al-Aasm, D. T. A. Symons, M. T. Lewchuk, and K. P. Gillen (2000), Correlating paleomagnetic, geochemical and petrographic evidence to date diagenetic and fluid flow events in the Mississippian Turner Valley Formation, Moose Field, Alberta, Canada, Sedimentary Geology, 131(3-4), 109-129.

Cioppa, M. T., J. S. Lonnee, D. T. A. Symons, I. S. Al-Aasm, and K. P. Gillen (2001), Facies and lithological controls on paleomagnetism; an example from the Rainbow South Field, Alberta, Canada, Bulletin of Canadian Petroleum Geology, 49(3), 393-407.

Cioppa, M. T., J. Lonnee, D. T. A. Symons, I. S. Al-Aasm, K. P. Gillen, and Anonymous (2000), Dating dolomitization/recrystallization events using petrologic, geochemical and paleomagnetic techniques, in AAPG Bulletin, edited, p. 1381, American Association of Petroleum Geologists, Tulsa.

Crouzet, C., P. Gautam, E. Schill, and E. Appel (2003), Multicomponent magnetization in western Dolpo (Tethyan Himalaya, Nepal); tectonic implications, in Tectonophysics, edited by A. Morris and J. Tait, pp. 179-196, Elsevier, Amsterdam.

Dekkers, M. J. (1988), Magnetic properties of natural pyrrhotite; Part I, Behaviour of initial susceptibility and saturation-magnetization-related rock-magnetic parameters in a grain-size dependent framework, in Physics of the Earth and Planetary Interiors, edited by F. Heller, K. M. Storetvedt and J. D. A. Zijderveld, pp. 376-393, Elsevier, Amsterdam.

Dekkers, M. J. (1989), Magnetic properties of natural pyrrhotite; II, High- and low-temperature behaviour of J (sub rs) and TRM as function of grain size, Physics of the Earth and Planetary Interiors, 57(3-4), 266-283.

Dekkers, M. J., J. L. Mattei, G. Fillion, and P. Rochette (1989), Grain-size dependence of the magnetic behavior of pyrrhotite during its low-temperature transition at 34 K, Geophysical Research Letters, 16(8), 855-858.

Elmore, R. D., J. Kelley, M. Evans, and M. T. Lewchuk (2001), Remagnetization and orogenic fluids; testing the hypothesis in the Central Appalachians, Geophysical Journal International, 144(3), 568-576.

Elmore, R. D., J. L.-E. Foucher, M. Evans, M. Lewchuk, and E. Cox (2006), Remagnetization of the Tonoloway Formation and the Helderberg Group in the Central Appalachians; testing the origin of syntilting magnetizations, Geophysical Journal International, 166(3), 1062-1076.

Enkin, R. J., K. G. Osadetz, J. Baker, and D. Kisilevsky (2000), Orogenic remagnetizations in the front ranges and inner foothills of the southern Canadian Cordillera; chemical harbinger and thermal handmaiden of Cordilleran deformation, Geological Society of America Bulletin, 112(6), 929-942.

Evans, M. A., R. D. Elmore, and M. T. Lewchuk (2000), Examining the relationship between remagnetization and orogenic fluids; central Appalachians, in Journal of Geochemical Exploration, vol.69-70, edited by J. J. Pueyo, E. Cardellach, K. Bitzer and C. Taberner, pp. 139-142, Elsevier, Amsterdam-New York.

Font, E., R. I. F. Trindade, and A. Nedelec (2006), Remagnetization in bituminous limestones of the Neoproterozoic Araras Group (Amazon craton); hydrocarbon maturation, burial diagenesis, or both?, Journal of Geophysical Research, 111, no.B6, 17.

Gillett, S. L., and R. E. Karlin (2004), Pervasive late Paleozoic-Triassic remagnetization of miogeoclinal carbonate rocks in the Basin and Range and vicinity, SW USA; regional results and possible tectonic implications, Physics of the Earth and Planetary Interiors, 141(2), 95-120.

Hall, A. J. (1986), Pyrite-pyrrhotite redox reactions in nature, Mineralogical Magazine, 50, Part 2(356), 223-229.

Harrison, R. J., and J. M. Feinberg (2008), FORCinel: An improved algorithm for calculating first-order reversal curve distributions using locally weighted regression smoothing, Geochemistry, Geophysics, Geosystems G, 9(5).

Horng, C.-S., and A. P. Roberts (2006), Authigenic or detrital origin of pyrrhotite in sediments? Resolving a paleomagnetic conundrum, Earth and Planetary Science Letters, 241(3-4), 750-762.

Housen, B. A., S. K. Banerjee, B. M. Moskowitz, and V. Courtillot (1996), Low-temperature magnetic properties of siderite and magnetite in marine sediments, Geophysical Research Letters, 23(20), 2843-2846.

Hudson, M. R., R. L. Reynolds, and N. S. Fishman (1989), Synfolding magnetization in the Jurassic Preuss Sandstone, Wyoming-Idaho-Utah thrust belt, Journal of Geophysical Research, 94(B10), 13,681-613,705.

Hunt, C. P., S. K. Banerjee, J. Han, P. A. Solheid, E. Oches, W. Sun, and T. Liu (1995), Rock-magnetic proxies of climate change in the loess-Palaeosol sequences of the western Loess Plateau of China, Geophysical Journal International, 123(1), 232-244.

Jackson, M. (1990), Diagenetic sources of stable remanence in remagnetized Paleozoic cratonic carbonates; a rock magnetic study, Journal of Geophysical Research, 95(B3), 2753-2761.

Jackson, M., H.-U. Worm, and S. K. Banerjee (1990), Fourier analysis of digital hysteresis data; rock magnetic applications, Physics of the Earth and Planetary Interiors, 65(1-2), 78-87.

Jackson, M. J., W. Sun, and J. P. Craddock (1992), The rock magnetic fingerprint of chemical remagnetization in midcontinental Paleozoic carbonates, Geophysical Research Letters, 19(8), 781-784.

Jackson, M., P. Rochette, G. Fillion, S. Banerjee, and J. Marvin (1993), Rock magnetism of remagnetized Paleozoic carbonates; low-temperature behavior and susceptibility characteristics, Journal of Geophysical Research, 98(B4), 6217-6225.

Katz, B., R. D. Elmore, and M. H. Engel (1998), Authigenesis of magnetite in organic-rich sediment next to a dike; implications for thermoviscous and chemical remagnetizations, Earth and Planetary Science Letters, 163(1-4), 221-234.

Katz, B., R. D. Elmore, M. Cogoini, and S. Ferry (1998), Widespread chemical remagnetization; orogenic fluids or burial diagenesis of clays?, Geology, 26(7), 603-606.

Kirschvink, J. L. (1980), The least-squares line and plane and the analysis of palaeomagnetic data, Geophysical Journal of the Royal Astronomical Society, 62(3), 699-718.

Kruiver, P. P., M. J. Dekkers, and D. Heslop (2001), Quantification of magnetic coercivity components by the analysis of acquisition curves of isothermal remanent magnetisation, Earth and Planetary Science Letters, 189(3-4), 269-276.

Lewchuk, M. T., R. D. Elmore, and M. Evans (2002), Remagnetization signature of Paleozoic sedimentary rocks from the Patterson Creek Mountain Anticline in West Virginia, Physics and Chemistry of the Earth, 27(25-31), 1141-1150.

Lewchuk, M. T., I. S. Al-Aasm, D. T. A. Symons, and K. P. Gillen (1998), Dolomitization of Mississippian carbonates in the Shell Waterton gas field, southwestern Alberta; insights from paleomagnetism, petrology and geochemistry, Bulletin of Canadian Petroleum Geology, 46(3), 387-410.

Lewchuk, M. T., I. S. Al-Aasm, D. T. A. Symons, and K. P. Gillen (2000), Late Laramide dolomite recrystallization of the Husky Rainbow "A" hydrocarbon Devonian reservoir, northwestern Alberta, Canada; paleomagnetic and geochemical evidence, Canadian Journal of Earth Sciences = Revue Canadienne des Sciences de la Terre, 37(1), 17-29.

Lowrie, W. (1990), Identification of ferromagnetic minerals in a rock by coercivity and unblocking temperature properties, Geophysical Research Letters, 17(2), 159-162.

McCabe, C., and R. D. Elmore (1989), The occurrence and origin of late Paleozoic remagnetization in the sedimentary rocks of North America, Reviews of Geophysics, 27(4), 471-494.

McCabe, C., and J. E. T. Channell (1994), Late Paleozoic remagnetization in limestones of the Craven Basin (northern England) and the rock magnetic fingerprint of remagnetized sedimentary carbonates, Journal of Geophysical Research, 99(B3), 4603-4612.

McCabe, C., M. Jackson, and B. Saffer (1989), Regional patterns of magnetite authigenesis in the Appalachian Basin; implications for the mechanism of late Paleozoic remagnetization, Journal of Geophysical Research, 94(B8), 10,429-410,443.

McMechan, M. E., and R. I. Thompson (Eds.) (1989), Structural style and history of the Rocky Mountain fold and thrust belt, 47-71 pp., Can. Soc. Pet. Geol., Calgary, AB, Canada, Calgary, AB.

Monger, J. W. H., and R. A. Price (1979), Geodynamic evolution of the Canadian Cordillera; progress and problems, Canadian Journal of Earth Sciences = Revue Canadienne des Sciences de la Terre, 16(3, Part 2), 771-791.

O'Brien, V. J., K. M. Moreland, R. D. Elmore, M. H. Engel, and M. A. Evans (2007), Origin of orogenic remagnetizations in Mississippian carbonates, Sawtooth Range, Montana, Journal of Geophysical Research, 112(B6).

Özdemir, O., and D. J. Dunlop (2000), Intermediate magnetite formation during dehydration of goethite, Earth and Planetary Science Letters, 177(1-2), 59-67.

Özdemir, O., D. J. Dunlop, and B. M. Moskowitz (1993), The effect of oxidation on the Verwey transition in magnetite, Geophysical Research Letters, 20(16), 1671-1674.

Parry, L. G. (1982), Magnetization of immobilized particle dispersions with two distinct particle sizes, Physics of the Earth and Planetary Interiors, 28(3), 230-241.

Peters, C., and M. J. Dekkers (2003), Selected room temperature magnetic parameters as a function of mineralogy, concentration and grain size, in Physics and Chemistry of the Earth, edited by E. Petrovsky, M. Urbat and T. von Dobeneck, pp. 659-667, Pergamon, Oxford-New York-Toronto.

Price, R. A., G. D. Mossop, and I. Shetsen (Eds.) (1994), Cordilleran tectonics and the evolution of the Western Canada sedimentary basin, 2-24 pp., Geological Survey of Canada, Calgary, AB.

Roberts, A. P. (1995), Magnetic properties of sedimentary greigite (Fe_3S_4), Earth and Planetary Science Letters, 134(3-4), 227-236.

Roberts, A. P., R. L. Reynolds, K. L. Verosub, D. P. Adam, and V. Courtillot (1996), Environmental magnetic implications of greigite (Fe_3S_4) formation in a 3 m.y. lake sediment record from Butte Valley, Northern California, Geophysical Research Letters, 23(20), 2859-2862.

Rochette, P., G. Fillion, J.-L. Mittei, and M. J. Dekkers (1990), Magnetic transition at 30-34 Kelvin in pyrrhotite; insight into a widespread occurrence of this mineral in rocks, Earth and Planetary Science Letters, 98(3-4), 319-328.

Saffer, B., and C. McCabe (1992), Further studies of carbonate remagnetization in the northern Appalachian Basin, Journal of Geophysical Research, 97(B4), 4331-4348.

Stamatakos, J., A. M. Hirt, and W. Lowrie (1996), The age and timing of folding in the Central Appalachians from paleomagnetic results, Geological Society of America Bulletin, 108(7), 815-829.

Suk, D., and S. L. Halgedahl (1996), Hysteresis properties of magnetic spherules and whole rock specimens from some Paleozoic platform carbonate rocks, Journal of Geophysical Research, 101(B11), 25,053-025,076.

Sun, W., and M. Jackson (1994), Scanning electron microscopy and rock magnetic studies of magnetic carriers in remagnetized early Paleozoic carbonates from Missouri, Journal of Geophysical Research, 99(B2), 2935-2942.

Symons, D. T. A., R. J. Enkin, and M. T. Cioppa (1999), Paleomagnetism in the Western Canada sedimentary basin; dating and fluid flow and deformation events, Bulletin of Canadian Petroleum Geology, 47(4), 534-547.

Tauxe, L., T. A. T. Mullender, and T. Pick (1996), Potbellies, wasp-waists, and superparamagnetism in magnetic hysteresis, Journal of Geophysical Research, 101(B1), 571-583.

Weaver, R., A. P. Roberts, and A. J. Barker (2002), A late diagenetic (syn-folding) magnetization carried by pyrrhotite; implications for paleomagnetic studies from magnetic iron sulphide-bearing sediments, Earth and Planetary Science Letters, 200(3-4), 371-386.

Weil, A. B., and R. Van der Voo (2002), Insights into the mechanism for orogen-related carbonate remagnetization from growth of authigenic Fe-oxide; a scanning electron microscopy and rock magnetic study of Devonian carbonates from northern Spain, Journal of Geophysical Research, 107, no.B4, 15.

Xu, W., R. Van der Voo, and D. R. Peacor (1998), Electron microscopic and rock magnetic study of remagnetized Leadville carbonates, central Colorado, Tectonophysics, 296(3-4), 333-362.

Zegers, T. E., M. J. Dekkers, and S. Bailly (2003), Late Carboniferous to Permian remagnetization of Devonian limestones in the Ardennes; role of temperature, fluids, and deformation, Journal of Geophysical Research, 108, no.B7, 19.

Zijderveld, J. D. A. (1967), A.c. demagnetization of rocks: analysis of results. *In* Collinson, D.E. et al., eds., Methods in Paleomagnetism. New York, Elsevier Science, pp. 254-286.

Chapter 3: Origin and timing of complex remagnetizations in folded Mississippian-Triassic carbonates in the Canadian Cordillera, SW Alberta and SE British Columbia

M.S. Zechmeister*, S. Pannelal, E.B. Manning, M.A. Engel, & R.D. Elmore*

*The ConocoPhillips School of Geology and Geophysics, the University of Oklahoma, Norman, OK 73019, USA (*zechmeim@ou.edu; delmore@ou.edu*

Abstract

Determining the timing and origin of fluid-related diagenetic events relative to orogenesis is crucial for understanding the interaction between thin skinned tectonics and diagenesis. In order to investigate this issue a combination of geochemical, petrographic and fluid inclusion analysis is needed to determine the nature of various diagenetic events and then paleomagnetic analysis can be used to date chemical remanent magnetizations (CRM's) formed by these events. Two folds in Mississippian carbonates and one fold in Pennsylvanian and Triassic carbonates and siliclastics have been investigated in the Front Range of the Southern Canadian Cordillera in order to test for a link between fluid flow, hydrocarbon migration/alteration and a the formation of a multi-component remagnetization. The characteristic remanent magnetization (ChRM) is contained in magnetite and is pre-tilting to early syntilting and was acquired in the Early to Late Cretaceous. An intermediate temperature component is a late syntilting to post tilting Tertiary age remagnetization contained in pyrrhotite. Both components are pervasive within both limestones and dolostones and are interpreted as CRMs. A Paleomagnetic vein contact test conducted on bedding parallel veins shows direct correlation to the magnetite component where as tectonic veins show a relationship to pyrrhotite. Elevated $^{87}Sr/^{86}Sr$ data from the host matrix indicate that the

rocks have been altered by fluids with a radiogenic signature. C/O isotopes of calcite veins show a wide range of light $\delta^{18}O$ over a narrow range of $\delta^{13}C$, suggesting formation due to a wide range of warm fluids. This interpretation is confirmed by fluid inclusion homogenization temperatures . The geochemical results are consistent with the interpretation that the magnetite CRM formed as a result of the migration of hydrocarbons and/or evolved basinal fluids into the unit. The timing of remagnetization relative to folding suggesting acquisition due to fluid migration ahead of the deformation front. The pyrrhotite component is interpreted to be the result of thermal sulfate reduction (TSR), caused by warm fluids moving into the carbonates along faults and fractures. This is based on the observation of sulfur enriched bitumen, barite and sphalerite which are common by-products of TSR.

1. Introduction

Paleomagnetic studies of remagnetized carbonates in fold and thrust belts can provide useful information on the timing of diagenetic events relative to orogenesis [e.g., Kent, 1985; McCabe and Elmore, 1989; Stamatakos et. al., 1995; Enkin et al., 2000; Katz et. al., 2000; Elmore et al., 2001; O'Brien et. al., 2007]. Diagenesis and tectonism are fundamentally separate geological processes, however, in terms of fold and thrust belts these processes are inherently linked. During orogenesis tectonic stacking of thrust sheets along with uplift and erosion increases burial in foreland basins which leads to increased burial temperatures. Increased burial temperatures can cause the acquisition of chemical remanent magnetizations (CRMs) through clay diagenesis [Katz et al., 2000] and maturation of organic matter [Banerjee, et al., 1997]. Thermoviscous remanent magnetizations (TVRMs) may also form through thermal

resetting of magnetizations due to moderate to high burial temperatures [e.g., Kent, 1985]. Orogenic processes also cause fluid migration events either by gravitational recharge [e.g., Ge and Garvin, 1994] or tectonically induced fluid flow [Oliver, 1986; Mache and Cavell, 1999]. Diagenetic alteration caused by fluid migration events are commonly cited as forming authigenic magnetic minerals and acquisition of CRMs in fold and thrust belts [e.g., McCabe and Elmore, 1989; Enkin et al., 2000; O'Brien et al., 2007]. Stress reorganization of domain walls [e.g., Hudson et al., 1989; Borradaile, 1997] or strain alteration of preexisting magnetizations during deformation [e.g., Kodama, 1988; Elmore et al., 2006] have also been proposed as remagnetization mechanisms.

The purpose of this study is to combine the results of detailed rock magnetic characterization [Chapter 1] with the results of paleomagnetic, geochemical and petrographic studies in order to determine the origin and timing of both the ChRM and an intermediate temperature component that are common throughout the Canadian Cordillera. Paleomagnetic analysis utilized tilt tests on individual folds and vein conduit tests to investigate the relationship between folding, fluid migration, and multiple remagnetization events. Geochemical analysis (stable Carbon and Oxygen isotopes and $^{86}Sr/^{87}Sr$ isotopes), and a variety of petrographic techniques where used to investigate the diagenetic features. Transmitted light and electron microprobe microscopy was used to determine lithology, identify diagenetic features and investigate the origin of magnetic minerals. Cathodoluminescence (CL) and fluid inclusion microscopy was used to investigate the nature of the vein forming fluids.

2. Geological/Tectonic Setting

The foreland fold and thrust belt in the Canadian Cordillera is divided into three sub units from west to east: The Main Ranges, the Front Ranges, and the Foothills (Figure 1) and is the result of west to east directed horizontal compression due to terrane accretion which accommodated up to 200 km of horizontal shortening [e.g., Price and Mountjoy, 1970; Price, 1981; Fermor and Moffat, 1992]. Contraction in the foreland fold and thrust belt was expressed as thin-skinned detachment thrusting and folding of Mesoproterozoic to Cretaceous strata over Cretaceous and older strata [e.g. Monger and Price, 1979; McMechan and Thompson, 1989; Price, 1994]. Deformation was active from the late Jurassic to the Eocene overlapping both the Columbian (Mid Jurassic–Late Cretaceous) and Laramide orogenies (Late Cretaceous to Paleocene) with most of the shortening occurring in the Late-Cretaceous (~89M) [Price, 1994].

Obduction of exotic terranes onto the North American pericratonic terranes began in the Late Triassic and continued into the Eocene which initiated shortening and thickening in the Omencia Belt west of the Foreland belt along both east and west directed faults and folds [Evenchick et al., 2007 and references there in]. This led to significant uplift in the Omencia Belt by the Late Middle Jurassic and the first appearance of western derived sediments and increased subsidence in the foreland belt due to tectonic loading [Poulton et al., 1993]. Initiation of thrusting in the western most portion of the foreland belt began in the Early Cretaceous and progressed eastward [Carr and Simony, 2006]. The majority of shortening occurred during the Late Cretaceous-to Eocene, with the major motions along the Lewis and McConnell thrust sheets occurred [Price, 1981] that effectively doubled the width of the foreland belt.

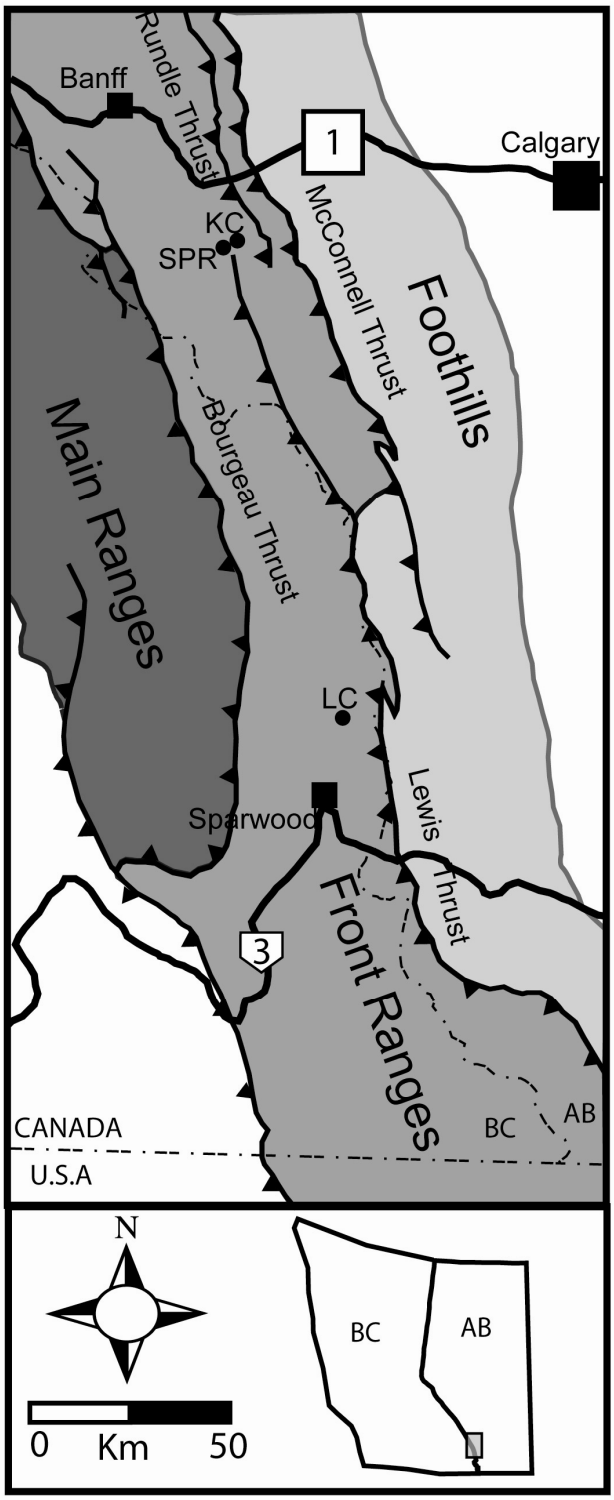

Figure 1: Generalized tectonic map of the Canadian Fold and Thrust belt highlighting major tectonic units and thrusts (Modified from Enkin et al., 2000). Sampling locations, Mt. Kidd anticline-syncline (KC), Line Creek anticline (LC) and Kent Anticline (SPR), are indicated by the black dots.

This was followed by cessation of contractional deformation which led to exhumation and erosion [Price and Mountjoy, 1970].

The folds of interest in this study are located within the eastern Front Ranges of the Southern Canadian Cordillera. In SW Alberta two folds were sampled within Kananaskis Country Provincial Park (KC & SPR; Figure 1). In SE British Columbia a fold was sampled within the Lewis thrust sheet along Line Creek on the property of Teck Coal (LC; Figure 1). In Kananaskis Country the first fold sampled was Mt. Kidd, located along both Kananaskis Road (HWY-40) and Spray Lakes Road (Figure 2A & B). This structure which is contained in the Rundle Trust Sheet is a plunging asymmetrical anticline-syncline pair (Plunge, Trend of fold axis: S14, 182 and S17, 178 respectively) within the Mississippian Banff, Livingstone, Mount Head and Etherington Formations (Rundle Group; Figure 2A & B) [McMechan, 1995], The tight folding observed is accommodated by flexural slip, brittle fracturing and ductile thinning in the steep east dipping limb and ductile thickening within the nose (Figure 3A). Kent Anticline was the second fold sampled is in Kananaskis country and is contained within the Sulphur Mountain thrust sheet [McMechan, 1995]. The structure is comprised of the Pennsylvanian Misty and Kananaskis Formations (Pennsylvanian-Permian Rocky Mountain Group) and Triassic Sulphur Mountain Formation [Norris, 1965] along the Smith-Dorrian Trail (Figure 2C). This structure is a plunging asymmetrical anticline (Figure 2C; Plunge, Trend of fold axis: S14, 166) with a west dipping shallow back limb (Figure 3C) and steep east dipping front limb (Figure 3D). At Line Creek the fold sampled was an asymmetrical upright fold (Fold Axis: 2, 169) contained in the Mississippian Mount Head and Etherington Formations (Rundle

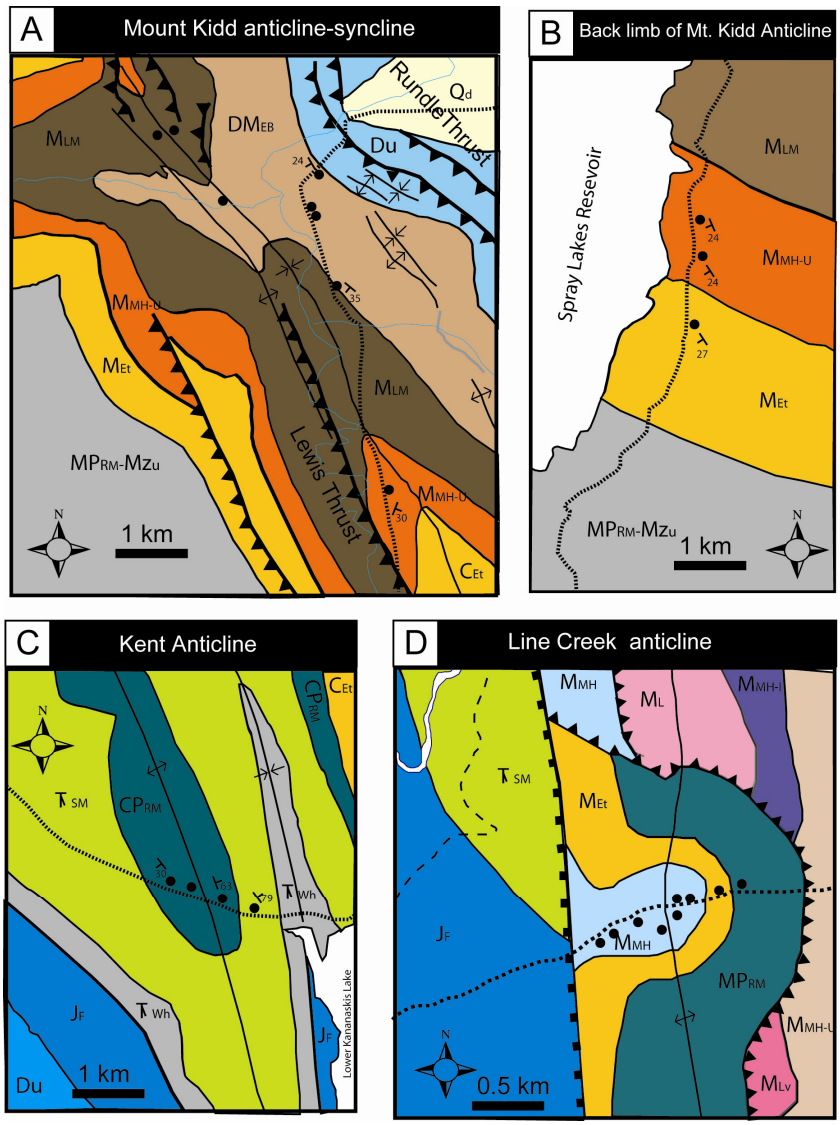

Figure 2: Geological maps of structures sampled. Black dots indicate major outcrops sampled. A) Mt. Kidd syncline, Kananaskis Country, AB (modified from McMechan, 1995). Qd = Quaternary alluvium; PPr_{RM}-Mz_U = Pennsylvanian-Permian Rocky Mountain Group-Mezezoic undivided; M_{ET} = Mississippian Etherington Fms., M_{MH-U} = Mississippian Mount Head Upper part, M_{LM} = Mississippian Livingstone-Mount Head upper part undivided, DM_{EB} = upper Devonian Exshaw-Lower Mississippian Banff undivided, D_U = Devonian undivided. B) Back limb of Mt. Kidd anticline (modified from McMechan, 1995). M_{ET} = Mississippian Etherington Fms., M_{MH-U} = Mississippian Mount Head Upper part, M_{LM} = Mississippian Livingstone-Mount Head upper part undivided, DM_{EB} = upper Devonian Exshaw-Lower Mississippian Banff undivided, D_U = Devonian undivided. C) Kent Anticline, Kananaskis Country, AB (modified from McMechan, 1995). J_F = Jurassic Fernie Fms., T_{WH} = Triassic White Horse Fms., T_{SM} = Triassic Sulphar Mountian Fms., PPr_{RM} = Pennsylvanian-Permian Rocky Mountain Group; M_{ET} = Mississippian Etherington Fms., D_U = Devonian undivided. D) Line Creek Anticline, BC (modified from Price et al., 1992). J_F = Jurassic Fernie Fms., T_{SM} = Triassic Sulphar Mountian Fms., PPr_{RM} = Pennsylvanian-Permian Rocky Mountain Group; M_{ET} = Mississippian Etherington Fms.,M_{MH} = Mount Head Undivided; M_{MH-U} = Mississippian Mount Head upper part, M_{MH-L} = Mississippian Mount Head Lower part, M_{LV} = Mississippian Livingstone Fms.

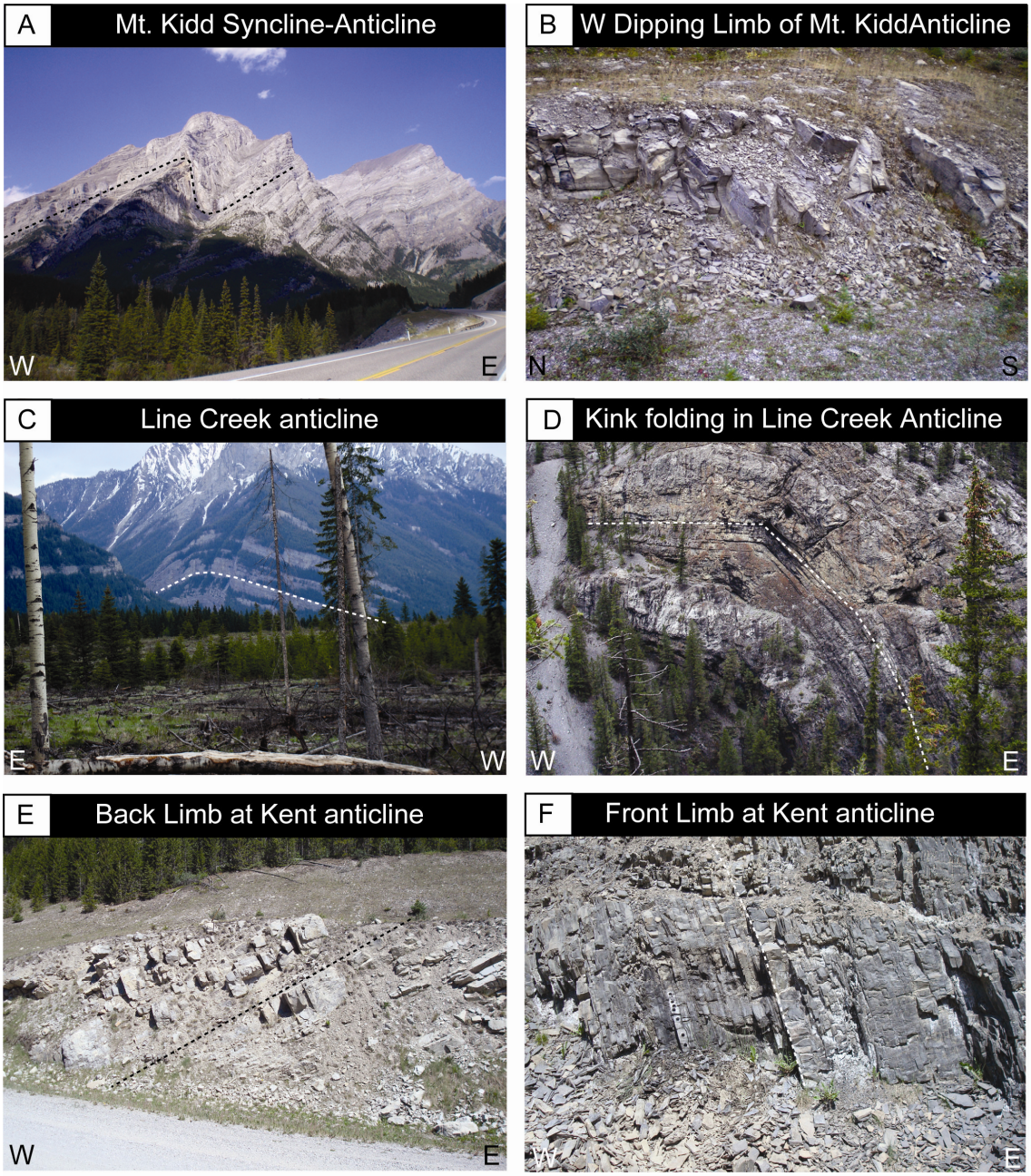

Figure 3: Field photos of structures sampled. A) Mt. Kidd anticline-syncline pair. B) West dipping back limb of Mt. Kidd anticline. C) Line Creek anticline. D) Kink folding in hinge zone of Line Creek anticline. E) Shallow back limb of Kent anticline. F) Steep front limb of Kent anticline.

Group; Figure 2D) [Price et al., 1992]. The structure is characterized by a shallow west dipping back limb a broad crest and steep west dipping front limb with deformation being accommodated by flexural slip, kink folding and brittle fracturing (Figure 3E & F).

The Mississippian Rundle Group and the Permian Rocky Mountain Group are considered to be predominantly platform to basin carbonates deposited within a passive margin setting [e.g. Hardebol et al., 2006]. Multiple workers have proposed that these carbonates were actually deposited in a foreland basin setting relating during the Late Devonian-Early Mississippian Antler Orogeny [e.g., Root, 2001 and references therein]. The Triassic units are considered to record the transition from Paleozoic carbonate dominated facies to the Jurassic-Cretaceous siliclastic dominated facies during the formation of the Laramide foreland basin [e.g., Davies, 1997]. The Triassic Sulphur Mountain Formation is considered to have formed in the continental margin-shoreline sag basin [Edwards et al., 1994] in between the North American margin and volcanic island arcs to the west [Ross et al., 1997].

Since deposition the Mississippian carbonates have undergone various diagenetic alterations creating a complex paragenetic sequence which involves early matrix dolomitization due to both marine pore waters and meteoric dominated systems [Al-Aasm, 2000]. This was followed by pervasive meso-dolomite recrystallization from both meteoric and hydrothermal fluids during burial [Al-Aasm, 2000] and very late formation of vug rimming saddle dolomites and sulfide mineralization**.** Hydrocarbon generation and migration is believed to have occurred within the Carboniferous and lower Triassic rocks during the Late Jurassic-Early Cretaceous in the

Front Ranges [Kalkreuth and McMechan, 1988] prior to Laramide burial and during the Late Cretaceous-Eocene time in the Western Canada Sedimentary Basin [e.g. Hitchon. 1984; Bustin, 1991]. Hydrocarbon emplacement was then followed by Thermo Sulphate Reduction (TSR) of the hydrocarbons, creating extensive sour gas reservoirs throughout the Canadian Cordillera and Western Canada Sedimentary Basin (WCSB) [Orr, 1974**;** Machel, 1987; Machel et al., 1995; Roure et al., 2005; Vandeginste et al., 2009].

3. Previous Paleomagnetic and Rock Magnetic Studies in the Canadian Cordillera

Paleomagnetic and rock magnetic results obtained from Mississippian carbonates at Line Creek anticline and Mt. Kidd anticline-syncline suggests the presence of a multi-component natural remanent magnetization (NRM) carried by magnetite and pyrrhotite [Chapter 2]. Several paleomagnetic studies conducted on remagnetized Paleozoic carbonates within the Canadian Cordillera also isolated a similar multi-component NRM [e.g. Lewchuk et al., 1998; Enkin et al., 2000; Robion et al., 2004]. Enkin et al. [2000] focused on determining the regional extent of remagnetizations throughout the Canadian Rockies and did not focus in detail on individual structures. Most of the other studies focused on drill cores obtained from Paleozoic hydrocarbon reservoirs on the western edge of the Western Canada Sedimentary Basin [WCSB, e.g., Lewchuk et al., 1998; Symons et al., 1999; Cioppa et al., 2000; 2001; 2003]. The purpose of these studies were to investigate whether the timing of remagnetizations could be related to: (1) dolomitization [Lewchuk et al., 1998; Roure et al., 2005], (2) fluid flow [Enkin et al., 2000; Lewchuk et al., 2000; Cioppa et al., 2000] and (3) hydrocarbon generation [Cioppa and Symons, 2000]. Many

of these studies concluded that a widespread multi-component remagnetization was present throughout the Canadian Rockies. The characteristic remanent magnetization (ChRM) was determined to be a CRM contained in magnetite with an intermediate temperature component interpreted to be a TVRM also residing in magnetite [e.g., Lewchuk et al., 1998; Enkin et al., 2000; Robion et al., 2004]. In most of these studies pyrrhotite was not considered to carry a remanence [i.e., Lewchuk et al., 1998; Cioppa et al., 2001], although one study of the Debolt Formation interpreted an intermediate component, similar to the TVRM, to be carried by pyrrhotite or a pyrrhotite/magnetite mixture. The carrier of the component was not conclusively identified [Cioppa et al., 2003].

4. Methodology

Samples for paleomagnetic and rock magnetic analysis were collected from three localities in the Front Ranges (Figure 1) within the Mississippian Etherington, Mount Head, Livingstone and Banff formations as well as the Pennsylvanian-Permian Rocky Mountain Super Group and Triassic Sulphur Mountain Formation. Cores were collected with a portable gasoline drill and oriented with an inclinometer and Brunton compass. Forty-three sites were collected from the anticline-syncline pair within the Mississippian carbonates in Kananaskis Country Provincial Park, AB (Figure 1). Thirty-six of those sites were drilled in the syncline along Kananaskis Road (Figure 2A) and 7 sites were drilled on the west dipping limb of the anticline along Spray Lakes Reservoir on the Western edge of the park (Figure 2B). Sampling was primarily confined to the syncline due to the structural coherence of the exposures. Also within Kananaskis Country 12 sites were drilled on the Kent Anticline along the Spray Lakes

Road/Smith Dorrian Trail within Permian-Triassic units (Figure 2C). Fifty-six sites were collected in Mississippian Carbonates within the asymmetrical anticline from an almost continuous exposure of outcrops along Line Creek, BC (Figure 1) on the property of The Teck Coal Company (Formerly Elk Valley Coal Company; Figure 2D).

Two vein conduit tests were also conducted in order to investigate the relationship between vein forming fluids and remagnetizations. At KC a 95 cm long traverse was conducted across three ~2.0 cm thick bedding parallel veins. At LC no definitive large scale isolated veins were observed so a modified version of the test was conducted. This test was performed by comparing the results from sites drilled within beds devoid of veins with a site collected from a bed containing intense thin veining. Both of the sites came from the same outcrop and were only a few meters apart.

Paleomagnetic samples were marked and cut to standardized lengths (~2.2 cm) with an ASC Scientific dual blade saw. Natural Remanent Magnetizations (NRMs) were measured using a 2G-Enterprises cryogenic magnetometer with DC squids in the shielded paleomagnetic lab at the University of Oklahoma. Prior to thermal demagnetization the samples were submerged in liquid nitrogen twice for two hours and warmed to room temperature in a zero field to remove the unstable remanence from Multi-Domain (MD) grains [Dunlop and Argyle, 1991]. The NRM was measured again after each treatment. Cores were then subjected to stepwise thermal demagnetization in 22 steps from 100 to 580°C using an ASC scientific Thermal Specimen Demagnetizer.

Demagnetization data was plotted on Zijderveld (1967) diagrams using the Super IAPD program, which was also used for Principal Component Analysis [PCA, Kirschvink, 1980] to determine the components. Site means were calculated using

Fisher (1953) statistics in Super IAPD. The optimal clustering (OC) tilt test [Watson and Enkin, 1993] and the direction-correction (DC) tilt test [Enkin, 2003] were performed using the PMGSC version 4.2 software program [Enkin, 2004]. Prior to conducting the tilt tests the plunges of the KC and SPR folds were removed. This was accomplished by considering that the site mean vector data as a line on the surface of a particular bed. Then following a modified version of the method of tracking a line during the unfolding of a plunging fold as outlined in Marshak and Mitra (1988; Method 6-14 pg 119-120). The plunge of the fold was removed and the orientation of the site mean vector on a bed which is unfolding around a particular fold axis could be determined. Paleopoles as well as their errors where calculated using the PMGSC version 4.2 software program [Enkin, 2004]. The poles were plotted on the Mesozoic portion of the apparent polar wander path (APWP) for North America [Besse and Courtillot, 2002] in order to determine the age of the magnetizations.

In order to investigate the magnetic mineralogy Isothermal Remanent Magnetization (IRM) acquisition was performed first by AF demagnetizing samples at 120 mT using a 2G Automated Degaussing System. The specimens were then subjected to a 26 step IRM acquisition up to 2500 mT using an ASC Scientific Impulse Magnetometer. The samples were then subjected again to AF demagnetization at 120 mT. Finally the samples had an IRM imparted on three mutually perpendicular directions at 120, 500, and 2500 mT respectively, then thermally demagnetized to produce tri-axial decay curves [Lowrie, 1990].

Petrographic analysis was conducted on thin sections produced from oriented cores as well as hand samples. Transmitted light microscopy was conducted using a

Zeiss Axio Imager.Z1 petrographic microscope in order to determine lithology as well as to investigate diagenetic features and opaque minerals. Cathodoluminescence microscopy was conducted using an Olympus BX50 system microscope with a CITL CCL 8800 MK4 Cathodoluminescence Stage.

Doubly polished thin sections from calcite and dolomite filled veins were prepared for preliminary fluid inclusion analysis. Petrographic analysis was performed on a Zeiss Research microscope using a Zeiss 40x long working distance objective. Fluid inclusion microthermometry was carried out using a Linkam TH-600 heating/freezing stage connected to a Linkam TMS 90 control unit. The temperature at which the vapor bubble disappeared in an individual inclusion was recorded as the homogenization temp (T_h). These temperatures were recorded in increased order so that lower temp inclusions were not damaged. Careful observations were made to look for stretching of the inclusions. No inclusions studied exhibited stretching. The small size of the inclusions (>10um) made it difficult to obtain ice melting temps (T_m).

An automated Cameca SX50 electron probe micro-analyzer that is equipped with an integrated energy-dispersive x-ray analyzer at the University of Oklahoma was used to investigate the nature of common opaque minerals observed in the various carbonates. Backscatter electron imaging (BSEI) was used to image the opaques while energy dispersive x-ray analysis (EDXA) was used to for qualitative analysis of the composition of the opaque minerals

Carbon and Oxygen isotopes were determined in the isotope geochemistry lab at the University of Oklahoma. About 200-300 μg of carbonate was loaded into 12 ml borosilicate exetainer vials (Labco 938 W) which were sealed with butyl rubber septa

caps. The vials were then placed in a thermostated sample tray heated at 50°C and flushed with ultra high purity He (99.999%) using a Thermo Gas Bench II equipped with a Combi PAL auto-sampler flushing needle for 360 seconds to remove the air. Then 0.4 ml of 100% phosphoric acid was manually injected into vials with a syringe and the reaction was allowed to proceed for at least 1 ½ hours. The vials were then sampled with the PAL measurement needle and the headspace CO_2 was analyzed for $\delta^{13}C$ and $\delta^{18}O$ using a Thermo Delta V Plus isotope ratio mass spectrometer.

The carbon and oxygen composition are reported in standard δ-notation:

$$\delta \text{ (sample)} = (R_{sample}/R_{sample}\text{-}1)1000 \text{ ‰}$$

Where R is $^{13}C/^{12}C$ for carbon and $^{18}O/^{16}O$ for oxygen. The average δ value of 10 sample pulses is expressed relative to PDB on a scale such that $\delta^{13}C$ and $\delta^{18}O$ of NBS-19 is +1.95 ‰and -2.20 ‰, respectively.

Strontium isotope analysis was performed at the University of Texas (Austin) in two batches (years 2008 and 2009) according to the methods described by *Gao et al*. [1992]. Four samples where ran from Mississippian Carbonates at Line Creek and 7 samples from Mississippian Carbonates at Mt. Kidd and 2 samples from the Permian-Triassic units at Kent Anticline. Samples consisted of dolomitized limestones so after removal of the exchangeable and water-soluble Sr the samples were dissolved in 4% acetic acid for 20 minutes to remove as much calcite as possible before dissolving them in 8% acetic acid to dissolve the dolomite. The NIST SRM 987 standard mean value for the 2008 samples was 0.710264 ± 0.000007 (2σ = 0.000015, n = 33) For the 2009 batch the NIST SRM 987 standard mean was 0.71026 ± 0.000005 (2σ = 0.000012, n= 35).The strontium values were normalized relative to the National Bureau of Standards' NBS

987 = 0.71014. The $^{87}Sr/^{86}Sr$ values were then plotted and compared to the coeval seawater values for Mississippian to Triassic seawater [Denison et al., 1994; McArthur et al., 2001].

5. Results and interpretations

5.1 Paleomagnetism

Based on the orthogonal projections the Mississippian carbonates in KC and LC contain two stable components after removal of a modern viscous remanent magnetization (VRM) by 200°C (Figure 4A, B). An intermediate temperature (IT) component with southerly declinations and steep up inclinations was removed between 220-340°C in specimens from most sites (Figure 4A, B). The maximum unblocking temperature suggests pyrrhotite carries the component. On the back limb of the KC anticline along Spray lakes the pyrrhotite appeared to be present but was unable to be picked due to noisy data and high MAD angles. The characteristic remanent magnetization (ChRM) is a high temperature (HT) component which has northerly directions and steep down inclinations (Figure 4A, B). The maximum unblocking temperature of the ChRM (540°C) suggests that magnetite carries the component. The temperature range for both components can be clearly seen on graphs of percent NRM verses thermal demagnetization step (Figures 4A, B). Specimens taken from the Permian to Triassic rocks at Kent Anticline in Kananaskis Country, however, do not contain the reversed IT component (Figure 4C). These only display the ChRM which unblocks between 220-560°C, suggesting a single component magnetization residing in magnetite. Low-temperature treatment prior to thermal demagnetization shows an overall decrease in the NRM intensity for the specimens at all localities but the decrease

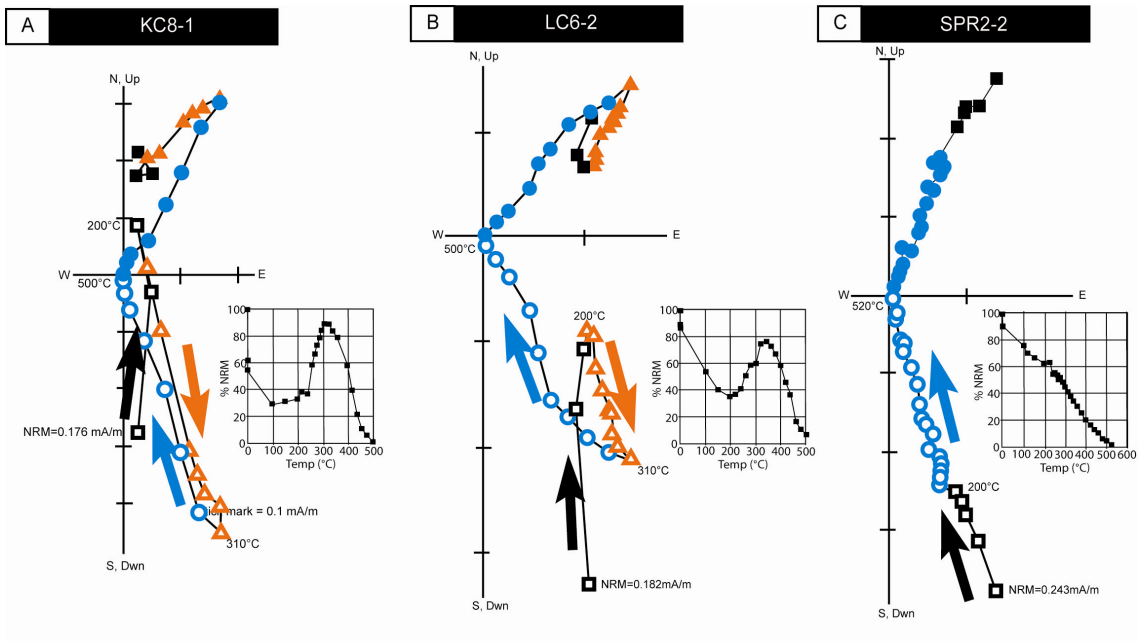

Figure 4: Representative orthogonal projections (Zijderveld diagrams) in geographic coordinates for stepwise thermal demagnetization of A) KC B) LC and C) SPR specimens. Open circles represent the vertical component and the closed circles indicate the horizontal component. The normal polarity ChRM is indicated by circles, the reversed polarity intermediate component is indicated by triangles and the modern VRM is indicated by squares. Arrows indicate the direction of thermal decay. The small insert map shows the percentage of magnetization removed by a particular temperature during stepwise demagnetization.

varies from site to site (5-41% for KC; 10-30% for LC; 4-17% for SPR), suggesting a highly variable concentration of MD grains.

5.2 Kananaskis Country, AB

5.2.1 Site Statistics and Tilt Tests for KC

Out of the 43 sites sampled at KC, 87% of these sites had specimens which displayed the ChRM. Out of these sites, 70% contained specimens with low MAD angles (<10) and low α95 values (<15°). The majority of these sites had more than 7 specimens used to determine the site mean statistics (Table 1). The k values ranged from 33.6 to 1019.4 and most α95 values were less than 9° (Table 1). Thirteen percent of the total sites had specimens with very weak NRM values (<0.010 mA/m) and/or displayed erratic decay which did not allow for the components to be resolved.

Upon 100% un-tilting of the HT site mean data for the KC syncline the remanence vectors display a crossover geometry and do not fully group (Figure 5). This observation is confirmed by both the OC [Watson and Enkin, 1993] and DC tilt tests [Enkin, 2003]. The OC tilt test shows that optimal un-tilting is achieved at 84.9% ± 4% un-tilting (Figure 5) and the DC tilt test shows similar results with optimal un-tilting at 85.6% ± 10.3% (Figure 5). These results suggest that the magnetization was acquired early in the folding process. In order to examine the anticline at KC a tilt test was performed using the data from the western limb along Spray lakes Reservoir and the eastern limb data from the KC syncline. When 100% tilt correction was applied the remanence vectors appeared to come together with a few sites displaying some crossover suggesting a pre-tilting to early syn-tilting acquisition (Figure 6). The OC tilt test shows that the best grouping occurs at 91.6% ± 7.2% (Figure 6) and the DC tilt test

Table 1: Site statistics for HT component at Mt. Kidd anticline-syncline, AB

				Statistics			Geographic		Stratigraphic	
Site	**Lat / Long**	**Lithology**	**Strike/Dip**	**N/N0**	**K**	**α95**	**Dec**	**Inc**	**Dec**	**Inc**
KC1	N50.826 / W115.165	OFGS	026.3 / 28E	7/8	63.16	7.7	276.1	58	304.2	81.5
KC2	N50.826 / W115.165	FGS	021.3 / 30E	8/8	91.39	5.8	268.1	53.5	280	81.1
KC3	N50.826 / W115.165	FPS	021.3 / 30E	7/8	59.73	7.9	276.1	53.1	305	78.9
KC4	N50.826 / W115.165	OFPS	021.3 / 45E	6/8	67.38	8.2	272.5	55.7	109.2	82.6
KC5	N50.826 / W115.165	OFGS	021.3 / 30E	Component present but Mad angle and α95 to high						
KC6	N50.861 / W115.175	DGS	136.3 / 42W	7/8	77.13	6.9	34.9	60.7	305.2	75.4
KC7	N50.861 / W115.175	DGS	166.3 / 42W	8/8	345.71	3	43.5	59.9	323.9	60.1
KC8	N50.862 / W115.175	DGS	151.3 / 42W	8/8	178.85	4.2	43.4	63.9	306.8	69.5
KC9	N50.862 / W115.175	ChCD	155.3 / 35W	7/7	137.98	5.2	39.3	56.9	2.1	60.8
KC10	N50.868 / W115.173	WS-PS	155.3 / 26W	8/8	80.28	6.2	22.3	81.1	300.5	66.9
KC11	N50.868 / W115.173	WS-PS	153.3 / 27W	8/8	79.52	6.2	37.6	79.7	300.4	69.8
KC12	N50.868 / W115.173	DWS	153.3 / 27W	7/7	338.94	3.3	55.4	75.5	310.9	74.4
KC13	N50.931 / W115.318	FPS	146.3 / 24W	7/8	1087.3	1.7	53.3	69.6	346.7	76.1
KC14	N50.933 / W115.318	FPS	146.3 / 24W	6/7	33.46	11.8	45	81.4	297.9	74.6
KC15	N50.933 / W115.318	DFPS	156.3 / 24W	6/7	92.03	7	54.7	71.2	338.1	73.5
KC16	N50.934 / W115.318	CD	156.3 / 24W	7/7	39.57	9.7	42.8	73	329.9	70.3
KC17	N50.934 / W115.318	DMS	136.3 / 30W	7/7	288.85	3.6	47.2	67.1	335.1	80.1
KC18	N50.934 / W115.318	DWS	146.3 / 26W	8/8	181.09	4.1	57.6	70.8	333.6	78.8
KC20	N50.934 / W115.318	PS	151.3 / 24W	8/8	125	4.6	58	69	351.9	81.7
KC21	N50.826 / W115.165	PFGS	028.3 / 34E	Component present but Mad angle and α95 to high						
KC22	N50.826 / W115.165	OFGS	028.3 / 34E	7/7	101.83	6	285.5	56.8	336.6	83.4
KC23	N50.826 / W115.165	OFGS	028.3 / 34E	Components present but Mad angle and α95 to high						
KC24	N50.826 / W115.165	FPS	028.3 / 34E	6/12	88.17	7.2	290.1	57.6	351.9	81.7
KC25	N50.826 / W115.165	OFGS	028.3 / 34E	Component present but Mad angle and α95 to high						
KC26	N50.861 / W115.175	CD	151.3 / 34W	7/7	264.48	3.7	42.5	52.9	354.2	66
KC27	N50.861 / W115.175	DGS	152.3 / 44W	7/7	53.04	8.4	46.1	46.1	349	68.3
KC28	N50.862 / W115.175	PS -WS	151.3 / 42W	Component present but Mad angle and α95 to high						
KC29	N50.862 / W115.175	ChCD	155.3 / 35W	6/7	117.96	6.2	47.1	56.1	346.7	68.3
KC30	N50.871 / W115.191	GS-PS	111.3 / 34W	Weak and incoherent						
KC31	N50.871 / W115.192	DGS-PS	028.3 / 9E	Weak and incoherent						
KC32	N50.871 / W115.192	FPS	028.3 / 9E	Weak and incoherent						
KC33	N50.871 / W115.192	FGS	356.3 / 37E	Weak and incoherent						
KC34	N50.871 / W115.192	DGS	336.3 / 35E	6/7	36.37	11.3				
KC35	N50.871 / W115.192	DGS	026.3 / 35E	Weak and incoherent						
KC36	N50.861 / W115.175	FPS	166.3 / 45W	Weak and incoherent						
KC37	N50.861 / W115.175	DGS	151.3 / 38W	3/4	270.25	7.5	30.9	37.1	0.2	51.5
KC38	N50.862 / W115.175	DGS	151.3 / 38W	4/4	103.24	9.1	30.8	39.5	357.4	53.2
KC39	N50.868 / W115.173	DWS	165.3 / 25W	6/7	124.03	6	51.3	68.4	318	66
KC40	N50.868 / W115.173	DWS	154.3 / 28W	8/9	1019.4	1.7	52.8	70.4	295.6	70.2
KC41	N50.868 / W115.173	WS-PS	146.3 / 25W	4/4	5.66	42.4				
KC42	N50.868 / W115.173	DMS	144.3 / 20W	7/7	140.13	5.1	55.5	74.9	342.9	78.1
KC43	N50.868 / W115.173	DPGS	156.3 / 25W	9/9	229.34	3.4	41.4	69.6	336	68.8

Notes: N/N_o is the number of specimens with direction versus the number of demagnetized specimens; k is a measure of grouping, a_{95} is the 95% cone of confidence. Dec is declination; Inc is inclination in both geographic and stratigraphic coordinates; Lithology: CD = crystalline dolomite, FPS = fossiliferous packstone, DFP = dolomitzed fossilifersou packstone, DFG = dolomitized fossiliferous grainstone, FGS = fossiliferous grainstone, DFWS = dolomitzed fossiliferous wackstone, DWS = dolomitized wackstones, OFGS = oolitic fossiliferous grainstone, PFGS = pelloidal fossiliferous grainstone, PS = packstone, WS = wackstone, GS = grainstone DMs = dolomitzed mudstone, DP = dolomitzed packstone, DPGS = dolomitized pellodial grainstone, DGS = dolomitized grainstone, ChCD = cherty crystalline dolomite, [Dunham, 1962].

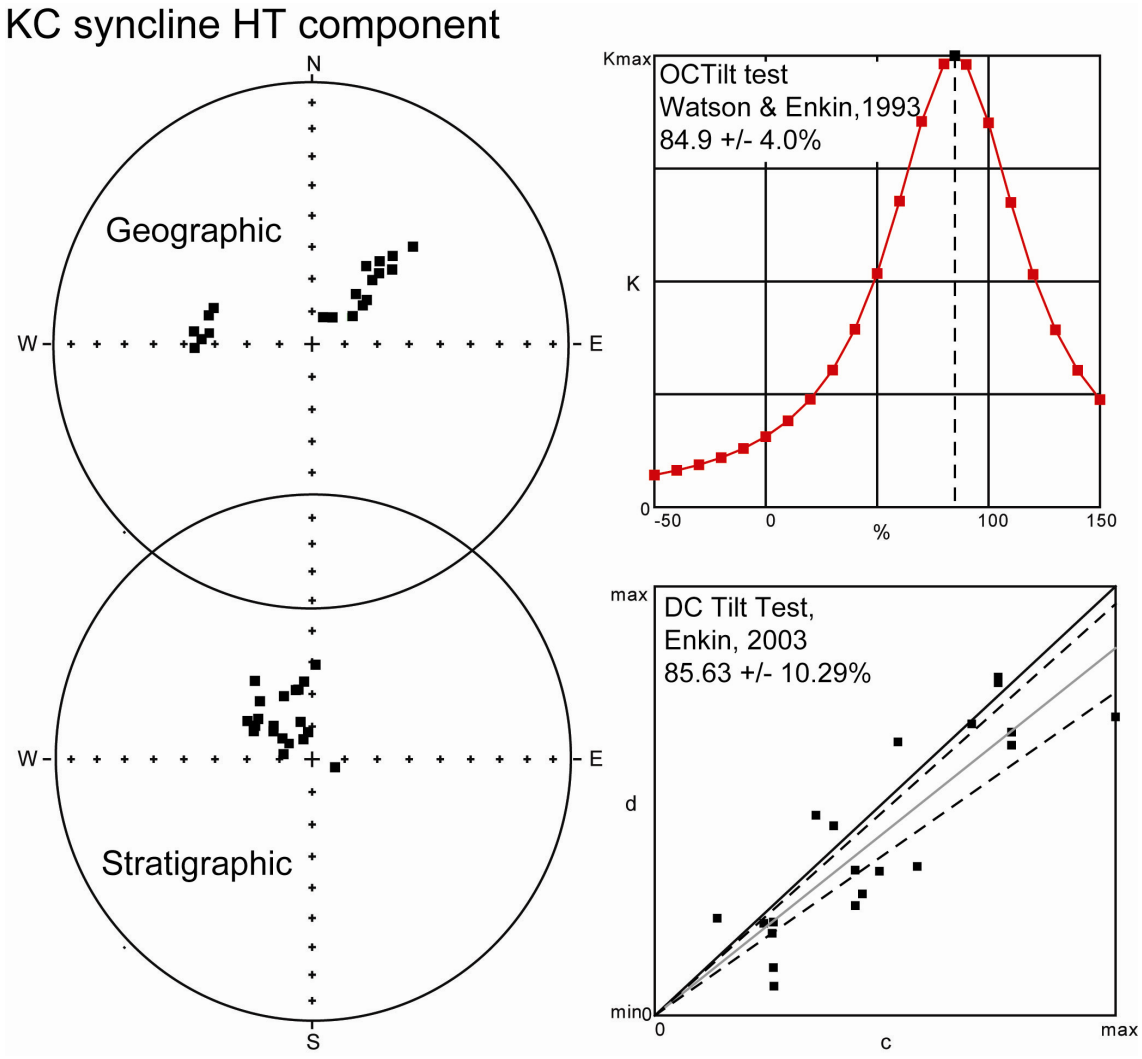

Figure 5: Tilt test results for the high temperature CRM at the Mt. Kidd syncline. A) Equal Area projections of site mean data ($k > 10$, $\alpha95 < 15$) in both geographic (upper) and stratigraphic (lower) coordinates. B) Optimal clustering (OC) tilt test (Watson and Enkin, 1993). C) Direction Correction (DC) tilt test (Enkin, 2003).

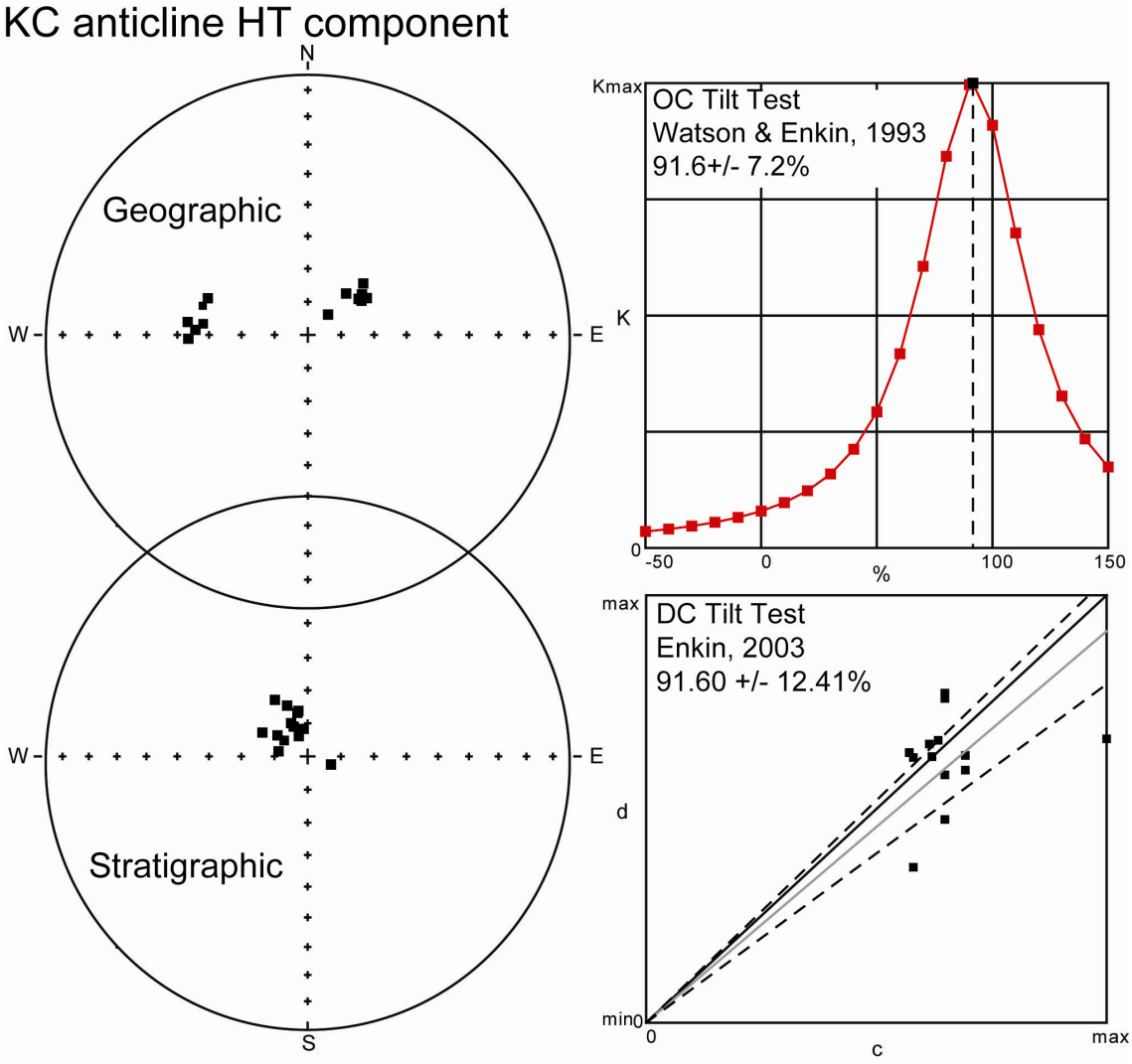

Figure 6: Tilt test results for the ChRM at the Mt. Kidd anticline. A) Equal Area projections of site mean data ($k > 10$, $\alpha 95 < 15$) in both geographic (upper) and stratigraphic (lower) coordinates. B) Optimal clustering (OC) tilt test (Watson and Enkin, 1993). C) Direction Correction (DC) tilt test (Enkin, 2003).

shows 91.6% ± 12.4% (Figure 6). The error in the OC tilt test does not overlap the 100% un-tilting suggesting an early syn-tilting acquisition whereas the error from the DC tilt test did overlap the 100% un-tilting suggesting a pre-tilting magnetization.

Eighty eight percent of the sites from the KC anticline-syncline contained the IT component,. On the west dipping limb of the anticline along Spray lakes reservoir, only one specimen (KC13-20) from all the sites had a well defined IT component. The majority of the sites used in the site statistics had at least 6 specimens to determine the site statistics, with k values ranging from 22.4 to 656.0 and most α95 values were less than 8°.

The best grouping of the IT site mean data for the KC syncline occurs at ~0% un-tilting with the remanence vectors moving away from each other upon 100% un-tilting (Figure 7). This suggests that the IT component is post-tilting. The k- parameter tilt test shows that optimal grouping occurs at -3.6% ± 8.0% (Figure 7) and the DC tilt test shows optimal grouping occurs at -3.5% ± 10.1% (Figure 7). These results suggest that the IT component was acquired after the units had been folded.

5.3 Line Creek anticline, BC

5.3.1 Site Statistics and Tilt Tests for LC

Out of the 56 sites collected from LC, 91% of the sites contained specimens with the ChRM. Out of these sites, 70%, had specimens which could be used to create site statistics suitable for tilt tests ($k > 10$, $\alpha95 < 15$). Four of the sites had a well defined ChRM but the α95 value for these site means were greater than 15° so these sites were left out of the tilt tests. The majority of the reliable sites used more than 6

Table 2: Site statistics for IT component at Mt. Kidd anticline-syncline, AB

				Statistics			Geographic		Stratigraphic	
Site	**Lat / Long**	**Lithology**	**Strike/Dip**	**N/N**	**k**	**α95**	**Dec**	**Inc**	**Dec**	**Inc**
KC1	N50.826 / W115.165	OFGS	026.3 / 28E	6/8	24.30	13.9	190.9	-61.4	239.3	-56.6
KC2	N50.826 / W115.165	FGS	021.3 / 30E	6/8	37.90	11.0	237.2	-76.5	273.9	-50.7
KC3	N50.826 / W115.165	FPS	021.3 / 30E	Component present but Mad angle and α95 to high						
KC4	N50.826 / W115.165	OFPS	021.3 / 45E	5/8	240.55	4.9	212.9	-65.5	261.3	-35.8
KC5	N50.826 / W115.165	OFGS	021.3 / 30E	Component present but Mad angle and α95 to high						
KC6	N50.861 / W115.175	DGS	136.3 / 42W	6/8	90.65	7.1	224.7	-67.2	48.2	-70.8
KC7	N50.861 / W115.175	DGS	166.3 / 42W	8/8	288.43	3.3	214.5	-71.5	101.1	-59.7
KC8	N50.862 / W115.175	DGS	151.3 / 42W	8/8	656.02	2.2	218.1	-72.4	76.7	-63.4
KC9	N50.862 / W115.175	ChCD	155.3 / 35W	6/7	226.45	4.5	208.3	-70.6	97	-67.6
KC10	N50.868 / W115.173	WS-PS	155.3 / 26W	7/8	22.99	12.9	161.9	-75.1	98.1	-61.8
KC11	N50.868 / W115.173	WS-PS	153.3 / 27W	7/8	22.43	13	175.1	-71.6	105.2	-64
KC12	N50.868 / W115.173	DWS	153.3 / 27W	7/7	89	7.1	207	-65	130	-74.2
KC13	N50.931 / W115.318	FPS	146.3 / 24W	Component present but swamped by HT comp.						
KC14	N50.933 / W115.318	FPS	146.3 / 24W	Component present but swamped by HT comp.						
KC15	N50.933 / W115.318	DFPS	156.3 / 24W	Component present but swamped by HT comp.						
KC16	N50.934 / W115.318	CD	156.3 / 24W	Component present but swamped by HT comp.						
KC17	N50.934 / W115.318	DMS	136.3 / 30W	Component present but swamped by HT comp.						
KC18	N50.934 / W115.318	DWS	146.3 / 26W	Component present but swamped by HT comp.						
KC20	N50.934 / W115.318	PS	151.3 / 24W	Component present but swamped by HT comp.						
KC21	N50.826 / W115.165	PFGS	028.3 / 34E	Component present but Mad angle and α95 to high						
KC22	N50.826 / W115.165	OFGS	028.3 / 34E	4/7	68.51	11.2	208.4	-73.8	270.9	-52.7
KC23	N50.826 / W115.165	OFGS	028.3 / 34E	Component present but Mad angle and α95 to high						
KC24	N50.826 / W115.165	FPS	028.3 / 34E	Component present but Mad angle and α95 to high						
KC25	N50.826 / W115.165	OFGS	028.3 / 34E	Component present but Mad angle and α95 to high						
KC26	N50.861 / W115.175	CD	151.3 / 34W	7/7	122.32	5.5	207.9	-64.5	110.2	-71.7
KC27	N50.861 / W115.175	DGS	152.3 / 44W	7/7	124.31	5.4	212.3	-66.7	89.1	-64
KC28	N50.862 / W115.175	PS -WS	151.3 / 42W	Component present but Mad angle and α95 to high						
KC29	N50.862 / W115.175	ChCD	155.3 / 35W	6/7	69.41	8.1	216	-68	100.1	-71.2
KC30	N50.871 / W115.191	GS-PS	111.3 / 34W	Weak and incoherent						
KC31	N50.871 / W115.192	DGS-PS	028.3 / 9E	Weak and incoherent						
KC32	N50.871 / W115.192	FPS	028.3 / 9E	Weak and incoherent						
KC33	N50.871 / W115.192	FGS	356.3 / 37E	Component present but Mad angle and α95 to high						
KC34	N50.871 / W115.192	DGS	336.3 / 35E	4/7	11.07	28.9	196.6	-52.9	215.7	-25.4
KC35	N50.871 / W115.192	DGS	026.3 / 35E	Weak and incoherent						
KC36	N50.861 / W115.175	FPS	166.3 / 45W	Weak and incoherent						
KC37	N50.861 / W115.175	DGS	151.3 / 38W	4/4	191.49	6.7	237.2	-64.1	69.7	-77.7
KC38	N50.862 / W115.175	DGS	151.3 / 38W	4/4	294.56	5.4	211.8	-68.5	90.6	-68.4
KC39	N50.868 / W115.173	DWS	165.3 / 25W	6/7	35.29	11.4	204.1	-62.6	128	-63.2
KC40	N50.868 / W115.173	DWS	154.3 / 28W	7/9	381.56	3.1	198.3	-64.9	107.5	-63.5
KC41	N50.868 / W115.173	WS-PS	146.3 / 25W	4/4	268.38	5.6	173	-70.3	92.2	-59.1
KC42	N50.868 / W115.173	DMS	144.3 / 20W	7/7	37.18	10	196.2	-68.1	134.1	-76.5
KC43	N50.868 / W115.173	DPGS	156.3 / 25W	8/9	97.87	5.6	173.3	-61.6	127.9	-58.9

Notes: N/N_o is the number of specimens with direction versus the number of demagnetized specimens; k is a measure of grouping, a_{95} is the 95% cone of confidence. Dec is declination; Inc is inclination in both geographic and stratigraphic coordinates; Lithology: same as described in table 1.

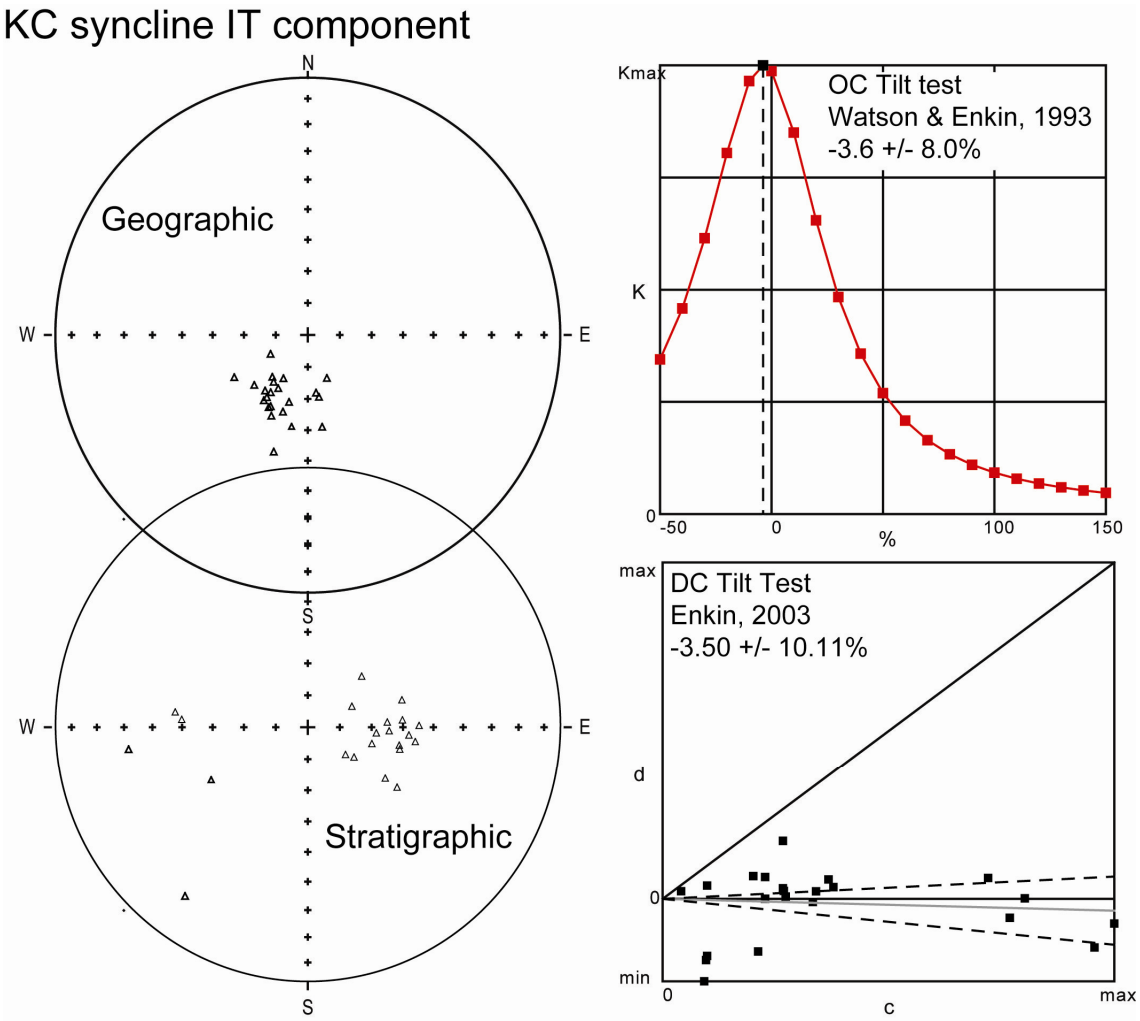

Figure 7: Tilt test results for the intermediate temperature component at the Mt. Kidd syncline. A) Equal Area projections of site mean data ($k > 10$, $\alpha 95 < 15$) in both geographic (upper) and stratigraphic (lower) coordinates. B) Optimal clustering (OC) tilt test (Watson and Enkin, 1993). C) Direction Correction (DC) tilt test (Enkin, 2003).

specimens to determine site means, with k values ranging from 18.8 to 282.9 and α95 values that were less than 11° (Table 3).

For the LC anticline 100% un-tilting of the HT site mean data appear to generate the best grouping with no crossover of data, suggesting a pre-tilting magnetization. (Figure 8). This is confirmed by both tilt tests, with the OC tilt test showing optimal grouping at 97.1.7% ± 3.1% (Figure 8) and the DC tilt test showing the best grouping at 96.6% ± 6.0% (Figure 8). Since the errors for both tests overlap the 100% un-tilting these tests indicate that the un-tilting of the site means is more like 100% un-tilting so the remagnetization was acquired prior to folding.

For the IT component 95% of the sites contained specimens with a well defined component and out of these 79% had had a component that could be reliably identified using the PCA program. As with the ChRM a few sites had site mean α95 values greater than 15 and were excluded from the tilt tests. The majority of the reliable sites contain at least 5 specimens per site, had k values ranging from 28.9 to 1276.5 and α95 values less than 11°.

The site mean data for the IT component have two distinct groupings prior to tilt correction, and display a crossover geometry during untilting (Figure 9). The OC tilt test shows the best grouping is at 69.5% ± 2.5% (Figure 9) and the DC tilt test shows the optimal grouping is achieved at 69.8% ± 7.3% (Figure 9). These results suggest that the IT component was acquired during the early stages of folding.

5.4 Vein conduit Tests (VCT)

Vein conduit tests from both the KC (Figure 10) and LC (Figure 11) localities show interesting relationships between the veins and the magnetic component

Table 3: Site Statistics for HT component at Line Creek anticline, BC

				Statistics			Geographic		Stratigraphic	
Site	**Lat / Long**	**Lithology**	**Strike/Dip**	**N/N0**	**K**	**α95**	**Dec**	**Inc**	**Dec**	**Inc**
LC01	N49.892 / W114.831	OFGS	185.8/20W	5/5	88.27	8.2	50	60.7	9.4	69.4
LC02	N49.892 / W114.831	FPS	185.8/20W	4/7	55.92	12.4	40.7	53.7	10.8	60.8
LC03	N49.892 / W114.831	OFPS	159.8/32W	Component present but Mad angle and α95 to high						
LC04	N49.892 / W114.831	FGS	153.5/31W	6/8	20.5	15.1	28.7	55.4	329.2	71
LC05	N49.892 / W114.830	DFWS	158.8/32W	7/8	151.63	4.9	29.3	56.8	325.1	69
LC06	N49.892 / W114.829	DWS	179.8/34W	8/8	48.28	8.1	42.3	51.8	348.3	62.3
LC07	N49.892 / W114.829	PGS	153.8/25W	9/9	25.96	10.3	353.4	64.8	301.6	61.7
LC10	N49.892 / W114.829	DWS	169.5/11W	7/7	208.53	4.2	353.8	74.7	317.5	71.9
LC11	N49.893 / W114.826	ChCD	157.8/10W	6/7	115.83	6.3	42.1	73.6	12.2	81.5
LC12	N49.893 / W114.826	PGS	157.8/10W	Component present but Mad angle and α95 to high						
LC13	N49.893 / W114.826	DPS	157.5/10W	6/6	62.53	8.5	1.9	72.9	327.7	74.2
LC14	N49.893 / W114.823	OPGS	341.8/64E	Component present but Mad angle and α95 to high						
LC15	N49.893 / W114.823	PGS	345.5/63E	8/9	18.84	13.1	268.8	27.8	352.4	78.2
LC16	N49.893 / W114.823	DMS	328.5/55E	6/8	12.26	19.9	281.3	41.3	352.2	56.1
LC17	N49.893 / W114.823	OGS	328.8/55E	Component present but Mad angle and α95 to high						
LC18	N49.894 / W114.821	***DPS***	340.8/65E	Component present but Mad angle and α95 to high						
LC19	N49.894 / W114.821	PS-GS	345.5/70E	7/8	53.38	8.3	272.6	11.2	319.9	71.3
LC20	N49.894 / W114.821	CD	349.8/72E	Component present but Mad angle and α95 to high						
LC21	N49.894 / W114.821	FPS	340.8/66E	Component present but Mad angle and α95 to high						
LC22	N49.894 / W114.820	OGS	351.8/80E	Component present but Mad angle and α95 to high						
LC23	N49.894 / W114.820	DWS	350.8/84E	3/3	282.91	7.3	294.8	-83.5	264.4	-0.6
LC24	N49.892 / W114.831	PS-GS	350.8/84E	4/	14.12	25.3	270.6	-20.6	280.4	61.7
LC25	N49.892 / W114.831	OFGS	163.8/27W	Component present but Mad angle and α95 to high						
LC26	N49.892 / W114.831	DWS	175.8/46W	7/7	62.83	7.7	58.2	53.9	317.1	69.5
LC27	N49.892 / W114.831	PS	155.8/32W	7/8	27.53	11.7	45.3	66.3	286.1	77.4
LC28	N49.892 / W114.830	DFPS	159.8/36W	8/8	24.78	11.3	32.8	59.7	308.9	69.3
LC29	N49.892 / W114.830	OFPS	180.8/37W	Weak and incoherent						
LC30	N49.892 / W114.830	DWS-PS	155.8/32W	8/8	221.72	3.7	59.7	51.1	36.1	82.3
LC31	N49.892 / W114.829	FGS	166.8/25W	8/16	114.06	5.2	31.6	66.3	322.2	71.7
LC32	N49.892 / W114.829	OPS	168.8/25W	6/9	117.8	6.2	54.7	57.5	10.7	76.3
LC33	N49.894 / W114.822	PFPS	351.8/79E	6/8	131.14	5.9	283.1	8.3	346.4	68.8
LC34	N49.894 / W114.822	PFPS	352.8/72E	6/8	45.68	10	280.1	25.7	26.7	71.2
LC35	N49.894 / W114.822	FGS	342.8/71E	Weak and incoherent						
LC36	N49.894 / W114.822	FGS	342.8/71E	Weak and incoherent						
LC37	N49.894 / W114.822	DFPS	339.8/79E	7/8	66.1	7.5	282.8	12.1	340.3	57.8
LC38	N49.894 / W114.822	-----	356.8/70E	6/6	97.74	6.8	280.4	14	334.1	75.7
LC39	N49.894 / W114.822	DFPS	350.8/76E	8/8	132.48	4.8	279.3	10.6	328.2	70.3
LC40	N49.893 / W114.822	FGS-PS	348.8/73E	6/8	52.18	9.4	276.2	15.6	353.1	73.2
LC41	N49.893 / W114.822	PPS	345.8/69E	3/3	16.01	31.9	266.7	26	14.5	78.8
LC42	N49.893 / W114.822	DPS	331.8/71E	9/9	211.62	3.5	273.8	17	272.8	10.2
LC43	N49.893 / W114.822	WS-PS	342.8/78E	Component present but Mad angle and α95 to high						
LC44	N49.893 / W114.822	DPS	345.8/70E	8/8	130.35	4.9	275.1	18.1	343.1	71.7
LC45	N49.892 / W114.823	FGS	185.8/23W	Weak and incoherent						
LC46	N49.892 / W114.823	PS	335.8/37E	5/7	12.37	22.6	306.1	46.3	350.9	51.6
LC47	N49.892 / W114.823	DWS	330.8/30E	8/8	22.69	11.9	288.6	46.6	326.7	59.3
LC48	N49.893 / W114.827	DWS	330.8/39E	9/9	59.79	6.7	273.1	37.1	312.1	63.3
LC50	N49.893 / W114.827	CD		8/8	57.03	7.4	26.8	63.1	351.8	64.2
LC51	N49.893 / W114.827	-----	185.8/17W	Weak and incoherent						
LC52	N49.892 / W114.829	DFPS	160.8/22W	8/10	101.31	5.5	48.4	62.1	2.2	79
LC54	N49.892 / W114.830	-----	155.8/25W	7/7	82.44	6.7	74.5	62	122.1	85.1

Notes: N/N_o is the number of specimens with direction versus the number of demagnetized specimens; k is a measure of grouping, a_{95} is the 95% cone of confidence. Dec is declination; Inc is inclination in both geographic and stratigraphic coordinates; Lithology: Same nomenclature as described in Table 1 .

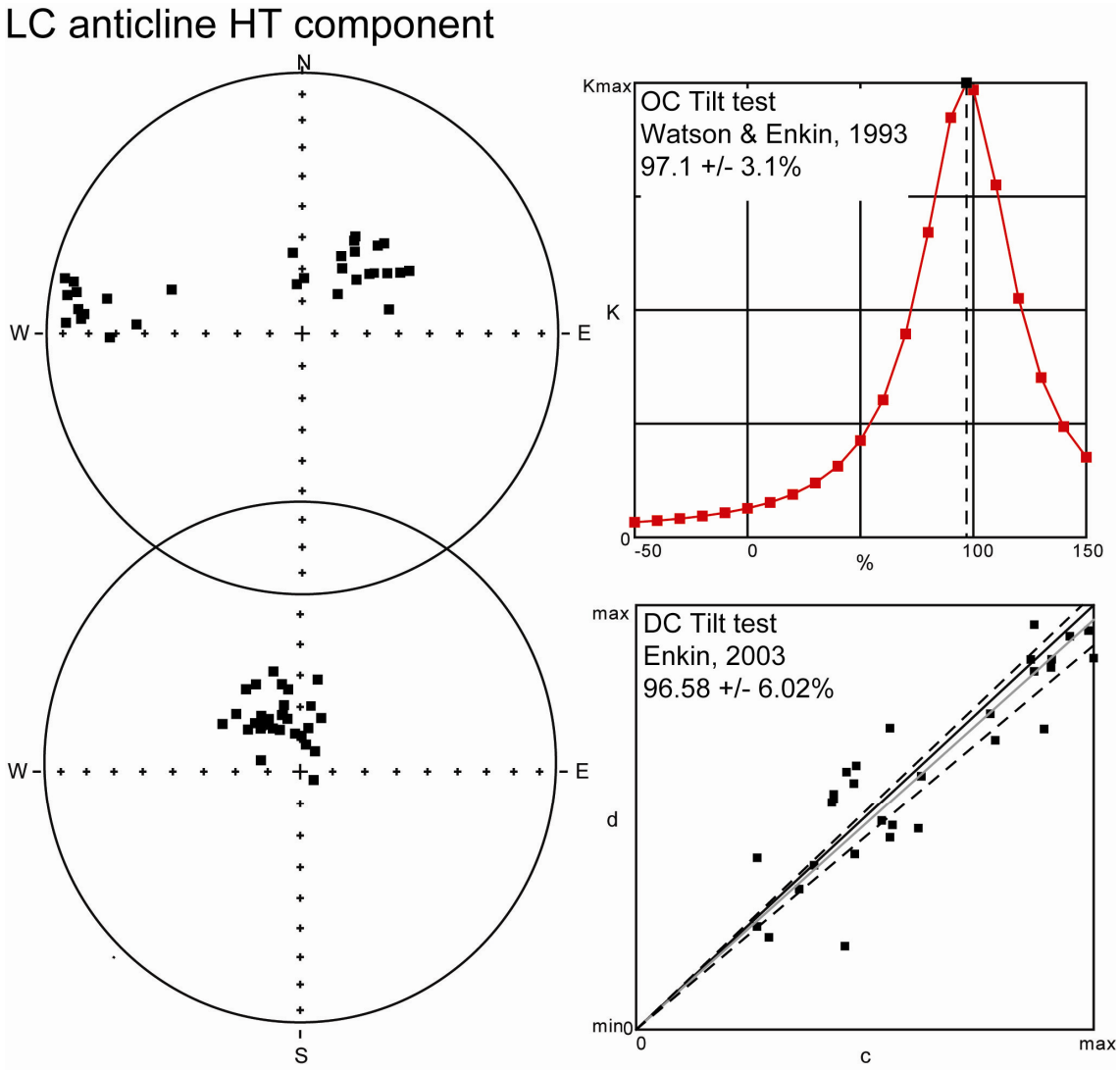

Figure 8: Tilt test results for the ChRM at the Line Creek anticline. A) Equal Area projections of site mean data ($k > 10$, $\alpha95 < 15$) in both geographic (upper) and stratigraphic (lower) coordinates. B) Optimal clustering (OC) tilt test (Watson and Enkin, 1993). C) Direction Correction (DC) tilt test (Enkin, 2003).

Table 4: Site Statistics for IT component at Line Creek anticline, BC

				Statistics			Geographic		Stratigraphic	
Site	**Lat / Long**	**Lithology**	**Strike/Dip**	**N/N0**	**K**	**α95**	**Dec**	**Inc**	**Dec**	**Inc**
LC01	N49.892 / W114.831	OFGS	185.8/20W	7/7	56.04	8.1	220.7	-79	129.7	-73.7
LC02	N49.892 / W114.831	FPS	185.8/20W	Component present but Mad angle and α95 to high						
LC03	N49.892 / W114.831	OFPS	159.8/32W	Component present but Mad angle and α95 to high						
LC04	N49.892 / W114.831	FGS	153.5/31W	6/8	35.0	11.5	214.1	-83.8	70.5	-64.2
LC05	N49.892 / W114.830	DFWS	158.8/32W	8/8	62.42	7.1	173.4	-69	108.5	-57.1
LC06	N49.892 / W114.829	DWS	179.8/34W	7/8	48.55	8.7	187.3	-66	130.6	-51.9
LC07	N49.892 / W114.829	PGS	153.8/25W	4/4	13.92	25.5	126.7	-58.7	102.6	-42.4
LC10	N49.892 / W114.829	DWS	169.5/11W	7/7	31.69	10.9	119.5	-65.2	108.4	-56.1
LC11	N49.893 / W114.826	ChCD	157.8/10W	6/7	53.28	9.3	134.7	-72.9	111.9	-67.1
LC12	N49.893 / W114.826	PGS	157.8/10W	Component present but Mad angle and α95 to high						
LC13	N49.893 / W114.826	DPS	157.5/10W	5/6	72.14	14.6	110.8	-59.2	101.7	-51.3
LC14	N49.893 / W114.823	OPGS	341.8/64E	Component present but Mad angle and α95 to high						
LC15	N49.893 / W114.823	PGS	345.5/63E	5/9	77.81	8.7	104.9	-22.9	163.3	-63.1
LC16	N49.893 / W114.823	DMS	328.5/55E	6/8	24.69	13.8	113.6	-46.4	181.5	-47.6
LC17	N49.893 / W114.823	OGS	328.8/55E	Component present but Mad angle and α95 to high						
LC18	N49.894 / W114.821	DPS	340.8/65E	Component present but Mad angle and α95 to high						
LC19	N49.894 / W114.821	PS-GS	345.5/70E	7/8	130.86	5.3	103.8	-21.6	174	-63.5
LC20	N49.894 / W114.821	CD	349.8/72E	Component present but Mad angle and α95 to high						
LC21	N49.894 / W114.821	FPS	340.8/66E	Component present but Mad angle and α95 to high						
LC22	N49.894 / W114.820	OGS	351.8/80E	7/	107.29	5.9	108.3	-34	221.3	-55.4
LC23	N49.894 / W114.820	DWS	350.8/84E	7/	51.5	8..5	84.1	-21.4	249.4	-74.3
LC24	N49.892 / W114.831	PS-GS	350.8/84E	3/3	117.2	11.4	105.5	-27.7	216.4	-58.1
LC25	N49.892 / W114.831	OFGS	163.8/27W	Component present but Mad angle and α95 to high						
LC26	N49.892 / W114.831	DWS	175.8/46W	6/7	28.99	12.7	250.9	-75.1	107.3	-73.8
LC27	N49.892 / W114.831	PS	155.8/32W	6/8	42.54	10.4	216.6	-67.7	107.3	-73.6
LC28	N49.892 / W114.830	DFPS	159.8/36W	6/8	6.52	28.4	195.3	-68.2	109	-61.4
LC29	N49.892 / W114.830	OFPS	180.8/37W	3/3	232.02	8.1	223.1	-67.4	130	-63.2
LC30	N49.892 / W114.830	DWS-PS	155.8/32W	5/8	144.21	6.4	224.8	-69.4	95.9	-75.4
LC31	N49.892 / W114.829	FGS	166.8/25W	9/16	67.67	6.3	197.3	-73.6	118.2	-68.4
LC32	N49.892 / W114.829	OPS	168.8/25W	5/9	725	2.8	204.5	-66.6	139.9	-68.4
LC33	N49.894 / W114.822	PFPS	351.8/79E	5/8	133.97	6.6	105.1	-18	191.8	-66.4
LC34	N49.894 / W114.822	PFPS	352.8/72E	Weak and incoherent						
LC35	N49.894 / W114.822	FGS	342.8/71E	Weak and incoherent						
LC36	N49.894 / W114.822	FGS	342.8/71E	Weak and incoherent						
LC37	N49.894 / W114.822	DFPS	339.8/79E	3/8	124.99	11.1	112.9	-14.4	169.2	-47.9
LC38	N49.894 / W114.822	-----	356.8/70E	6/6	38.59	10.9	101.6	-17	167.2	-75.7
LC39	N49.894 / W114.822	DFPS	350.8/76E	6/8	70.41	8	104.2	-17.9	183.8	-67.2
LC40	N49.893 / W114.822	FGS-PS	348.8/73E	5/8	56.67	10.3	110.4	-22.4	184.3	-59.8
LC41	N49.893 / W114.822	PPS	345.8/69E	3/3	35.71	20.9	100.8	-19.7	167.1	-66.5
LC42	N49.893 / W114.822	DPS	331.8/71E	8/9	66.54	6.8	103.1	-23.7	166.3	-51.4
LC43	N49.893 / W114.822	WS-PS	342.8/78E	Component present but Mad angle and α95 to high						
LC44	N49.893 / W114.822	DPS	345.8/70E	8/8	72.37	6.6	101	-21.9	174.9	-66.4
LC45	N49.892 / W114.823	FGS	185.8/23W	Component present but Mad angle and α95 to high						
LC46	N49.892 / W114.823	PS	335.8/37E	Component present but Mad angle and α95 to high						
LC47	N49.892 / W114.823	DWS	330.8/30E	5/8	29.28	14.4	117	-64.9	186	-64.5
LC48	N49.893 / W114.827	DWS	330.8/39E	6/9	33.41	11.8	118.8	-37	155	-47.2
LC50	N49.893 / W114.827	CD		5/8	54.37	10.5	195	-60.7	165.3	-59
LC51	N49.893 / W114.827	-----	185.8/17W	Component present but Mad angle and α95 to high						
LC52	N49.892 / W114.829	DFPS	160.8/22W	7/10	74.99	7	224.3	-71.1	130.2	-80.3
LC54	N49.892 / W114.830	-----	155.8/25W	7/7	7.54	23.5	267.4	-61.6	326.4	-79.8

Notes: N/N_o is the number of specimens with direction versus the number of demagnetized specimens; k is a measure of grouping, a_{95} is the 95% cone of confidence. Dec is declination; Inc is inclination in both geographic and stratigraphic coordinates; Lithology: Same nomenclature as described in Table 1

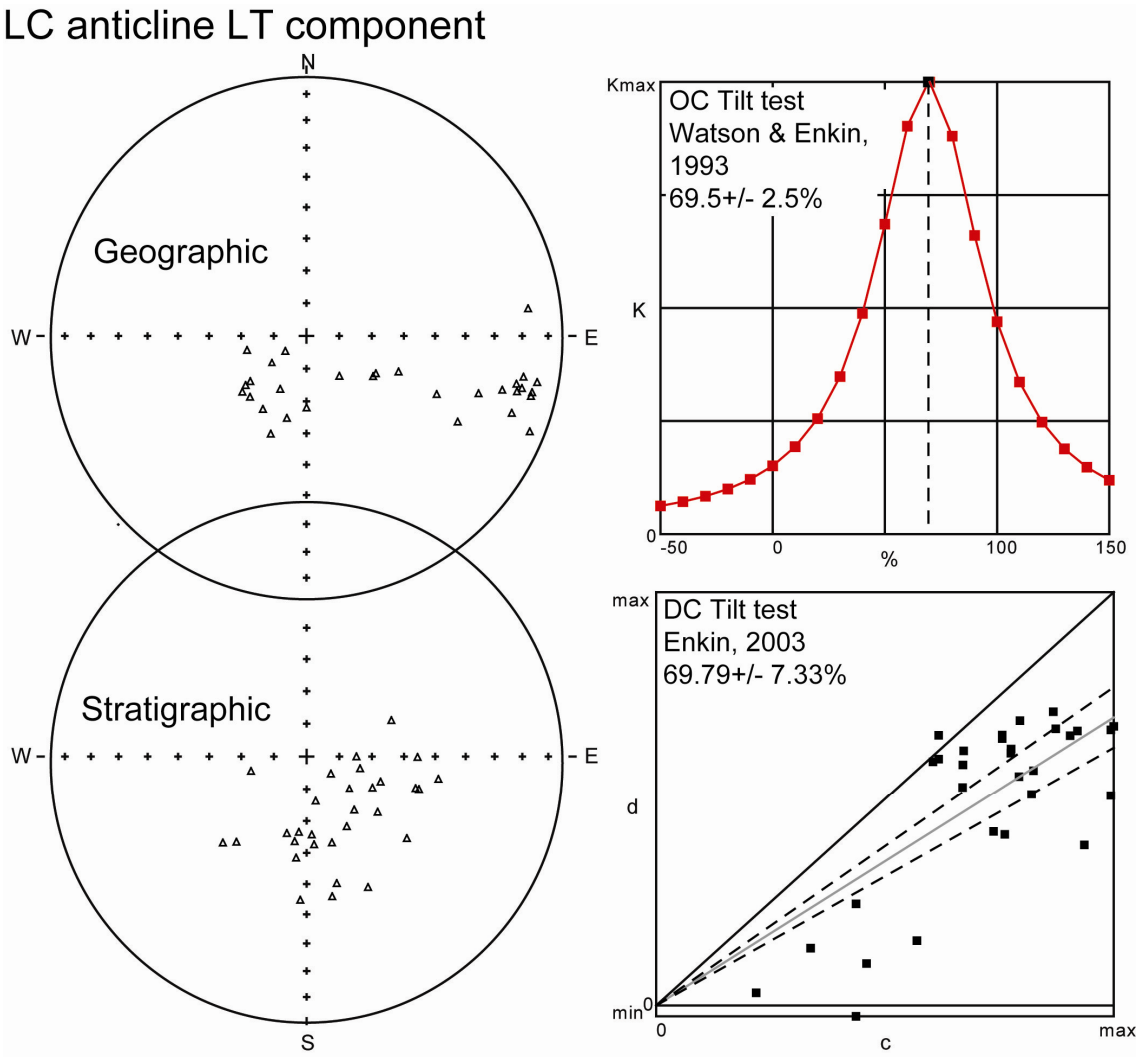

Figure 9: Tilt test results for the intermediate temperature component at the Line Creek anticline. A) Equal Area projections of site mean data ($k > 10$, $\alpha95 < 15$) in both geographic (upper) and stratigraphic (lower) coordinates. B) Optimal clustering (OC) tilt test (Watson and Enkin, 1993). C) Direction Correction (DC) tilt test (Enkin, 2003).

intensities. The VCT at KC which was conducted using 12 specimens taken along a profile which crossed three bedding parallel veins. Both components exist in the specimens based on orthogonal projections (Figure 12A), however, a large spike in total magnetic intensity of the ChRM and not the IT component is observed at each of the three veins suggesting a relationship between bedding parallel veins and the ChRM (Figure 10B). The ChRM is interpreted to reside in magnetite so the component intensity is a combination of the VRM contained in MD magnetite, which is calculated from the intensity drop caused by the liquid nitrogen treatment and the total intensity of the ChRM (PSD to SD grains). The MD intensity was added to the PSD/SD intensities because both are concluded to form during the same event.

The VCT at LC examined tectonic veins and is considered to be unconventional in the sense that it tested an un-veined bed (Figure 11A) versus a bed containing intense thin veining (Figure 11B). Both components are observed in the un-veined bed (Figure 12B) and have similar component intensities (Figure 11A). Unlike the other sites at LC the ChRM is reversed (Figure 12B). For the highly veined bed, multiple specimens displayed only the IT component (Figure 12C), however, a few specimens did display a weak and noisy ChRM. It appears that the magnetic intensity of the IT component overwhelms the ChRM (Figure 11B). A drop due to liquid nitrogen treatment was observed in the veined specimens suggesting MD magnetite, however, this data was not included in the component intensity data for the magnetite component due to the lack of a well defined magnetite ChRM in the veined specimens. These results suggest that the fluids filling these tectonic veins may have had exerted a strong control on the IT component.

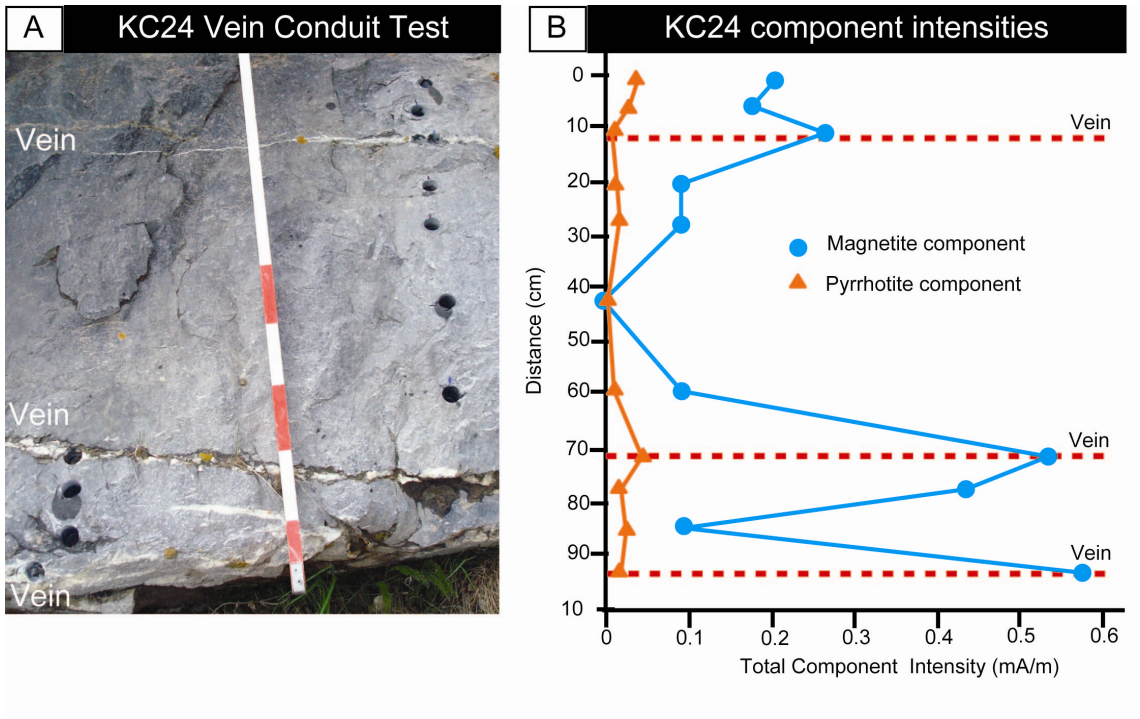

Figure 10: Bedding parallel vein conduit (contact) test from Kananaskis Country. A) Field photo showing veins and core locations. Cores holes are 1 inch in diameter. B) Component intensities verses distance from the veins, Circles = Magnetite component intensity; Triangles = Pyrrhotite component intensity

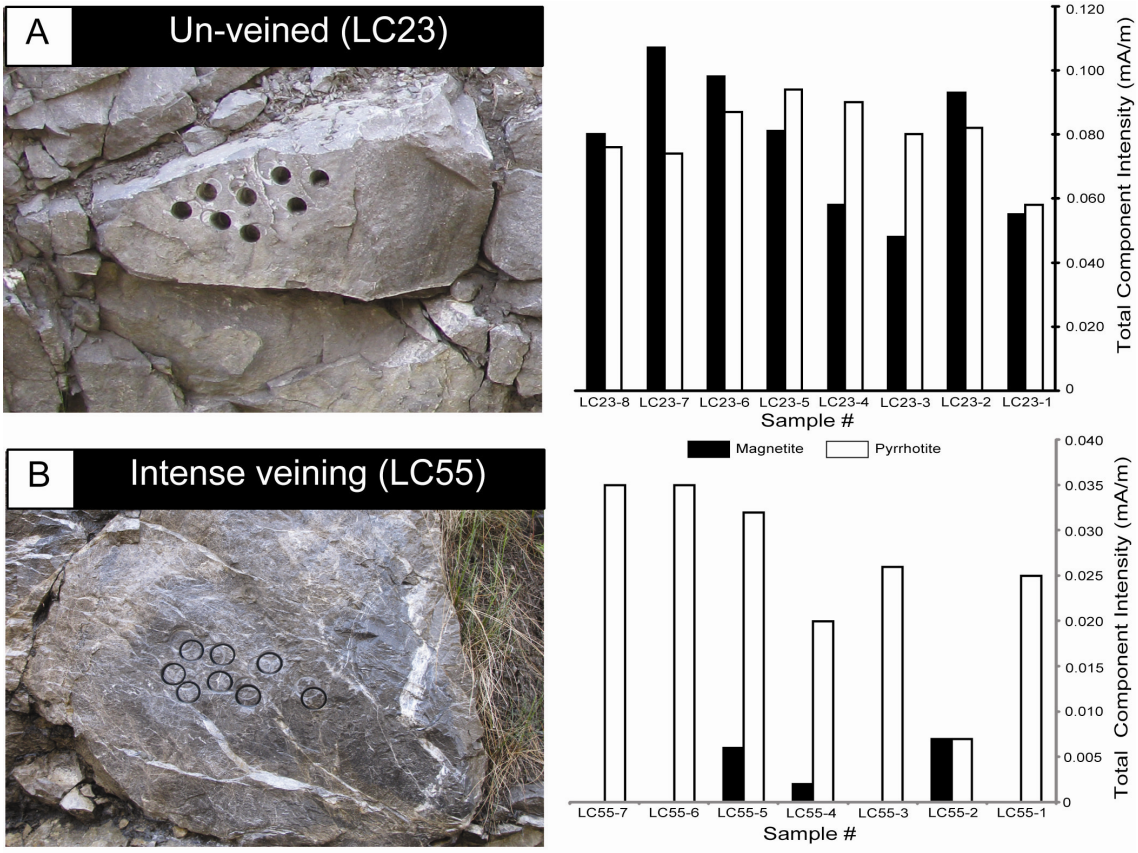

Figure 11: Tectonic vein conduit (contact) test from Line Creek. A) Un-veined sample (LC23). Left = Field Photo of unveined rock, cores holes are 1 inch in diameter. Right = Component intensity of both components for each specimen. B) Intensely veined sample, Left = Field Photo showing intense veining; Right = Component intensity of both components for each specimen. Black bars = Magnetite; White bars = Pyrrhotite.

These differences between the sites can also be observed in both IRM acquisition curves and tri-axial decay curves (Figure 13). The un-veined specimen (LC23-7) has a curve with a fairly sharp transition to saturation with 80% of the magnetization acquired below 100 mT (Figure 13A). This suggests a large amount of lower coercivity magnetite compared to pyrrhotite. The veined specimen (LC55-8) has a much more gentle curve with 80% saturation achieved just below 200 mT (Figure 13B) suggesting a larger concentration of higher coercivity pyrrhotite compared to magnetite. Tri-axial decay curves for both samples are full demagnetized by 580°C. In the veined samples, 85-90% of the IRM for the low and moderate coercivity curves is removed by 325°C whereas only 60-70% is removed in the unveined sample (Figure 13B). This also suggests a larger concentration of pyrrhotite compared to magnetite in the veined sample.

5.5 Spray lakes Road (Kent Anticline), AB

5.5.1 Site Statistics and Tilt Tests for SPR

Out of the 12 sites collected in Pennsylvanian and Triassic units from the Kent Anticline, 10 contained the ChRM with a maximum unblocking temperature of 560°C with none of the samples showing the IT component (Figure 5C). A minimum of 5 specimens were used to calculate the site statistics. The k values ranged from 30.5 to 174.9 and α95 values were less than 15 (Table 5).

At 100% un-tilting the site mean data from each limb came together suggesting a pre-tilting magnetization (Figure 14). The best grouping for the OC tilt test was 96.5% +/- 3.2% (Figure 14). The DC tilt test gave similar results with the best grouping achieved at 96.7% +/- 9.3% un-tilting (Figure 14).

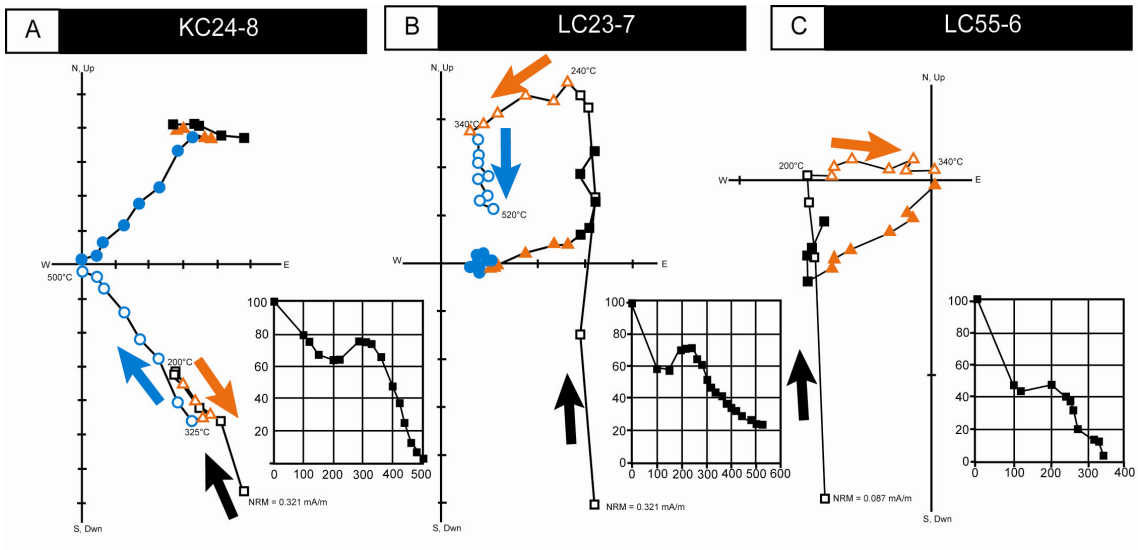

Figure 12: Orthogonal projections (Zijderveld diagrams) in geographic coordinates for stepwise thermal demagnetization of A) KC sample B) LC unveined sample. C). LC veined sample Open symbols represent the vertical component and the closed circles indicate the horizontal component. The high temperature ChRM is indicated by circles, the intermediate component is indicated by triangles and the modern VRM is indicated by squares. Arrows indicate the direction of thermal decay. The small insert map shows the percentage of magnetization removed by a particular temperature during stepwise demagnetization.

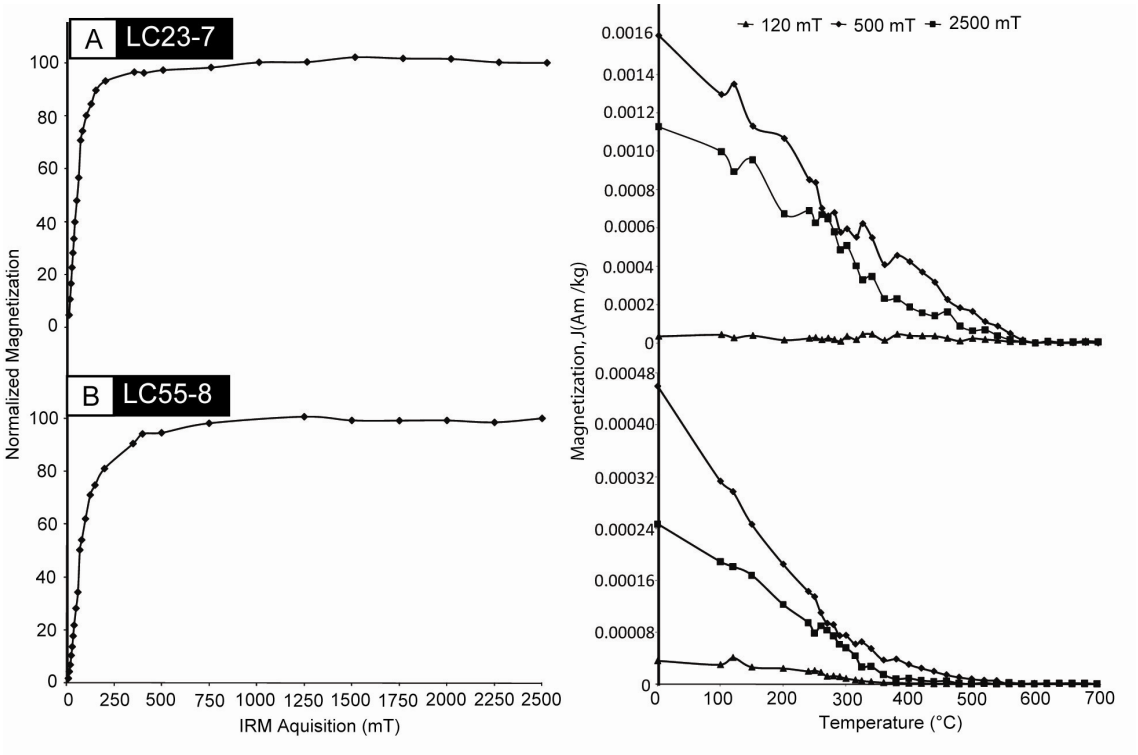

Figure 13: IRM Acquisition and tri-axial thermal decay curves for LC vein conduit tests. A) Unveined sample (LC23-7) B) Intensely veined sample (LC55-8).

Table 5: Site Statistics for HT component at Kent anticline, AB

				Statistics			Geographic		Stratigraphic	
Site	**Lat / Long**	**Lithology**	**Strike/Dip**	**N/N0**	**K**	**α95**	**Dec**	**Inc**	**Dec**	**Inc**
SPR1	N50.695 / W115.167	-----	131.3/30W	5/8	45.2	11.5	41.9	51.2	40.5	81.2
SPR2	N50.695 / W115.165	-----	127.3/25W	5/8	174.9	5.8	20.5	54.4	348.7	76.5
SPR3	N50.691/ W115.152	-----	346.3/72W	5/8	30.5	14.1	276.7	26.8	25.2	69.2
SPR4	N50.691 / W115.153	-----	354.3/63E	5/8	42.2	11.9	277.5	20.9	338.9	76.5
SPR9	N50.695 / W115.165	-----	136.3/22W	5/8	100.5	7.9	46.1	63.9	0.9	74.3
SPR11	N50.695 / W115.164	-----	145.3/29W	5/8	137.1	6.6	23.5	55.3	326.6	72.5
SPR12	N50.693 / W115.159	Q-SS-M	351.3/72E	5/8	125.7	5.6	276.7	20.2	354.5	71.0
SPR13	N50.693 / W115.157	CD-Q	354.3/63E	4/8	72.6	8.7	280.5	24.7	343.2	68.7
SPR14	N50.692 / W115.153	DMS	355.3/74W	5/8	139.3	5.1	278.9	21.9	7.8	72.8
SPR15	N50.692 / W115.152	DGS-Shl	346.3/79W	4/8	174.2	7.0	283.5	7.1	351.9	62.9

Notes: Notes: N/N_o is the number of specimens with direction versus the number of demagnetized specimens; k is a measure of grouping, a_{95} is the 95% cone of confidence. Dec is declination; Inc is inclination in both geographic and stratigraphic coordinates; Lithology: QSSM = Quartz sandstone with micrite. CDQ = crystalline dolomite with quartz, DMS = dolomitized mudstone, ShDGS = shaley dolomitized grainstone

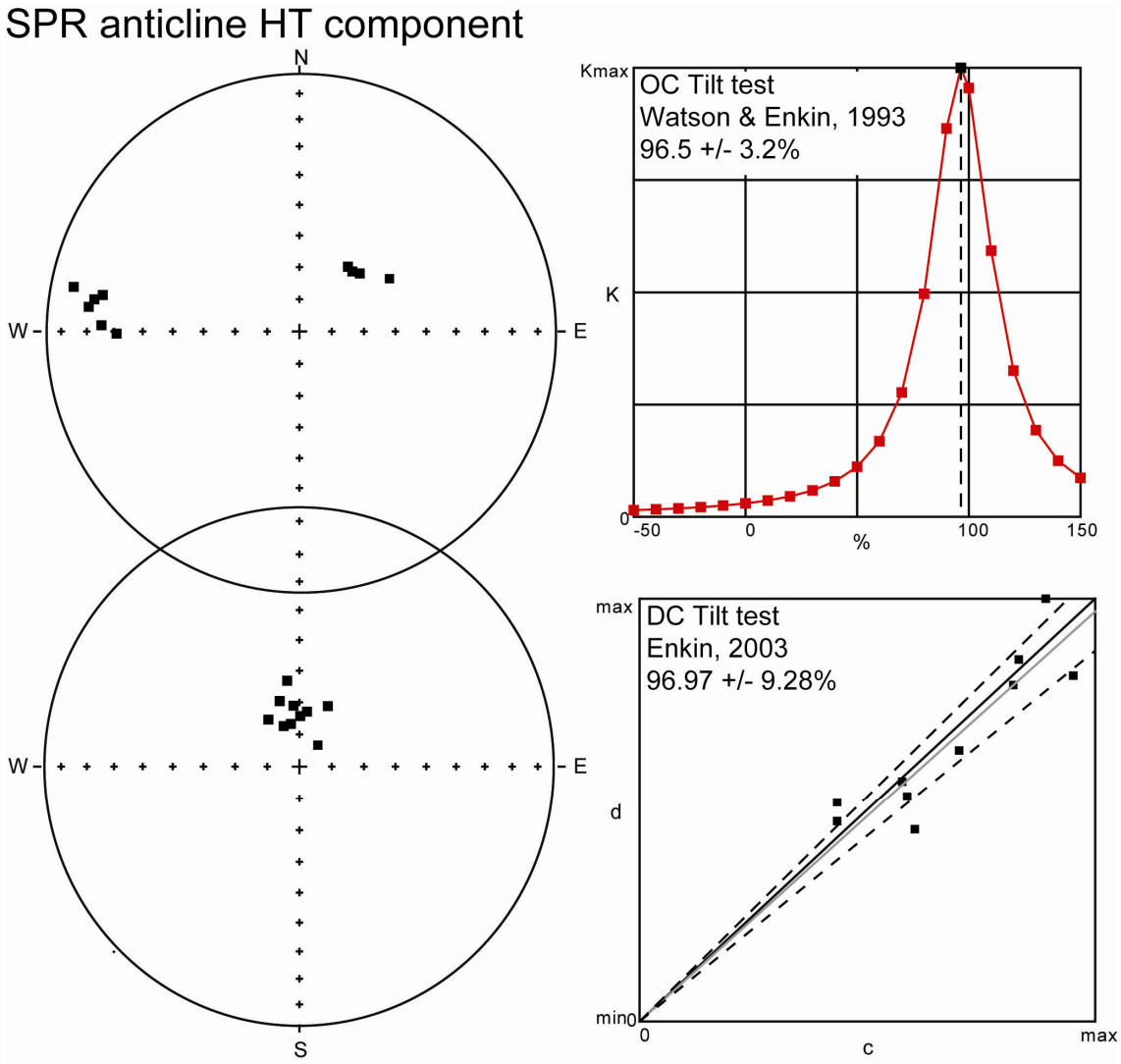

Figure 14: Tilt test results for the ChRM at the Kent anticline. A) Equal Area projections of site mean data (k > 10, α95 < 15) in both geographic (upper) and stratigraphic (lower) coordinates. B) Optimal clustering (OC) tilt test (Watson and Enkin, 1993). C) Direction Correction (DC) tilt test (Enkin, 2003).

5.6 Paleopoles and the Apparent Polar Wander Path (APWP)

The paleopole for the pre-tilting ChRM (74.7°N, 194.0°E; dp/dm = 6.2° /5.5°) at LC falls along the Mesozoic portion of the APWP in the Early Cretaceous (Aptian; ~120-110 Ma; Figure 15). The paleopole from the syn-tilting KC syncline (70.6°N, 202.1°E; dp/dm =7.5°/6.9°) and the pre-tilting KC anticline (65.4°N, 219.5°E; dp/dm = 6.3°/5.6°) fall to the east of the Early Cretaceous portion of the APWP and the errors do not overlap any portion of the path (Figure 15). The syn-tilting IT pole at LC falls off the path near the late Jurassic-Early Cretaceous portion of the path (62.5N, 170.9E; dp/dm = 7.3/6.0; Figure 15) and the post-tilting IT pole for the KC syncline plots off the path near the north pole (74.5°N, 325.8°E; dp/dm = 5.7/4.7; Figure 15) The paleopole for the pre-tilting SPR anticline (80.1°N, 220.9°E; dp/dm = 8.1°/7.3°) plots near the Late Cretaceous to Eocene portion of the path (Figure 15).

5.7 Rock Magnetism

5.7.1 Previous Rock Magnetic Work conducted on KC and LC samples

Detailed rock magnetic characterization has been conducted on the KC and LC samples as part of this comprehensive study of secondary magnetizations in the Canadian Cordillera [Chapter 2]. Based on a combination of thermal demagnetization, cumulative log Gaussian analysis, High-Field hysteresis measurements and low temperature experiments, these samples contain up to three distinct components. 1) a modern VRM which is unblocked below 200°C and resides MD magnetite. 2) an IT component carried by SD pyrrhotite. 3) a ChRM contained in PSD-SD magnetite. Superparamagnetic magnetite as well as high coercivity oxidized phases (hematite or goethite) are also found in various amounts in these samples [Chapter 2]. These grains

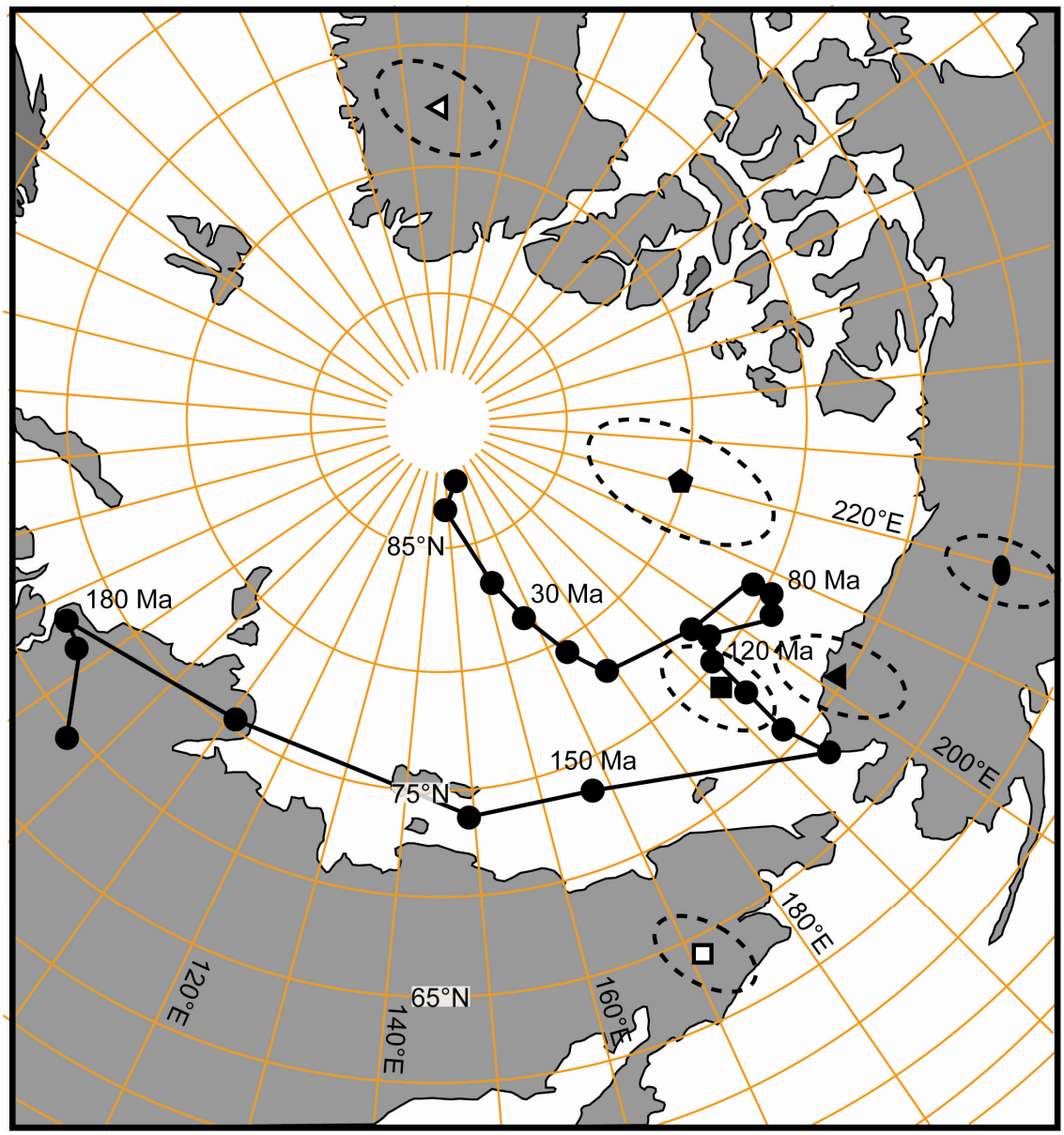

Figure 15: Mesozoic section of the apparent polar wander path for North America (modified from Besse and Courtillot, 2000). Squares = Mt. Kidd syncline; Oval = Mt. Kidd anticline Triangles = Line Creek anticline; Pentagon = Kent anticline Open symbol represent the ChRM and closed symbols indicate the intermediate temperature component. dp/dm errors are indicated by the dashed ovals.

can have a strong influence on the bulk rock magnetic properties but do not affect the NRM of these remagnetized carbonates.

5.7.2 Rock magnetic analysis of SPR samples

In order to confirm the magnetic mineralogy observed in thermal demagnetization of the SPR samples, a series of rock magnetic were also conducted. IRM aquisition curves show that for SPR9-2 partial saturation is acheived around 100 mT, suggesting magnetite. The magnetization does not ever reach full saturation by 2500 mT, suggesting the presence of hematite (Figure 16A). Thermal decay of a triaxial IRM shows that both of the lower coercivity curves have the majority of the magnetization and decay by 580°C, confirming the presence of magnetite (Figure 16A). The remaining magnetization in the lower coercivity curves as well as the high coercivity curve is removed by 680°C indicating hematite. For SPR14-4 the IRM acqustion curve shows a sharp transition to full saturation below 120 mT suggesting magnetite (Figure 16B). The presence of magnetite is confirmed by total removal of the triaxial IRM by 580°C (Figure 16B). Pyrrhotite is not considered to be present in these specimens based on the thermal demagnetization of the NRM results. This absence is confirmed by the lack of a gentle transition to saturation below 200mT as observed in the Mississippian carbonates from Chapter 2

5.8 Petrology

5.8.1 Transmitted light

At Line Creek 22 representative lithologies were sampled (Tables 3 & 4) and classified according to Dunham [1962]. These samples range from pure limestone with no dolomitization to samples that have been completely dolomitized. The most

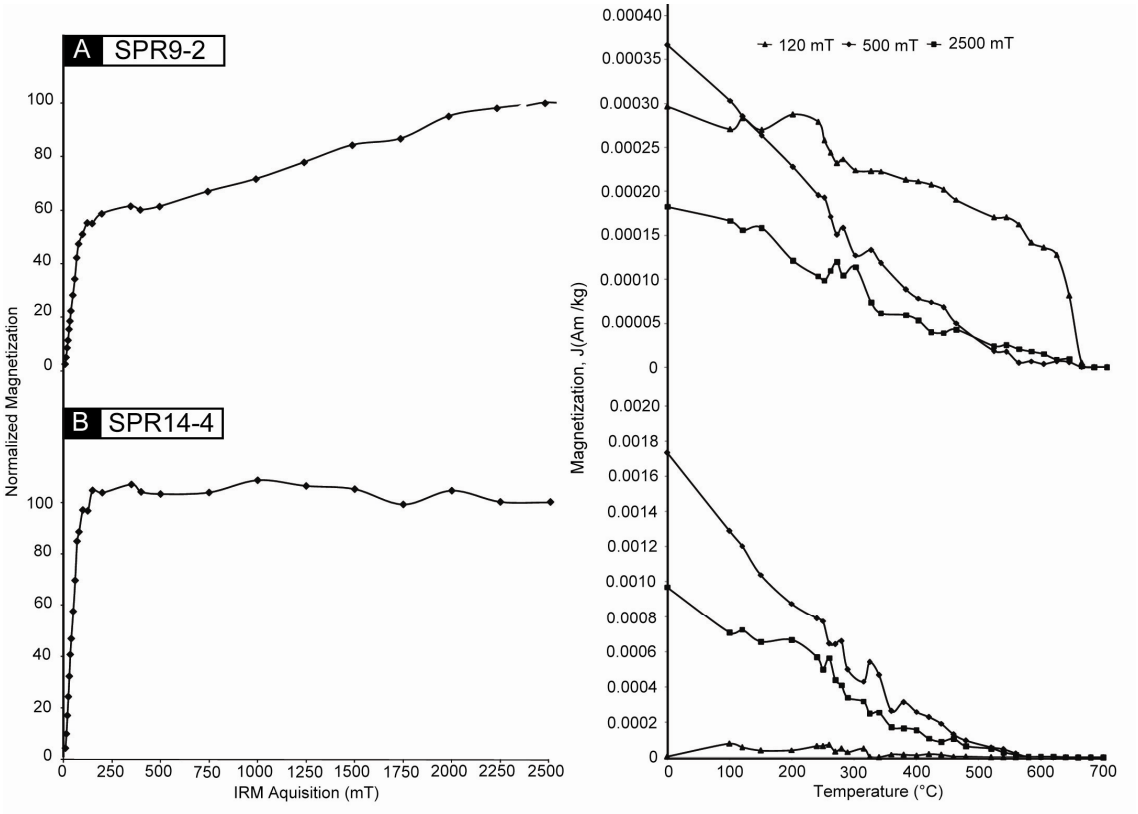

Figure 16: Representative IRM Acquisition and Tri-axial thermal decay curves for representative samples from Kent Anticline. A) SPR9-2. B) SPR14-4.

abundant lithologies sampled were dolomitized wackstones and fossiliferous grainstones. These are followed by dolomitized fossiliferous grainstones, dolomitized packstones, pelloidal grainstones and crystalline dolomite. The remaining lithologies are minor variations of these six predominate lithologies (Table 3 & 4). The samples show various concentrations of detrital siliclastic material (quartz and feldspar), opaque minerals (pyrite, hematite and magnetite), and degraded hydrocarbons (i.e. bitumen).

At Kananaskis Country the Mississippian carbonates are similar to Line Creek and also show a large variation in lithologies and dolomitization, with 16 different lithologies sampled (Tables 1 & 2). The most predominate lithologies sampled were dolomitized grainstones and fossiliferous packstones followed by dolomitized wackstones, oolitic fossiliferous grainstones, wackstone-packstones and crystalline dolomites. Again the remaining lithologies are slight variations of the 6 common lithologies (Tables 1 & 2). As with the Line Creek samples the Mississippian carbonates also contain various amounts of detrital siliclastic material (with some quartz grains displaying overgrowths), opaque minerals, and degraded hydrocarbons. It is worth noting that at both locations is that there is no observable relationship between coherent and incoherent sites and the petrographic characteristics. In addition, there is not a relationship between the components and type or amount of dolomitization.

Calcite veins were milky and the only observable inclusions were too small for analysis. The vein dolomites contained large two phase aqueous brine inclusions along growth planes (Figure 17). Preliminary analysis of these inclusions suggests fluids with homogenization temperatures between 140-212°C.

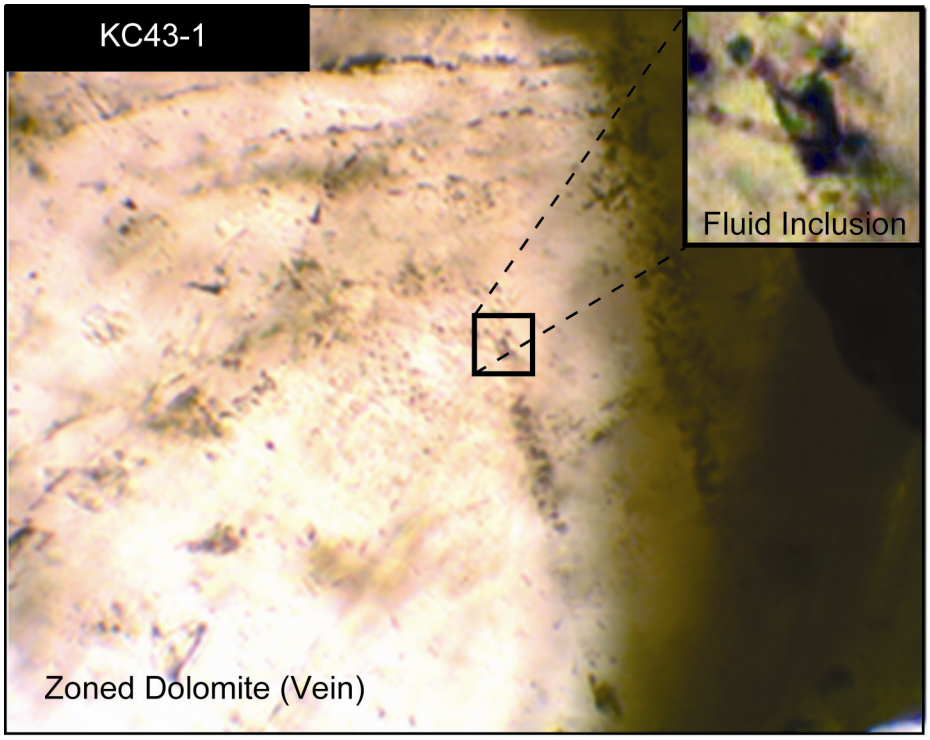

Figure 17: Representative Fluid inclusions along a growth plane in a tectonic dolomite vein from the west dipping limb of the Mt. Kidd syncline.

For Kent Anticline in Kananaskis Country the sites sampled were carbonates as well as siliclastics. The majority of the sites drilled were in the Pennsylvanian-Permian Rock Mountain Super Group. The lithologies consisted of a quartzarenite with a lime mud matrix and a crystalline dolomite or dolomitized mudstone. The Triassic Sulphur Mountain Formation was a dolomitized laminated shaley grainstone. All of the samples contained abundant pyrite and detrital material similar to the Mississippian units but they did not contain observable solid bitumen.

5.8.2 Cathodoluminescence (CL)

CL microscopy was performed on vein material from specimens used in the vein conduit tests to determine if any variations exist between the vein material [e.g., Marshall, 1988]. If variations exist they could reflect differences in the Mn to Fe ratios of the vein forming fluids. The bedding parallel vein (KC24-11) shows two distinct mineralogies in transmitted light. The primary vein forming mineral is calcite, with un-twinned dolomite observed as a late stage interstitial vug filling material (Figure 18A). Under CL the calcite shows a faint red luminescence while the dolomite shows a bright red luminescence (Figure 18B). The tectonic veins at LC also show interfingering mineral phases composed of dolomite and calcite (Figure 18C), suggesting multiple veining events. Based on cross-cutting relationships the primary veining material is dolomite followed by a later calcite. Under CL the dolomite has a bright red luminescence similar to the late stage dolomite in the bedding parallel veins, whereas the late stage calcite is quenched (Figure 18D). Based on the CL results it appears that the dolomite in both vein tests precipitated from fluids with similar Mn to Fe ratios while the calcite precipitated from fluids with different Mn to Fe ratios.

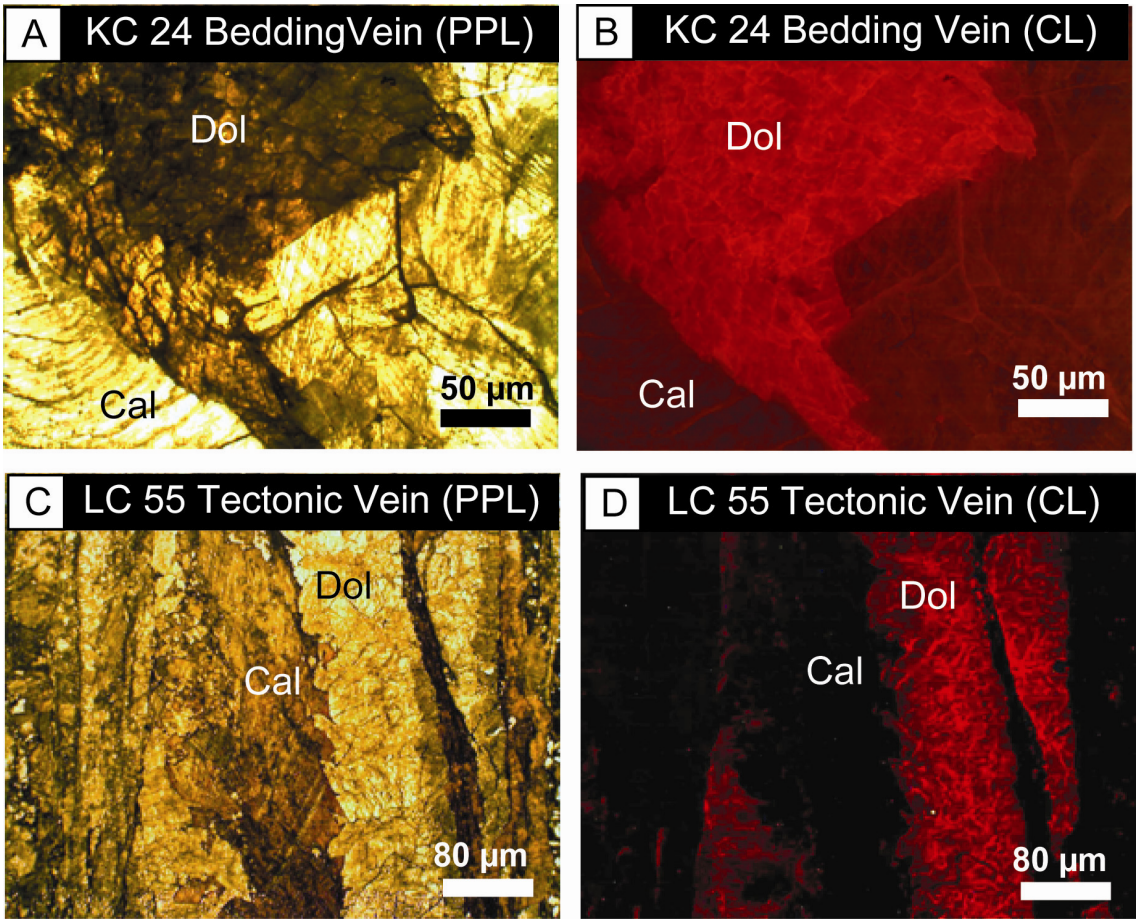

Figure 18: Petrography of vein material from the vein conduit tests. A) KC24-11, Plane polarized light (PPL). B) LC55-6, PPL. C) KC24-11, Cathodoluminescence (CL) image. D) LC55-6, CL image

5.8.3 Electron Microprobe results

The origin of the opaque minerals observed within the matrix and degraded hydrocarbons where ambiguous in bright field reflected light so backscatter electron microscopy (BSEL) and Energy Dispersive X-Ray Analysis (EDXA) was employed to determine composition. Degraded hydrocarbons are abundant throughout the samples examined (Figure 19) and opaque minerals are common in the hydrocarbons. Pyrite grains were the most abundant and commonly were partially replaced by hematite (Figure 19A). The EDXA showed that the solid bitumen (Figure 19B) is enriched in sulfur with the weight percent sulfur ranging from 12.25 to 29.12%. Sphalerite (Figure 19C) and barite (Figure 19A) were also observed. Based on EDXA frambodial pyrrhotite (Figure 19D) was identified, however, due to the small crystal size compared to the beam size it is possible that the EDXA signal was a representation of pyrite and hematite, which has a spectrum that looks similar to pyrrhotite.

5.9 Geochemistry

5.9.1 Carbon/Oxygen Results

Carbon^{13} and Oxygen^{18} isotopes were analyzed to characterize the nature of the vein material as well as the nature of vug material. The LC vein and vugs had a very narrow range of positive carbon values ranging from 1.39 to 3.58 and a very wide range of negative oxygen values ranging from -4.23 to -22.94 (Figure 20). The Kananaskis veins, vugs and slickensides were similar in terms of a narrow range of carbon values (2.72 to -1.89; Figure 20) with the exception of one vug sample which has a highly depleted carbon value (-10.42). These samples also display a wide range of oxygen values (-4.92 to -24.36; Figure 20). The This narrow range of carbon values over a

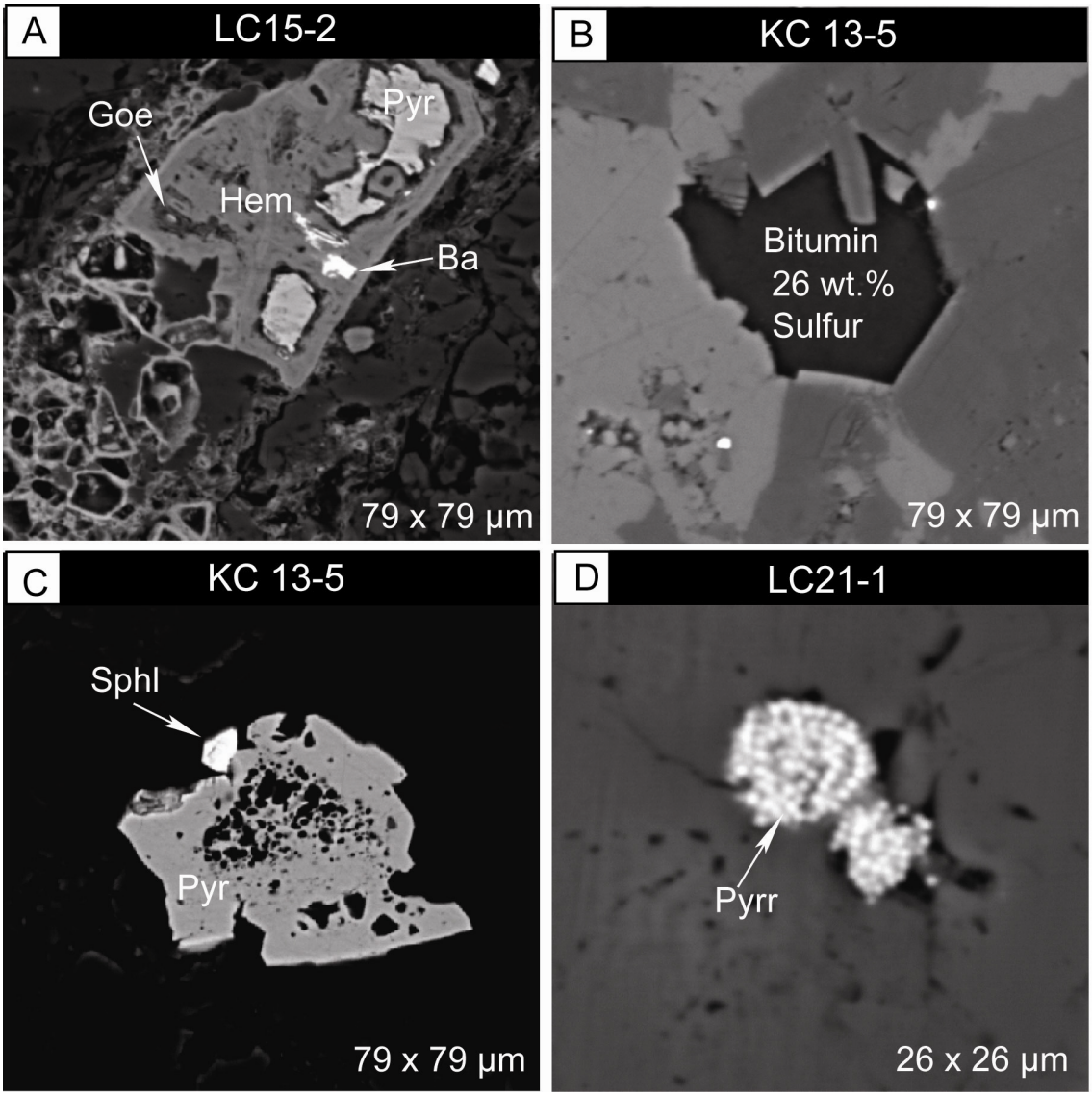

Figure 19: Electron backscatter images from host rock. A) Pyrite being replaced by hematite. B) Sulphar rich solid bitumen. C) Spahlerite on pyrite. D) Framboidal Pyrrhotite.

wide range of oxygen value suggests vein forming fluids which had variable range of high temperatures [e.g., Nelson et al., 2002], although the very low oxygen values may reflect equilibration with meteoric waters. Also observed in only three samples was a liner trend of increasingly negative carbon values linked to increasingly negative oxygen values (Figure 20).

5.9.2 $^{87}Sr/^{86}Sr$ Results

Strontium isotope data was collected from 17 samples to investigate possible fluid alteration. Out of the 15 samples from the Mississippian carbonates, 7 were host composed of calcite, 4 were host composed of dolomite, 2 were calcite veins and 2 were dolomite veins. Also one sample was tested from the Pennsylvanian-Permian Rock Mountain Super Group and one from the Triassic Sulphur Mountain Formation, both of which are dolomite rich rock. All Mississippian samples examined have elevated $^{87}Sr/^{86}Sr$ values when compared to coeval seawater values for Mississippian carbonates (Figure 21) [McArthur et al., 2001]. The calcite hosts have a mean value of 0.708128 ± 0.000006 and the dolomite hosts have a slightly lower mean value of 0.708040 ± 0.000006. The vein material shows similar results (calcite veins mean value of 0.707970 ± 0.000005 and the dolomite veins mean value of 0.708015 ± 0.000006). The Rock Mountain Super Group sample has a ratio which plots below the lower Pennsylvanian section of the seawater curve (Figure 21), while the Sulphur Mountain Formation sample plots much higher that the Triassic section of the seawater curve (Figure 21).

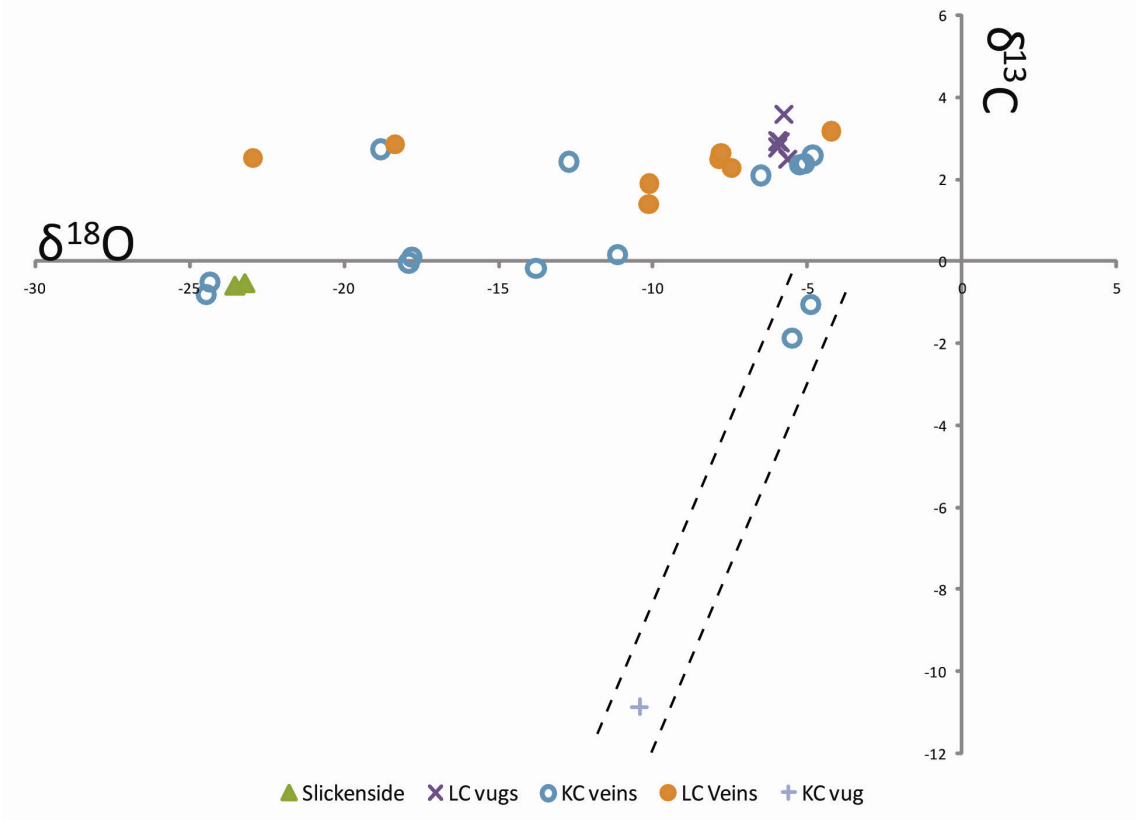

Figure 20: Plot of stable Carbon-Oxygen isotope results from veins, vugs and slickensides from both field areas.

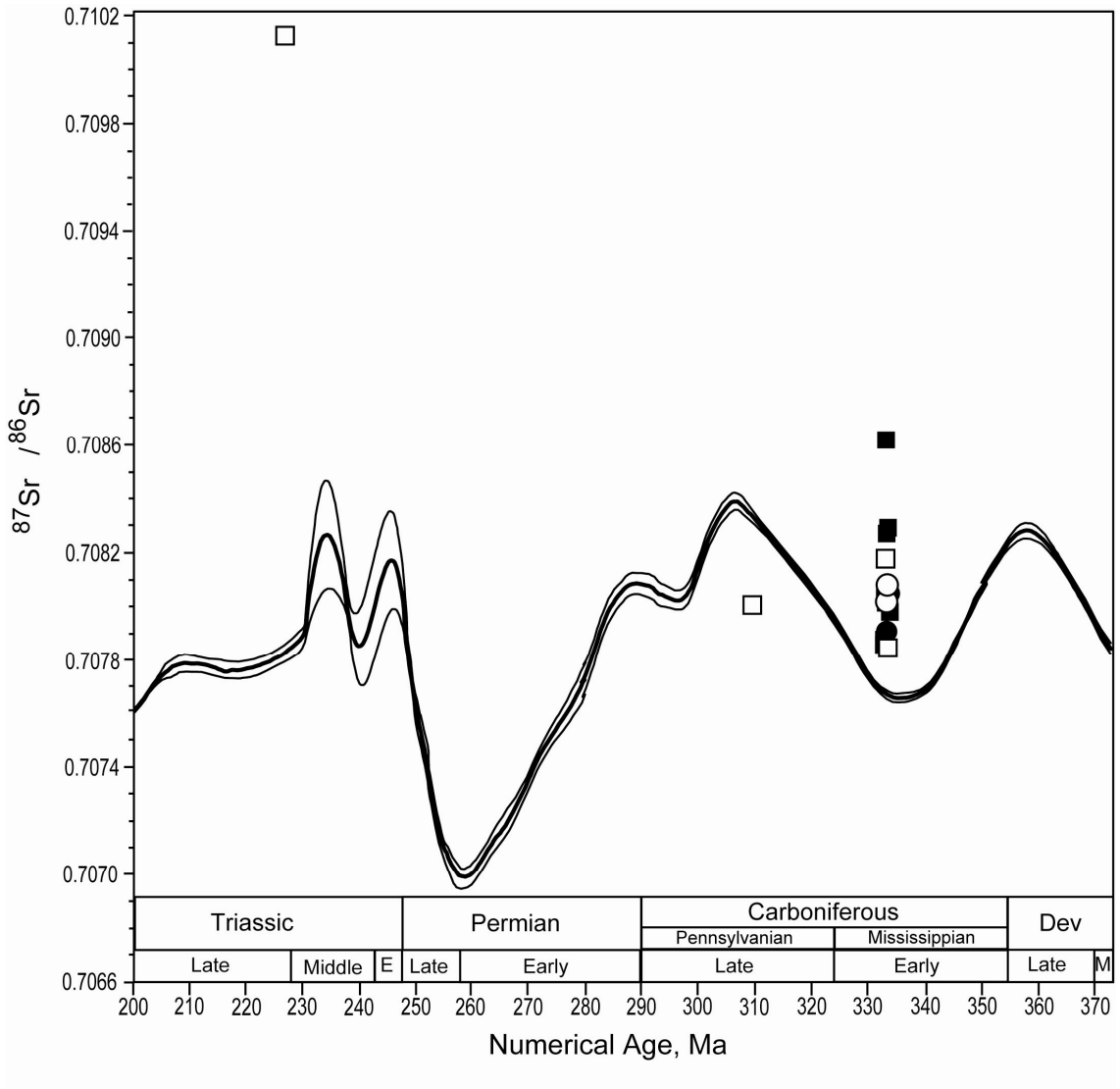

Figure 21: Plot of $^{87}Sr/^{86}Sr$ results for both host rock and vein material. Squares = Host carbonates; Circles indicate vein material; Solid symbols indicate calcite and open symbols indicate dolomite. Data plotted on the Triassic to Devonian coeval seawater curve (modified from MacArthur, 2001).

6. Discussion

Detailed paleomagnetic analysis has uncovered a multi-component remagnetization in organic rich Mississippian carbonates from two fault related folds. The folds are located within the Front Ranges of the Canadian Cordillera and the normal and reversed nature of the multiple remagnetization is similar to what has been observed in other areas of the Canadian Cordillera [e.g., Lewchuk et al., 1998; Enkin et al., 2000; Cioppa et al., 1999; Robion et al., 2004]. The ChRM in both folds is a normal polarity ChRM with a maximum unblocking temperature of 540°C and is interpreted as a CRM due to relatively low burial temperatures (180-250°C). This is based on magnetite relaxation time-unblocking temperature curves for SD grains [e.g., Middleton and Schmidt, 1982; Dunlop et al., 2000], which is applicable for are samples since the MD contribution has been removed by liquid nitrogen treatment. The second component is an IT reversed polarity component with a maximum unblocking temperature of 340°C. The maximum unblocking temperature, combined with the results of extensive rock magnetic experiments [Chaptere 2], indicates that this component resides in SD pyrrhotite. The pyrrhotite component is also considered to be a CRM based on the SD pyrrhotite relaxation time-unblocking temperature curves [Dunlop et al., 2000]. In previous studies the IT component has been interpreted to be a TVRM in magnetite [e.g., Enkin et al., 2000; Robion et al., 2004]. The results of Chapter 2 as well as this study, have demonstrated that the IT component resides in pyrrhotite as a CRM and is not a TVRM in magnetite.

The presence of pyrrhotite as a stable remanence carrier has important implications on what diagenetic processes may have affected a particular suite of rocks.

In recent years pyrrhotite has been increasingly recognized as an important carrier of a paleomagnetic signal [e.g., Dekkers et al., 1989; Rochette et al., 1990; Jackson et al., 1993; Xu et al., 1998; Crouzet et al., 2002; Weaver et al., 2002; Gillet and Karlin, 2004; Font et al., 2006; Preeden et al., 2008]. Pyrrhotite is considered an important redox indicator that may form as a result of diagenesis [Hall, 1986], and has been shown to be a useful in geothermometry [Dunlop et al., 2000; Schill et al., 2002]. One reason that pyrrhotite may have been discounted as a dominant remanence carrier in the past is due to the fact pyrrhotite and magnetite have overlapping room temperature coercivites. Another possible reason is because pyrrhotite may be interpreted as thermally remagnetized magnetite. Pyrrhotite is generally considered to have a maximum unblocking temperature of 325°C although temperatures as high as 350°C have been reported [Rochette et al., 1990], which may contribute to this misinterpretation. Jackson et al., [1993] has suggested that the Cenozoic TVRM widely reported throughout the Appalachian Fold and thrust belt may in fact be a CRM contained in pyrrhotite.

The Line Creek Anticline in BC contains an Early Cretaceous pre-tilting ChRM and at Mt. Kidd in Kananaskis Country, AB the ChRM appears to have formed also formed in the Early Cretaceous, as pre-tilting remagnetization in the anticline and an early syn-tilting remagnetization in the syncline. The fact that the pre-tilting result for the Mt. Kidd anticline has a paleopole that is significantly different than the pre-tilting Line Creek pole suggest that a structural complication may exist and will be discussed in detail in Chapter 3. The pyrrhotite component is syn-tilting at the Line Creek Anticline and post-tilting at Mt. Kidd. The timing based on the paleopole for the pyrrhotite component is inconclusive. The post-tilting CRM at Mt. Kidd appears to be

late Tertiary in age, however, the pole plots off of the path near the North Pole. This may be because the process forming the remagnetization occurred to rapidly and did not average out secular variation and will be discussed below. The syn-tilting Line Creek pole plots off the path near the Late Jurassic portion of the path. This would make it older than the pre-tilting magnetite pole. This may be due to secular variation not being averaged out or that sampling may have uncovered multiple remagnetization events. A Late Cretaceous pre-tilting single polarity normal component has also been observed in Pennsylvanian and Triassic rocks at Kent Anticline in Kananaskis Country. Based on unblocking temperatures and rock magnetic experiments the component is contained in magnetite, with no evidence for pyrrhotite observed.

These results raise an interesting question regarding the timing of deformation in the Kananaskis region. It is unlikely that the Mt. Kidd fold would have a syn-tilting remagnetization that was ~30Ma older than a pre-tilting remagnetization at Kent Anticline which is located only a few km's to the south. Also, an Early Cretaceous syn-tilting magnetization would predate the inferred initiation of movement of the McConnell Thrust which was Late Cretaceous-Eocene time [Price, 1981]. The age of motion along the Rundle and Sulphur Mountain thrusts containing each structure have also been determined to have occurred in the Late Cretaceous (68.4-72.7 Ma) using authogenic illite from fault gouge along the thrusts [van der Pluijm et al., 2006]. This supports the assertion that the Early Cretaceous syn-tilting nature of the Mt. Kidd syncline is the result of a strain or stress modification of a pre-tilting remagnetization, although the validity of using authogenic illite to date fault movement is currently under

debate [e.g., Price, 2007; Pevear et al., 2007]. The effect of strain/stress modification of pre-tilting remagnetizations will be discussed in detail in Chapter 3.

6.2 Origin of ChRM

The Mississippian carbonates examined from both field locations show elevated strontium isotope compared to Mississippian coeval seawater suggesting alteration by externally derived fluids. This coupled with the observation of a strong correlation between bedding parallel veins and the magnetite component provides evidence that the CRM contained in magnetite is the result of a regional pervasive fluid migration of evolved fluids. This is in direct contrast to a recent study which proposed that regional fluid flow was not sufficient to cause regional remagnetization in the Canadian Cordillera, opting for burial diagenesis as a possible mechanism [e.g., Machel and Cavall, 1999].

Hydrocarbon maturation [Cioppa and Symons, 2000] and clay diagenesis [Machel and Cavall, 1999] has been invoked as a remagnetization mechanisms in the Canadian Cordillera Burial clay diagenesis is not considered to be a likely remagnetization mechanism, due to a relatively negligible clay content observed in the samples. Dolomitization which has also been invoked as a possible remagnetization mechanism in the Canadian Cordillera [e.g., Lewchuk et al., 1998; Symons et al., 1998; Roure et al., 2005] can be discounted due to the presence of the magnetite component is in both limestones and dolostones at each locality. Even if direct dolomitization either early or late in the diagenetic history is not a source of remagnetization is still plays an important role by creating porosity for later fluid migration. This idea is highlighted by the fact that dolomitized mudstones and wackstones also contain the magnetite

component, which was probably aided by dolomitization which increased porosity and permeability.

Roure et al., [2005] proposed that recrystallization of fine crystalline dolomite during layer parallel shortening (LPS) in a low water circulation environment as the driving mechanism for regional remagnetization in the Canadian Cordillera. This model was based on the observation of a magnetic lineation based on anisotropy of magnetic susceptibility data, which correlated to LPS styolitic cleavage (Roure et al., 2005). Pressure solution due to LPS has been shown to lead to liberation of preexisting magnetic grains which then reorient within styolites leading to remagnetization [e.g., Evans et al, 2006; Olivia-Urica et al., 2007].

Since the timing of the ChRM relative to folding is considered pre-tilting at LC the fluids would have needed to migrate through these units prior to or just at the onset of deformation. Laramide deformation is believed to have initiated in the westernmost portion of the Alberta foreland Basin by around 135 Ma [Evenchick et al., 2007]. This suggests that the observed Early Cretaceous (~120 Ma; Aptian) remagnetization event could have been sourced from the Omencia highlands to the west and/or by the initiation Laramide shortening in the foreland fold and thrust belt. The origin of the fluids (meteoric or deep basinal) is unclear and it is not possible to determine which orogenic fluid flow mechanism (tectonically induced or gravitational recharge) was responsible.

The origin of the single polarity pre-tilting magnetite component in the Pennsylvanian and Triassic rocks at Kent Anticline is not clear. Preliminary Sr-isotope data from the Triassic dolomites are highly radiogenic while values from the

Pennsylvanian dolomites appear to be primary. Also the remagnetization is much younger (Late Cretaceous), which is difficult to reconcile with the Early Cretaceous regional fluid related remagnetization in the Mississippian carbonates. This along with the lack of any vein conduit tests makes it difficult to assess the potential of fluids being responsible for the remagnetization with the same amount of certainty as the Mississippian carbonates. One possibility is that the remagnetization is the result of a later and stratigraphically higher fluid migration event prior to deformation. In terms of the other possible remagnetization mechanisms, hydrocarbon migration and/or maturation can be ruled out since these units are devoid of degraded hydrocarbons (i.e. solid bitumen). On the other hand many of the beds do contain large amounts of clay so the smectite to illite transformation [e.g., Katz et al., 2000] is a plausible remagnetization mechanism. More detailed petrographic and geochemical studies as well as clay analysis needs to be conducted on these units in order to accurately determine the true remagnetization mechanism.

6.2 Origin of the IT Component

Authigenic pyrrhotite can carry a CRM in black shales and dark limestones and may be formed through multiple processes. Processes include the transformation of primary magnetite in the presence of pyrite and organic matter in the lower greenshist facies (~300°C) and the breakdown of pyrite around 400°C [Rochette, 1987]. Recently pyrrhotite has been shown to form during anaerobic oxidation of methane associated with gas hydrate dissociation in neogene sediments [Larrasoãna et al., 2007; van Dongen et al., 2007; Rowan and Roberts, 2008]. Another possibility is formation of pyrrhotite by bacterial sulphate reduction (BSR) or thermo sulphate reduction (TSR)

which converts hydrocarbons into sour gas [e.g., Pierce et al., 1998]. At Line Creek the burial temperatures did not exceed 180°C based on vitrinite reflectance data for the overlying Jurassic coals [~120°C; Per. Comm. J.Halko]. Slightly higher temperatures are observed at Mt. Kidd, but did not reach greenshist temperatures based on a lack of metamorphic minerals and calcite twin morphology [Ferrill et al., 2004], so low grade metamorphism can be ruled out. Sulphate reduction on the other hand has been known to have occurred throughout the Canadian Cordillera due to warm sulphate rich formational waters moving up along faults and fractures [e.g., Goldhaber and Reynolds, 1991; Pierce et al., 1998; Mountjoy et al., 1999] and could provide a viable remagnetization mechanism.

6.2.1 Process and products of TSR/BSR

Bacterial sulphate reduction occurs in low temperature diagenetic environments due to sulphate reducing bacteria (0-80°C) which above 80°C cease to metabolize [e.g., Machel and Foght, 2000]. TSR is the result of a redox-reaction that occurs during deep burial diagenesis within a temperature range of ~100 to 200°C through sulfate reduction of hydrocarbons with concomitant oxidation of the organic compounds [e.g. Machel 2001]. It is a common and widespread process within the Devonian-Mississippian carbonate reservoirs in Western Canada and is responsible for the formation of sour gas fields [Krouse et al., 1988; Hutcheon et al., 1995]. BSR and TSR form similar products and by-products and it can be difficult to separate the two processes. BSR and TSR processes require dissolved sulphate (SO_4^{2-}) that is derived from seawater, pore waters, or from dissolution of gypsum and anhydrite [Machel, 2001]. BSR and TSR occur when dissolved sulphate comes into contact with organic

compounds such as kerogen, crude oil, microbial methane, and thermogenic gas, and/or gas condensate. H_2S (sour gas) is the most abundant product [e.g. Machel, 1998a] and the amount of H_2S generated by TSR and BSR is controlled primarily by the availability of organic reactants and sulphate but also on the availability of base and transition metals, such as Fe, Pb, Zn, Mn, and metal sulfides. The most common metal sulfides produced are iron sulfides (pyrite and pyrrhotite), galena, and spahlerite can be produced. Due to the low solubility of metal sulfides, formation can occur even if only trace amounts of the metals are present [Machel, 2001]. BSR processes typically form greater amounts of iron sulfides due to an abundance of Fe in near surface diagenetic environments, whereas iron sulfides are rare by comparison as by-products of TSR due to availability of iron.

The most common iron sulfide observed in sour gas reservoirs is pyrite although pyrrhotite has recently been reported as a by-product of TSR [Pierce et al., 1998]. Carbonate precipitation is also common with calcite and dolomite being the most prominent phases formed by TSR and aragonite and calcite being the most common phases formed during BSR. Typical carbon isotope values are -25 to -30‰ PDB for BSR and as low as -12‰ PDB for TSR [Machel et al., 1995]. TSR calcites and dolomites are also characterized by elevated fluid inclusion temperatures. Other common by-products include elemental sulfur and sulfur enriched solid bitumen. The size and duration of TSR zones is controlled by the duration of physical contact between organic compound and sulphate, with data suggesting that formation occurs in narrow reaction zones (~10-100m) over a time scale of tens of thousands to hundreds of thousands years. BSR on the other hand is considered to be nearly instantaneous and

formation rates are extremely high in most geological settings although they can be relatively slow due to slow influx of one of the primary reactants.

6.2.2 Evidence for TSR/BSR as a remagnetization mechanism in the Canadian Cordillera

Evidence that TSR/BSR has occurred in the Mississippian carbonates comes from the observation of multiple common TSR/BSR by-products. These include authigenic pyrite, frambodial pyrrhotite, spahlerite, sulfur enriched bitumen (29.12 Wt% sulfur) within host dolomites and limestones, as well as, zoned dolomite crystals with elevated fluid inclusion temperatures (140-212°C). The $\delta^{13}C$ and $\delta^{18}O$ values for the majority of veins examined do not show evidence of TSR, however, 3 samples (2 veins and 1 Vug) display a linear trend represented by a increasingly negative $\delta^{18}O$ values coupled with a increasingly negative $\delta^{13}C$ values (Figure 21). The vug has $\delta^{13}C$ values near the maximum negative values observed in TSR dolomites (-10.87‰ PDB). This feature has been observed in other TSR calcite/dolomites [e.g., Machel and Cavell, 1999; Machel 2001; Vandeginste et al., 2009]. The majority of the veins examined have a narrow range of $\delta^{13}C$ (~-1 to +4‰ PDB) and heavily depleted $\delta^{18}O$ –isotopes (-10 to -25‰ PDB) which, do not directly reflect TSR water, but does reflects fluids with variable elevated temperatures [Nelson et al., 2002] and/or transfer of oxygen from the SO_4^{2-} into the CO_3^{2-} group [e.g., Machel, et al., 1995] which are required for TSR to occur.

Additional support for TSR/BSR as a remagnetization mechanism is based not on evidence of TSR/BSR, but on the absence of the pyrrhotite component in the Pennsylvanian and Triassic rocks at Kent Anticline. These units are located within Kananaskis Country only a few km's from Mt. Kidd, however, they have not been

affected by the same diagenetic event which created the pervasive pyrrhotite remagnetization within the Mississippian carbonates. The most probable reason for this is due to the fact that these units appear to lack the same concentration of organic matter which is a crucial reactant required for TSR/BSR. If TSR is indeed the cause of the pyrrhotite than a lack of organic matter would prohibit the formation of any TSR/BSR by-product, such as pyrrhotite.

6.2.3 Relationship of TSR to fluid migration along faults and fractures

It has been proposed that TSR is the result of warm fluids moving upwards along faults and fractures [e.g., Goldhaber and Reynolds, 1991; Pierce et al., 1998; Mountjoy et al., 1999]. In order to investigate this idea CL imaging was conducted on the vein conduit tests in order to investigate relationships between vein forming fluids with different Mn to Fe ratios and both the magnetite and pyrrhotite components. The bedding parallel calcite veins at Mt. Kidd have a red luminescence as does a late stage vug filling dolomite within the vein. The tectonic vein conduit test from the Line Creek Anticline shows an increase in the pyrrhotite intensities along with a decrease in the magnetite intensities when compared to unveined rock. The primary vein forming mineral is red luminenescent dolomite which is followed by a later calcite vein which displays a quenched luminescence. In order to form pyrrhotite TSR needs to have Fe in the system and there are several possible sources. First the late stage calcite fluids are quenched which means they contain more Fe relative to Mn [e.g., Marshall, 1988] and they may have been the source of the Fe which allowed TSR to produce the pyrrhotite component. Iron in organics or preexisting pyrite present in the rocks may also have been the source. Lastly, the intense tectonic veining probably resulted in a large enough

volume of warm sulphate rich water to be in contact with magnetite which could be the source of the Fe. This may have allowed the Fe in the magnetite to be consumed to form pyrrhotite during TSR. This may explain the drop in magnetite intensity in the highly veined zone. Since the pyrrhotite is a pervasive remagnetization, minor amounts of the warm fluids must have migrated out into the un-veined sections leading to pervasive TSR and formation of pyrrhotite at the expense of magnetite, although preserving enough magnetite to form the ChRM. The interpretation that fluids moving along fractures were responsible for the pyrrhotite component is important because it suggests that pyrrhotite formed prior to exhumation to shallow depths. This would suggest that pyrrhotite formation would have occurred as a result of TSR and not BSR.

6.2.4 Nature of TSR and its relationship to the timing of remagnetization

Based on the paleomagnetic, rock magnetic, petrographic, and geochemical data the most probable remagnetization mechanism for the pyrrhotite component is TSR. As a result paleomagnetic analysis may be a powerful tool in terms investigating the timing of TSR in important sour gas reservoirs. The nature of TSR, however, may lead to problems when trying to date these events using paleomagnetism. The first issue is the time span in which TSR occurs. TSR formation of sour gas reservoirs typically occurs over time periods of tens of thousands to hundreds of thousands of years under the right conditions and at most they may require a few million years [Goldhaber and Orr, 1995]. If TSR occurs at the lower end of the spectrum than it is possible that the formation of pyrrhotite may not average out secular variation, which is typically on the order of $\sim 10^5$ years. This may be reflected at Mt. Kidd by the fact that the paleopole plots off of the Late Tertiary portion of the path. Another issue relating to the nature of TSR is the

limited stratigraphic extent of TSR (~10-100m). This may result in multiple events occurring at different time intervals within a single structure. At Mt. Kidd the exposure of the units lead sampling to be confined to a relatively small vertical section within the structure. The results from the tilt-tests at Mt. Kidd gave a post-tilting remagnetization, which is what would be expected for a Late Tertiary TSR. At Line Creek, however, the exposure was much more expansive, allowing sampling across a stratigraphic section comprising several 100 meters. The results from the tilt test gave a syn-tilting result (~60% un-tilting). It is also possible that the stepwise demagnetization uncovered two separate post-tilting events in the front and back limb. If this is indeed the case attempting to perform a tilt-test on the entire structure would give erroneous results. Another unresolved issue is the overprint by a later pyrrhotite forming remagnetization event due to BSR during exhumation to shallow levels, which would further complicate the paleomagnetic signal. More work needs to be done to resolve these issues before paleomagnetic dating of TSR/BSR can be considered reliable.

7. Conclusions

Detailed Paleomagnetic analysis of three folds in the Front Ranges of the Canadian cordillera has uncovered a multi-component remagnetization in Mississippian carbonates at Mt. Kidd and at the Line Creek Anticline and a single component remagnetization in Pennsylvanian and Triassic rocks at Kent Anticline. Based on unblocking temperatures and rock magnetic experiments [Chapter 2], the ChRM observed at all three folds is a CRM contained in magnetite and the IT reversed component observed in the Mississippian carbonates is a CRM contained in pyrrhotite. The magnetite component is Early Cretaceous in both folds containing Mississippian

carbonates and is pre-tilting at the Line Creek Anticline. The remagnetization is early syn-tilting at Mt. Kidd syncline and pretilting in the Mt. Kidd anticline, although these results may be influenced by structural complications. The magnetite component at Kent Anticline is a Late Cretaceous pre-tilting magnetization. Both the Kent and Line Creek anticlines have the majority of their deformation taken up by flexural slip and brittle faulting/ fracturing. The Mt. Kidd structure shows that steepening and thinning of the east dipping limb was accommodated by ductile deformation. This coupled with the location of the paleopoles for the pre-tilting remagnetization at Kent Anticline, which appears ~30 Ma younger than the syn-tilting remagnetization at Mt. Kidd located only a few km to the north suggest that remagnetization at Mt. Kidd may have been altered by strain. Based on elevated Sr-isotopes in the host dolomites and limestones in the Mississippian carbonates and positive correlations between bedding parallel veins and the magnetite component, the most probable origin of the remagnetization is a regional fluid flow event related to the initiation of thrusting and folding in the Main Ranges of the foreland belt prior to the onset of Laramide deformation in the Front Ranges.

The origin of the pyrrhotite component observed in the Mississippian carbonates is consistent with warm Fe rich fluids migrating along faults and fractures causing TSR of hydrocarbons, which led to the formation of sour gas reservoirs. This model is based on the petrographic observation of multiple common by-products of TSR which include: authigenic pyrite, frambodial pyrrhotite, spahlerite, sulfur enriched bitumen and zoned dolomite crystals with elevated fluid inclusion temperature (140-212°C). The exact timing of pyrrhotite remagnetization is unclear due to the general

nature of TSR. At Mt. Kidd the pyrrhotite component is post-tilting and appears to be Late Tertiary in age.

Appendix

In order to perform this technique with the site mean data, the β axis of the fold was calculated using GEOrient 9.2 [Holcombe, 2005], once the plunge and trend of the fold was known, both the bedding orientation and the declination/inclination of the magnetizations were recalculated. This was accomplished by taking the pole to the bedding and importing this data into the SuperIAPD program as if it was declination and inclination data. Once the pole to the bedding data was imported the plunge and trend of the fold axis was converted to a strike and dip following the right-hand rule and the plunge was removed using the "bedding correction for the mean" option in SuperIAPD. Finally the corrected bedding was determined by converting the plunge corrected pole back to bedding. The bedding correction for the mean option was also used to remove the plunge from the site mean data. Once all the corrections had been applied, the data could be used in both of the aforementioned tilt tests. After the plunge corrected bedding and site mean data was untilted back to horizontal (stratigraphic position) the results were checked using GeoCalculator 4.9 [Holcombe, 2007], which allows for the un-tilting of beds around a fold axis while tracking a line on the surface.

References Cited

Al-Aasm, I. S. (2000), Chemical and isotopic constraints for recrystallization of sedimentary dolomites from the Western Canada Sedimentary Basin, Aquatic Geochemistry, 6(2), 227-248.

Banerjee, S., R. D. Elmore, and M. H. Engel (1997), Chemical remagnetization and burial diagenesis; testing the hypothesis in the Pennsylvanian Belden Formation, Colorado, Journal of Geophysical Research, 102(B11), 24,825-824,842.

Banerjee, S., D. Fruit, R. D. Elmore, and Anonymous (1995), CRM related to diagenesis of organic matter; Belden Formation, Colorado, International Union of Geodesy and Geophysics, General Assembly, 21, Week B, 137.

Banerjee, S., D. Fruit, R. D. Elmore, and Anonymous (1995), Orogenic fluids and regional chemical magnetizations, Belden Formation, Colorado, Annual Meeting Expanded Abstracts - American Association of Petroleum Geologists, 4, 6.

Bayona, G., W. A. Thomas, and R. Van der Voo (2003), Kinematics of thrust sheets within transverse zones; a structural and paleomagnetic investigation in the Appalachian thrust belt of Georgia and Alabama, Journal of Structural Geology, 25(8), 1193-1212.

Besse, J., and V. Courtillot (2002), Apparent and true polar wander and the geometry of the geomagnetic field over the last 200 Myr, Journal of Geophysical Research, 107, no.B11, 31.

Blumstein, A. M., R. D. Elmore, M. H. Engel, C. Elliot, and A. Basu (2004), Paleomagnetic dating of burial diagenesis in Mississippian carbonates, Utah, Journal of Geophysical Research, B, Solid Earth and Planets, 109, no.4, 16.

Blumstein, R. D., R. D. Elmore, M. H. Engel, J. Parnell, and M. Baron (2005), Multiple fluid migration events along the Moine thrust zone, Scotland, Journal of the Geological Society of London, 162(6), 1031-1045.

Borradaile, G. J. (1997), Deformation and paleomagnetism, Surveys in Geophysics, 18(4), 405-435.

Borradaile, G. J., K. Lucas, and R. S. Middleton (2004), Low-temperature demagnetization isolates stable magnetic vector components in magnetite-bearing diabase, Geophysical Journal International [Geophys. J. Int.]. 157(2), 526-536.

Bustin, R. M. (1991), Organic maturity in the Western Canada sedimentary basin, International Journal of Coal Geology, 19, 1-4.

Carr, S. D., and P. S. Simony (1993), Ductile thrusting versus channel flow in the southeastern Canadian Cordillera; evolution of a coherent crystalline thrust sheet, Geological Society Special Publications, D-1, 561-587.

Channell, J. E. T., and C. McCabe (1994), Comparison of magnetic hysteresis parameters of unremagnetized and remagnetized limestones, Journal of Geophysical Research, 99(B3), 4613-4623.

Cioppa, M. T., and D. T. A. Symons (2000), Timing of hydrocarbon generation and migration; paleomagnetic and rock magnetic analysis of the Devonian Duvernay Formation, Alberta, Canada, in Journal of Geochemical Exploration, vol.69-70, edited by J. J. Pueyo, E. Cardellach, K. Bitzer and C. Taberner, pp. 387-390, Elsevier, Amsterdam-New York.

Cioppa, M. T., D. T. A. Symons, and M. Flore (2002), Initial analysis of the Jurassic "Nordegg Member", Fernie Formation; using paleomagnetism to date source rock thermal maturation, in Physics and Chemistry of the Earth, edited by C. Aubourg, D. Elmore, A. Hirt, L. J. Pesonen, C. Peters, E. Petrovsky and R. Scholger, pp. 1161-1168, Pergamon, Oxford-New York-Toronto.

Cioppa, M. T., D. T. A. Symons, I. S. Al-Aasm, and K. P. Gillen (2002), Evaluating the timing of hydrocarbon generation in the Devonian Duvernay Formation;

paleomagnetic, rock magnetic and geochemical evidence, in Marine and Petroleum Geology, edited by I. S. Al-Aasm, I. C. Scotchman and H. Verweij, pp. 275-287, Elsevier, Oxford.

Cioppa, M. T., I. S. Al-Aasm, D. T. A. Symons, and K. P. Gillen (2003), Dating penecontemporaneous dolomitization in carbonate reservoirs; paleomagnetic, petrographic, and geochemical constraints, AAPG Bulletin, 87(1), 71-88.

Cioppa, M. T., I. S. Al-Aasm, D. T. A. Symons, M. T. Lewchuk, and K. P. Gillen (2000), Correlating paleomagnetic, geochemical and petrographic evidence to date diagenetic and fluid flow events in the Mississippian Turner Valley Formation, Moose Field, Alberta, Canada, Sedimentary Geology, 131(3-4), 109-129.

Cioppa, M. T., J. S. Lonnee, D. T. A. Symons, I. S. Al-Aasm, and K. P. Gillen (2001), Facies and lithological controls on paleomagnetism; an example from the Rainbow South Field, Alberta, Canada, Bulletin of Canadian Petroleum Geology, 49(3), 393-407.

Cioppa, M. T., J. Lonnee, D. T. A. Symons, I. S. Al-Aasm, K. P. Gillen, and Anonymous (2000), Dating dolomitization/recrystallization events using petrologic, geochemical and paleomagnetic techniques, in AAPG Bulletin, edited, p. 1381, American Association of Petroleum Geologists, Tulsa.

Cox, E., R. D. Elmore, and M. Evans (2005), Paleomagnetism of Devonian red beds in the Appalachian Plateau and Valley and Ridge Provinces, Journal of Geophysical Research, 110, no.B8, 16.

Crouzet, C., P. Gautam, E. Appel, and E. Schill (2001), Discussion on new paleomagnetic results from Tethyan Himalaya (western Nepal); tectonic and geodynamic implications, in Journal of Asian Earth Sciences, edited by B. Grasemann and K. Stuewe, p. 11, Pergamon, Oxford.

Crouzet, C., P. Gautam, E. Schill, and E. Appel (2003), Multicomponent magnetization in western Dolpo (Tethyan Himalaya, Nepal); tectonic implications, in Tectonophysics, edited by A. Morris and J. Tait, pp. 179-196, Elsevier, Amsterdam.

Davidson, M., J. Egger, R. D. Elmore, M. H. Engel, S. D. Woods, and M. Abraham (2000), Orogenic fluids and secondary magnetizations; testing the relationship in the South Wales Coalfield foreland basin, Journal of Geochemical Exploration, 69-70, 581-584.

Davies, G. R. (1997), The Triassic of the Western Canada sedimentary basin; tectonic and stratigraphic framework, paleogeography, paleoclimate and biota, Bulletin of Canadian Petroleum Geology, 45(4), 434-460.

Dekkers, M. J. (1988), Magnetic properties of natural pyrrhotite; Part I, Behaviour of initial susceptibility and saturation-magnetization-related rock-magnetic parameters in a grain-size dependent framework, in Physics of the Earth and Planetary Interiors, edited by F. Heller, K. M. Storetvedt and J. D. A. Zijderveld, pp. 376-393, Elsevier, Amsterdam.

Dekkers, M. J. (1989), Magnetic properties of natural pyrrhotite; II, High- and low-temperature behaviour of J (sub rs) and TRM as function of grain size, Physics of the Earth and Planetary Interiors, 57(3-4), 266-283.

Dekkers, M. J., P. Rochette, and G. L. Nord, Jr. (1990), Magnetic monitoring of pyrrhotite alteration during thermal demagnetization, in Geophysical Research Letters, edited, pp. 779-782, American Geophysical Union, Washington.
Dekkers, M. J., J. L. Mattei, G. Fillion, and P. Rochette (1989), Grain-size dependence of the magnetic behavior of pyrrhotite during its low-temperature transition at 34 K, Geophysical Research Letters, 16(8), 855-858.
Denison, R. E., R. B. Koepnick, W. H. Burke, E. A. Hetherington, and A. Fletcher (1994), Construction of the Mississippian, Pennsylvanian and Permian seawater (super 87) Sr/ (super 86) Sr curve, Chemical Geology, 112, 1-2.
Elmore, R.D, J. Lee-Egger Foucher, M. Evans, M. Lewchuk, and E. Cox (1062), Remagnetization of the Tonoloway Formation and the Helderberg Group in the Central Appalachians: testing the origin of syntilting magnetizations, Geophysical Journal International [Geophys. J. Int.]. 166(3), 1062-1076.
Dulin, S., and R. D. Elmore (2008), Paleomagnetism of the Weaubleau Structure, southwestern Missouri, Special Paper - Geological Society of America, 437, 55-64.
Dunham, R. J. (1962), Classification of carbonate rocks according to depositional texture, Memoir American Association of Petroleum Geologists, pp.
Dunlop, D. J., and K. S. Argyle (2007), Separating multidomain and single-domain-like remanences in pseudo-single-domain magnetites (215-540 nm) by low-temperature demagnetization, Journal of Geophysical Research, 96(B2), 2007-2017.
Dunlop, D. J., O. Ozdemir, D. A. Clark, and P. W. Schmidt (2000), Time-temperature relations for the remagnetization of pyrrhotite (Fe (sub 7) S (sub 8)) and their use in estimating paleotemperatures, Earth and Planetary Science Letters, 176(1), 107-116.

Edwards, D. E., J. E. Barclay, D. W. Gibson, G. E. Kvill, and E. Halton (Eds.) (1994), Triassic strata of the Western Canada sedimentary basin, 259-275 pp., Geological Survey of Canada, Calgary, aB.
Ehrlich, H. L. Geomicrobiology.
Elmore, R. D., and M. C. Leach (1990), Remagnetization of the Rush Springs Formation, Cement, Oklahoma; implications for dating hydrocarbon migration and aeromagnetic exploration, Geology, 18(2), 124-127.
Elmore, R. D., and Anonymous (1993), Chemical remagnetization and paleomagnetic dating of fluid migration events; testing the orogenic fluid hypothesis, AAPG Bulletin, 77(11), 2019-2020.
Elmore, R. D., K. Cates, G. Gao, and L. Land (1994), Geochemical constraints on the origin of secondary magnetizations in the Cambro-Ordovician Royer Dolomite, Arbuckle Mountains, southern Oklahoma, Physics of the Earth and Planetary Interiors, 85(1-2), 3-13.
Elmore, R. D., J. Kelley, M. Evans, and M. T. Lewchuk (2001), Remagnetization and orogenic fluids; testing the hypothesis in the Central Appalachians, Geophysical Journal International, 144(3), 568-576.

Elmore, R. D., R. Blumstein, M. Engel, and J. Parnell (2003), Palaeomagnetic dating of fluid flow events along the Moine thrust fault, Scotland, Journal of Geochemical Exploration, 78-79(2003), 45-49.

Elmore, R. D., J. L.-E. Foucher, M. Evans, M. Lewchuk, and E. Cox (2006), Remagnetization of the Tonoloway Formation and the Helderberg Group in the Central Appalachians; testing the origin of syntilting magnetizations, Geophysical Journal International, 166(3), 1062-1076.

Enkin, R. J. (2003), The direction-correction tilt test; an all-purpose tilt/fold test for paleomagnetic studies, Earth and Planetary Science Letters, 212, 1-2.

Enkin, R. J. (2004), Paleomagnetism Data Analysis: Version 4.2. Geological Survey of Canada. *On* www.pgc.nrcan.gc.ca/tectonic/enkin.htm.

Enkin, R. J., and G. S. Watson (1996), Statistical analysis of palaeomagnetic inclination data, Geophysical Journal International, 126(2), 495-504.

Enkin, R. J., K. G. Osadetz, J. Baker, and D. Kisilevsky (2000), Orogenic remagnetizations in the front ranges and inner foothills of the southern Canadian Cordillera; chemical harbinger and thermal handmaiden of Cordilleran deformation, Geological Society of America Bulletin, 112(6), 929-942.

Evans, M. A., and R. D. Elmore (2006), Fluid control of localized mineral domains in limestone pressure solution structures, Journal of Structural Geology, 28(2), 284-301.

Evans, M. A., R. D. Elmore, and M. T. Lewchuk (2000), Examining the relationship between remagnetization and orogenic fluids; central Appalachians, in Journal of Geochemical Exploration, vol.69-70, edited by J. J. Pueyo, E. Cardellach, K. Bitzer and C. Taberner, pp. 139-142, Elsevier, Amsterdam-New York.

Evans, M. A., R. D. Elmore, and M. T. Lewchuk (2000), Examining the relationship between remagnetization and orogenic fluids; central Appalachians, Journal of Geochemical Exploration, 69-70, 139-142.

Evenchick, C. A., M. E. McMechan, V. J. McNicoll, and S. D. Carr (2007), A synthesis of the Jurassic–Cretaceous tectonic evolution of the central and southeastern Canadian Cordillera: Exploring links across the orogen, GSA Special Papers 2007, 433, 117-145.

Fermor, P. R., and I. W. Moffat (1992), Tectonics and structure of the Western Canada foreland basin, AAPG Memoir, 55, 81-105.

Ferrill, D. A., A. P. Morris, M. A. Evans, M. Burkhard, R. H. Groshong, Jr., and C. M. Onasch (2004), Calcite twin morphology; a low temperature deformation geothermometer, Journal of Structural Geology, 26(8), 1521-1529.

Fisher, R. A. (1953), Dispersion on a sphere, *Proc. R. Soc. London, Ser. A, 217*, 295-305.

Font, E., R. I. F. Trindade, and A. Nedelec (2006), Remagnetization in bituminous limestones of the Neoproterozoic Araras Group (Amazon craton); hydrocarbon maturation, burial diagenesis, or both?, Journal of Geophysical Research, 111, no.B6, 17.

Fruit, D., R. D. Elmore, M. Engel, S. W. Imbus, M. Leach, and Anonymous (1991), Hydrocarbons and magnetizations in sedimentary rocks, in AAPG Bulletin, edited, p. 577, American Association of Petroleum Geologists, Tulsa.

Gao, G., R. D. Elmore, and L. S. Land (1992), Geochemical constraints on the origin of calcite veins and associated limestone alteration, Ordovician Viola Group, Arbuckle Mountains, Oklahoma, U.S.A, Chemical Geology, 98, 3-4.

Ge, S., and G. Garven (1994), A theoretical model for thrust-induced deep groundwater expulsion with application to the Canadian Rocky Mountains, Journal of Geophysical Research, 99(B7), 851-813.

Gill, J. D., R. D. Elmore, and M. H. Engel (2002), Chemical remagnetization and clay diagenesis; testing the hypothesis in the Cretaceous sedimentary rocks of northwestern Montana, in Physics and Chemistry of the Earth, edited by C. Aubourg, D. Elmore, A. Hirt, L. J. Pesonen, C. Peters, E. Petrovsky and R. Scholger, pp. 1131-1139, Pergamon, Oxford-New York-Toronto.

Gill, J. D., R. D. Elmore, and M. H. Engel (2002), Chemical remagnetization and clay diagenesis; testing the hypothesis in the Cretaceous sedimentary rocks of northwestern Montana, Physics and Chemistry of the Earth, 27(25-31), 1131-1139.

Gillett, S. L. (2003), Paleomagnetism of the Notch Peak contact metamorphic aureole, revisited; pyrrhotite from magnetite+pyrite under submetamorphic conditions, Journal of Geophysical Research, 108, no.B9, 11.

Gillett, S. L., and Anonymous (1990), Paleomagnetism of the Notch Peak contact metamorphic aureole, revisited; pyrrhotite CRM and implications for magnetite preservation during deep burial, Eos, Transactions, American Geophysical Union, 71(43), 1285.

Gillett, S. L., and Anonymous (1991), Low-temperature formation of pyrrhotite from magnetite (super +) pyrite; evidence from low-grade metamorphism and implications for magnetite preservation during deep burial, in AAPG Bulletin, edited, p. 581, American Association of Petroleum Geologists, Tulsa.

Gillett, S. L., and Anonymous (1991), Low-temperature formation of pyrrhotite from magnetite (super +) pyrite; evidence from low-grade metamorphism and implications for magnetite preservation during deep burial, AAPG Bulletin, 75(3), 581.

Gillett, S. L., and R. E. Karlin (2004), Pervasive late Paleozoic-Triassic remagnetization of miogeoclinal carbonate rocks in the Basin and Range and vicinity, SW USA; regional results and possible tectonic implications, Physics of the Earth and Planetary Interiors, 141(2), 95-120.

Goldhaber, M. B., and R. L. Reynolds (1991), Relations among hydrocarbon reservoirs, epigenetic sulfidization, and rock magnetization; examples from the South Texas coastal plain, Geophysics, 56(6), 748-757.

Goldhaber, M. B., and W. L. Orr (1995), Kinetic Controls on Thermochemical Sulfate Reduction as a Source of Sedimentary H~2S, American Chemical Society Symposium Series, 612 412-425.

Grabowski, J., and J. Nawrocki (2001), Palaeomagnetism of some Devonian carbonates from the Holy Cross Mts. (central Poland); large pre-Permian rotations or strain modified palaeomagnetic directions?, Geological Quarterly, 45(2), 165-178.

Gray, M. B., and J. Stamatakos (1997), New model for evolution of fold and thrust belt curvature based on integrated structural and paleomagnetic results from the Pennsylvania Salient, Geology, 25(12), 1067-1070.

Halgedahl, S. L., and J. Ye (2000), Observed effects of mechanical grain-size reduction on the domain structure of pyrrhotite, Earth and Planetary Science Letters, 176(3-4), 457-467.
Hall, A. J. (1986), Pyrite-pyrrhotite redox reactions in nature, Mineralogical Magazine, 50, Part 2(356), 223-229.
Hardebol, N. J., J.-P. Callot, J.-L. Faure, G. Bertotti, and F. Roure (Eds.) (2007), Kinematics of the SE Canadian fold-and-thrust belt; implications for the thermal and organic maturation history, 179-202 pp., Springer Berlin Heidelberg.
Harrison, R. J., and J. M. Feinberg (2008), FORCinel: An improved algorithm for calculating first-order reversal curve distributions using locally weighted regression smoothing, Geochemistry, Geophysics, Geosystems G, 9(5).
Hirt, A. M., K. F. Evans, and T. Engelder (1995), Correlation between magnetic anisotropy and fabric for Devonian shales on the Appalachian Plateau, Tectonophysics, 247(1-4), 121-132.
Hitchon, B. (1984), Geothermal gradients, hydrodynamics, and hydrocarbon occurrences, Alberta, Canada, AAPG Bulletin, 72(11), 1395-1410.
Horng, C.-S., and A. P. Roberts (2006), Authigenic or detrital origin of pyrrhotite in sediments? Resolving a paleomagnetic conundrum, Earth and Planetary Science Letters, 241(3-4), 750-762.
Housen, B. A., S. K. Banerjee, B. M. Moskowitz, and V. Courtillot (1996), Low-temperature magnetic properties of siderite and magnetite in marine sediments, Geophysical Research Letters, 23(20), 2843-2846.
Hudson, M. R., R. L. Reynolds, and N. S. Fishman (1989), Synfolding magnetization in the Jurassic Preuss Sandstone, Wyoming-Idaho-Utah thrust belt, Journal of Geophysical Research, 94(B10), 13,681-613,705.
Hunt, C. P., S. K. Banerjee, J. Han, P. A. Solheid, E. Oches, W. Sun, and T. Liu (1995), Rock-magnetic proxies of climate change in the loess-Palaeosol sequences of the western Loess Plateau of China, Geophysical Journal International, 123(1), 232-244.
Hutcheon, I., J. Cody, G. Simpson, S. McLellan, and H. Abercrombie (1995), Sulfate reduction, reservoir properties, H (sub 2) S and sulfur (S) in natural gas, Annual Meeting Expanded Abstracts American Association of Petroleum Geologists, 4(46).
Jackson, M. (1990), Diagenetic sources of stable remanence in remagnetized Paleozoic cratonic carbonates; a rock magnetic study, Journal of Geophysical Research, 95(B3), 2753-2761.
Jackson, M., and H.-U. Worm (2001), Anomalous unblocking temperatures, viscosity and frequency-dependent susceptibility in the chemically-remagnetized Trenton Limestone, in Physics of the Earth and Planetary Interiors, edited by D. J. Dunlop and M. Prevot, pp. 27-42, Elsevier, Amsterdam.
Jackson, M., H.-U. Worm, and S. K. Banerjee (1990), Fourier analysis of digital hysteresis data; rock magnetic applications, Physics of the Earth and Planetary Interiors, 65(1-2), 78-87.
Jackson, M. J., W. Sun, and J. P. Craddock (1992), The rock magnetic fingerprint of chemical remagnetization in midcontinental Paleozoic carbonates, Geophysical Research Letters, 19(8), 781-784.

Jackson, M., C. McCabe, M. M. Ballard, and R. Van der Voo (1988), Magnetite authigenesis and diagenetic paleotemperatures across the northern Appalachian Basin, Geology, 16(7), 592-595.

Jackson, M., J. P. Craddock, M. M. Ballard, R. Van der Voo, and C. McCabe (1989), Anhysteretic remanent magnetic anisotropy and calcite strains in Devonian carbonates from the Appalachian Plateau, New York, Tectonophysics, 161(1-2), 43-53.

Jackson, M., P. Rochette, G. Fillion, S. Banerjee, and J. Marvin (1993), Rock magnetism of remagnetized Paleozoic carbonates; low-temperature behavior and susceptibility characteristics, Journal of Geophysical Research, 98(B4), 6217-6225.

Kalkreuth, W., and M. E. McMechan (1395), Burial history and thermal maturity, Rocky Mountain Front Ranges, foothills, and foreland, east-central British Columbia and adjacent Alberta, Canada, AAPG Bulletin, 72(11), 1395-1410.

Kalkreuth, W., and M. E. McMechan (1988), Burial history and thermal maturity, Rocky Mountain Front Ranges, foothills, and foreland, east-central British Columbia and adjacent Alberta, Canada, AAPG Bulletin, 72(11), 1395-1410.

Katz, B., R. D. Elmore, and M. H. Engel (1998), Authigenesis of magnetite in organic-rich sediment next to a dike; implications for thermoviscous and chemical remagnetizations, Earth and Planetary Science Letters, 163(1-4), 221-234.

Katz, B., R. D. Elmore, M. Cogoini, and S. Ferry (1998), Widespread chemical remagnetization; orogenic fluids or burial diagenesis of clays?, Geology, 26(7), 603-606.

Katz, B., D. R. Elmore, M. Cogoini, M. H. Engel, and S. Ferry (2000), Associations between burial diagenesis of smectite, chemical remagnetization, and magnetite authigenesis in the Vocontian Trough, SE France, Journal of Geophysical Research, 105(B1), 851-868.

Kent, D. V. (1985), Thermoviscous remagnetization in some Appalachian limestones, Geophysical Research Letters, 12(12), 805-808.

Kent, D. V. (1988), Further paleomagnetic evidence for oroclinal rotation in the central folded Appalachians from the Bloomsburg and the Mauch Chunk formations, Tectonics, 7(4), 749-759.

Kilgore, B., and R. D. Elmore (1989), A study of the relationship between hydrocarbon migration and the precipitation of authigenic magnetic minerals in the Triassic Chugwater Formation, southern Montana, Geological Society of America Bulletin, 101(10), 1280-1288.

Kirschvink, J. L. (1980), The least-squares line and plane and the analysis of palaeomagnetic data, Geophysical Journal of the Royal Astronomical Society, 62(3), 699-718.

Kodama, K. P. (1988), Remanence rotation due to rock strain during folding and the stepwise application of the fold test, Journal of Geophysical Research, 93(B4), 3357-3371.

Krouse, H. R., C. A. Viau, L. S. Eliuk, A. Ueda, and S. Halas (1988), Chemical and isotopic evidence of thermochemical sulphate reduction by light hydrocarbon gases in deep carbonate reservoirs, Nature, 333(6172), 415-419.

Kruiver, P. P., M. J. Dekkers, and D. Heslop (2001), Quantification of magnetic coercivity components by the analysis of acquisition curves of isothermal remanent magnetisation, Earth and Planetary Science Letters, 189(3-4), 269-276.

Larrasoaña, J. C., A. P. Roberts, R. J. Musgrave, E. Gracia, E. Pinero, M. Vega, and F. Martinez-Ruiz (2007), Diagenetic formation of greigite and pyrrhotite in gas hydrate marine sedimentary systems, Earth and Planetary Science Letters, 261(3-4), 350-366.

Lewchuk, M. T., R. D. Elmore, and M. Evans (2002), Remagnetization signature of Paleozoic sedimentary rocks from the Patterson Creek Mountain Anticline in West Virginia, in Physics and Chemistry of the Earth, edited by C. Aubourg, D. Elmore, A. Hirt, L. J. Pesonen, C. Peters, E. Petrovsky and R. Scholger, pp. 1141-1150, Pergamon, Oxford-New York-Toronto.

Lewchuk, M. T., R. D. Elmore, and M. Evans (2002), Remagnetization signature of Paleozoic sedimentary rocks from the Patterson Creek Mountain Anticline in West Virginia, Physics and Chemistry of the Earth, 27(25-31), 1141-1150.

Lewchuk, M. T., M. Evans, and R. D. Elmore (2003), Synfolding remagnetization and deformation; results from Paleozoic sedimentary rocks in West Virginia, Geophysical Journal International, 152(2), 266-279.

Lewchuk, M. T., M. Evans, and R. Douglas Elmore (2003), Synfolding remagnetization and deformation: results from Paleozoic sedimentary rocks in West Virginia, Geophysical Journal International [Geophys. J. Int.]. 152(2), 266-279.

Lewchuk, M. T., I. S. Al-Aasm, D. T. A. Symons, and K. P. Gillen (1998), Dolomitization of Mississippian carbonates in the Shell Waterton gas field, southwestern Alberta; insights from paleomagnetism, petrology and geochemistry, Bulletin of Canadian Petroleum Geology, 46(3), 387-410.

Lewchuk, M. T., I. S. Al-Aasm, D. T. A. Symons, and K. P. Gillen (2000), Late Laramide dolomite recrystallization of the Husky Rainbow "A" hydrocarbon Devonian reservoir, northwestern Alberta, Canada; paleomagnetic and geochemical evidence, Canadian Journal of Earth Sciences = Revue Canadienne des Sciences de la Terre, 37(1), 17-29.

Lowrie, W. (1990), Identification of ferromagnetic minerals in a rock by coercivity and unblocking temperature properties, Geophysical Research Letters, 17(2), 159-162.

Machel, H. G. (1974), Bacterial and thermochemical sulfate reduction in diagenetic settings; old and new insights, Sedimentary Geology, 58(11), 2295-2318.

Machel, H. G. (1989), Saddle dolomite as a by-product of chemical compaction and thermochemical sulfate reduction, Carbonates and Evaporites, 4(2), 137-152.

Machel, H. G. (1991), Relationships between sulphate reduction and oxidation of organic compounds to carbonate diagenesis, hydrocarbon accumulations, salt domes, and metal sulphide deposits, Bulletin of Canadian Petroleum Geology, 39(2), 219.

Machel, H. G. (1998), Gas souring by thermochemical sulfate reduction at 140 degrees C; discussion, AAPG Bulletin, 82(10), 1870-1873.

Machel, H. G. (1999), Gas souring by thermochemical sulfate reduction at 140 degrees C; discussion, Bulletin of Canadian Petroleum Geology, 47(4), 487-509.

Machel, H. G. (2001), Thermochemical sulfate reduction in the Devonian Nisku Formation, Alberta, Canada; a unique sour gas play with generally applicable characteristics, Sedimentary Geology, 140(1-2), 143-175.
Machel, H. G., and E. W. Mountjoy (1987), General constraints on extensive pervasive dolomitization and their application to the Devonian carbonates of Western Canada, Bulletin of Canadian Petroleum Geology, 15(10), 936-940.
Machel, H. G., and E. A. Burton (1991), Chemical and microbial processes causing anomalous magnetization in environments affected by hydrocarbon seepage, Geophysics, 56(5), 598-605.
Machel, H. G., and P. A. Cavell (1999), Low-flux, tectonically-induced squeegee fluid flow ("hot flash") into the Rocky Mountain foreland basin, Bulletin of Canadian Petroleum Geology, 47(4), 510-533.
Machel, H. G., and J. Foght (2000), Products and depth limits of microbial activity in petroliferous subsurface settings.
Machel, H. G., and J. Foght (Eds.) (2000), Products and depth limits of microbial activity in petroliferous subsurface settings, 106-120 pp., Springer-Verlag Berlin Heidelberg.
Machel, H. G., H. R. Krouse, and R. Sassen (1995), Products and distinguishing criteria of bacterial and thermochemical sulfate reduction, Applied Geochemistry, 108(9), 1108-1119.
Machel, H. G., P. A. Cavell, and K. S. Patey (1997), Isotopic evidence for carbonate cementation and recrystallization, and for tectonic expulsion of fluids into the Western Canada Sedimentary Basin, Bull. Geol. Soc. Am., 27(7-8), 507-521.
Machel, H. G., P. A. Cavell, B. E. Buschkuehle, and K. Michael (2000), Tectonically induced fluid flow in Devonian carbonate aquifers of the Western Canada Sedimentary Basin, AAPG Bulletin, 84(9), 1458-1459.
Manzano, B. K., M. G. Fowler, and H. G. Machel (1998), The influence of thermochemical sulphate reduction on hydrocarbon composition in Nisku reservoirs, Brazeau River area, Alberta, Canada, Organic Geochemistry, 82(10), 1870-1873.
Marshak, S., and G. Mitra (Eds.) (1988), Basic methods of structural geology; Part 1, Elementary techniques; Part 2, Special topics, 446 pp., Prentice-Hall, Englewood Cliffs, NJ, United States (USA).
Marshall, D. J. (Ed.) (1988), Cathodoluminescence of geological materials, 146 pp., Allen Unwin.
McArthur, J. M., R. J. Howarth, and T. R. Bailey (2001), Strontium isotope stratigraphy; LOWESS Version 3; best fit to the marine Sr-isotope curve for 0-509 Ma and accompanying look-up table for deriving numerical age, Journal of Geology, 109(2), 155-170.
McCabe, C., and Anonymous (1988), Mountain building, regional diagenesis, and magnetite authigenesis in Alleghenian foredeep, in AAPG Bulletin, edited, p. 220, American Association of Petroleum Geologists, Tulsa.
McCabe, C., and R. D. Elmore (1989), The occurrence and origin of late Paleozoic remagnetization in the sedimentary rocks of North America, Reviews of Geophysics, 27(4), 471-494.

McCabe, C., and J. E. T. Channell (1994), Late Paleozoic remagnetization in limestones of the Craven Basin (northern England) and the rock magnetic fingerprint of remagnetized sedimentary carbonates, Journal of Geophysical Research, 99(B3), 4603-4612.

McCabe, C., M. Jackson, and B. Saffer (1989), Regional patterns of magnetite authigenesis in the Appalachian Basin; implications for the mechanism of late Paleozoic remagnetization, Journal of Geophysical Research, 94(B8), 10,429-410,443.

McCabe, C., R. Van der Voo, D. R. Peacor, C. R. Scotese, and R. Freeman (1983), Diagenetic magnetite carries ancient yet secondary remanence in some Paleozoic sedimentary carbonates, Geology, 11(4), 221-223.

McMechan, M. E., and R. I. Thompson (Eds.) (1989), Structural style and history of the Rocky Mountain fold and thrust belt, 47-71 pp., Can. Soc. Pet. Geol., Calgary, AB, Canada, Calgary, AB.

McMechan, M. E. (1995), Geology Rocky Mountain Foothills and Front Ranges in Kananaskis Country, Alberta, Geological Survey of Canada GSC1865A.

Menyeh, A., and W. O'Reilly (1998), Thermoremanence in monoclinic pyrrhotite particles containing few domains, Geophysical Research Letters, 25(18), 3461-3464.

Michael, K., S. Bachu, and H. G. Machel (2000), Groundwater flow in response to ground surface topography, erosional rebound, and hydrocarbon generation in Cretaceous strata in the Alberta Basin, Canada, Journal of Geochemical Exploration, 69(70), 213-217.

Middleton, M. F., and P. W. Schmidt (1982), Paleothermometry of the Sydney Basin, Journal of Geophysical Research, 87(B7), 5351-5359.

Miller, J. D., and D. V. Kent (1986), Paleomagnetism of the Upper Devonian Catskill Formation from the southern limb of the Pennsylvania Salient; possible evidence of oroclinal rotation, Geophysical Research Letters, 13(11), 1173-1176.

Miller, J. D., and D. V. Kent (1988), Regional trends in the timing of Alleghanian remagnetization in the Appalachians, Geology, 16(7), 588-591.

Monger, J. W. H., and R. A. Price (1979), Geodynamic evolution of the Canadian Cordillera; progress and problems, Canadian Journal of Earth Sciences = Revue Canadienne des Sciences de la Terre, 16(3, Part 2), 771-791.

Mountjoy, E. W., J. E. Amithor, and H. G. Machel (1991), A new look at Leduc dolomites; implications for fluid-flow systems, AAPG Bulletin, 76(7), 1093-1094.

Mountjoy, E. W., D. Green, H. G. Machel, J. Duggan, and A. E. Williams-Jones (2000), Devonian matrix dolomites and deep burial carbonate cements; a comparison between the Rimbey-Meadowbrook reef trend and the deep basin of west-central Alberta, Journal of Geochemical Exploration, 69(70), 657-661.

Mountjoy, E. W., D. Green, H. G. Machel, J. Duggan, A. E. Williams-Jones, and Anonymous (1999), Devonian matrix dolomites and deep burial carbonate cements; a comparison between the Rimbey-Meadowbrook reef trend and the deep basin of west-central Alberta, Bulletin of Canadian Petroleum Geology, 47(4), 487-509.

Muttoni, G. (1995), "Wasp-waisted" hysteresis loops from a pyrrhotite and magnetite-bearing remagnetized Triassic limestone, Geophysical Research Letters, 22(23), 3167-3170.
Nelson, J., S. Paradis, J. Christensen, and J. Gabites (2002), Canadian Cordilleran Mississippi valley-type deposits; a case for Devonian-Mississippi back-arc hydrothermal origin, Economic Geology and the Bulletin of the Society of Economic Geologists, 97(5), 1013-1036.
Norris, D. K. (1965), Stratigraphy of the Rocky Mountain Group in the southeastern Cordillera of Canada, Bulletin Geological Survey of Canada, 82.
O'Brien, V. J., K. M. Moreland, R. D. Elmore, M. H. Engel, and M. A. Evans (2007), Origin of orogenic remagnetizations in Mississippian carbonates, Sawtooth Range, Montana, Journal of Geophysical Research, 112(B6).
Oliva-Urcia, B., E. L. Pueyo, and J. C. Larrasoaña (2008), Magnetic reorientation induced by pressure solution: A potential mechanism for orogenic-scale remagnetizations, Earth and Planetary Science Letters, 265, 525-534.
Oliver, J. (1986), Fluids expelled tectonically from orogenic belts; their role in hydrocarbon migration and other geologic phenomena, Geology, 14(2), 99-102.
O'Reilly, W. O., V. Hoffmann, A. C. Chouker, H. C. Soffel, and A. Menyeh (2000), Magnetic properties of synthetic analogues of pyrrhotite ore in the grain size range 1-24 mu, Geophysical Journal International, 142(3), 669-683.
Orr, W. L. (1974), Changes in Sulfur Content and Isotopic Ratios of Sulfur during Petroleum Maturation; Study of Big Horn Basin Paleozoic Oils, AAPG Bulletin, 68(6), 713-743.
Orr, W. L., M. B. Goldhaber, and Anonymous (1995), H (sub 2) S abundance in natural gas with emphasis on thermochemical sulfate reduction, Annual Meeting Expanded Abstracts American Association of Petroleum Geologists, 4(73).
Ozdemir, O., and D. J. Dunlop (2000), Intermediate magnetite formation during dehydration of goethite, Earth and Planetary Science Letters, 177(1-2), 59-67.
Ozdemir, O., D. J. Dunlop, and B. M. Moskowitz (1993), The effect of oxidation on the Verwey transition in magnetite, Geophysical Research Letters, 20(16), 1671-1674.
Pares, J. M., and B. A. van der Pluijm (2002), Evaluating magnetic lineations (AMS) in deformed rocks, Tectonophysics, 350(4), 283-298.
Pares, J. M., and B. A. van der Pluijm (2004), Correlating magnetic fabrics with finite strain; comparing results from mudrocks in the Variscan and Appalachian orogens, Geologica Acta, 2(3), 213-220.
Parry, L. G. (1982), Magnetization of immobilized particle dispersions with two distinct particle sizes, Physics of the Earth and Planetary Interiors, 28(3), 230-241.
Peck, C., R. D. Elmore, and R. L. DuBois (1986), Early and late Paleozoic remagnetization of the Cambrian Peerless Formation, Colorado, Physics of the Earth and Planetary Interiors, 43(4), 274-282.
Peters, C., and M. J. Dekkers (2003), Selected room temperature magnetic parameters as a function of mineralogy, concentration and grain size, in Physics and Chemistry of the Earth, edited by E. Petrovsky, M. Urbat and T. von Dobeneck, pp. 659-667, Pergamon, Oxford-New York-Toronto.

Pierce, J.W., S.A. Goussev, R.A. Charters, H.J. Ambercrombie and G.R. DePaoli (1998), Intrasedimentary magnetization by vertical fluid flow and exotic geochemistry, The Leading Edge, January 1998 .

Poulton, T. P., W. K. Braun, M. M. Brooke, and E. H. Davies (Eds.) (1993), Jurassic, sub chapter 4H, 321-357 pp., Geological Survey of Canada, Geology of Canada.

Preeden, U., J. Plado, S. Mertanen, and V. Puura (2008), Multiply remagnetized Silurian carbonate sequence in Estonia, Estonian Journal of Earth Sciences, 57(3), 170-180.

Price, R. A. (2007), Fault Dating in the Canadian Rocky Mountains: Evidence for late Cretaceous and eatly Eocene orogenic pulses: Comment, Geology, 34.

Price, R. A. (1981), The Cordilleran foreland thrust and fold belt in the southern Canadian Rocky Mountains, Special Publication Geological Society of London, no, 9(9), 427-448.

Price, R. A., and E. W. Mountjoy (1970), Geologic structure of the Canadian rocky mountains between bow and Athabasca rivers - a progress report, Special Paper Geological Association of Canada, pp, 7-25.

Price, R. A., D. A. Grieve, and C. Patenaude (1992), Geology, Tornado Mountain British Columbia-Alberta, Geological Survey of Canada. GSC1823A

Price, R. A., G. D. Mossop, and I. Shetsen (Eds.) (1994), Cordilleran tectonics and the evolution of the Western Canada sedimentary basin, 2-24 pp., Geological Survey of Canada, Calgary, AB.

Quidelleur, X., J.-P. Valet, and N. Thouveny (1992), Multicomponent magnetization in paleomagnetic records of reversals from continental sediments in Bolivia, Earth and Planetary Science Letters, 111(1), 23-39.

Roberts, A. P. (1995), Magnetic properties of sedimentary greigite (Fe (sub 3) S (sub 4)), Earth and Planetary Science Letters, 134(3-4), 227-236.

Robion, P., and G. J. Borradaile (2001), Stress remagnetization in pyrrhotite-calcite synthetic aggregates, Geophysical Journal International, 144(1), 96-104.

Rochette, P. (1987), Metamorphic control of the magnetic mineralogy of black shales in the Swiss Alps; toward the use of "magnetic isograde", Earth and Planetary Science Letters, 84(4), 446-456.

Rochette, P., G. Fillion, J.-L. Mittei, and M. J. Dekkers (1990), Magnetic transition at 30-34 Kelvin in pyrrhotite; insight into a widespread occurrence of this mineral in rocks, Earth and Planetary Science Letters, 98(3-4), 319-328.

Root, K. G. (2001), Devonian Antler fold and thrust belt and foreland basin development in the southern Canadian Cordillera; implications for the Western Canada Sedimentary Basin, Bulletin of Canadian Petroleum Geology, 268, 561-587.

Ross, G. M., G. E. Gehrels, and P. J. Patchett (1997), Provenance of Triassic strata in the Cordilleran miogeocline, Western Canada, Bulletin of Canadian Petroleum Geology, 45(4), 461-473.

Roure, F., R. Swennen, F. Schneider, J.L. Faure, H. Ferket, N. Guilhaumou, K. Osadetz, P. Robion and V. Vandeginste (2005), Incidence and importance of tectonics and natural fluid migration on reservoir evolution in foreland fold-and-thrust belts, Oil & Gas Science and Technology, 60, (1), 67-106.

Rowan, C. J., and A. P. Roberts (2008), Widespread remagnetizations and a new view of Neogene tectonic rotations within the Australia-Pacific plate boundary zone, New Zealand, Journal of Geophysical Research, 113(B3).

Saffer, B., and C. McCabe (1992), Further studies of carbonate remagnetization in the northern Appalachian Basin, Journal of Geophysical Research, 97(B4), 4331-4348.

Schill, E., E. Appel, and P. Gautam (2002), Towards pyrrhotite/magnetite geothermometry in low-grade metamorphic carbonates of the Tethyan Himalayas (Shiar Khola, central Nepal), in Journal of Asian Earth Sciences, edited by C. Wang, C. J. L. Wilson and M. P. Searle, pp. 195-201, Pergamon, Oxford.

Schill, E., E. Appel, O. Zeh, V. K. Singh, and P. Gautam (2001), Coupling of late-orogenic tectonics and secondary pyrrhotite remanences; towards a separation of different rotation processes and quantification of rotational underthrusting in the western Himalaya (northern India), Tectonophysics, 337(1-2), 1-21.

Schill, E., E. Appel, L. Godin, C. Crouzet, P. Gautam, and K. R. Regmi (2003), Record of deformation by secondary magnetic remanences and magnetic anisotropy in the Nar-Phu Valley (central Himalaya), in Tectonophysics, edited by A. Morris and J. Tait, pp. 197-209, Elsevier, Amsterdam.

Schill, E., E. Appel, C. Crouzet, P. Gautam, F. Wehland, and M. Staiger (2004), Oroclinal bending versus regional significant clockwise rotations in the Himalayan arc; constraints from secondary pyrrhotite remanences, Special Paper - Geological Society of America, 383, 73-85.

Stamatakos, J., and K. P. Kodama (1991), Flexural flow folding and the paleomagnetic fold test; an example of strain reorientation of remanence in the Mauch Chunk Formation, Tectonics, 10(4), 807-819.

Stamatakos, J., and A. M. Hirt (1994), Paleomagnetic considerations of the development of the Pennsylvania Salient in the Central Appalachians, Tectonophysics, 231(4), 237-255.

Stamatakos, J., A. M. Hirt, and W. Lowrie (1996), The age and timing of folding in the Central Appalachians from paleomagnetic results, Geological Society of America Bulletin, 108(7), 815-829.

Suk, D., and S. L. Halgedahl (1996), Hysteresis properties of magnetic spherules and whole rock specimens from some Paleozoic platform carbonate rocks, Journal of Geophysical Research, 101(B11), 25,053-025,076.

Suk, D., R. Van der Voo, and D. R. Peacor (1992), SEM/STEM observation of magnetic minerals in presumably unremagnetized Paleozoic carbonates from Indiana and Alabama, Tectonophysics, 215(3-4), 255-272.

Suk, D., R. Van der Voo, D. R. Peacor, and T. Torgersen (1991), SEM/STEM observations of magnetite in carbonates of eastern North America; evidence for chemical remagnetization during the Alleghenian Orogeny, in Geophysical Research Letters, edited, pp. 939-942, American Geophysical Union, Washington.

Suk, D., R. Van der Voo, D. R. Peacor, and K. C. Lohmann (1993), Late Paleozoic remagnetization and its carrier in the Trenton and Black River carbonates from the Michigan Basin, Journal of Geology, 101(6), 795-808.

Sun, W., and M. Jackson (1994), Scanning electron microscopy and rock magnetic studies of magnetic carriers in remagnetized early Paleozoic carbonates from Missouri, Journal of Geophysical Research, 99(B2), 2935-2942.
Sun, W., M. Jackson, and J. P. Craddock (1993), Relationship between remagnetization, magnetic fabric and deformation in Paleozoic carbonates, Tectonophysics, 221(3-4), 361-366.
Symons, D. T. A., and M. T. Cioppa (2002), Conodont CAI and magnetic mineral unblocking temperatures; implications for the Western Canada Sedimentary Basin, in Physics and Chemistry of the Earth, edited by C. Aubourg, D. Elmore, A. Hirt, L. J. Pesonen, C. Peters, E. Petrovsky and R. Scholger, pp. 1189-1193, Pergamon, Oxford-New York-Toronto.
Symons, D. T. A., and M. T. Cioppa (2002), Conodont CAI and magnetic mineral unblocking temperatures; implications for the Western Canada Sedimentary Basin, Physics and Chemistry of the Earth, 27(25-31), 1189-1193.
Symons, D. T. A., M. T. Lewchuk, and D. F. Sangster (1998), Laramide orogenic fluid flow into the Western Canada sedimentary basin; evidence from paleomagnetic dating of the Kicking Horse Mississippi valley-type ore deposit, Economic Geology and the Bulletin of the Society of Economic Geologists, 93(1), 68-83.
Symons, D. T. A., R. J. Enkin, and M. T. Cioppa (1999), Paleomagnetism in the Western Canada sedimentary basin; dating and fluid flow and deformation events, Bulletin of Canadian Petroleum Geology, 47(4), 534-547.
Symons, D. T. A., M. J. Harris, C. J. R. Hart, W. H. Blackburn, F. Cook, and P. Erdmer (1998), Geotectonics in the Northern Cordillera from paleomagnetism and geobarometry; progress report and recent results from the Eocene White Pass dikes and Jurassic Fourth of July Batholith, Lithoprobe Report, Report, 64, 171-180.
Tauxe, L., T. A. T. Mullender, and T. Pick (1996), Potbellies, wasp-waists, and superparamagnetism in magnetic hysteresis, Journal of Geophysical Research, 101(B1), 571-583.
van der Pluijm, B. A., P. J. Vrolijk, D. R. Pevear, C. M. Hall, and J. Solum (2006), Fault dating in the Canadian Rocky Mountains: Evidence for late Cretaceous and early Eocene orogenic pulses, Geology, 34(10), 837-840.
van Dongen, B. E., A. P. Roberts, S. Schouten, W.-T. Jiang, F. Florindo, and R. D. Pancost (2007), Formation of iron sulfide nodules during anaerobic oxidation of methane, Geochimica et Cosmochimica Acta, 71(21), 5155-5167.
Vandeginste, V., R. Swennen, S. A. Gleeson, R. M. Ellam, K. Osadetz, and F. Roure (1987), Zebra dolomitization as a result of focused fluid flow in the Rocky Mountains Fold and Thrust Belt, Canada, Sedimentology, 35(2), 143-158.
Vandeginste, V., R. Swennen, S. A. Gleeson, R. M. Ellam, K. Osadetz, and F. Roure (2009), Thermochemical sulphate reduction in the Upper Devonian Cairn Formation of the Fairholme carbonate complex (South-West Alberta, Canadian Rockies): evidence from fluid inclusions and isotopic data, Sedimentology, 56(2), 439-460.
Vandeginste, V., R. Swennen, S. A. Gleeson, R. M. Ellam, K. Osadetz, and F. Roure (2009), Thermochemical sulphate reduction in the Upper Devonian Cairn Formation of the Fairholme carbonate complex (South-West Alberta, Canadian

Rockies): evidence from fluid inclusions and isotopic data, Sedimentology, 56(2), 439-460.
Watson, G. S., and R. J. Enkin (1993), The fold test in paleomagnetism as a parameter estimation problem, Geophysical Research Letters, 20(19), 2135-2137.
Weaver, R., A. P. Roberts, and A. J. Barker (2002), A late diagenetic (syn-folding) magnetization carried by pyrrhotite; implications for paleomagnetic studies from magnetic iron sulphide-bearing sediments, Earth and Planetary Science Letters, 200(3-4), 371-386.
Wehland, F., A. Stancu, P. Rochette, M. J. Dekkers, and E. Appel (2005), Experimental evaluation of magnetic interaction in pyrrhotite bearing samples, Physics of the Earth and Planetary Interiors, 153(4), 181-190.
Weil, A. B., and R. Van der Voo (2002), Insights into the mechanism for orogen-related carbonate remagnetization from growth of authigenic Fe-oxide; a scanning electron microscopy and rock magnetic study of Devonian carbonates from northern Spain, Journal of Geophysical Research, 107, no.B4, 15.
Weil, A. B., and R. Van der Voo (2002), The evolution of the paleomagnetic fold test as applied to complex geologic situations, illustrated by a case study from northern Spain, in Physics and Chemistry of the Earth, edited by C. Aubourg, D. Elmore, A. Hirt, L. J. Pesonen, C. Peters, E. Petrovsky and R. Scholger, pp. 1223-1235, Pergamon, Oxford-New York-Toronto.
Weissenberger, J. A. W., K. Potma, W. Kalkreuth, and M. E. McMechan (2001), Burial history and thermal maturity, Rocky Mountain Front Ranges, foothills, and foreland, east-central British Columbia and adjacent Alberta, Canada, Bulletin of Canadian Petroleum Geology, 49(1), 7-36.
Woods, S. D., R. D. Elmore, and M. H. Engel (2000), The occurrence of pervasive chemical remanent magnetizations in sedimentary basins; implications for dating burial diagenetic events, in Journal of Geochemical Exploration, vol.69-70, edited by J. J. Pueyo, E. Cardellach, K. Bitzer and C. Taberner, pp. 381-385, Elsevier, Amsterdam-New York.
Xu, W., R. Van der Voo, and D. R. Peacor (1998), Electron microscopic and rock magnetic study of remagnetized Leadville carbonates, central Colorado, Tectonophysics, 296(3-4), 333-362.
Ye, J., and S. L. Halgedahl (2000), Theoretical effects of mechanical grain-size reduction on GEM domain states in pyrrhotite, Earth and Planetary Science Letters, 178(1-2), 73-85.
Zegers, T. E., M. J. Dekkers, and S. Bailly (2003), Late Carboniferous to Permian remagnetization of Devonian limestones in the Ardennes; role of temperature, fluids, and deformation, Journal of Geophysical Research, 108, no.B7, 19.
Zijderveld, J. D. A. (1967), A.c. demagnetization of rocks: analysis of results. *In* Collinson, D.E. et al., eds., Methods in Paleomagnetism. New York, Elsevier Science, pp. 254-286.

.

Chapter 4: Testing the origin of a syn-tilting remagnetization in Mississippian Carbonates from the Canadian Cordillera, using Small Circle and Calcite Strain analysis

Zechmeister[a], M.S., Evans[b], M.A., & Elmore[a], R.D.

[a]*The ConocoPhillips School of Geology and Geophysics, the University of Oklahoma, Norman, OK 73019, USA (*zechmeim@ou.edu; delmore@ou.edu*

[b]*Department of Physics and Earth Science, Central Connecticut State University, New Britain, CT 06050*

Abstract

The use of conventional tilt tests in studies in fold and thrust belts has been shown to be a powerful tool when investigating pre- and post tilting results. In the case of syn-tilting, however, many structural complications such as block rotations, small out of plane bedding rotations, spurious rotations of magnetic vectors, and strain/stress alterations exist which are undetected using conventional tilt tests. To address this issue, an integrated study of the results from conventional tilt tests, small circle intersection analysis (SCI), and calcite twin strain has been conducted on two folds containing a multi-component remagnetization in Mississippian carbonates within the Front Ranges of the Southern Canadian Cordillera. The results of this study show that the Line Creek anticline acquired a high temperature chemical remanent magnetization (CRM) in the Early Cretaceous (~Aptian) prior to folding. The Line Creek anticline represents an ideal fold for paleomagnetic analysis. This fold formed under low to moderate burial temperatures (170-180°C) and low deviatoric strain (0.27-0.84%) via kink folding and brittle processes during transportation of the hanging wall over a simple frontal ramp. On the other hand, the Mt. Kidd anticline-syncline contains multiple structural complications that affect the high temperature CRM. These structural complications create discrepancies between the conventional tilt tests and SCI

analysis in terms of the untilting percentages and age determination. The primary structural complications involve subtle out of plane rotations or spurious rotations within certain sites which were only identified using the SCI analysis. This analysis indicates that the portion of the Mt. Kidd anticline was complicated by imbricate thrust sheets and therefore is not valid for paleomagnetic analysis. Removal of sites from the east dipping limb which appeared to be rotated with respect to the other sites within the Mt. Kidd syncline data set removed the discrepancies between the conventional tilt tests and the SCI analysis. This allowed for the determination of an early syn-tilting remagnetization. The origin of the syn-tilting result is attributed to either strain modification or spurious rotation of a pre-tilting high temperature CRM. The Mt. Kidd syncline formed under high burial temperatures (≥ 200°C) and high deviatoric strain (3.6-8.7%) via ductile deformation during transportation over a frontal and oblique ramp. The conventional tilt tests and SCI analysis of the intermediate temperature chemical remanent magnetization at the Line Creek anticline yielded a Late Jurassic syn-tilting result which is attributed to either secular variation not being averaged out or multiple remagnetization events. The intermediate temperature CRM at the Mt. Kidd syncline is a Late Tertiary post tilting remagnetization event that has not been influenced by any structural complications.

1. Introduction

When a magnetization is acquired from a single depositional or diagenetic event it forms a resultant vector which is considered to be similar to a lineation. This allows paleomagnetists to infer the timing of magnetization relative to folding within fold and thrust belts by determining when these remanence vectors achieve parallelism which

represents the paleofield at the time of acquisition (e.g., Hudson et al., 1989; McFadden, 1990; Stamatokos et al., 1996; Enkin et al., 2000; Lewchuk et al., 2003; O'Brien et al., 2007; Shipunov et al., 2008). This is accomplished by applying an incremental bedding correction or tilt test (e.g., Watson and Enkin, 1993; Enkin, 2003). The tilt test is one of the more powerful field tests in paleomagnetism and has had many formulations since the original test was developed by Graham (1949), however, all follow the basic assumption that untilting of two opposing limbs occurs around a single horizontal axis via rigid body rotation. If parallelism is achieved without any bedding correction (i.e. in situ or geographic position) the magnetization is considered to have been acquired post folding. If parallelism is achieved after bedding has been corrected to horizontal (i.e. tilt corrected or stratigraphic position) the magnetization is considered to have been acquired pre-tilting. Tilt corrections can also result in crossover geometries with parallelism achieved at an intermediate stage of folding and are referred to as syn-tilting remagnetizations (e.g., Scotese and Van der Voo, 1983). Syn-tilting remagnetizations are common, but the origin and usefulness such secondary magnetizations has been debated (e.g., McFadden, 1998; Weil et al., 2002; Elmore et al., 2006).

The objective of this study is to investigate the origin of syn-tilting remagnetizations within asymmetrical folds in the Front Ranges of the Canadian Cordillera. Critical attention will be paid to the results obtained from multiple tilt tests utilized in this study. The syn-tilting nature of these folds has been previously established in Chapter 2 using the optimal cluster (OC) tilt test (Watson and Enkin, 1993) and direction correction (DC) tilt tests (Enkin, 2003). In order to gain a clearer picture regarding the origin of syn-tilting remagnetizations, small circle intersection

(SCI) analysis (Shipunov, 1997; Waldhöer and Appel, 2006) was conducted on the aforementioned data set in conjunction with fold kinematic analysis and calcite twin strain analysis (e.g., Groshong, 1974). This integrated study will be used to evaluate the results of the conventional tilt tests as well as to investigate if any structural complexities such as block rotations and internal stress/strain have biased the results.

2. Origin of syn-tilting magnetizations

Syn-tilting remagnetization have been recognized from various fold and thrust belts from around the world and three major classes have been recognized (e.g., Hudson et al., 1989). The first class is considered to be a "true" syn-tilting remagnetizations, which formed during the actual folding process, either by: (1) chemical precipitation of magnetic minerals (e.g., Kent and Opdyke, 1985), (2) thermal resetting of preexisting magnetic minerals, (e.g., Kent, 1985), or (3) stress enhanced acquisition of piezoremanent magnetization (PRM; e.g. Hudson et al., 1989; Borradaile, 1997). "True" syn-tilting remagnetizations are considered the only geologically significant class, however, incremental tilt test results are not unique when folding is not symmetrical, particularly in asymmetrical folds. The second class is a contaminated syntilting result due to unresolved combinations of pre-, syn- and post-tilting remagnetizations with similar coercivity and unblocking characteristics (e.g., Miller & Kent, 1988; Hudson et al., 1989). The third class is remagnetizations resulting from structural modification of pre-tilting magnetization via strain. Several models have been proposed to explain such modifications. For example, over steepening of fold limbs during shear slip folding (e.g., Tarling, 1983) or the concentration and rotation of preexisting magnetic minerals within styolites (Olivia-Ulric et al., 2007). Grain scale strain has also been proposed to

have a direct impact, by deflection of preexisting magnetizations due to: (1) remanence vectors behaving as passive markers which are deflected during internal strain (Kligfield et al., 1983; Hirt et al., 1986; Kodama, 1988). (2) Physical reorientation of magnetic grains by rigid body rotation during layer parallel shear (e.g., Van der Pluijm, 1987; Kodama, 1988) or during mechanical twining of calcite within grains or along grain boundaries (e.g., Evans et al., 2003). Contamination due to multiple remagnetizations or stress/strain modifications of pre-tilting magnetizations create "false" syn-tilting results. Interpreting a "false" syn-tilting result as a "true" syn-tilting result may lead to erroneous amounts of inferred vertical axis rotation as well as erroneous timing of folding/faulting and/or diagenetic alteration events. Although strain studies are commonly performed in fold and thrust belts, relatively few paleomagnetic studies have integrated strain/stress studies with tilt test results (Kodama, 1988; Hudson et al., 1989; Stamatokos and Kodama, 1991; Lewchuk et al., 2003; Evans et al., 2003; Elmore et al., 2006).

Apart from direct stress and strain alteration of preexisting magnetizations several structural complications related to fold kinematics can influence tilt test results and also generate erroneous results (e.g., Stewart, 1995; Pueyo et al., 2003; Waldhöer and Appel, 2006). Commonly folds have inclined fold axis with the plunge forming concurrent with folding or by a subsequent overall tilt. Inclined fold axes can be resolved by removing the plunge and subsequent untilting around the resultant horizontal fold axis as long as the plunge forms by rotation of each limb around lines parallel to a fold hinge. If the structure in question is an interference fold formed by rotation around non-parallel horizontal axis, then complications arise because multiple

fold hinges may exist, making determination of the correct fold hinge for rotation difficult (e.g., Stewart, 1995). Numerical modeling of paleomagnetic vectors that are transported in hanging wall over footwall ramps geometries has also shown that interactions between frontal and oblique ramps can lead to the formation of spurious rotations of paleomagnetic vectors (Pueyo et al., 2003). Vertical axis rotations formed either by oroclinal bending (e.g., Van der Voo et al., 1997; Weil et al., 2002) or block rotation (e.g., Aubourg & Chabet-Peliline, 1999; Grabowoski & Nawrocki, 2001) can also significantly alter paleomagnetic vectors. Recently, subtle out of plane bedding rotations (Waldhöer and Appel, 2006) and layer parallelization (Waldhöer and Appel, 2009) have been proposed to have a profound effect on paleomagnetic vectors. In order to gain geologically significant paleomagnetic information from fold and thrust belts each one of these issues need to be evaluated.

3. Evolution of Tilt Tests

As stated above paleomagnetic tilt tests have undergone several modifications since their inception, and will be briefly summarized below. For a more detailed explanation of the modification of tilt tests over the years see Weil et al. (2002; and references therein). The initial tilt test was simple and was based on the rotation of measured vectors around a local strike to investigate pre-and post tilting magnetizations (Graham, 1949). This test, however, lacked statistical criteria for assessing the significance of the tilt test results. This led McElhinny (1964) to modify this test by introducing Fisher (1953) k-parameter statistics to estimate the degree of clustering of directional data on a sphere, in order to investigate the significance of a particular result. The significance tilt tests, however, only investigate the nature of pre- and post tilting

magnetizations and did not provide information on magnetizations acquired during folding (i.e., syn-tilting). This led to the development of an incremental tilt test (Scotese and Van der Voo, 1983) which calculated the statistical significance of various clusters at an incremental stage of untilting. The incremental test was subsequently modified to rely more on optimal clustering estimation which determined confidence limits from Fisher statistics as opposed to statistical significance (e.g., Tauxe et al., 1991; Watson and Enkin, 1993). McFadden, (1998) argued that although the optimal clustering tilt tests were simple and relatively intuitive they were flawed by the assumption that magnetizations are most tightly clustered when the beds are tilted to their proper orientation at the time of acquisition, which may result in the erroneous observation of syn-tilting magnetizations. Instead, McFadden (1998) argued for a test which is based on correlation between distributions of both magnetic directions and tectonic information, by investigating the correlation of the cluster of two groups of Fisher-distributed site means on opposing limbs. One disadvantage to this type of test is that it requires very detailed and strategic sampling (McFadden and Jones, 1981; McFadden, 1990). Enkin, (2003) addressed this issue by creating the Direction Correction (DC) tilt test which combines the correlation test (McFadden, 1990) with optimal clustering tilt tests (Watson and Enkin, 1993). This test involves a graph showing whether or not the geographic site mean directions are correlated to their corresponding bedding tilt corrections. The DC tilt test offers an analytical rather than numerical method of determining optimal degree of untilting. As an alternative to conventional tilt tests, several authors have proposed a test based on the intersection of remanence small circles which follow the path of remanence vectors during tilt

correction. This approach can be used to investigate the effect of structural complications and assess the validity of results determined from conventional tilt tests (McClelland-Brown, 1983; Shipunov, 1997; Waldhöer and Appel, 2006). Another form of SCI analysis was proposed by Enkin et al. (2000), which used optimal differential untilting (ODU) to determine the greatest concentration of vectors during untilting, Unfortunately details on the procedure was not published in detail. SCI has not been widely implemented in the paleomagnetic community even though it has been shown to be rather sensitive to many issues related to fold geometry and vertical axis rotations (e.g., Henry et al., 2004; Waldhöer and Appel, 2006).

The concept of SCI analysis is explained in detail in Shipunov (1997) and Waldhöer and Appel (2006). It is based on the motion of remanence vectors within a particular bed as a bedding correction is applied and the concept is displayed in Figure 1. During untilting the bedding pole moves along the π-circle of bedding (e.g., Ramsay and Huber, 1987) while the remanence vector moves along a parallel small circle tied to a particular bed, termed the remanence small circle. Remanence small circles tilted to different directions will intersect at a common point indicating the paleofield direction during acquisition (Figure 1B; McClelland-Brown, 1983; Shipunov, 1997; Waldhöer and Appel, 2006). This method is not applicable to perfectly cylindrical folds because the small circles will never intersect, however in nature the majority of folds have significant variations in bedding strike which does create a sufficient number of small circle intersections (Waldhöer and Appel, 2006). The paleofield direction at the time of magnetization is determined using a least squares method, which means that the paleofield direction during acquisition is retained in the small circle at the point closest

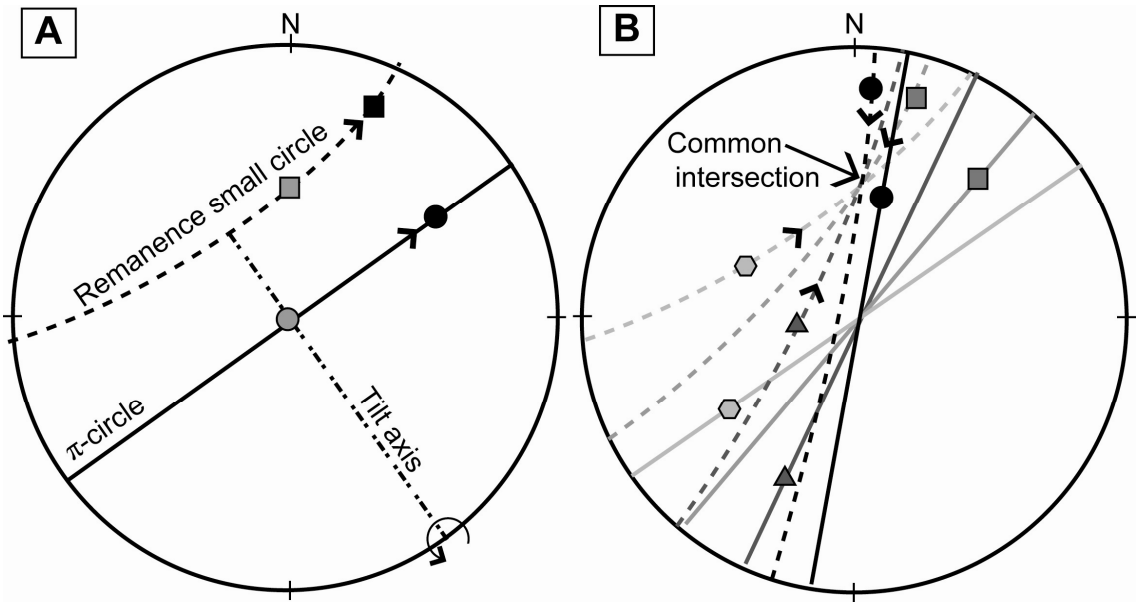

Figure 1: Basic concept of small circle intersection (SCI) analysis (modified from Waldoer and Appel, 2006). A) Equal area projection showing a site mean of an imagnetization aquired prior to tilting (Dec/Inc.0/60; gray square) and the location after tilting about a horizontal axis (black square). Motion of the site mean is tied to a remanence small circle, which is parallel to the π-circle. The π-circle is a great circle which contains the motion during the tilting (black circle) of the bedding pole for an originally horizontal bed (grey circle). B) π-circles (solid lines) and corresonding bedding poles for beds which have been tilted about a horizontal axis in opposite directions. Different symbols represent the in situ location of the site means and tie the remanence small circles (dashed lines) to their corresponding π-circles. Paleofield direction (dec/inc: 0/60) is determined from the common intersection of all small circles (Shipunov, 1997) and arrows show direction in which site means will move during untilting. Paleofield direction can only be determined if there is sufficent variation in strike of tilted beds.

to the best intersection (Henry et al., 2004). Shipunov (1997) proposed a least-squares method which utilized the point in the x-y plane that lies closest to all remanence small circles intersections. This method has all points on the sphere projected orthogonally onto the projection plane and does not utilize angular distances which may promote a geometric bias (e.g., Henry et al., 2004). Because of this a modified least squares method which utilizes angular distances was proposed by Waldhöer and Appel (2006) and will be employed in this study. Also of interest is the fact that where the remanence vectors lie along the remanence small circle is considered to be independent from where the intersection occurs (e.g., Waldhöer and Appel, 2006). The best intersection of small circles occurring from variable untilting angles at each site has been used to constrain the fold geometry at the time of acquisition (e.g., Henry et al., 2004). The error in the untilting percentages is determined by the standard deviation of untilting angles divided by the mean dip of the beds which may result in large errors when beds on opposing limbs are similar and shallow.

4. Geological Setting of the Canadian Cordillera

The foreland fold and thrust belt in the Canadian Cordillera is divided into three sub units from west to east: The Main Ranges, the Front Ranges, and the Foothills (Figure 2) and is the result of west to east directed horizontal compression due to terrane accretion which accommodated up 200 km of horizontal shortening (e.g., Price and Mountjoy, 1970; Price, 1981; Fermor and Moffat, 1992). Contraction in the foreland fold and thrust belt was expressed as thin-skinned detachment thrusting and folding of Mesoproterozoic to Cretaceous strata over Cretaceous and older strata [e.g. Monger and Price, 1979; McMechan and Thompson, 1989; Price, 1994]. Deformation

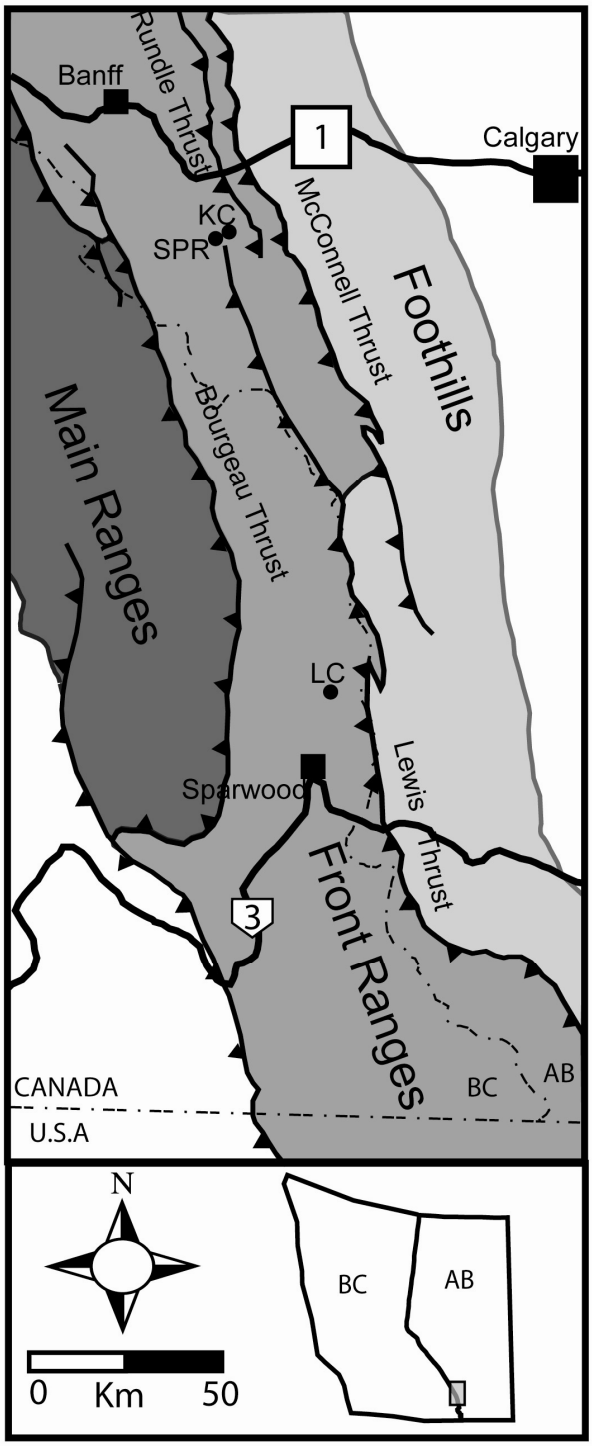

Figure 2: Generalized tectonic map of the Canadian Fold and Thrust belt highlighting major tectonic units (Main Ranges, Front Range, and Foothills; Modified from Enkin et al., 2000). Sampling locations, Mt. Kidd (KC), Line Creek (LC) are indicated by the black dots.

was active from the late Jurassic to the Eocene overlapping both the Columbian (Mid Jurassic–Late Cretaceous) and Laramide orogenies (Late Cretaceous to Paleocene) with the majority of the shortening occurring in the Late-Cretaceous (~89Ma; Price, 1994).

Obduction of terranes onto the North American pericratonic terranes began in the Late Triassic and continued into the Eocene which initiated shortening and thickening in the Omencia Belt west of the Foreland belt along both east and west directed faults and folds (Evenchick et al., 2007 and references therein). Initiation of thrusting in the western most portion of the foreland belt began in the Early Cretaceous and progressed eastward (Carr and Simony, 2006). This motion resulted in the formation of a wide variety of thin-skinned folding (e.g., Erslev and Mayborn, 1997) and duplexing (e.g., McMechan, 2001). The majority of shortening due to major thrust motions along the Lewis and McConnell thrusts occurred during the Late Cretaceous-to Eocene (Price, 1981). This effectively doubled the width of the foreland belt, which was followed by cessation of contractional deformation and led to exhumation and erosion (Price and Mountjoy, 1970).

The folds of interest in this study are located within the eastern Front Ranges of the Southern Canadian Cordillera (Figure 2) and are contained in the Mississippian Rundle Group. In SE British Columbia an anticline was sampled within the Lewis thrust sheet along Line Creek on the property of Tek Coal (LC; Figure 3). In SW Alberta the Mt. Kidd anticline was sampled within the Rundle thrust where as the Mt. Kidd syncline was sampled within Rundle thrust at the contact with the Lewis thrust located in Kananaskis Country Provincial Park (KC; Figure 4). The Mississippian Rundle Group is considered to be predominantly platform to basin carbonates deposited within

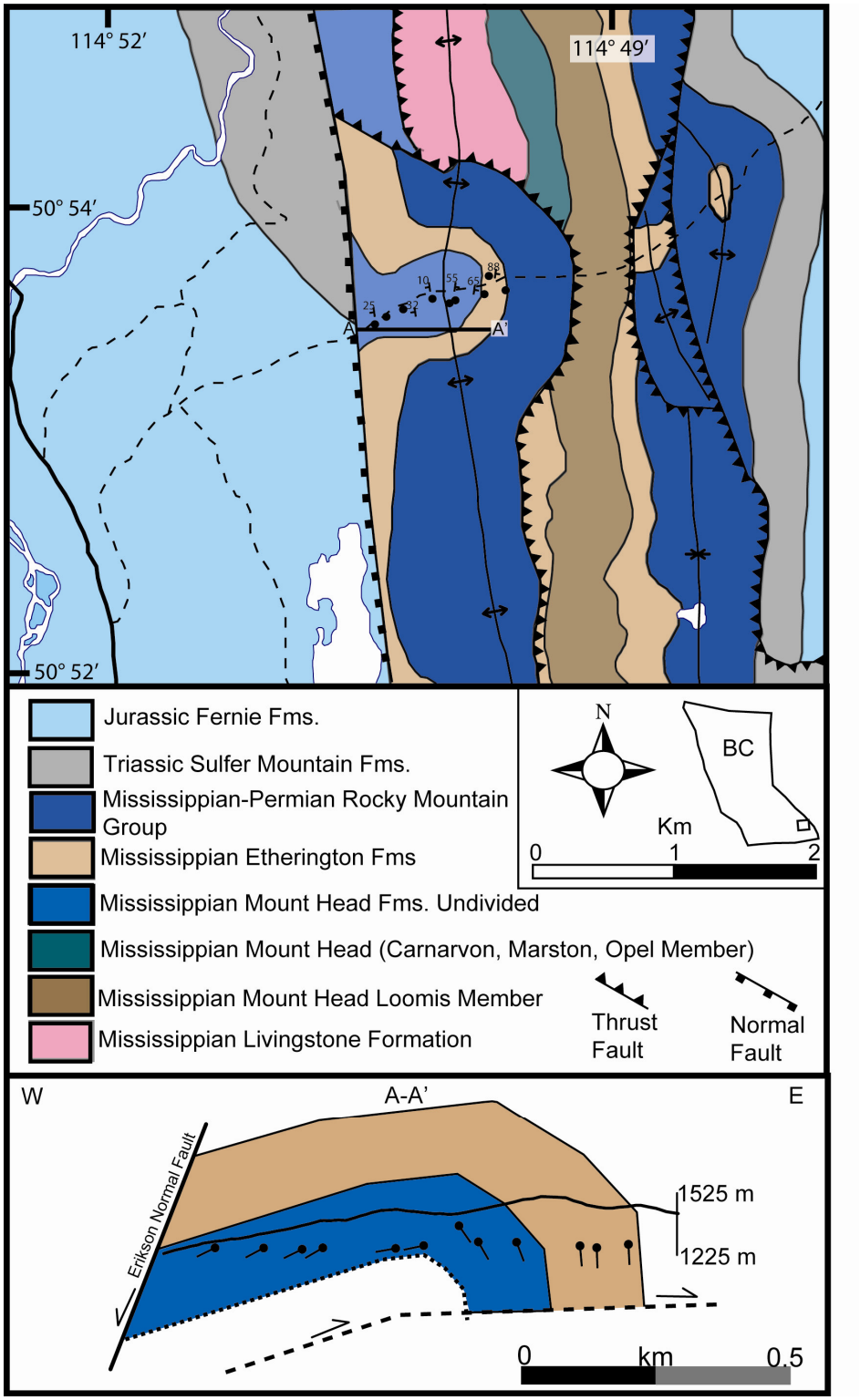

Figure 3: Geologic map (modified from Price et al.,1992) and cross section with dip symbols for the Line Creek anticline. Dashed line shows hypothesized ramp-flat geometry of thrust fault.

a passive margin setting (e.g. Hardebol et al., 2006) although multiple workers have proposed that these carbonates were actually deposited in a foreland basin setting during the Late Devonian-Early Mississippian Antler Orogeny (e.g., Root, 2001 and references therein). Since deposition the Mississippian carbonates have undergone various diagenetic alterations creating a complex paragenetic sequence which involves early matrix dolomitization due to both marine pore waters and meteoric dominated systems (Al-Aasm, 2000). This was followed by pervasive meso-dolomite recrystallization from both meteoric and hydrothermal fluids during burial (Al-Aasm, 2000) and very late formation of vug rimming saddle dolomites and sulfide mineralization**.** Hydrocarbon generation and migration is believed to have occurred within the Mississippian rocks in the Front Ranges during the Late Jurassic-Early Cretaceous (Kalkreuth and McMechan, 1988) prior to Laramide deep. Hydrocarbon emplacement was then followed by Thermo Sulphate Reduction (TSR) of the hydrocarbons, creating extensive sour gas reservoirs throughout the Canadian Cordillera and Western Canada Sedimentary (Machel, 1987; Machel et al., 1995; Roure et al., 2005; Vandeginste et al., 2009).

4.1 Line Creek Anticline, BC

At Line Creek the fold sampled was an asymmetrical upright anticline (Fold Axis: S2, 169) contained in the Mississippian Mount Head and Etherington Formations (Figure 3; Price et al., 1992). The structure is characterized by a shallow west dipping back limb, a broad shallow west dipping crest, and steep west dipping front limb (Figure 3, 5A and B). Deformation was accommodated primarily by flexural slip and kink folding (Figure 5C). Thinning was observed in the steep front limb, however, it was accommodated by brittle fracturing and small scale faulting (Figure 5C). The back

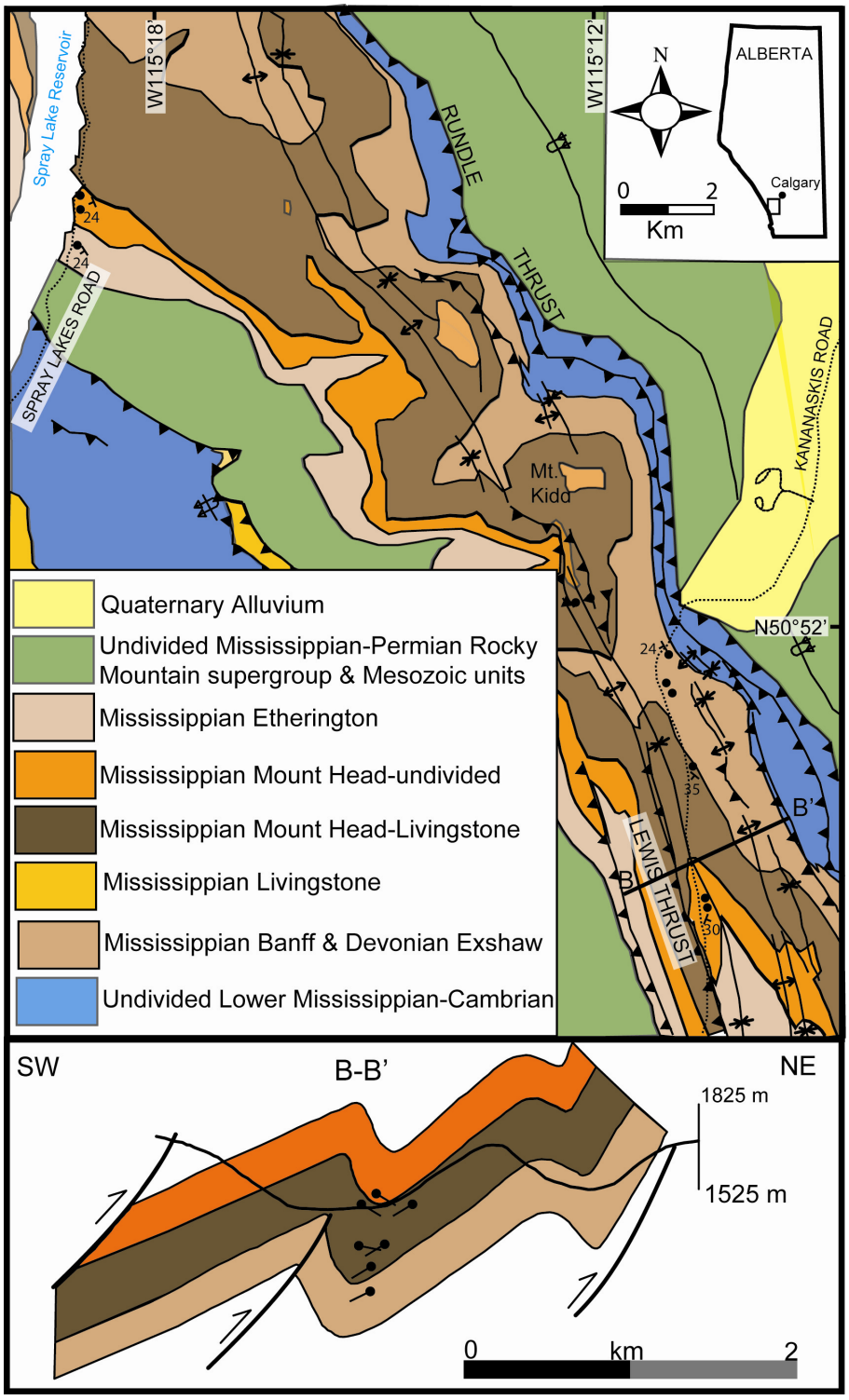

Figure 4: Geologic map (modified from McMechan, 1995) and cross section with dip symbols for Mt. Kidd anticline-syncline anticline.

limb contains small scale duplexing and back thrusting related to steepening of the front limb and tightening of the fold core (Figure 5D). One normal fault displaying minor offset was also observed which was interpreted to be related to Eocene extension on the major Erickson normal fault west of the structure.

4.2 Mt. Kidd Anticline-Syncline, AB

In Kananaskis Country, Mt. Kidd is a plunging asymmetrical anticline-syncline pair (Plunge, trend of the fold Axis: S14, 182 and S17, 178 respectively) located along both Kananaskis Road (HWY-40) and Spray Lakes Road (Figure 4). The fold is composed of the Mississippian Banff, Livingstone, Mount Head and Etherington Formations (Figure 4; McMechan, 1995). The anticline is characterized by a shallow west dipping back limp with a tight fold hinge which progresses into an east dipping front limb which is steep and asymetrical near the core of the syncline and progressively shallows up section and becomes more symetrical (Figure 4). Folding was accommodated by flexural slip, brittle fracturing and ductile thinning in the east dipping limb which thickens into the nose of the syncline (Figure 6B) and proceeds into the west dipping limb of the syncline. The west dipping shallow limb of the syncline contains brittle fracturing and small scale duplexing. A left lateral transverse fault was identified by the presence of horizontal slickensides bounding the northern edge of Mount Kidd (Figure 6C), a common feature observed in Kananaskis Country (Moffat and Spang, 1984; McGugan, 1987; McMechan, 1995).

5. Previous paleomagnetic studies at Mt. Kidd and Line Creek

The timing and origin of a multi-component fluid related remagnetizations in

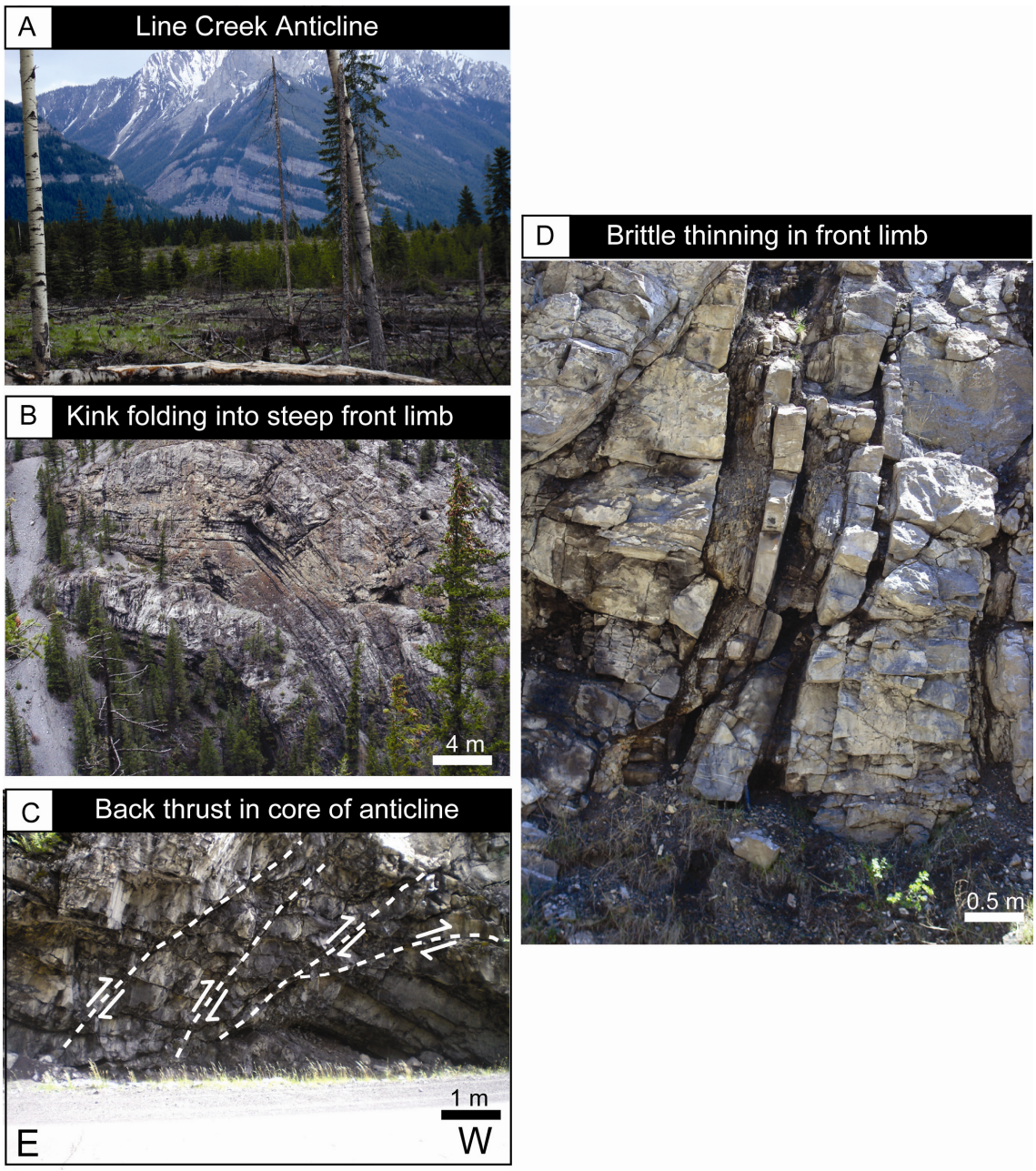

Figure 5: Field photos of major structural features at Line Creek anticline. A) Shallow back limb and crest. B) Kink folding during transition from crest into the steep front limb. C) Back thrusting in core of the anticline. D) Thinning of steep front limb via brittle fracturing and faulting

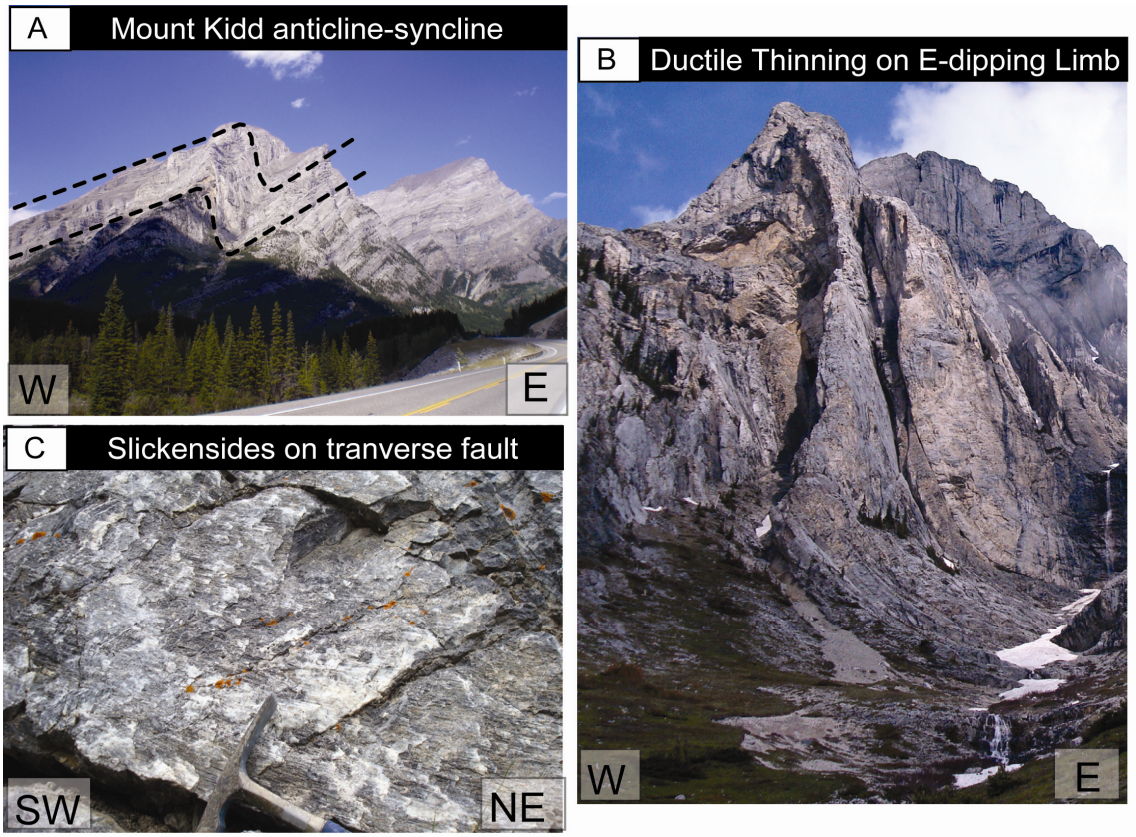

Figure 6: Field photos of major structural features at Mt. Kidd anticline-syncline. A) Asymmetrical anticline-syncline pair highlighting tight fold hinges. B) Horizontal slickensides marking location of transverse fault at the northern edge of the study area. C) Ductile thinning in the front limb of the anticline accompanied by thickening into the nose of the syncline.

Mississippian carbonates from the two folds of interest in this study were detailed in Chapters 1 and 2 (Figure 7). The characteristic remanent magnetization (ChRM) has a maximum unblocking temperature of 540°C and has been interpreted as a high temperature chemical remanent magnetization (high temperature CRM) residing in magnetite. An intermediate temperature (IT) reversed component has a maximum unblocking temperature of 340°C and is interpreted to be an CRM residing in pyrrhotite (intermediate temperature CRM). Conventional tilt tests results (OC and DC) suggest the high temperature CRM at Line Creek anticline is pre-tilting and Early Cretaceous. The high temperature CRM at the Mt. Kidd anticline is pre-tiling and apparently Early Cretaceous while the Mt. Kidd syncline is interpreted to be an apparent Early Cretaceous, early syn-tilting remagnetization. The discrepancy between the two untilting percentages may be related to structural complications. Both paleopoles from Mt. Kidd plot to the south and east of the Line Creek paleopole (Chapter 2; Table 1). The intermediate temperature CRM at Line Creek is syn-tilting and plots below the Late Jurassic portion of the path (Table 1). At Mt. Kidd the intermediate temperature CRM is post tilting and plots near the North Pole, which is attributed to be the result of secular variation it is considered to be a Late Tertiary remagnetization.

6. Methodology

6.1 Paleomagnetic sampling, analysis and Small Circle Intersection Analysis

Cores for paleomagnetic analysis were collected in the field with a portable gasoline drill and oriented with an inclinometer and Brunton compass. Forty-three sites were collected from the anticline-syncline pair within the Mississippian carbonates at Mt. Kidd (Figure 4). Thirty-six of those sites were drilled in the syncline along

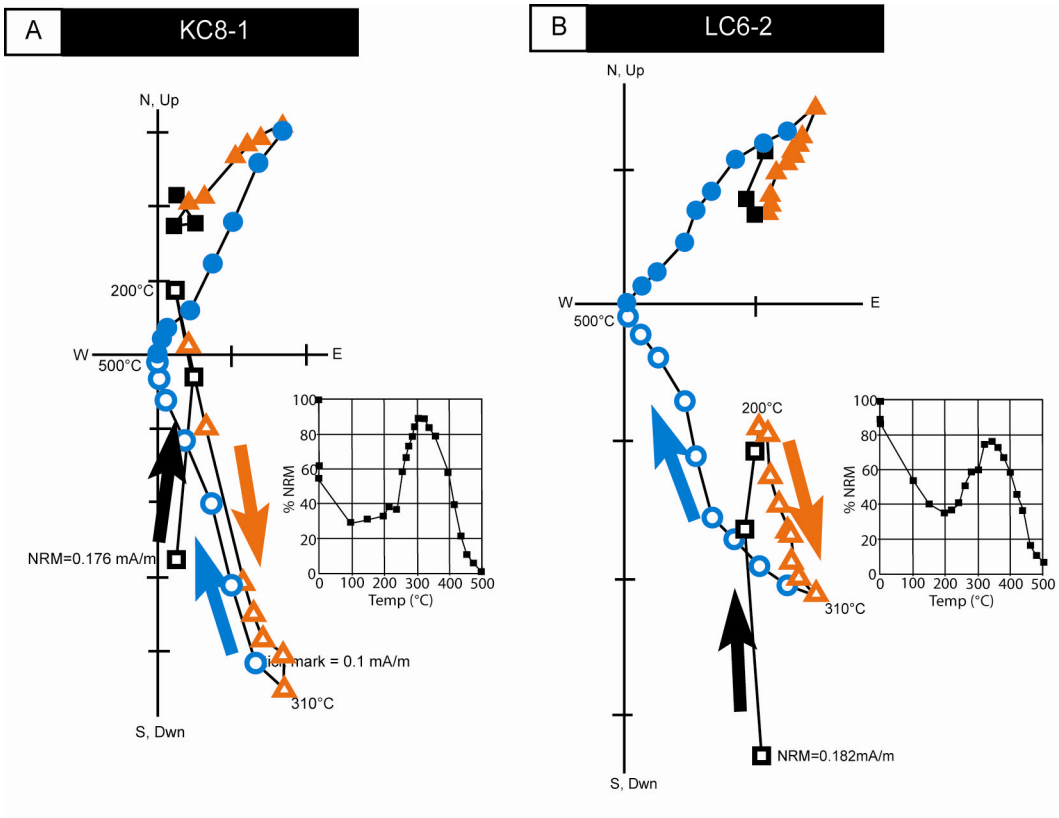

Figure 7: Representative orthogonal projections (Zijderveld diagrams) in geographic coordinates for stepwise thermal demagnetization of A) KC B) LC. Open circles represent the vertical component and the closed circles indicate the horizontal component. The normal polarity ChRM is indicated by circles, the reversed polarity intermediate component is indicated by triangles and the modern VRM is indicated by squares. Arrows indicate the direction of thermal decay. The small insert map shows the percentage of magnetization removed by a particular temperature during stepwise demagnetization.

Table 1: Summary of conventional tilt test results

HTCRM	N	D (°)	I (°)	k	α_{95} (°)	% Unfolding	Pole	dp(°)	dm(°)
KC Anticline									
OC Tilt test	13	327.7	80	129.6	3.7	91.5 ± 7.4	N65.4 / E219.5	6.3	5.6
DC tilt test	13	----	----	----	----	91.6 ± 12.41	----	----	----
KC Syncline									
OC Tilt test	20	330.9	75.3	63.3	4.1	84.9 ± 4.0	N70.6 / E202.1	7.5	6.9
DC tilt test	20	----	----	----	----	85.63 ± 10.29	----	----	----
LC Anticline									
OC Tilt test	31	338.6	72.6	55.02	3.5	97.7 ± 3.1	N74.7 / E194.0	6.4	5.7
DC tilt test	31	----	----	----	----	96.6 ± 6.02	----	----	----
ITCRM	**N**	**D (°)**	**I (°)**	**k**	**α_{95} (°)**	**% Unfolding**	**Pole**	**dp(°)**	**dm(°)**
KC Syncline									
OC Tilt test	19	202.4	-68.8	102.7	3.3	-1.8 ± 5.3	N74.5 / 325.8	7.3	6.0
DC tilt test	19	----	----	----	----	-2.13 ± 10.76	----	----	----
LC Anticline									
OC Tilt test	30	137.0	-66.8	37.4	4.4	64.5 ± 2.5	N62.5 / E170.9	5.7	4.7
DC tilt test	30	----	----	----	----	69.8 ± 7.3	----	----	----

Notes: N is the number of sites used in the tilt tests; D is declination; I is inclination; k is a statistical measure of grouping, α_{95} is the 95% cone of confidence. Percent untilting and confidence interval from direction-correction (DC) tilt test [Enkin, 2003] and the optimal clustering (OC) tilt tests(Watson and Enkin, 1993) tilt test; The pole represents the inferred location at during acquisition; dp/dm is the semi minor and semi major axis, respectively, of the 95% error ellipse.

Kananaskis Road (Figure 4) and 7 sites were drilled on the west dipping limb of the anticline along Spray Lakes Reservoir on the Western edge of the park ~12 km NW of the front limb (Figure 4). Seven sites from the syncline were drilled in the vicinity of the right lateral transverse fault at the northern edge of the structure. Sampling was primarily confined to the syncline due to the structural coherence of the exposures. Fifty-six sites were collected in Mississippian Carbonates within an asymmetrical anticline from an almost continuous exposure of outcrops, within a water gap along Line Creek, BC (Figure 3) on the property of The Tek Coal Company (Formerly Elk Valley Coal Company; Figure 3). At Line Creek, care was taken not to sample within the small scale duplexes, back thrusted, or late normal-faulted areas.

Paleomagnetic samples were marked and cut to standardized lengths (~2.2 cm) with an ASC Scientific dual blade saw. Natural Remanent Magnetizations (NRMs) were measured using a 2G-Enterprises cryogenic magnetometer with DC squids in the shielded paleomagnetic lab at the University of Oklahoma. Prior to thermal demagnetization the samples were submerged in liquid nitrogen twice for two hours and warmed to room temperature in a zero field to remove the unstable remanence from Multi-Domain (MD) grains (Dunlop and Argyle, 1991). The NRM was measured again after each treatment. Cores were then subjected to stepwise thermal demagnetization in 22 steps from 100 to 580°C using an ASC scientific Thermal Specimen Demagnetizer.

Demagnetization data was plotted on Zijderveld (1967) diagrams using the Super IAPD program, which was also used for Principal Component Analysis (PCA, Kirschvink, 1980) to determine the components. Site means were calculated using Fisher (1953) statistics in Super IAPD. Small circle intersection (SCI) analysis was

conducted using the software generated by (Waldhöer and Appel, 2006). The data from KC was analyzed for both the unplunge and plunge corrected data sets. Removal of the plunge was accomplished by considering that the site mean vector data as a line on the surface of a particular bed. Then following a modified version of the method of tracking a line during the unfolding of a plunging fold, outlined in Marshak and Mitra, (1988; Method 6-14 pg 119-120), the plunge of the fold was removed and as a result, the orientation of the site mean vectors on a bed unfolded around a particular fold axis could be determined. Based on the results of the SCI analysis both the OC tilt test (Watson and Enkin, 1993) and the DC tilt test (Enkin, 2003) were performed on modified data sets using the PMGSC version 4.2 software program [Enkin, 2004].

Paleopoles were determined based on the declination and inclination of the greatest concentration of small circle intersections determined from SCI analysis and the optimal clustering from the OC tilt test. Errors where calculated using the α95 of the resulting intersections and clusters. The poles were calculated using the PMGSC version 4.2 software program (Enkin, 2004). The poles were then plotted on the Mesozoic portion of the apparent polar wander path (APWP) for North America (Besse and Courtillot, 2002) in order to investigate the age of remagnetization relative to folding.

6.2 Calcite Strain Gauge

The calcite strain gauge (CSG) method (Groshong, 1972, 1974; Evans and Groshong, 1994) is a least squares calculation which determines intergranular twinning strains. The CSG analysis was conducted on 2 mutual perpendicular thin sections created from opposing limbs at both folds (4 sites total) to investigate strain variations

between the two folds. The samples examined were coarse grained packstones at Line Creek and dolomitized grainstones at Mt. Kidd. The reference slide was cut parallel to the bedding and the second slide was cut perpendicular to bedding. Measurements were conducted on a Leitz 4-axis Universal Stage with a 40x Nikon extra long working distance (ELWD) objective attached to a Nikon Opti-Phot petrographic microscope following the method outlined by Turner and Weiss, (1963) and Groshong (1974). At least 25 calcite twin orientations and calcite C-axis were measured on each slide and photographs were taken at 10x magnification after each measurement to ensure that no grain was measured twice. GeoCalculator v4.9 (Holcomb, 2007) was used to ensure that the proper angle of 26.5±3 was achieved between the calcite twin and the C-axis. Once the measurements were complete the data sets were cleaned to reduce error by eliminating 20% of the twin sets with the largest deviation from the mean (Groshong, 1974). After removal of the largest deviations the square root of the second strain invariant ($\sqrt{J_2}$) or total distortion by twinning (TDT) was calculated using the Calcite Strain Gauge (CSG) v1.2 software developed by Evans (2005). The TDT is a measure of the total deviatoric strain in a particular sample (Jager and Cook, 1979). Twin intensity (twin planes/mm) and average twin width, were also calculated in order to approximate maximum burial temperatures (Ferrill, 1991; Ferrill et al., 2004).

7. Results

7.1 Small Circle Analysis

7.1.1 Line Creek Anticline

Equal area projections displaying the small circle tracks from opposing limbs for the high temperature and intermediate CRMs at Line Creek are shown in Figure 8A and

9A. The plunge of the Line Creek Anticline is insignificant (~2°) and no plunge correction has been applied to the data set. The opposing limbs of the fold exhibit enough variation in bedding strike to generate a sufficient number of the remanence small circle intersections (m_R/m_P = 0.6; Table 2) needed to perform SCI analysis (Figure 8A and 9A) and the results are summarized in Table 2. SCI analysis of the high temperature CRM at Line Creek shows that the greatest concentration of intersections occurs at 95.6% ± 25.6 untilting (Table 2), suggesting a pre-tilting magnetization with the greatest concentration of remanence small circles intersections occurring at a declination of 333.4° and an inclination of 72.8°. The paleopole falls on the Late Cretaceous portion of the APWP (N72.7°, E191.2°; Figure 10) similar to the results obtained from the conventional tilt tests (Table 1).

The SCI analysis of the intermediate temperature CRM at the Line Creek anticline displays a syn-tilting result (66.4% ± 31.9) and the maximum number of remanence small circles occurs at a declination of 141.1° and an inclination of -68.5° (Table 2). These locations correspond to a paleopole of N65.7°, E174.7° and plots below the Late Jurassic portion of the path (Figure 10), which is similar to the results obtained from the conventional tilt tests (Table 1).

7.1.2 Mt. Kidd Anticline-Syncline

For the plunging (~15°) Mt. Kidd anticline-syncline pair, equal area projections for the unplunge corrected data sets show a high concentration of remanence small circle intersections (Figure 8B, C and 9B) due to large bedding strike variations resulting from plunge formation (m_R/m_P = 0.85 and 0.76 respectively; Table 2). Upon removal of the plunge the number of remanence small circle intersections decrease

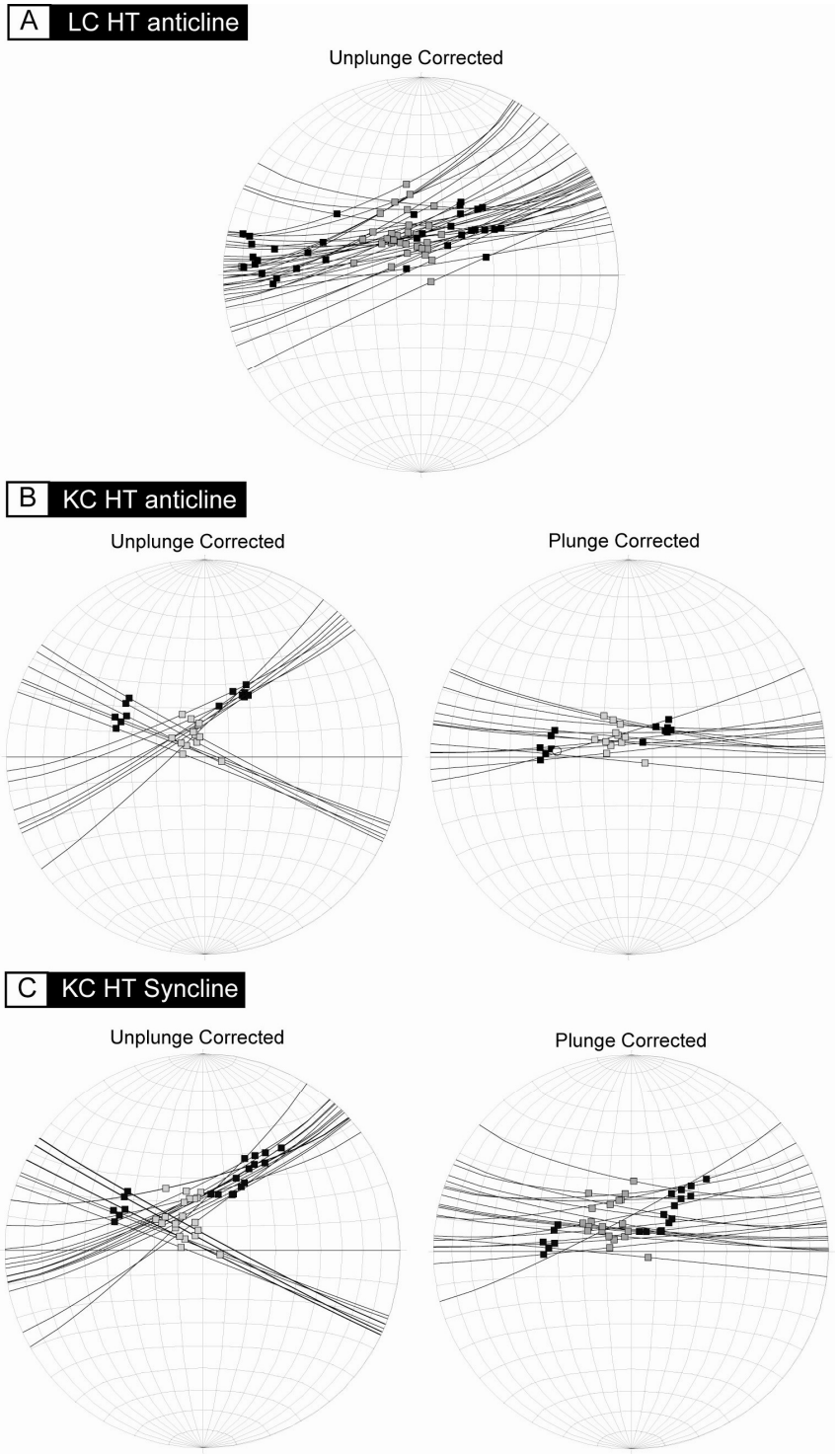

Figure 8: Equal area projections of the results from small circle intersection analysis of the high temperature CRM for all structures. Black squares indicate in situ site means. Gray squares indicate tilt corrected site means. Black lines indicate remanence small circles. A) Unplunge corrected data from the Line Creek anticline. B) Unplunge corrected and plunge corrected data from Mt. Kidd anticline. C) Unplunge corrected and plunge corrected data from Mt. Kidd syncline.

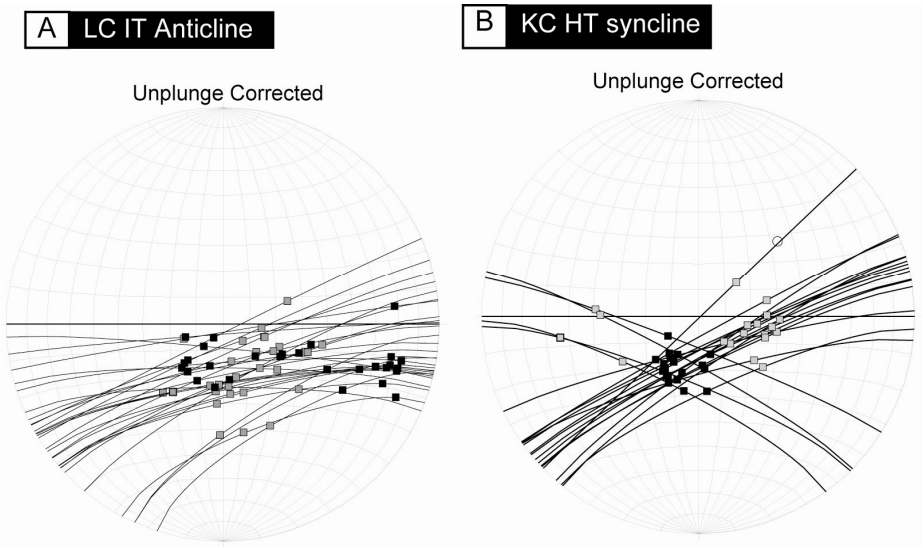

Figure 9: Equal area projections of the results from small circle intersection analysis of the intermediate temperature pyrrhotite component. Black squares indicate in situ site means. Gray squares indicate tilt corrected site means. Black lines indicate remanence small circles. A) Unplunge corrected data from the Line Creek anticline. B) Unplunge corrected data from Mt. Kidd syncline.

Table 2: Summary of small circle intersection (SCI) analysis results

HTCRM	N	m_R/m_P	D (°)	I (°)	k	α_{95} (°)	% Untilt	Pole	dp(°)	dm(°)
KC Anticline										
Unplunge Corrected	13	0.85	299.9	74.6	206	2.7	93.3 ± 50.6	N56.2, E196.0	4.9	4.5
Plunge corrected	13	0.67	65.5	66.5	129.7	3.4	98.0 ± 56.2	N49.2, 310.3	5.6	4.6
KC Syncline										
Unplunge Corrected	20	0.76	298.6	65.6	109.5	3	107.0 ± 43.5	N51.0, E174.4	4.9	4
Plunge corrected	20	0.54	318.2	76.6	47.9	4.5	102.4 ± 41.8	N64.5, 202.4	8.4	7.8
LC Anticline										
Unplunge Corrected	29	0.6	333.4	72.8	43.4	4	95.6% ± 25.6	N72.7, E191.2	6.3	5
ITCRM										
KC Syncline										
Unplunge Corrected	19	0.7	200.3	-68.8	98.7	3.2	-2.1 ± 25.7	N77.3, E323.0	5.4	4.6
LC Anticline										
Unplunge Corrected	28	0.52	141.1	-68.5	31.6	4.7	66.4 ± 31.9	N65,7, E174.7	7.4	5.9

Notes: Notes: N is the number of sites used in the tilt tests; m_R/m_P is the intersection factor where m_R represents the number of realized intersections and m_P represents the number of possible intersections; D is declination; I is inclination; k is a statistical measure of grouping, α_{95} is the 95% cone of confidence. Percent untilting and confidence interval from SCI analysis (Waldhöer and Appel, 2006); the pole represents the inferred location at during acquisition; dp/dm is the semi minor and semi major axis, respectively, of the 95% error ellipse.

(Table 2) due to rotation towards a cylindrical fold geometry, but there are still enough intersections (m_R/m_P = 0.67 and 0.54 respectively; Table 2) to perform SCI analysis. The removal of the plunge results in an increase in the α95 and a decrease in the k values, as well as a deviation between the declination and inclination of the intersections at each structure (Table 2).

Prior to plunge correction the percentage untilting for the high temperature CRM at the Mt. Kidd anticline is 93.3% ±50.6 and after plunge correction it is 98.0% ±56.2, both of which are similar to the results obtained using conventional tilt tests and suggest a pre-tilting magnetization (Table 1). Large errors exist in the untilting percentages, most likely due to the similar and shallow bedding dip on both limbs (Table 2). In terms of declination and inclination prior to plunge correction the highest concentration of remanence small circles occurs at declination of 299.9° and inclination of 74.6° resulting in a paleopole of N56.2°, E196.0° (Table 2). After plunge correction the declination becomes 065.5° and the inclination becomes 66.5° resulting in a paleopole of N49.2°, E310.3°. This paleopole differs significantly from the paleopole obtained using conventional tilt tests (Table 1 and 2), perhaps because the intersections are being influenced by structural complications. This issue will be discussed in detail in the discussion section.

At the Mt. Kidd syncline a similar pattern is observed in terms of the behavior of the remanence small circles during removal of the plunge from the high temperature CRM data set (Figure 8C; Table 2). The untilting percentage obtained from SCI analysis, however, differ from the results obtained from the conventional tilt tests (Table 1 and 2). Based on the OC and DC tilt tests the Mt. Kidd syncline is determined

to be early syn-tilting (85.6 ± 10.3%, Table 1), however, SCI analysis gives a pre-tilting result (102.4% ± 41.8, Table 2). As with the Mt. Kidd anticline large errors in the untilting percentages exist. The declination and inclination of the unplunge corrected high temperature CRM data set at the Mt. Kidd syncline determined from SCI analysis is 318.2°, 76.6° resulting in a paleopole at N51.0°, E174.4° (Table 2), which plots far south of the Late Jurassic portion of the APWP. After plunge correction the declination and inclination of the high temperature CRM becomes 298.6°, 65.6° resulting in a paleopole at N64.5°, E202.4° (Table 1) which plots near the Early Cretaceous portion of the APWP (Figure 10). It is significantly different than either the Line Creek or Mt. Kidd anticline high temperature CRM paleopoles.

For the intermediate temperature CRM at the Mt. Kidd syncline the conventional tilt tests determined a post tilting result (Table 1). Because of this no plunge correction was applied to the data set (Figure 9B). The results from the SCI analysis are very similar to the conventional tilt tests, with maximum remanence small circle intersection occurring at -2.1% ±25.7 untilting, corresponding to a declination and inclination of 220.3°, 68.3° and a paleopole at N77.3°, E323.0° (Table 2). This pole is similar to the conventional tilt test results (Table 1), plotting near the North Pole (Figure 10), and is considered a Late Tertiary remagnetization.

7.2. Calcite Twinning Strain

Variations in calcite twin morphology are observed between the two folds of interest in this study and are summarized in Table 3. At Line Creek a pelloidal fossiliferous packstone was examined from the shallow back limb and a dolomitized packstone was examined from the steep front limb. Both limbs exhibited thin twins

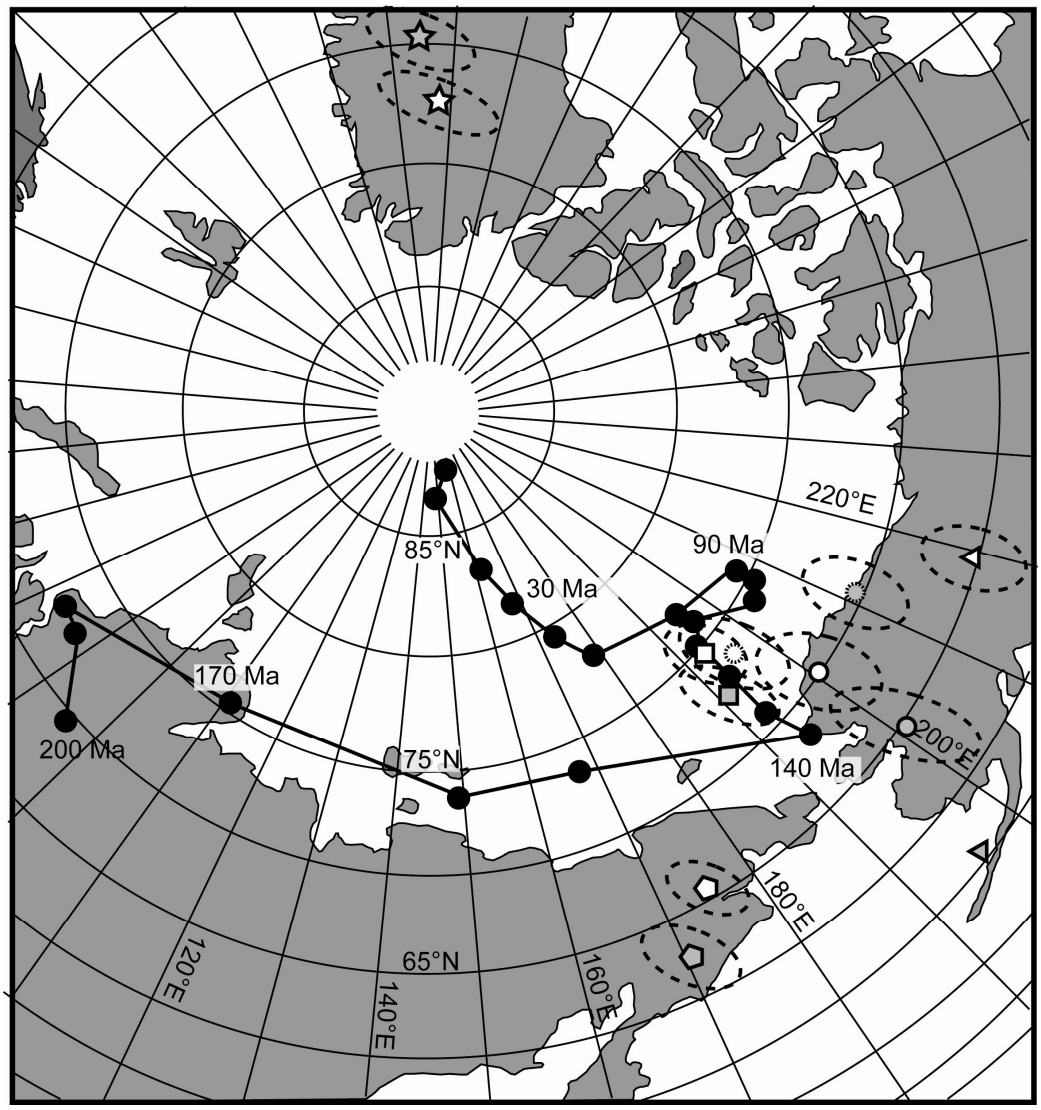

Figure 10: Mesozoic section of the apparent polar wander path for North America (Besse and Courtillot, 2000). Squares = ChRM at Line Creek anticline; Circles = high temperature CRM at Mt. Kidd syncline; Triangles = high temperature CRM at Mt. Kidd anticline anticline; Pentagon = intermediate temperature CRM at Line Creek anticline; Star = intermediate temperature CRM at Mt. Kidd syncline White fill represents original tilt test results; Grey fill represent SCI results Dashed circle represents the modified tilt test results. dp/dm errors are indicated by the dashed ovals.

(type 1 twins, Burkhard, 1993) generally observed as single twin sets (average thickness 0.12μm; Figure 11A) and have a twin intensity (twins/mm) in the back and front limb of 38.1 and 91.2 respectively. Total deviatoric strain ($\sqrt{J_2}$) from the back and front limb was low (0.27% TDT and 0.84% TDT respectively). The maximum burial temperature approximated from the data set was < 170°C, which falls in the range of the maximum burial temperature of ~180°C extrapolated from vitrinite reflectance data from the overlying Jurassic coals (J. Halko, per. comm.).

At the Mt. Kidd syncline the twins were measured in dolomitized grainstones from both the steep front limb and shallow back limb. The twins were a mixture of thick and thin twins, however, thick twins were predominate (Type 2; Burkhard, 1993). The grains examined predominantly contained two twin sets per grain (Figure 11B). The average twin width was 2.25 μm for the west dipping back limb and 3.3 μm for the east dipping front limb with twin intensities (twins/mm) of 22.73 and 39.75 respectively. These results correlate with a temperature range of 170-200°C, based on calcite geothermometry graphs (Ferrill et al., 2004). Also observed in thin sections taken from the nose of the syncline were bent thick twins (Type 3; Burkhard, 1993) suggesting that the maximum was probably slightly higher than 200°C. The total deviatoric strain ($\sqrt{J_2}$) was orders of magnitude higher than at Line creek with the back limb having 3.7% TDT and the front limb having 8.7% TDT. Based on deformation maps for calcite constructed from constitutive equations and flow laws for calcite (Evans et al., 2006), the predominate deformation mechanisms in samples subjected to maximum burial temperatures below 250°C are pressure solution and twinning. Because of this the TDT is a good approximation of the strain variations between the two folds in this study.

Table 3: Summary calcite twin strain results

Sample	# twins sets	Intesity (twins/mm)	Avg width (μm)	$\sqrt{J_2}$ (%)
KC34	42	39.8	3.3	8.7
KC38	42	22.7	2.3	3.6
LC33	40	91.2	0.12	0.84
LC52	40	38.1	0.12	0.27

Notes: Results presented are after removal of 20% of twins representing the largest deviations from mean. Total distortion by twinning, $\sqrt{J_2} = -(e_2e_3 + e_3e_1 + e_1e_2)^{1/2}$

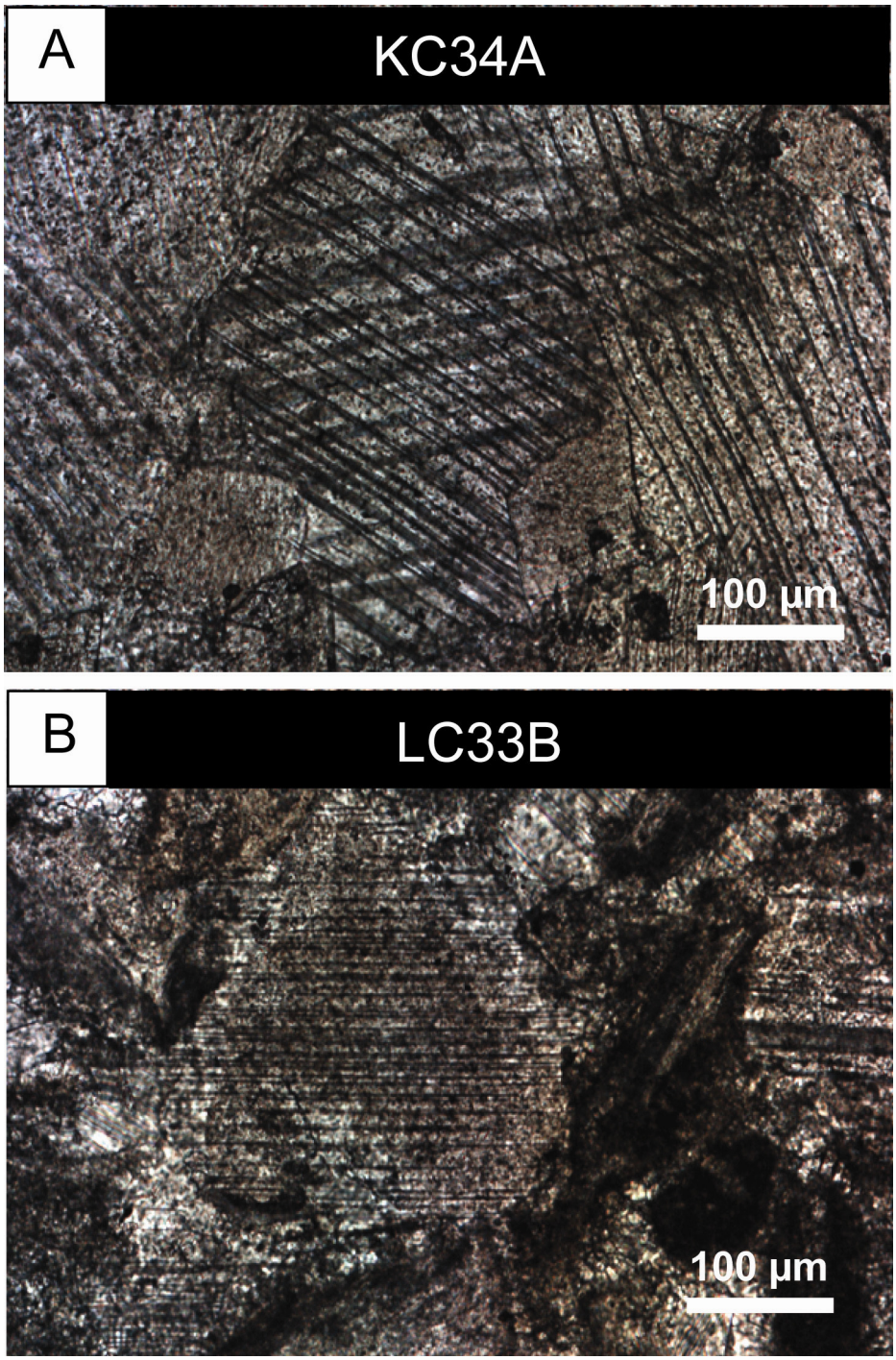

Figure 11: Representative calcite twin morphology (Burkhard et al., 1993) from both structures. A) Type 2 dual sets thick and thin twins at Mt. Kidd syncline. B) Type 1 single set thin twins at Line Creek anticline.

8. Discussion

8.1 Effects of folding kinematics and deformation mechanism on the high temperature CRM

8.1.1 Line Creek Anticline

The SCI analysis and the conventional tilt tests at Line Creek produce similar untilting percentages and paleopoles for the high temperature CRM, although the SCI analysis produces large errors. This suggests the remagnetization was acquired prior to folding in the Early Cretaceous (~Aptian). This is most likely the result of the kinematic history as well as the predominate deformation mechanisms involved in the folding process. The Line Creek anticline has an almost horizontal fold axis (~2° plunge), suggesting that the hanging wall was transported over a simple frontal ramp which did not generate any spurious rotation of paleomagnetic vectors (e.g., Pueyo et al., 2003). Equal area projections show a few remanence small circles which have large deviations compared to the majority of small circles (Figure 8A), suggesting the influence of structural complications such as out of plane bedding rotations. Because of the large data set (49 sites) these discrepancies do not significantly influence the SCI analysis or tilt test results.

Other structural complications such as small scale duplexing in the back limb and back thrusting within the fold core due to steepening of the front limb and tightening in the fold core were observed at Line Creek, however, these areas were avoided during sampling. Also the Line Creek fold has planar limb segments formed via kink folding. This allows for the application of simple rigid body rotation about the bedding strike of the opposing limb, which is one of the main assumptions in all tilt tests proposed. Another complication to the tilt tests, that is avoided at Line Creek, is

high tectonic strain, which can result in strain alteration of a preexisiting CRM (e.g., Kodma, 1988) or the formation of a PRM due to high stresses (e.g., Borradaile, 1997). Based on calcite deformation twinning the rocks in this anticline experienced low deviatoric strain (0.27-0.84% TDT), which resulted in brittle fracturing under low to moderate burial temperatures (170-180°C) being the dominant deformation mechanism accommodating steepening of the front limb and tightening of the fold core. Based on these results it appears that the Line Creek anticline may represent an ideal structure for paleomagnetic analysis within fold and thrust belts as long as areas that contain obvious structural complications (i.e., duplexing and back thrusting) are avoided. Because of this the pole generated for the Line Creek anticline can be considered the true timing of acquisition of the HTCRM.

8.1.3 Mt. Kidd syncline

At the Mt. Kidd syncline which is located on the McConnell thrust sheet near the contact with the Rundle thrust, the conventional tilt tests gives an early syn-tilting result (85.6% ± 10.3) whereas the SCI estimate gives a pre-tilting result with large errors (102.4% ± 41.8). The resultant paleopoles plot close to each other but both paleopoles plot south and east of the pre-tilting Line Creek pole (Figure 10) making them appear older. A true syn-tilting result is considered suspect since motion along the Rundle thrust has been determined to have occurred in the Late Cretaceous (68.4-72.7 Ma) using authigenic illite from fault gouge along the thrusts (van der Pluijm et al., 2006). This suggests that the Early Cretaceous syn-tilting nature of the Mt. Kidd syncline may be the result of a strain or stress modification of a pre-tilting remagnetization, although the validity of using authogenic illite to date fault movement

is currently under debate (e.g., Price, 2007; Pevear et al., 2007). This would also contradict a west to east migrating fluid front being responsible for the high temperature CRM as proposed in Chapter 2, since Mt. Kidd is east of the Line Creek anticline. These discrepancies between the untilting percentages and paleopoles may be the result of one or more structural complications.

One possible origin of these discrepancies may be the result of an overall deformation event perpendicular to the fold axis occurring after folding resulting in the significant plunge observed in the structure (~15°). An overall tilt post folding is unlikely since during removal of the plunge k values decrease and α95 values increase (Table 2). Modeling of synthetic paleomagnetic data conducted by Waldhöer and Appel (2006) showed that k values will increase and α95 values will decrease during plunge correction if a subsequent overall tilt occurs post folding. This suggests that the plunge formed during folding, most likely due the interaction of the hanging wall being transported over a frontal and oblique ramp. Another complication is observed in the tracks of remanence small circles from three sites in the plunge corrected data from the east dipping limb. During tilt correction these sites have small circles which follow an easterly path as opposed to the remainder of the sites which follow a more north easterly path (Figure 8C). When these sites are removed the untilting percentages for both the SCI and the conventional tilt test are both near 85% untilting (Table 4) and the resultant paleopoles from both tests migrate closer to, but still east of the pre-tilting Line Creek pole (Table 4; Figure 10). This modification reduced the errors for the untilting percentages, while increasing the k values and decreasing the α95 values in both tests (Table 1, 2, and 4). This suggests that these three sites were altered by small

out of plane bedding rotations, although spurious rotations of paleomagnetic vectors formed due to the complex ramp interactions cannot be discounted. These spurious rotations may be significant when the magnetic vectors are oriented at a high angle to the fold axis (Pueyo et al., 2003), which is also the case at Mt. Kidd.

In terms of the origin of the syn-tilting nature of the high temperature CRM at the Mt. Kidd syncline it must first be determined if the result indicates a "true" or a "false" syn-tilting result since true syn-tilting results may provide pertinent geological information when the fold appears to be symmetrical as is the case at the Mt. Kidd syncline. Based on the results of this study there is a strong indication that the syn-tilting nature is actually a "false" syn-tilting result formed by one or more deformation related alterations. A likely mechanism is strain modification of a pre-tilting high temperature CRM. Analysis of calcite deformation twinning shows evidence for burial temperatures at or above 200°C as well as moderate to high deviatoric strain (3.6%-8.7%). This high strain may have resulted in passive rotation of magnetic vectors (e.g., Kligfield et al., 1983; Hirt et al., 1986; Kodama, 1988), minor rigid body rotation of individual magnetic grains due to layer parallel shear (e.g., Van der Pluijm, 1987; Kodama, 1988) or calcite twin deformation (e.g., Evans et al., 2006). The higher burial temperatures at Mt. Kidd resulted in vastly different deformation mechanism during folding compared with Line Creek (Figures 3 & 4). At Line Creek the upper section of the Mississippian units (Mount Head–Etherington formations) were sampled and the folding was controlled by brittle deformation with the steepening and thinning of the front limb accommodated by fracturing and minor faulting. At Mt. Kidd, however, the lower sections of the Missippian units (Banff–Mount Head formations) were sampled

Table 4: Summary of modified tilt test and SCI results

HTCRM	N	D (°)	I (°)	k	α_{95} (°)	% Untilt	Pole	dp(°)	dm(°)
KC Anticline									
(sites 4, 15, 16, 20 removed)									
Plunge corr. OC Tilt test	9	320.2	80.4	253.5	3.2	98.6 ± 8.4	N63.8, E218.0	6.1	5.9
Plunge corr. DC tilt test	9	---	---	---	---	96.67 ± 16.04	---	---	---
Plunge corr. SCI analysis	9	320.9	81.4	281.0	2.8	99.3 ± 16.4	N62.1, E221.7	5.4	5.2
KC Syncline									
(Sites 1, 2, 4 removed)									
Plunge corr. OC Tilt test	17	334.3	73.5	76.5	4.1	85.4 ± 5.2	N73.1, E195.2	7.4	6.6
Plunge corr. DC tilt test	17	---	---	---	---	86.4 ± 13	---	---	---
Plunge corr. SCI analysis	17	334.7	77	63.2	4.3	83.5 ± 23.6	N70.6, E212.2	8.0	7.5

Notes: Notes: N is the number of sites used in the analysis after modification of the data set; D is declination; I is inclination; k is a statistical measure of grouping, α_{95} is the 95% cone of confidence. Percent untilting and confidence interval for the optimal clustering (OC) tilt tests(Watson and Enkin, 1993), direction-correction (DC) tilt test [Enkin, 2003] and SCI analysis (Waldhöer and Appel, 2006); The pole represents the inferred location at during acquisition; dp/dm is the semi minor and semi major axis, respectively, of the 95% error ellipse.

the steepening is accommodated by ductile deformation with thinning in the limb and thickening into the hinge of the syncline. The layer parallel shear, which lead to ductile thinning may have caused a subtle modification of the remanence vectors via one or more of the mechanisms described above, although spurious rotation of paleomagnetic vectors cannot be discounted as a source of this modification. This strain alteration may have created the early syn-tilting result but only slightly altered the paleopoles.

The possibility that the high temperature CRM was actually acquired during folding is unlikely for multiple reasons. First it is unlikely that the syn-tilting result is due to the formation of a PRM (e.g., Hudson et al., 1989; Borradaile, 1997), since PRMs are considered to predominantly affect only the coarse multi domain (MD) grains and the magnetization in these grains were removed by liquid nitrogen treatment prior to stepwise thermal demagnetization. The possibility that a regional fluid migration event affected the Mt. Kidd syncline and created an Early Cretaceous (~Aptian) early syn-tilting paleopole is unlikely since the major thrust movements responsible for the folding do not occur until ~89 Ma (Price, 1994). On the other hand, Moffat and Spang (1984) found field evidence of minor folding prior to major thrust motion in folds within the Rundle and Sulphur Mountain thrust, north of the Mt. Kidd syncline near Canmore, AB although they did not speculate on the timing of this minor folding. Folding prior to thrusting Mt. Kidd syncline cannot be ruled out at this time and requires more detailed field study in order to resolve the issue.

8.1.4 Mt. Kidd anticline

The untilting percentage determined from SCI analysis indicate a pre-tilting result at the Mt. Kidd anticline which is very similar to the results of the conventional

tilt tests, although as with the Line Creek anticline the SCI results contain large errors (Tables 1 and 2). A major discrepancy exists between the paleopoles obtained from conventional tilt tests and SCI analysis. The results of the OC tilt test generate a paleopole which plots ~25° east of the Early Cretaceous portion of the APWP (Table 1; Figure 10) while the results of the SCI analysis generate a paleopole which plots more than 80° off of the APWP (Table 2). Equal area projections of the remanence small circles show that there are three sites on the west dipping back limb which strongly influence the location of the greatest concentration of intersections, resulting in a declination of 65.6° and inclination of 66.5° (Figure 8B; Table 2) as opposed to 327.7°, 80.0° obtained from the tilt tests (Table 1). When the data set is modified by removing these sites the result is still pre-tilting (Table 4), although now the mean direction and resultant paleopole from the SCI analysis coincides with the OC tilt test results (Table 4). These three sites are apparently spurious, perhaps because of rotations.

These pretilting paleopoles plot at significantly different positions than the pre-tilting Line Creek pole (~ 25° east of the APWP; Figure 10) which is considered to represent the actual timing of acquisition of the high temperature CRM. Since the high temperature CRM is considered to have been formed during a single regional remagnetization (Chapter 2) these pre-tilting poles should coincide. The fact that they do not coincide even after removal of multiple sites which appear to contain structural complications, suggests that the Mt. Kidd anticline may not represent a continuous anticline as originally thought. The Mt. Kidd anticline is quite expansive and most of the structure was inaccessible due to rugged terrain, with sampling of the back limb occurring ~12 km NW of the front limb. Thrust imbrication is common between the

Rundle and Sulphur Mountain Thrusts (Moffat and Spang, 1984) which contain the Mt. Kidd anticline. It is likely that an unmapped imbrications occur within the inaccessible area resulting in multiple structures, which are not suitable for either conventional tilt tests or SCI analysis. This highlights the need to have strong structural controls on large scale structures used for paleomagnetic analysis, since any attempt to consider multiple structures as a single structure would result in biased and subsequently invalid untilting percentages and age determinations.

8.2 Folding affects on the intermediate temperature CRM

At Line Creek the syn-tilting intermediate temperature CRM appears to be older than the pre-tilting high temperature CRM based on the paleopole positions (Figure 10). Since there are no structural complications affecting the Line Creek anticline, another mechanism is needed to explain this discrepancy. One possibility is directly related to the remagnetization mechanism. In Chapter 2 the intermediate temperature CRM was concluded to have formed during TSR of hydrocarbons resulting in the formation of pyrrhotite. Since TSR is considered to occur very rapidly geologically, over very narrow stratigraphic intervals, it is possible that either secular variation was not averaged out or that sampling across the entire expanse of the Line Creek anticline uncovered multiple TSR events. At the Mt. Kidd syncline sampling was confined to a relatively narrow stratigraphic interval which was more likely to have sampled only one TSR event. The fact that the intermediate temperature CRM at the syncline was acquired post-folding, without any subsequent overall tilts, would suggest that there is no need to worry about structural complications, however, the paleopoles determined by

both methods plot off of the path near the North Pole. One likely cause of this discrepancy is that secular variation was not averaged out.

8.3 Conventional tilt tests vs. SCI Analysis

The results of this study have shown that integration of conventional tilt tests and SCI analysis can provide valuable information regarding the timing of remagnetization relative to folding. The main drawback with the conventional tilt tests is that by simple rotation of remanence vectors around strike many structural complications are not recognized. This does not pose any problems when there are no structural complications affecting the data set as with the Line Creek anticline as long as areas containing obvious structural complications (i.e., duplexing and back thrusting) were avoided during sampling. This highlights the need for a certain amount of structural coherency within a particular data set. In the case of the Mt. Kidd syncline, multiple structural complications exist and conventional tilt tests are not appropriate by themselves. SCI analysis on the other hand offers insight into the pathways that remanence vectors move during tilt correction via small circles. This allows for visual determination of which sites may contain structural complications such as minor out of plane bedding rotations. Without SCI analysis it would not have been possible to identify which sites on the east dipping limb of the Mt. Kidd syncline were altering the results. The main drawback with SCI analysis is due to the large errors produced, which can make interpretation of untilting percentages difficult. This is especially the case when the mean dip of both limbs is low compared to the standard deviation of the untilting percentages.

This issue can be reconciled when SCI analysis is integrated with conventional tilt tests. It appears that when both the untilting percentages of the conventional tilt tests and SCI analysis are in good agreement, as in the case of the unmodified Line Creek anticline data set and the modified Mt. Kidd syncline data set, then the results of the conventional tilt tests can be considered valid. For this assumption to work detailed structural knowledge of the complete structure is required as highlighted by the Mt. Kidd anticline and certain areas within the Line Creek anticline. The Mt. Kidd anticline showed good agreement between the pre-tilting results from both methods, however, the paleopoles from this data set did not coincide with the pre-tilting pole from Line Creek. This discrepancy was probably due to a lack of structural data, such as knowledge of imbricate thrusts between the front and back limb, which led to the assumption that the anticline represented a continuous structure when in reality it did not.

8.4 Effect of structural complications on regional studies

One of the fundamental observations of this study is that subtle structural complications can have a profound effect on a particular paleomagnetic data set, even within a well defined structure. These structural complications can alter untilting percentages as well as resultant paleopoles. This may be amplified in studies of individual structures lacking detailed structural data, as with the Mt. Kidd anticline or in regional studies which combine paleomagnetic results from multiple structures (e.g. Enkin et al., 2000). An important paleomagnetic study in the Canadian Cordillera was a regional investigation where samples were collected from multiple across strike transects through different portions of the Canadian Cordillera (Enkin et al., 2000).

This study reported early syn-tilting to pre-tilting results and had paleopoles which showed a wide range in ages around the Tertiary-Late Jurassic sections of the APWP. The discrepenciy in ages were determined to simply relate to vertical axis rotations in the thrust sheets (Enkin et al., 2000). The majority of the other paleomagnetic studies in the Canadian Cordillera were conducted on drill cores from hydrocarbon reservoirs which sampled only one limb of complex structures and no tilt tests were performed (e.g., Lewchuk et al., 1998; Cioppa et al., 2000). These studies also had paleopoles which were quite variable. It is likely that the poles were contaminated by one or more structural complications such as plunging fold axis's, small out of plane bedding rotations, strain alterations and/or spurious rotations. If detailed sampling had been conducted on individual structures as in this study it may have been possible to recognize many of these subtle structural complications. This would have allowed for the modification of these data sets which may have generated more refined and accurate paleomagnetic poles. Although regional studies as well as studies of subsurface units provide valuable information about the nature and extent of remagnetizations in fold and thrust belts a lack of structural knowledge complicates accurate age determination. The only way to accurately date remagnetizations in complex structures is to conduct detailed studies on individual folds which allow for a strong control on the deformation mechanisms and kinematic history, in order to avoid or recognize subtle structural complications.

9. Conclusions

Based on the results of a combined SCI and calcite twin strain analysis this study has shown that small and subtle structural variations can have a profound effect

on a particular paleomagnetic data set. These variations are influenced by both the kinematic history as well as the predominate deformation mechanism and three primary conclusions can be reached.

1) Subtle structural variation are generally not observable using conventional tilt tests alone while SCI analysis can be quite sensitive to these subtle variations and has been shown in this study to be a powerful tool when investigating remagnetizations in fold and thrust belts. Combining SCI and conventional tilt test analysis allowed the refinement of the age and confirmation of the syn-tilting nature of the remagnetization at the Mt. Kidd syncline. This was accomplished by highlighting and allowing for the modification of the data set by removing the sites that were subjected to structural complications, which strongly influenced the tilt test and SCI results. SCI analysis also showed no subsequent overall tilts at Mt. Kidd providing important kinematic information about the origin of the plunging fold axis, which can now be related to an interaction of a both a frontal and oblique ramp as opposed to later tilting event perpendicular to the fold axis.
2) In terms of the origin of the early syn-tilting remagnetization for the high temperature CRM at the Mt. Kidd Syncline, modified SCI and tilt test analysis has shown the magnetization was acquired around (~120Ma), which is much older than the motion of the major underlying thrust sheets. This suggests that the remagnetization is unlikely a "true" syn-tilting remagnetization and that some form of structural or strain modification has generated the syn-tilting result. Since the plunge in the structure may have formed due to the interaction

of both a frontal and oblique ramp there is a possibility that the syn-tilting remagnetization is the result of spurious rotation of the remanence vectors. The Mt. Kidd syncline has also been subjected to relatively high ductile strain as shown by calcite twin strain analysis and macroscopic observation of ductile thinning in the east dipping limb of the structure, which may have led to strain modification of a pre-tilting remagnetization.

3) Finally this study has also shown that certain structural criteria exist to predetermine what type of structure is the most suitable for paleomagnetic analysis in fold and thrust belts. The Line Creek anticline appears to be an ideal fold. This structure is an upright fold which formed by transport of the hanging wall over a simple frontal ramp removing the complication of spurious rotations due to complex ramp interactions. The structure also contains planer limbs formed via kink folding which is idea for application of conventional tilt tests which apply ridged body rotation of the limb segments. Finally the Line Creek anticline has been subjected to only low strain during moderate burial and the dominate deformation mechanism is brittle faulting and fracturing, which removes complications of strain alteration due to ductile deformation and allowing for a confident age determination.

References Cited

Al-Aasm, I. S. (2000), Chemical and isotopic constraints for recrystallization of sedimentary dolomites from the Western Canada Sedimentary Basin, Aquatic Geochemistry, 6(2), 227-248.

Aubourg, C., and C. Chabert-Pelline (1999), Neogene remagnetization of normal polarity in the Late Jurassic black shales from the southern subalpine chains

(French Alps); evidence for late anticlockwise rotations, Tectonophysics, 308(4), 473-486.

Besse, J., and V. Courtillot (2002), Apparent and true polar wander and the geometry of the geomagnetic field over the last 200 Myr, Journal of Geophysical Research, 107, no.B11, 31.

Burkhard, M. (1993), Calcite twins, their geometry, appearance and significance as stress-strain markers and indicators of tectonic regime; a review, Journal of Structural Geology, 15, 3-5.

Borradaile, G. J. (1997), Deformation and paleomagnetism, Surveys in Geophysics, 18(4), 405-435.

Bustin, R. M. (1991), Organic maturity in the Western Canada sedimentary basin, International Journal of Coal Geology, 19, 1-4.

Carr, S. D., and P. S. Simony (2006), Ductile thrusting versus channel flow in the southeastern Canadian Cordillera; evolution of a coherent crystalline thrust sheet, Geological Society Special Publications, D-1, 561-587.

Cioppa, M. T., I. S. Al-Aasm, D. T. A. Symons, M. T. Lewchuk, and K. P. Gillen (2000), Correlating paleomagnetic, geochemical and petrographic evidence to date diagenetic and fluid flow events in the Mississippian Turner Valley Formation, Moose Field, Alberta, Canada, Sedimentary Geology, 131(3-4), 109-129.

Dunlop, D. J., and K. S. Argyle (2007), Separating multidomain and single-domain-like remanences in pseudo-single-domain magnetites (215-540 nm) by low-temperature demagnetization, Journal of Geophysical Research, 96(B2), 2007-2017.

Elmore, R. D., J. L.-E. Foucher, M. Evans, M. Lewchuk, and E. Cox (2006), Remagnetization of the Tonoloway Formation and the Helderberg Group in the Central Appalachians; testing the origin of syntilting magnetizations, Geophysical Journal International, 166(3), 1062-1076.

Enkin, R. J. (2003), The direction-correction tilt test; an all-purpose tilt/fold test for paleomagnetic studies, Earth and Planetary Science Letters, 212, 1-2.

Enkin, R. J. (2004), Paleomagnetism Data Analysis: Version 4.2. Geological Survey of Canada. *On* www.pgc.nrcan.gc.ca/tectonic/enkin.htm.

Enkin, R. J., K. G. Osadetz, J. Baker, and D. Kisilevsky (2000), Orogenic remagnetizations in the front ranges and inner foothills of the southern Canadian Cordillera; chemical harbinger and thermal handmaiden of Cordilleran deformation, Geological Society of America Bulletin, 112(6), 929-942.

Erslev, E. A., and K. R. Mayborn (1997), Multiple geometries and modes of fault-propagation folding in the Canadian thrust belt, Journal of Structural Geology, 19, 3-4.

Evans, M. A., and R. H. Groshong, Jr. (1994), Microcomputer techniques and applications; a computer program for the calcite strain-gauge technique, Journal of Structural Geology, 16(2), 277-281.

Evans, M. A., M. T. Lewchuk, and R. D. Elmore (2003), Strain partitioning of deformation mechanisms in limestones; examining the relationship of strain and anisotropy of magnetic susceptibility (AMS), Journal of Structural Geology, 25(9), 1525-1549.

Evenchick, C. A., M. E. McMechan, V. J. McNicoll, and S. D. Carr (2007), A synthesis of the Jurassic–Cretaceous tectonic evolution of the central and southeastern Canadian Cordillera: Exploring links across the orogen, GSA Special Papers 2007, 433, 117-145.

Fermor, P. R., and I. W. Moffat (1992), Tectonics and structure of the Western Canada foreland basin, AAPG Memoir, 55, 81-105.

Ferrill, D. A. (1991), Calcite twin widths and intensities as metamorphic indicators in natural low-temperature deformation of limestone, Journal of Structural Geology, 13(6), 667-675.

Ferrill, D. A., A. P. Morris, M. A. Evans, M. Burkhard, R. H. Groshong, Jr., and C. M. Onasch (1994), Calcite twin morphology; a low temperature deformation geothermometer, Journal of Structural Geology, 26(8), 1521-1529.

Fisher, R. A. (1953), Dispersion on a sphere, *Proc. R. Soc. London, Ser. A, 217*, 295-305.

Grabowski, J., and J. Nawrocki (2001), Palaeomagnetism of some Devonian carbonates from the Holy Cross Mts. (central Poland); large pre-Permian rotations or strain modified palaeomagnetic directions?, Geological Quarterly, 45(2), 165-178.

Graham, J. W. (1949), The stability and significance of magnetism in sedimentary rocks, Journal of Geophysical Research, 54(2), 131-167.

Groshong, R. H., Jr. (1972), Strain Calculated from Twinning in Calcite, Geological Society of America Bulletin, 83(7), 2025-2037.

Groshong, R. H., Jr. (1974), Experimental Test of Least-Squares Strain Gage Calculation Using Twinned Calcite, Geological Society of America Bulletin, 85(12), 1855-1863.

Hardebol, N. J., J.-P. Callot, J.-L. Faure, G. Bertotti, and F. Roure (Eds.) (2007), Kinematics of the SE Canadian fold-and-thrust belt; implications for the thermal and organic maturation history, 179-202 pp., Springer Berlin Heidelberg.

Henry, B., H. Rouvier, and M. Le Goff (2004), Using syntectonic remagnetizations for fold geometry and vertical axis rotation: the example of the Cevennes border (France), Geophysical Journal International, 157(3), 1061-1070.

Hirt, A. M., W. Lowrie, and O. A. Pfiffner (1986), A paleomagnetic study of tectonically deformed red beds of the lower Glarus nappe complex, eastern Switzerland, Tectonics, 5(5), 723-731.

Hitchon, B. (1984), Geothermal gradients, hydrodynamics, and hydrocarbon occurrences, Alberta, Canada, AAPG Bulletin, 72(11), 1395-1410.

Hudson, M. R., R. L. Reynolds, and N. S. Fishman (1989), Synfolding magnetization in the Jurassic Preuss Sandstone, Wyoming-Idaho-Utah thrust belt, Journal of Geophysical Research, 94(B10), 13,681-613,705.

Jager, J. C., and N. G. W. Cook (Eds.) (1979), Fundamentals of Rock Mechanics, 3rd ed., Chapman and Hall, London.

Kalkreuth, W., and M. E. McMechan (1988), Burial history and thermal maturity, Rocky Mountain Front Ranges, foothills, and foreland, east-central British Columbia and adjacent Alberta, Canada, AAPG Bulletin, 72(11), 1395-1410.

Katz, B., D. R. Elmore, M. Cogoini, M. H. Engel, and S. Ferry (2000), Associations between burial diagenesis of smectite, chemical remagnetization, and magnetite

authigenesis in the Vocontian Trough, SE France, Journal of Geophysical Research, 105(B1), 851-868.
Kent, D. V., and N. D. Opdyke (1985), Multicomponent magnetizations from the Mississippian Mauch Chunk Formation of the Central Appalachians and their tectonic implications, Journal of Geophysical Research, 90(B7), 5371-5383.
Kirschvink, J. L. (1980), The least-squares line and plane and the analysis of palaeomagnetic data, Geophysical Journal of the Royal Astronomical Society, 62(3), 699-718.
Kligfield, R., W. Lowrie, A. Hirt, and A. W. B. Siddans (1983), Effect of progressive deformation on remanent magnetization of Permian redbeds from the Alpes Maritimes (France), Tectonophysics, 98, 1-2.
Kodama, K. P. (1988), Remanence rotation due to rock strain during folding and the stepwise application of the fold test, Journal of Geophysical Research, 93(B4), 3357-3371.
Lewchuk, M. T., I. S. Al-Aasm, D. T. A. Symons, and K. P. Gillen (1998), Dolomitization of Mississippian carbonates in the Shell Waterton gas field, southwestern Alberta; insights from paleomagnetism, petrology and geochemistry, Bulletin of Canadian Petroleum Geology, 46(3), 387-410.
Lewchuk, M. T., M. Evans, and R. D. Elmore (2003), Synfolding remagnetization and deformation; results from Palaeozoic sedimentary rocks in West Virginia, Geophysical Journal International, 152(2), 266-279.
Machel, H. G., and E. W. Mountjoy (1987), General constraints on extensive pervasive dolomitization and their application to the Devonian carbonates of Western Canada, Bulletin of Canadian Petroleum Geology, 15(10), 936-940.
Machel, H. G., H. R. Krouse, and R. Sassen (1995), Products and distinguishing criteria of bacterial and thermochemical sulfate reduction, Applied Geochemistry, 108(9), 1108-1119.
Marshak, S., and G. Mitra (Eds.) (1988), Basic methods of structural geology; Part 1, Elementary techniques; Part 2, Special topics, 446 pp., Prentice-Hall, Englewood Cliffs, NJ, United States (USA).
McCabe, C., and R. D. Elmore (1989), The occurrence and origin of late Paleozoic remagnetization in the sedimentary rocks of North America, Reviews of Geophysics, 27(4), 471-494.
McClelland-Brown, E. (1983), Palaeomagnetic studies of fold developmentand propagation in the Pembrokeshire old red sandstone, Tectonophysics, 98, 131–149.
McElhinny, M. W. (1964), Statistical significance of the fold test in palaeomagnetism., Geophysical Journal of the Royal Astronomical Society, 8, 338-340.
McFadden, P. L. (1990), A new fold test for palaeomagnetic studies, Geophysical Journal International, 103(1), 163-169.
McFadden, P. L. (1998), The fold test as an analytical tool, Geophysical Journal International, 135(2), 329-338.
McFadden, P. L., and D. L. Jones (1981), The fold test in palaeomagnetism, Geophysical Journal of the Royal Astronomical Society, 67(1), 53-58.

McGugan, A. (1987), "Horses" and transverse faults in the Lewis thrust sheet, Elk Range, Kananaskis Valley, Rocky Mountain Front Ranges, southwestern Alberta, Bulletin of Canadian Petroleum Geology, 35(3), 358-361.

McMechan, M. E. (1995), Geology Rocky Mountain Foothills and Front Ranges in Kananaskis Country, Alberta, Geological Survey of Canada.

McMechan, M. E. (2001), Large scale duplex structures in the McConnell thrust sheet, Rocky Mountains, Southwest Alberta, Bulletin of Canadian Petroleum Geology, 49(3), 408-425.

McMechan, M. E., and R. I. Thompson (Eds.) (1989), Structural style and history of the Rocky Mountain fold and thrust belt, 47-71 pp., Can. Soc. Pet. Geol., Calgary, AB, Canada, Calgary, AB.

Miller, J. D., and D. V. Kent (1988), Regional trends in the timing of Alleghanian remagnetization in the Appalachians, Geology, 16(7), 588-591.

Moffat, I. W., and J. H. Spang (1984), Origin of transverse faulting, Rocky Mountain Front Ranges, Canmore, Alberta, Bulletin of Canadian Petroleum Geology, 32(2), 147-161.

Monger, J. W. H., and R. A. Price (1979), Geodynamic evolution of the Canadian Cordillera; progress and problems, Canadian Journal of Earth Sciences = Revue Canadienne des Sciences de la Terre, 16(3, Part 2), 771-791.

O'Brien, V. J., K. M. Moreland, R. D. Elmore, M. H. Engel, and M. A. Evans (2007), Origin of orogenic remagnetizations in Mississippian carbonates, Sawtooth Range, Montana, Journal of Geophysical Research, 112(B6).

Oliva-Urcia, B., E. L. Pueyo, and J. C. Larrasoaña (2008), Magnetic reorientation induced by pressure solution: A potential mechanism for orogenic-scale remagnetizations, Earth and Planetary Science Letters, 265, 525-534.

Orr, W. L. (1974), Changes in Sulfur Content and Isotopic Ratios of Sulfur during Petroleum Maturation; Study of Big Horn Basin Paleozoic Oils, AAPG Bulletin, 68(6), 713-743.

Price, R. A. (2007), Fault Dating in the Canadian Rocky Mountains: Evidence for late Cretaceous and eatly Eocene orogenic pulses: Comment, Geology, 34.

Price, R. A. (1981), The Cordilleran foreland thrust and fold belt in the southern Canadian Rocky Mountains, Special Publication Geological Society of London, no, 9(9), 427-448.

Price, R. A., and E. W. Mountjoy (1970), Geologic structure of the canadian rocky mountains between bow and athabasca rivers - a progress report, Special Paper Geological Association of Canada, pp, 7-25.

Price, R. A., D. A. Grieve, and C. Patenaude (1992), Geology, Tornado Mountain British Columbia-Alberta, Geological Survey of Canada.

Price, R. A., G. D. Mossop, and I. Shetsen (Eds.) (1994), Cordilleran tectonics and the evolution of the Western Canada sedimentary basin, 2-24 pp., Geological Survey of Canada, Calgary, AB.

Pueyo, E. L., A. Pocovi, J. M. Pares, H. Millan, and J. C. Larrasoana (2003), Thrust ramp geometry and spurious rotations of paleomagnetic vectors, Studia Geophysica et Geodetica, 47(2), 331-357.

Ramsay, J. G., and M. I. Huber (Eds.) (1987), The techniques of modern structural geology; Volume 2; Folds and fractures.

Root, K. G. (2001), Devonian Antler fold and thrust belt and foreland basin development in the southern Canadian Cordillera; implications for the Western Canada Sedimentary Basin, Bulletin of Canadian Petroleum Geology, 268, 561-587.

Roure, F., R. Swennen, F. Schneider, J.L. Faure, H. Ferket, N. Guilhaumou, K. Osadetz, P. Robion and V. Vandeginste (2005), Incidence and importance of tectonics and natural fluid migration on reservoir evolution in foreland fold-and-thrust belts, Oil & Gas Science and Technology, 60, (1), 67-106.

Scotese, C. R., R. Van der Voo, and Anonymous (1983), Paleomagnetic dating of Alleghenian folding, Eos, Transactions, American Geophysical Union, 64(18).

Shipunov, S. V. (1997), Synfolding magnetization; detection, testing and geological applications, Geophysical Journal International, 130(2), 405-410.

Spang, J. H., and T. L. Wolcott (1981), Strain in the ramp regions of two minor thrusts, southern Canadian Rocky Mountains, Geophysical Monograph, no, 24, 243-250.

Stamatakos, J., and K. P. Kodama (1991), Flexural flow folding and the paleomagnetic fold test; an example of strain reorientation of remanence in the Mauch Chunk Formation, Tectonics, 10(4), 807-819.

Stamatakos, J., and A. M. Hirt (1994), Paleomagnetic considerations of the development of the Pennsylvania Salient in the Central Appalachians, Tectonophysics, 231(4), 237-255.

Stamatakos, J., A. M. Hirt, and W. Lowrie (1996), The age and timing of folding in the Central Appalachians from paleomagnetic results, Geological Society of America Bulletin, 108(7), 815-829.

Stewart, S. A. (1995), Palaeomagnetic analysis of plunging fold structures; errors and a simple fold test, Earth and Planetary Science Letters, 130, 1-4.

Tarling, D. H. (Ed.) (1983), Palaeomagnetism; principles and applications in geology, geophysics and archaeology.

Tauxe, L., N. Kylstra, and C. Constable (1991), Bootstrap statistics for paleomagnetic data, Journal of Geophysical Research, 96(B7), 723-711.

Turner, F. J., and L. E. Weiss (Eds.) (1963), Structural analysis of metamorphic tectonites.

van der Pluijm, B. A., P. J. Vrolijk, D. R. Pevear, C. M. Hall, and J. Solum (2006), Fault dating in the Canadian Rocky Mountains: Evidence for late Cretaceous and early Eocene orogenic pulses, Geology, 34(10), 837-840.

van der Pluijm, B. A. (1987), Grain-scale deformation and the fold test; evaluation of syn-folding remagnetization, Geophysical Research Letters, 14(2), 155-157.

Van der Voo, R., J. A. Stamatakos, and J. M. Pares (1997), Kinematic constraints on thrust-belt curvature from syndeformational magnetizations in the Lagos del Valle Syncline in the Cantabrian Arc, Spain, Journal of Geophysical Research, 102(B5), 105-110.

Vandeginste, V., R. Swennen, S. A. Gleeson, R. M. Ellam, K. Osadetz, and F. Roure (2009), Thermochemical sulphate reduction in the Upper Devonian Cairn Formation of the Fairholme carbonate complex (South-West Alberta, Canadian Rockies): evidence from fluid inclusions and isotopic data, Sedimentology, 56(2), 439-460.

Villalain, J. J., M. L. Osete, R. Vegas, V. Garcia-Duenas, and F. Heller (1994), Widespread Neogene remagnetization in Jurassic limestones of the South-Iberian palaeomargin (western Betics, Gibraltar Arc), Physics of the Earth and Planetary Interiors, 85, 1-2.

Waldhoer, M., and E. Appel (2006), Intersections of remanence small circles: new tools to improve data processing and interpretation in palaeomagnetism, Geophysical Journal International, 166(1), 33-45.

Waldhoer, M., and E. Appel (2009), Layer parallelisation; an unrecognised mechanism for palaeomagnetic rotations in fold belts, Tectonophysics, 474, 3-4.

Watson, G. S., and R. J. Enkin (1993), The fold test in paleomagnetism as a parameter estimation problem, Geophysical Research Letters, 20(19), 2135-2137.

Weil, A. B., and R. Van der Voo (2002), Insights into the mechanism for orogen-related carbonate remagnetization from growth of authigenic Fe-oxide; a scanning electron microscopy and rock magnetic study of Devonian carbonates from northern Spain, Journal of Geophysical Research, 107, no.B4, 15.

Weil, A. B., and R. Van der Voo (2002), The evolution of the paleomagnetic fold test as applied to complex geologic situations, illustrated by a case study from northern Spain, in Physics and Chemistry of the Earth, edited by C. Aubourg, D. Elmore, A. Hirt, L. J. Pesonen, C. Peters, E. Petrovsky and R. Scholger, pp. 1223-1235, Pergamon, Oxford-New York-Toronto.

Zijderveld, J. D. A. (1967), A.c. demagnetization of rocks: analysis of results. *In* Collinson, D.E. et al., eds., Methods in Paleomagnetism. New York, Elsevier Science, pp. 254-286

Chapter 5: Discussion and Major Conclusion

5.1 Cumulative model for the origin and timing relative to folding of the multi-component remagnetization.

5.1.1 Origin of the multi-component remagnetization event

Since deposition these Mississippian carbonates have undergone multiple diagenetic and tectonic events, which have had a profound effect on the units and have helped promote the acquisition of the observed multi-component remagnetization. Based on burial time-unblocking temperature diagrams (Dunlop et al., 2000) and detailed rock magnetic characterization, the high temperature component is has been determined to be a chemical remanent magnetization (CRM) residing in magnetite and the intermediate temperature component is CRM residing in pyrrhotite. Based on paleomagnetic field tests and paleopoles the magnetite component is Early Cretaceous in age and the pyrrhotite component is Tertiary in age.

The obduction of exotic terranes onto the North American pericratonic terranes began in the Late Triassic and continued into the Eocene which initiated shortening and thickening in the Omineca Belt west of the Foreland belt [Evenchick et al., 2007 and references there in]. This led to significant uplift in the Omineca Belt by the Late Middle Jurassic and the first appearance of western derived sediments. Tectonic loading and erosion of the Omineca highlands increased subsidence and burial in the foreland belt [Poulton et al., 1993], which led to hydrocarbon generation and subsequent migration within the Carboniferous and lower Triassic rocks during the Late Jurassic-Early Cretaceous [Kalkreuth and McMechan, 1988]. Initiation of thrusting in the western most portion of the foreland belt began in the Early Cretaceous and progressed eastward [Carr and Simony, 2006].

A regional fluid migration event, possibly related to maturation of organic matter and hydrocarbon migration, progressed eastward through the undeformed strata via one or more mechanisms: 1) gravitational recharge (Ge and Garvin, 1994) from the Omencia Highlands, 2) tectonically induced squeegee type flow in the direct vicinity of the active deformation front (Oliver, 1986; Machel and Cavell, 1999) or 3) basinward up dip migration towards the Western Canada Sedimentary Basin (Bachu, 1995). Pervasive meso-dolomite recrystallization is considered to have formed from both meteoric and hydrothermal fluids during burial [Al-Aasm, 2000], however, these fluids are not considered to have caused acquisition of the magnetite component since it has been found in both dolostones and limestones. Regional dolomitization was followed by another fluid migration event which led to the formation of the Early Cretaceous Aptian), pre-tilting pervasive remagnetization in magnetite within the Mississippian carbonates in the eastern Front Ranges. There is a direct relationship between the magnetite component and calcite in red luminescent, bedding parallel veins. This fluid event was pervasive throughout the Mississippian units examined as shown by red luminescent calcite cement.

This fluid migration event and hydrocarbon emplacement was followed by intense contraction in the Front Ranges during the Late Cretaceous-to Eocene, during which the major motions along the Lewis, Rundle and McConnell thrust sheets occurred [Price, 1981; van der Pluijm et al., 2006]. This contraction was expressed as thin-skinned detachment thrusting and folding of Mesoproterozoic to Cretaceous strata over Cretaceous and older strata [e.g. Monger and Price, 1979; McMechan and Thompson, 1989; Price, 1994]. Following and possibly during the latest stages of

folding warm dolomitizing sulphate rich fluids moved upward along faults and fractures, and came into contact with the hydrocarbons. This led to the formation of extensive sour gas reservoirs throughout the Canadian Cordillera via thermo sulphate reduction (TSR) of the hydrocarbons, [Machel, 1987; Machel et al., 1995; Roure et al., 2005; Vandeginste et al., 2009]. During TSR the alteration of the hydrocarbons led to the formation of coarse vein and vug filling dolomite, barite, sulphur enriched organics and sulphide mineralization (e.g., Machel et al., 1995; Pierce, et al., 1998). The Mississippian carbonates contain multiple TSR byproducts as well as the pervasive Tertiary, reversed polarity pyrrhotite component within the eastern Front Ranges. Based on a vein test, the pyrrhotite component shows a direct relationship to red luminescent dolomite in tectonic veins and vugs.

5.1.2 Origin of syn-tilting remagnetizations in the Canadian Cordillera

Syn-tilting remagnetizations have commonly been observed throughout the Canadian Cordillera and show a wide range of paleopoles [e.g., Enkin et al., 2000]. The origin of these syn-tilting remagnetizations can be related to both the kinematic history, the predominate deformation mechanisms associated with folding and thrusting, and the actual remagnetization mechanism. Since the intense contraction along the Lewis, Rundle and McConnell thrust sheets within the Front Ranges occurred during the Late Cretaceous-to Eocene [Price, 1981; van der Pluijm et al., 2006], any true syn-tilting remagnetizations should occur within this time span. Tilt test and SCI analysis for the magnetite component at the Mt. Kidd syncline shows an early syn-tilting result which has paleopoles that fall close to the Early Cretaceous (Barremian-Aptian) portion of the apparent polar wander path (APWP). This is almost 30 Ma years prior to the onset of

major motion on the trusts in which the structure is located. This is in direct contrast to an Early Cretaceous (Aptian) pre-tilting result obtained from the Line Creek anticline, also contained within the Lewis thrust sheet. This suggests that the syn-tilting nature of the Mt. Kidd syncline may be related to structural complications or strain alteration, although a non-unique solution due to differential folding may also be a factor.

At the Mt. Kidd syncline the lower section of the Mississippian carbonates (Banff to Lower Mount Head formations) were sampled. The plunging (~15°) tight asymmetrical syncline underwent significant layer parallel shear resulting in ductile thinning in the front limb and thickening in the nose. In contrast, the pre-tilting Line Creek anticline is an upright fold formed in the upper section of the Mississippian carbonates (upper Mount Head and Etherington formations) and formed as a result of kink folding and brittle faulting/fracturing during thrusting. The syn-tilting Mt. Kidd syncline experienced high deviatoric strain resulting in as high as 8.6% total distortion by twinning at burial temperatures which exceed 200°C. The pre-tilting Line Creek anticline, on the other hand, formed under low burial temperatures (~170°C) and low deviatoric strain (0.27-0.84%). The low strain and upright nature of the Line Creek anticline removes the possibility of unforeseen structural complication and makes the structure an good candidate for structural analysis. These results are consistent with strain alteration of a pre-tilting remagnetization at the Mt. Kidd syncline either by whole grain distortion during twinning (Evans et al., 2003) or rigid body rotation of magnetic grains due to layer parallel shear (van der Pluijm, 1987).

Another possibility for the syn-tilting result is related to structural complications such as overall tilts perpendicular to the fold axis (Stewart, 1995; Waldhöer and Appel,

2006) or spurious rotations of paleomagnetic vectors due to complex ramp geometries (Pueyo et al., 2003). Small circle intersection (SCI) analysis has shown that the plunge in the Mt. Kidd syncline was not the result of an overall tilt perpendicular to the fold axis. The presence of multiple transverse faults in the Rundle thrust sheet in the vicinity of Mt. Kidd suggests the existence of a complex ramp geometry so spurious rotation of paleomagnetic vectors cannot be completely discounted.

In terms of the pyrrhotite component at Line Creek the syn-tilting result appears to be Late Jurassic making it older than the pre-tilting magnetite component. Since the Line Creek anticline does not contain any un foreseen structural complications the syn-tilting nature most likely relates to either differential folding or multiple remagnetization events. The water gap at the Line Creek anticline is roughly perpendicular to strike and creates a almost continuous outcrop of the entire structure. Because of this sampling covered an extensive stratigraphic section at Line Creek. TSR, which is considered to be the remagnetization mechanism for the pyrrhotite component, can occur rapidly over a small stratigraphic section. It is possible, therefore, that the multiple TSR events were sampled which resulted in a "false" syn-tilting result.

5.2 Summary of major conclusions

1) Based on a combination of paleomagnetic and rock magnetic experiments, it is clear that the remagnetized Mississippian carbonates from the Canadian Rockies contain a complex and at times highly variable mixture of magnetic mineralogies and grain sizes. The results of this study suggest that determination of the remanence carriers in multi-component NRMs requires low temperature

experiments combined with thermal demagnetization and advanced rock magnetic techniques such as FORC analysis and Log Gaussian analysis.

2) Based on a combination of thermal demagnetization, cumulative Log Gaussian analysis and low temperature experiments, these samples contain up to three distinct components: 1) a modern VRM unblocks below 200°C and resides in MD magnetite 2) an intermediate temperature component unblocks between 310 and 325°C that was determined to be a CRM in SD pyrrhotite 3) a high temperature component with a maximum unblocking temperature of 540°C, which was determined to be a CRM in PSD-SD magnetite.
3) Based on elevated Sr-isotopes in the host dolomites and limestones in the Mississippian carbonates and positive correlations between bedding parallel veins and the magnetite component, the most probable origin of the remagnetization is a regional fluid flow event related to the initiation of thrusting and folding in the Main Ranges of the foreland belt prior to the onset of Laramide deformation in the Front Ranges.
4) The origin of the pyrrhotite component observed in the Mississippian carbonates is consistent with warm Fe rich fluids migrating along faults and fractures causing TSR of hydrocarbons, which led to the formation of sour gas reservoirs. This model is based on the petrographic observation of multiple common by-products of TSR which include: authogenic pyrite, frambodial pyrrhotite, spalerite, sulfur enriched bitumen and zoned dolomite crystals with elevated fluid inclusion temperatures (140-212°C). The exact timing of pyrrhotite

remagnetization is unclear due to the general nature of TSR. At Mt. Kidd the pyrrhotite component is post-tilting and appears to be Late Tertiary in age.

5) Subtle structural variations are generally not observable using conventional tilt tests alone while SCI analysis can be quite sensitive to the subtle variations, however, in this study SCI analysis was shown to be a useful tool when investigating remagnetizations in fold and thrust belts. In terms of the origin of the early syn-tilting remagnetization for the high temperature CRM at the Mt. Kidd Syncline, modified SCI and tilt test analysis has shown that the magnetization was acquired around (~120Ma), which is much older than the motion of the major underlying thrust sheets. This suggests that the remagnetization is unlikely a "true" syn-tilting remagnetization and that some form of structural or strain modification has generated the syn-tilting result. Since the plunging structure formed due to the interaction of both a frontal and oblique ramp, there is a possibility that the syn-tilting remagnetization is the result of spurious rotation of the remanence vectors. The Mt. Kidd syncline has also been subjected to relatively high ductile strain as shown by calcite twin strain analysis and macroscopic observation of ductile thinning in the east dipping limb of the structure, which may have led to strain modification of a pre-tilting remagnetization.

6) Finally, this study has also shown that certain structural criteria exist to predetermine what type of structure is the most suitable for paleomagnetic analysis in fold and thrust belts. The Line Creek anticline appears to be an ideal fold. This structure is an upright fold that formed by transport of the hanging

wall over a simple frontal ramp removing the complication of spurious rotations due to complex ramp interactions. The structure also contains planer limbs formed via kink folding, which is ideal for application of conventional tilt tests that apply ridged body rotation of the limb segments. Finally, the Line Creek anticline has been subjected to only low strain during moderate burial and the dominate deformation mechanism is brittle faulting and fracturing, which removes complications of strain alteration due to ductile deformation and allowing for a confident age determination.